SYNTHESIS OF DYSIHERBAINE AND SEPARASE INHIBITORS IN DRUG DEVELOPMENT FOR NEURAL DISORDERS AND BREAST CANCER

A Dissertation Presented to

the Faculty of the Department of Chemistry

University of Houston

In Partial Fulfillment

of the Requirements for the Degree

Doctor of Philosophy

By

Ha T. Do

August, 2015

SYNTHESIS OF DYSIHERBAINE AND SEPARASE INHIBITORS IN DRUG DEVELOPMENT FOR NEURAL DISORDERS AND BREAST CANCER

_____

Ha T. Do

APPROVED:

_____

Scott R. Gilbertson, Ph.D.
Committee Chair

_____

Olafs Daugulis, Ph.D.

_____

Jeremy A. May, Ph.D.

_____

Shiv P. Halasyamani, Ph.D.

_____

Greg D. Cuny, Ph.D.

_____

Dean, College of Natural Sciences and Mathematics

Acknowledgements

First and foremost, I would like to thank my advisor, Prof. Scott R. Gilbertson for his guidance and mentorship. Starting working in Gilbertson group, I was given the best research environment and constant support from him. I would like to express my sincere appreciation for everything he has done to help me in my Ph.D. studies.

I would also like to thank my committee members, Prof. Olafs Daugulis, Prof. Jeremy A. May, Prof. Greg D. Cuny, and Prof. Shiv P. Halasyamani for their insightful comments and suggestions on my dissertation. Additionally, I would like to thank Dr. James Korp for his time working on X-ray analysis in dysiherbaine project.

Furthermore, I would like to acknowledge all of labmates in the Gilbertson group, both past and present, for their support and friendship.

Finally, I would like to thank my family for unconditionally supporting me, especially my husband, Minh Nguyen, who always encourages and supports me during the hard times.

SYNTHESIS OF DYSIHERBAINE AND SEPARASE INHIBITORS IN DRUG DEVELOPMENT FOR NEURAL DISORDERS AND BREAST CANCER

An Abstract of a Dissertation

Presented to

the Faculty of the Department of Chemistry

University of Houston

In Partial Fulfillment

of the Requirements for the Degree

Doctor of Philosophy

By

Ha T. Do

August, 2015

ABSTRACT

Drug development has been playing an important role in the search for new medications for hard-to-treat diseases. The development of a new drug for a specific biological target mainly derives from two sources: natural products or small organic molecules. This dissertation presents our effort and accomplishments in the synthesis of the natural product dysiherbaine and small molecule inhibitors of the separase enzyme in drug development for neural disorders and breast cancer.

Ionotropic glutamate receptors (iGluRs) are synaptic receptors that are involved in brain signaling mechanisms and are also implicated in neuronal disorders. Dysiherbaine, isolated from the marine sponge *Dysidea herbacea*, has shown high affinity and selectivity for certain iGluRs making it a unique ligand to explore the complexity of these receptors. In this dissertation, we present the synthesis of dyshiherbaine by using a novel approach that allows the modification of important functionalities and their stereochemistry at a late stage of the synthesis. The synthetic route was established by using an intermediate with a carbon-carbon double bond between C8 and C9 to which various functional groups can be added. To install the aminohydroxyl functional group at C8 and C9 with the correct stereochemistry as the natural product, dysiherbaine, the ring opening and rearrangement of the Boc-protected aziridine was utilized. Furthermore, our extensive study in constructing the amino acid side chain at C4, using an optimized condition for asymmetric hydrogenation was a key step to obtain the natural product.

Additionally, a library of small molecule inhibitors of saparase enzyme was synthesized and utilized in a structure-activity relationship (SAR) study. Due to the

overexpression of separase enzyme in human cancer tumor cells, modulation of separase enzymatic activity could constitute a new therapeutic strategy for targeting resistant, separase-overexpressing aneuploid tumors, particularly hard-to-treat triple negative breast cancer. Herein, we report the synthesis, structural information, and SAR of novel separase inhibitors based on structural modification on three main regions of the lead molecule (2,2-dimethyl-5-nitro-2*H*-benzimidazol-1,3-dioxide). Various functional groups have been used to attach to the three modified regions and general trends have been observed on the effects of the substituting functionality. Our calculation and bioassay results indicate that the oxides on the lead compound could possibly be the binding site to separase enzyme.

Table of Contents

List of Tables

List of Figures

List of Schemes

Chapter 1: New Approach to Dysiherbaine - A Unique Ligand to Study Ionotropic Glutamate Receptors

1.1. INTRODUCTION

1.1.1. Glutamate and Its receptors

Glutamate (Glu) is the major excitatory neurotransmitter in the mammalian central nervous system (CNS). It is responsible for sending signals between nerve cells and is thought to play important roles in normal brain function.[1] Glutamate exerts its signaling function by activating its receptor proteins including the ionotropic glutamate receptors (iGluRs) and the metabotropic glutamate receptors (mGluRs).[2,3] The activation of these receptors by glutamate contributes to the mechanism of excitatory synaptic transmission and many forms of synaptic plasticity, a property of brain thought to be vital for memory and learning. The ionotropic receptors tend to be quicker in relaying information while the metabotropic are associated with a more prolonged stimulus.[1] Despite the role of glutamate receptors in brain cognition, their overstimulation can induce neuronal apoptosis which has been linked to many neurodegenerative diseases including epilepsy, Alzheimer's disease, and stroke. Understanding the structure and function of these receptors is critically important for developing potential therapies for neurological diseases.[4]

The ionotropic glutamate receptors

The iGluRs are group of ion channels located mainly on postsynaptic membrane. Upon the binding of Glu, the channel becomes activated and allows the flow of ions

including Ca^{2+}, Na^{+}, and K^{+} into the cell, which leads to membrane depolarization and produces excitatory synaptic transmission.[2] Three classes of iGluRs have been identified and named based on their selective agonists: NMDA (N-methyl-D-aspartate), AMPA ((S)-2-amino-3-(3-hydroxy-5-methyl-4-isoxazolyl)propionic acid), and KA (Kainic acid) (Figure 1.1).[5]

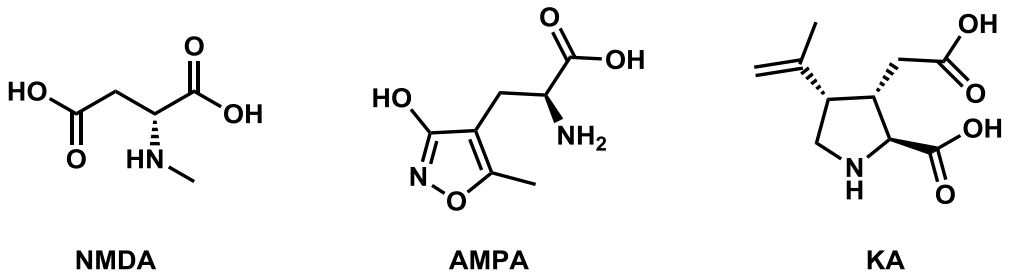

Figure 1.1. Structures of iGluRs' agonists

Each class has different receptor subunits which assemble as tetrameric complexes to form functional receptors. Each receptor subunit has a modular structure, including an extracellular amino-terminal domain (ATD, green) which participates in receptor assembly, trafficking and modulation; a ligand-binding domain (LBD, blue) which is defined by two segments of amino acid termed S1 and S2; a transmembrane domain (TMD, orange) which forms ion channel pores; and an intracellular carboxyl-terminal domain (CTD) which is involved in receptor localization and regulation. The TMD is composed of four segments in which M2 has a re-entrant loop and M4 is connected to the CTD (Figure 1.2).[5,6]

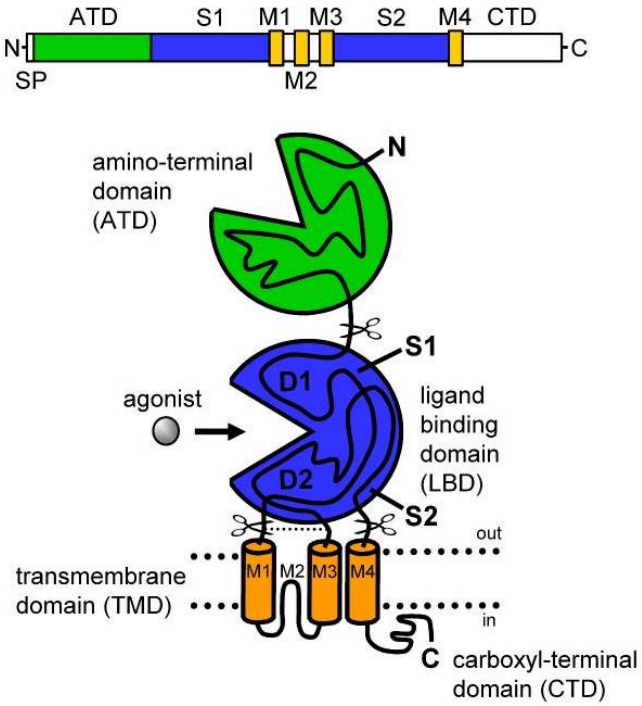

Figure 1.2. Schematic representation of iGluRs subunit structure. Adapted from ref. 5

NMDA receptors

There are seven NMDA receptor subunits including the GluN1, GluN2A-GluN2D, GluN3A, and GluN3B. The assembly of two GluN1 together with either two GluN2 or a combination of GluN2 and GluN3 is required to form functional NMDA receptors. Distinguished from other iGluRs, NMDA receptors demand the binding of not only glutamate but also a co-agonist, glycine to be activated. The GluN1 and GluN3 subunits provide the binding sites for glycine while the GluN2 ones form the binding sites for glutamate.[7] The activation of NMDA receptors also requires the release of Mg^{2+} block to allow the passage of its most permeable cation Ca^{2+} by high depolarization of postsynaptic membrane. These properties make the activation as well as the deactivation

rates of NMDA receptors much slower than other iGluRs. The slow deactivation of NMDA receptors governs the duration of the excitatory postsynaptic potential which is widely thought to be the basis for information storage at synapses, including learning and memory.[5,8]

AMPA receptors

AMPA receptors are composed of four subunits including GluA1 to GluA4 which also assemble as tetramers to form functional receptors. The great majority of AMPA receptors in the CNS exists as dimer of dimers of GluA2 and either GluA1, GluA3, or GluA4.[9] The ion permeation of AMPA receptors is regulated by the Q/R (glutamine/arginine) editing site located in the M2 loop of receptor subunit. When the glutamine is altered to the arginine, the additional charge is introduced into the pore, preventing the passage of a divalent cation Ca^{2+} due to the electrostatic repulsion. Most of AMPA receptors contain GluA2 arginine edited site and are impermeable to Ca^{2+}. This is different from NMDA receptors which permits the influx of Ca^{2+}. Furthermore, AMPA receptors show fast activation and deactivation rates within millisecond time scale, and are thus responsible for most of fast excitatory synaptic transmission in CNS.[10]

Kainate receptors (KAR)

KA receptors are composed of five subunits including GluK1 to GluK5 in which GluK1 to GluK3 can form both homo- and heteromeric receptors, while GluK4 and GluK5 only form functional receptors when coexpressed with GluK1 to GluK3.[11] Unlike AMPA and NMDA receptors, KA receptors are localized in both pre- and postsynaptic sites and play prominent roles in each site. They mediate the excitatory current in

postsynaptic site and modify both excitatory and inhibitory synaptic efficacy in the presynaptic site.[12] Mostly, KA receptors are permeable to K^+ and Na^+. Their Ca^{2+} ion permeability is slight and varies with their subunit composition. Interestingly, homomeric edited arginine form of KA receptors are no longer purely cation-selective, but are also permeable to Cl^-.[13] KA receptors also show relatively fast activation and deactivation compared to NMDA receptors.[11]

The metabotropic glutamate receptors

The mGluRs are G-protein coupled receptors which indirectly mediate the synaptic transmission by inducing intracellular metabolic processes via G-protein. The binding of glutamate causes the change in conformation of receptors, leading to the activation of G-protein. When G-protein gets activated, the GDP within its α-subunit gets exchanged with GTP, leading to the dissociation of α-subunit from G-protein complex (αβγ). The dissociated segments from G-protein will further interact with other proteins or ion channels to transfer intracellular messengers.[3]

Eight metabotropic glutamate receptor types including mGluR1 to mGluR8 have been identified and are classified into 3 groups based on their sequence homology, pharmacology, and transduction mechanisms. Group I including mGluR1 and 5 are expressed mostly at the postsynapse. Group II including mGluR2 and 3 were found both pre- and postsynaptically. Group III including mGluR4, 6, 7, and 8 are preferentially located in the presynaptic terminal.[3,14,15] Structurally, mGluRs contain a large extracellular N-terminal domain termed the Venus flytrap domain (VFD), a cysteine-rich domain, seven transmembrane domains, also known as hepatahelical domain (HD), and

an intracellular C-terminal domain (Figure 1.3).[3,15] The VFD provides the binding site for glutamate and mediates the receptor dimerization, while the C-domain interacts with G-protein to induce the signal transduction. The conformation changes of receptors induced by glutamate binding are propagated from the VFD via cysteine-rich domain to the HD and transferred from C-domain to G-protein.[3,16,17]

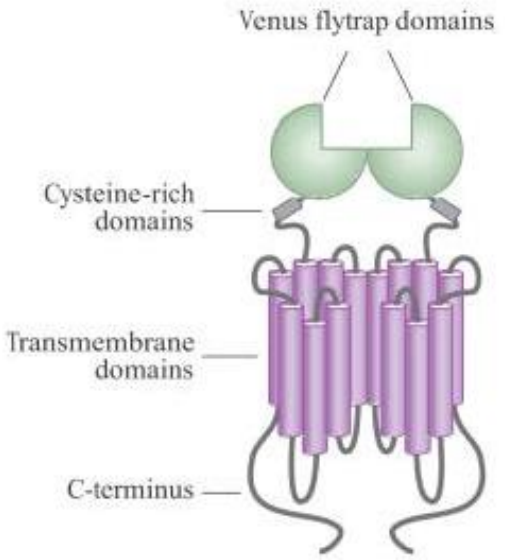

Figure 1.3. Schematic representation of mGluR structure. Adapted from ref. 3

In general, group I mGluRs couple to G_q/G_{11} and activate phospholipase C_β. This pathway leads to Ca^{2+} mobilization and activation of protein kinase C. The activation of group I mGluRs often leads to cell depolarization and increases in neuronal excitability. On the other hand, Group II and III mGluRs are coupled predominantly to $G_{i/o}$ proteins and inhibit adenylyl cyclase. They tend to reduce activity of postsynaptic potential by inhibiting the release of neurotransmitter and thus protect the nerve cells from excitotoxicity.[3,14]

1.1.2. Dysiherbaine and its biological activity to iGluRs

Even though there has been tremendous research on glutamate receptors over the past decade, their physiological and pathological processes in the human brain have not been completely elucidated. This is due to the homology of receptor structures and the lack of selective ligands that can discriminate well between them, particularly for AMPA and KA subtype receptors.[5] The development of pharmacological compounds that can target a specific receptor is a key strategy to address this issue, and naturally occurring molecules represent valuable tools for pharmacological research, as they often show high affinity and selectivity.

Dysiherbaine (DH) was isolated in 1997 from the marine sponge *Dysidea herbacea* by Sakai and co-workers in the course of study to find neurologically active compounds. Its structure was characterized as a unique *cis*-fused hexahydrofuro[3,2-*b*]pyran with four contiguous stereocenters (C6-C9), a quaternary center at C4, and a glutamic acid appendage (Figure 1.4).[18]

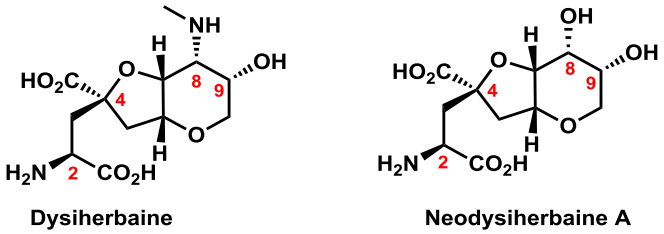

Figure 1.4. Structures of dysiherbaine and neodysiherbaine A

The administration of DH by intraperitoneal injection into mice induces chronic convulsion and seizure, even more intense than domic acid, a known neuroexcitotoxin

and also a potent agonist for KA receptors, suggesting that DH is a strong epileptogenic agent. Furthermore, a radioligand binding assay of DH toward iGluRs revealed that it possesses a high affinity for AMPA and KA receptors with more potent affinity for the later and has almost no effect on NMDA receptors (Table 1.1).[19] This information implicates that DH may be a potential ligand to study the role of KA receptors in iGluR system.

Table 1.1. K_i values of DH and glutamate on iGluRs by displacement of radiolabeled ligands from rat synaptic membrane

	KA receptors (nM)	AMPA receptors (nM)	NMDA receptors (nM)
DH	26 ± 4.0	153 ± 10	>100,000
Glutamate	89 ± 4.3	62 ± 2.3	62 ± 2.8

Detailed studies toward KA subunit receptors showed that DH has strong binding preference for recombinant homomeric GluK1 and GluK2 receptors with K_i values 0.48 nM and 1.28 nM, respectively, but not for GluK5 receptor (Table 1.2). Because of its high affinity for GluK1, DH promotes a desensitized state of the receptor that persists for at least 20 to 45 minutes after removal. This unique activity of DH was used to block GluK1 subunits in GluK1/GluK5 diheteromeric receptors, which revealed that glutamate evokes a desensitizing response from the remaining GluK5 subunits.[20]

In addition to DH, its natural cogener, neodysiherbaine A (Figure 1.4), was isolated in 2001 from the same marine sponge by Sakai and co-workers.[21] It also showed high binding affinity for GluK1 and GluK2 with K_i values 7.7 nM and 33 nM, respectively. These values are higher than those of DH and are consistent with a weaker

potent in seizure induction in mice of neoDH. For the GluK5 subunit, neoDH has a better binding affinity than DH (K_i = 0.6 μM for neoDH and 4.3 μM for DH).[22] The unique structural difference between these two compounds which is the functional group at C8 may contribute to the difference in their binding affinities.

Table 1.2. K_i values of DH and related compounds for the displacement of [^{3}H]kainate from KA subunit receptors

	GluK1 (nM)	**GluK2 (nM)**	**GluK5 (μM)**
DH	0.5 ± 0.1	1.3 ± 0.1	4.3 ± 0.8
NeoDH	7.7 ± 1.3	33 ± 9.0	0.6 ± 0.3
MSVIII-19	128 ± 21	>100,000	>100
8-deoxy-neoDH	1.1	42	36
9-deoxy-neoDH	168	>100,000	>100
8-epi-neoDH	34	32	>100
9-F-8-epi-neoDH	28	>100,000	>100
9-epi-neoDH	292	>100,000	>100
8,9-epi-neoDH	48	>100,000	>100

Several synthetic analogs of neoDH were further prepared for SAR study (Figure 1.5).[23,24] Most of these analogs retained a binding preference for GluK1 over GluK2 and GluK5 (Table 1.2). The C9-hydroxyl group seems to play a crucial role in the binding affinity since the deletion (9-deoxy-neoDH) or epimerization (9-epi-neoDH) of this position causes a profound loss in affinity to GluK1. However, the replacement of C9-hydroxyl group by a fluorine (9-F-8-epi-neoDH) did not strongly impact the affinity of

this analog to GluK1. Compared to the C9 position, the C8-hydroxyl group was less critical (Figure 1.5 and Table 1.2).[23,24] The removal of this position (8-deoxy-neoDH) did not induce severe change in the affinity compared to neoDH while its epimerization (8-epi-neoDH) showed a small decrease in affinity. Furthermore, alteration of both C8 and C9 effectively reduced affinity for all receptor subunits, including GluK1.

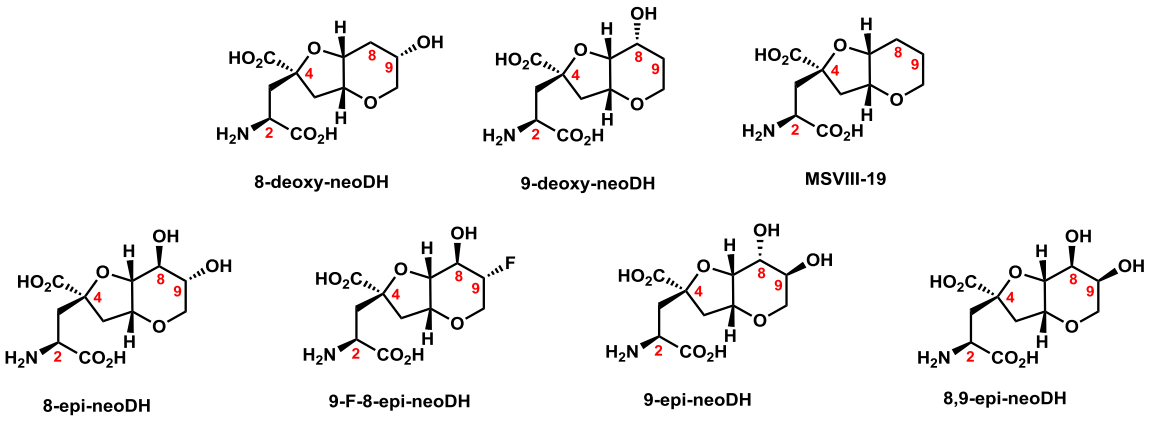

Figure 1.5. Synthetic analogs of neoDH

MSVIII-19 analog,[25] which has no functional groups at the C8 and C9 positions, binds to GluK1 with K_i values 128 nM.[22] Interestingly, MSVIII-19 was originally reported as a GluK1 antagonist, but crystallographic studies revealed that it induces full domain closure of the GluK1 LBD, promoting further functional studies showed that it is an agonist with low efficacy.[26] This information suggests that a small change in structure of DH and neoDH can profoundly impact their pharmacological properties and the C8-C9 region seems to play a significant role in their binding affinity.

1.1.3. Overview of published work in total synthesis of dysiherbaine

The high affinity and selectivity of DH for certain KA receptors makes this natural product a unique ligand to explore the complexity of iGluRs. There have been several reports of its total and formal synthesis described in the literature.[27] In all these reports, the general approach consists of the construction of four contiguous C6-C9 stereocenters on the pyran ring, followed by the cyclization to generate the tetrahydrofuran ring with stereocontrol of the C4 quaternary center, and finally the installation of the amino acid chain.

The first total synthesis of (–)-DH was accomplished by Snider and coworkers in 2000.[28] The main approach is using the intramolecular S_N2 substitutions of a carbamate anion on an epoxide and an alkoxide on a secondary mesylate to efficiently construct the bicyclic system. An allyl group was installed to introduce the glutamic acid side chain (Scheme 1.1).

Scheme 1.1. Key steps in first total synthesis of DH by Snider and coworkers[28]

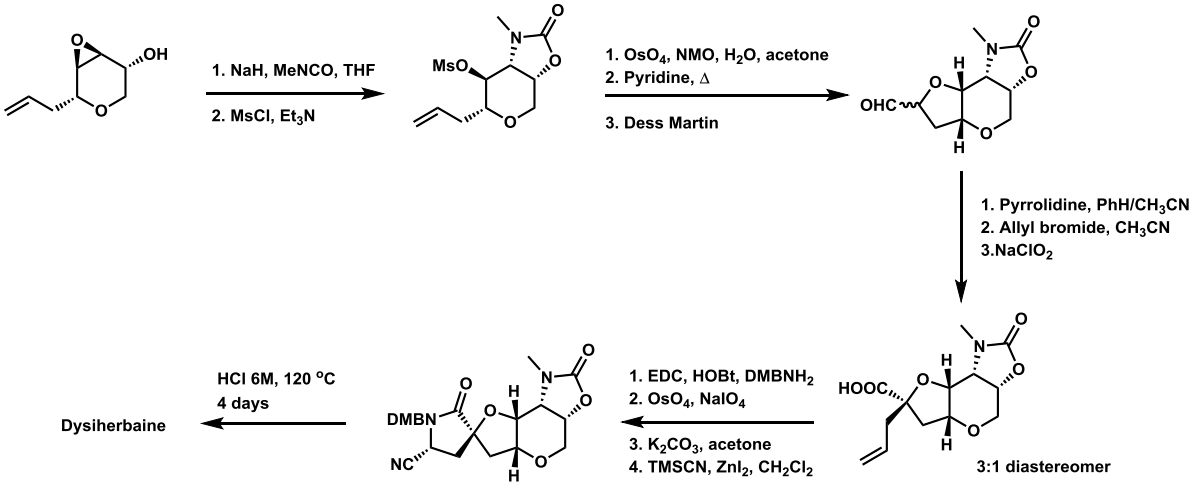

In the same year, Masaki and coworkers reported the second total synthesis of (–)-DH.[29] The functional groups at C8 and C9 were installed in early in the synthesis. A Pd-mediated Negishi-type coupling was successfully used to connect the alanine moiety to enol triflate. Cyclization to form furan ring was then carried out to accomplish DH in 21 steps (Scheme 1.2).

Scheme 1.2. Key steps in synthesis of DH by Masaki and coworkers[29]

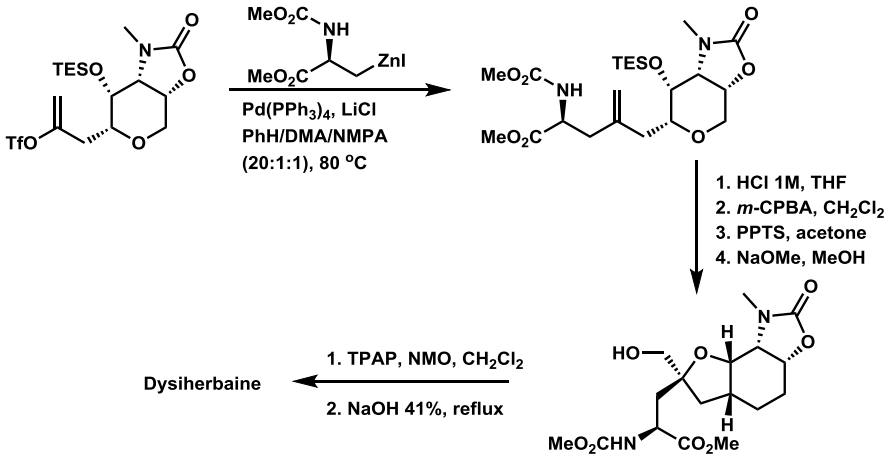

Scheme 1.3. Key steps in synthesis of DH by Phillips and coworkers[30]

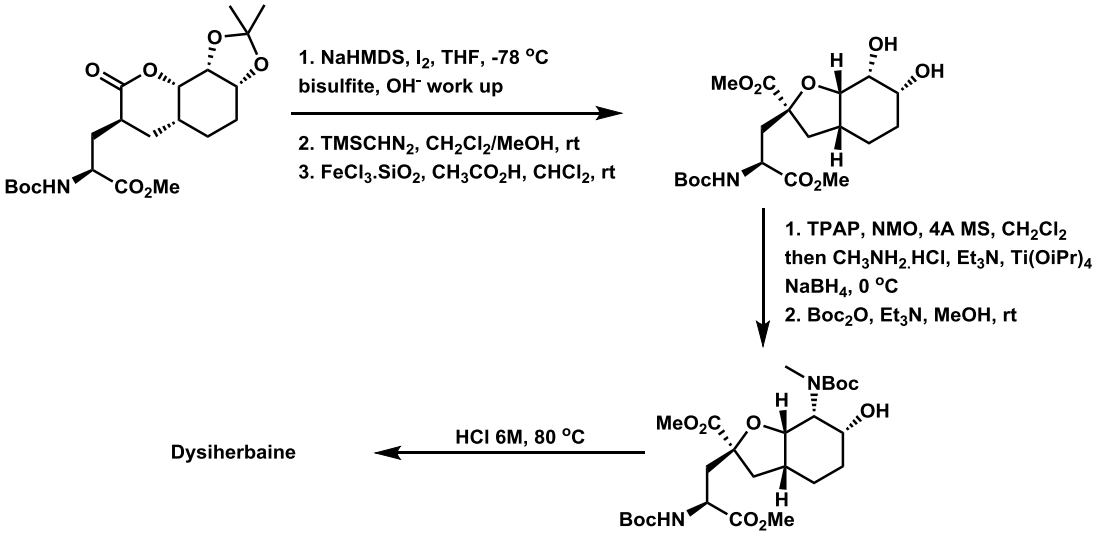

In 2002, Phillips and coworkers reported the next total synthesis of DH by using the Fleet ring contraction as a key step to generate the furan ring from the six-member ring lactone. The C8-methylamino group was introduced by one pot oxidation/reductive amination, leading to the accomplishment of the synthesis (Scheme 1.3).[30]

In 2008, Sasaki and coworkers reported the synthesis of DH based on their previous work on neoDH.[31] Their approach includes a Sharpless asymmetric dihydroxylation and the asymmetric hydrogenation to ensure the stereochemistry at C4 and C2, respectively. Horner-Wadsworth-Emmons olefination was used to construct the amino acid side chain. Different from previous approaches, the cyclization of the furan ring was carried out before the installation of amino acid side chain (Scheme 1.4).

Scheme 1.4. Key steps in synthesis of DH by Sasaki and coworkers[31]

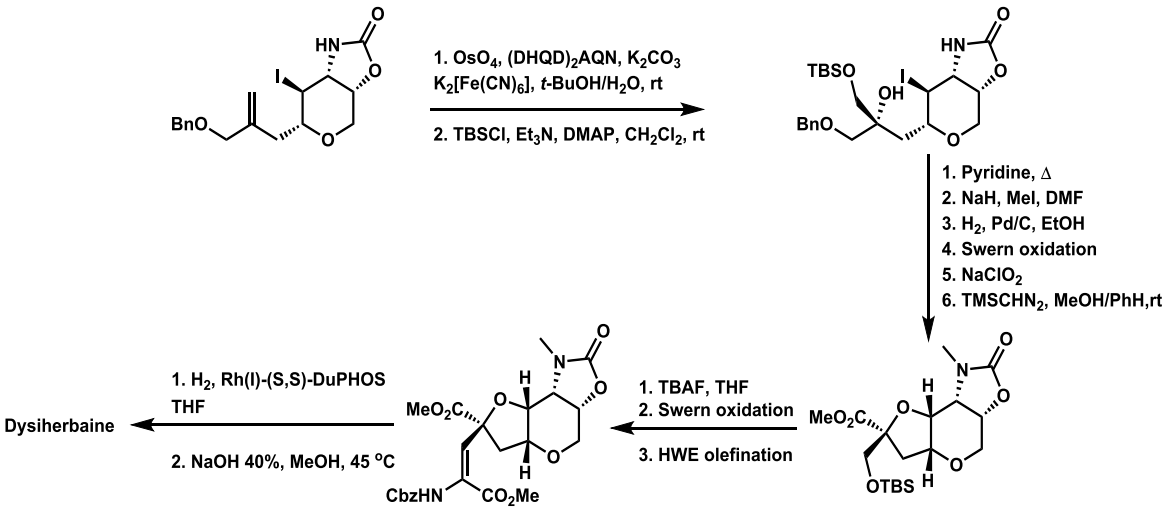

In 2012, Kang and coworkers reported the synthesis of DH with a different approach. The C4 stereocenter was constructed first, followed by the elaboration of the

bicyclic furopyran ring. The furan ring was formed by using oxone, followed by $CDCl_3$, furnished the desired *cis*-fused pyranofuran as the sole product (Scheme 1.5).[32]

Scheme 1.5. Key steps in synthesis of DH by Kang and coworkers[32]

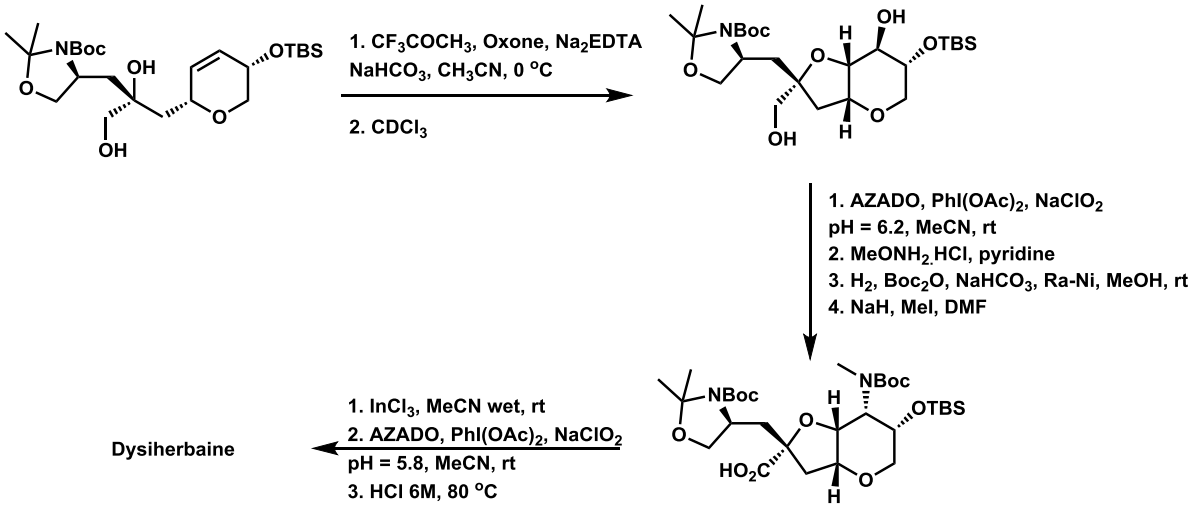

1.1.4. Previous work in our group and the scope of this research

Numerous approaches have been developed to access dysiherbaine. In most cases, the functional groups at C8-C9 were incorporated in the early stages of the synthesis, which limits the ability to modify these important pharmacological positions. The ultimate goal of this project is the synthesis of dysiherbaine and its derivatives by an efficient route in which the functional groups at C8-C9 will be installed in the late stage of the synthesis. We proposed intermediate **1.1** with carbon-carbon double bond between C8 and C9 (Figure 1.6) as a key intermediate in our approach. The double bond will be functionalized by using reactions including hydroxylation, hydrogenation, halogenation, alkylation, and amination. This approach helps maximize access to potentially important analogs of dysiherbaine while also providing a route to the parent compound.

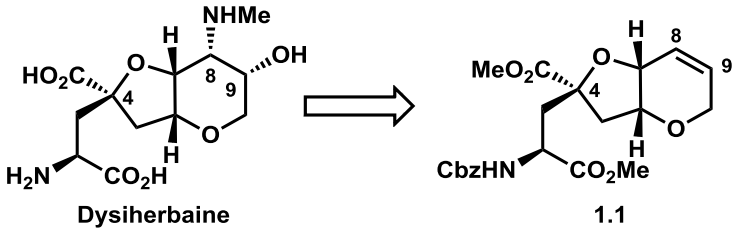

Figure 1.6. Structures of dysiherbaine and a key intermediate **1.1**

In our retrosynthetic analysis, the key intermediate **1.1** will be constructed from intermediate **1.2** by installation of amino acid side chain to the C4 position. To generate this C4 quaternary center, enolate chemistry will be elaborated and the desired stereochemistry will be controlled by the concave-shaped of **1.2**. Intermediate **1.2** will be generated by the ring closing metathesis of intermediate **1.3** which will be further constructed by the ring-opening of the epoxide **1.4** followed by allylation. Intermediate **1.4** will be fabricated by the directed-epoxidation of **1.5** which will be further constructed from *(S)*-Methyl glycidate (Scheme 1.6).

Scheme 1.6. Retrosynthetic route of key intermediate **1.1**

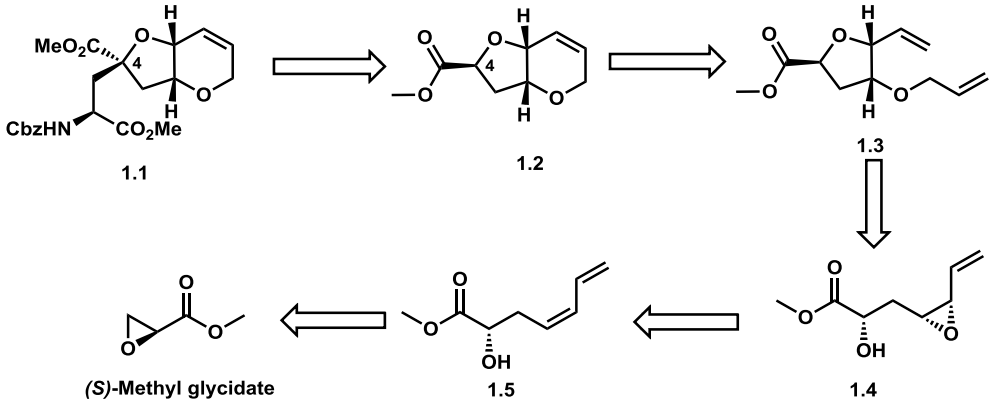

Previous work in our lab successfully established 8 synthetic steps to an early intermediate **1.2** (Scheme 1.7). The synthesis starts with *(S)*-methyl glycidate which is

commercially available or can be synthesized in gram scale by using Jacobsen hydrolytic kinetic resolution.[33]

Scheme 1.7. Eight synthetic steps to intermediate **1.2**

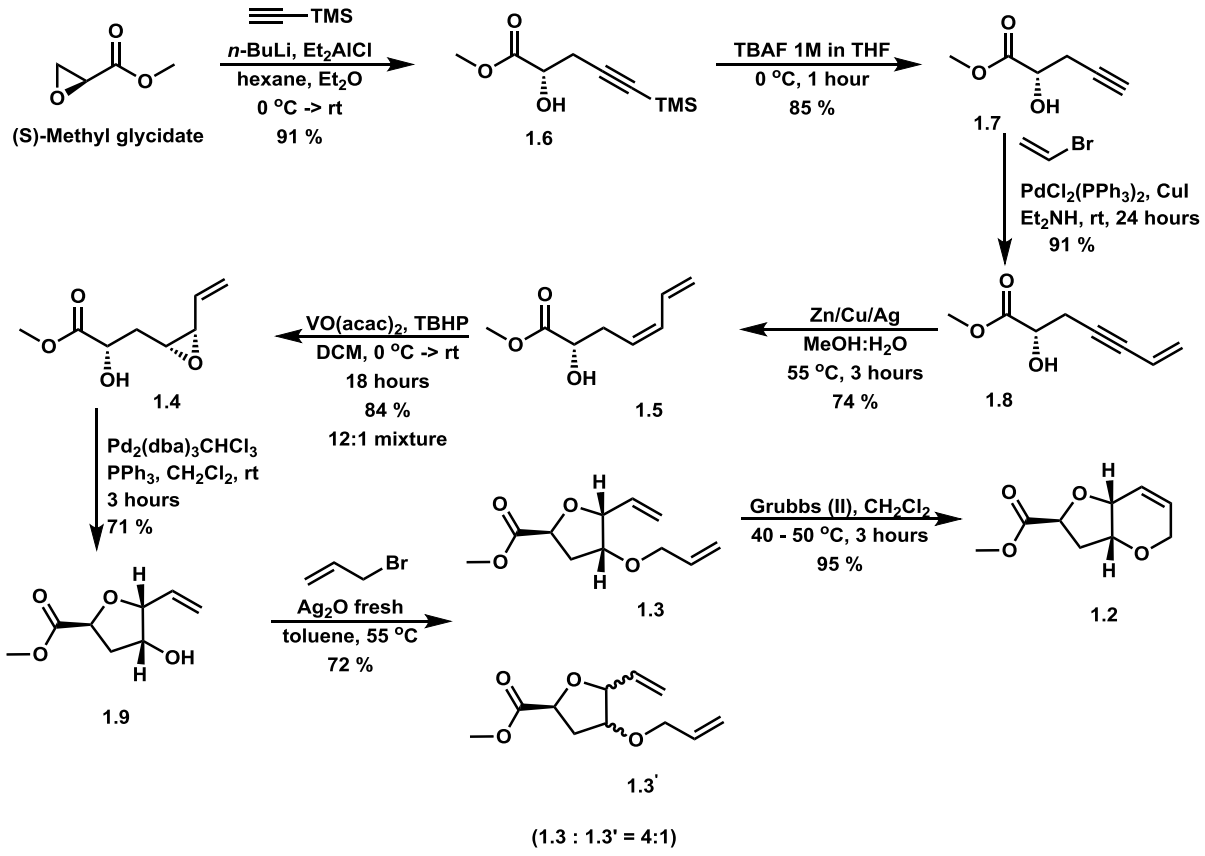

Trimethylsilylacetylene was used to open the epoxide, generating alcohol **1.6**. The removal of trimethylsilyl group by TBAF generated alkyne **1.7** which was further reacted with vinyl bromide under Sonogashira coupling conditions to give enyne **1.8**. Amalgam of Zn:Cu:Ag in mixture of MeOH and water was used to selectively reduce enyne **1.8**,[34] providing diene **1.5** with desired Z-configuration. Directed epoxidation of **1.5** was then performed by using $VO(acac)_2$ and TBHP to give epoxide **1.4**. Selective opening of

epoxide **1.4** by Pd-catalyst[35] generated desired furan ring which was further reacted with allyl bromide, generating a separable mixture of allylation products **1.3** and **1.3'** with 4:1 ratio. Intramolecular metathesis was then carried out to provide the intermediate **1.2**.

Following these studies, this dissertation will focus on examining intermediate **1.2** by working out the chemistry on the double bond of this molecule necessary to complete the natural product. The developed chemistry will be further applied to access dysiherbaine and its derivatives. The remaining challenges including the installation of aminohydroxyl group at C8-C9 and the construction of quaternary center at C4 with desired stereochemistry will be extensively studied in order to achieve dysiherbaine.

1.2. RESULTS AND DISCUSSION

1.2.1. Functionalization of C8-C9 double bond

Woodward-Prevost reaction

Dysiherbaine has a methyl amine group at C8 and hydroxyl group at C9 while neodysiherbaine has dihydroxyl groups at C8 and C9. The Sharpless asymmetric aminohydroxylation and dihydroxylation would be the shortest approach to these functional groups. However, the steric environment of intermediate **1.2** would provide the wrong diastereomer of the product with the groups being added to the double bond from the same face of the bicyclic system as the hydrogens at the ring juncture. Moreover, in the case of aminohydroxylation, the regiochemistry of the reaction needs to be controlled to prevent formation of the wrong regioisomer. The Woodward-Prevost reaction could potentially overcome these issues. Addition of iodine to the double bond will be favored from the convex face of the structure. *Trans* opening of the iodonium ion from the

concave face will give the iodoacetate complex **1.10**, which can potentially be transformed to aminohydroxyl **1.11** or dihydroxyl product **1.12** with desired stereochemistry (Scheme 1.8).[36,37]

Scheme 1.8. Woodward-Prevost reaction approach

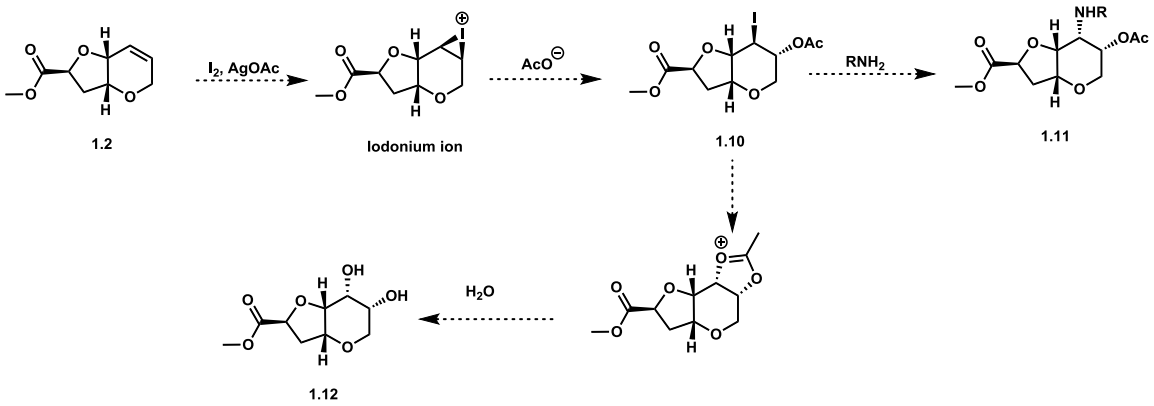

Treatment of intermediate **1.2** with I_2/AgOAc in acetic acid and water did not give the desired dihydroxyl product **1.12**. Instead, the iodoacetate **1.10** was formed as single stable product. This product did not undergo S_N2 reaction to provide the necessary second hydroxyl group. Attempted oxidation of the iodide in **1.10** to hypervalent iodide with *m*-CPBA to make it be a better leaving group did not lead to formation of the desired product.[38,39] CsOAc and AgOAc were also used but did not displace the iodide group (Scheme 1.9).

We further attempted to replace the iodide group on **1.10** by different nucleophiles to access the desired aminohydroxyl group at C8-C9. The first strategy was replacement of the iodide by an azide group. Reduction of the azide would provide the amine. A variety of azide sources (NaN_3, $TMSN_3$, LiN_3, $TMGN_3$) and different reaction conditions were attempted but none of them provided the desired product. A primary

amine were also attempted but could not substitute the iodide group (Scheme 1.9 and Table 1.3).

Scheme 1.9. Approach to dihydroxyl and aminohydroxyl group at C8-C9

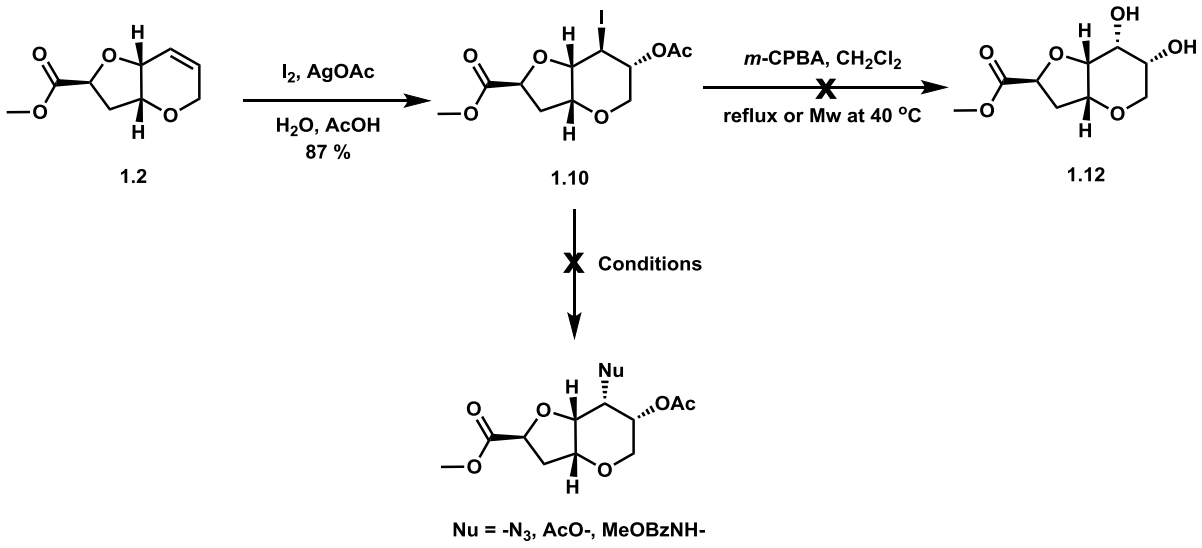

1.2 1.10 1.12

Table 1.3. Attempts on nucleophilic substitution of iodoacetate compound

Entry	Nucleophiles	Reaction conditions	Result
1	NaN_3	DMF, 75 – 120 °C	No reaction
2	NaN_3	15-crown-5, DMF, 60 °C	No reaction
3	NaN_3	Ag_2O, DMF, 70 °C	No reaction
4	NaN_3	$Bu_4N^+Br^-$, DMF, 80 °C	No reaction
5	$TMSN_3$	$SnCl_4$, CH_2Cl_2, 0 °C -> reflux	No reaction
6	LiN_3	CH_3CN : H_2O (1:1), 70 °C	No reaction
7	$TMGN_3$	DMF, rt	No reaction
8	CsOAc	DMF, 90 °C	No reaction
9	$MeOBzNH_2$	K_2CO_3, CH_3CN, reflux	No reaction

Dihydroxylation

Intermediate **1.2** was treated with OsO_4 and NMO to form a dihydroxylated product **1.13** in 70% yield. Due to its concave shape, hydroxyl groups were predicted to end up on the double bond at the top face. The stereochemical outcome was inverted compared to natural product neoDH. To obtain the amino and hydroxyl groups at C8-C9 with desired stereochemistry in DH, the hydroxyl group at C9 of **1.13** was selectively protected with pivaloyl chloride and Mitsunobu reaction was tried in order to convert the second hydroxyl group to an azide. Different conditions were attempted but desired product **1.16** was not generated.[40] The second hydroxyl group at C8 was converted to a mesylate (**1.15**). Reaction with NaN_3 did not provide the desired azide. Back-side substitution at C8 position has been proven to be difficult due to its steric environment and the likely conformation of the six-member ring which places the leaving group in an equatorial orientation.

Scheme 1.10. Formation of dihydroxyl product and its further modification

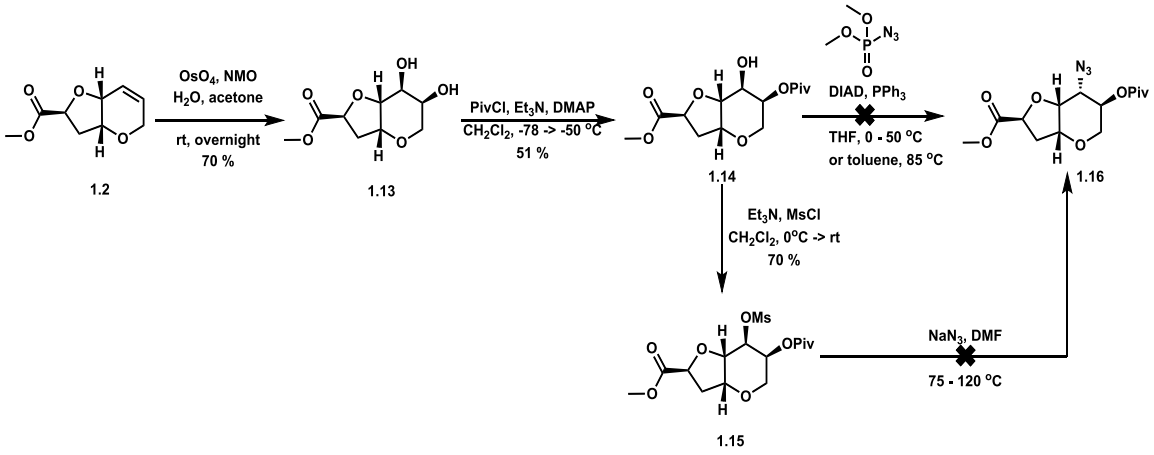

Other reactions

The reduction of **1.2** with H_2 and Pd/C gave **1.17** in high yield. Direct aziridination on the double bond was also performed. However, the protected aziridine **1.18** was formed in low yield (7%) and the mixture of isomers could not be separated. Various conditions were used to perform an epoxidation on **1.2**. Surprisingly, none of them generated the epoxide product. The Sharpless asymmetric dihydroxylation and hydroboration also did not provide the expected products (Scheme 1.11).

Scheme 1.11. Functionalization on double bond of intermediate **1.2**

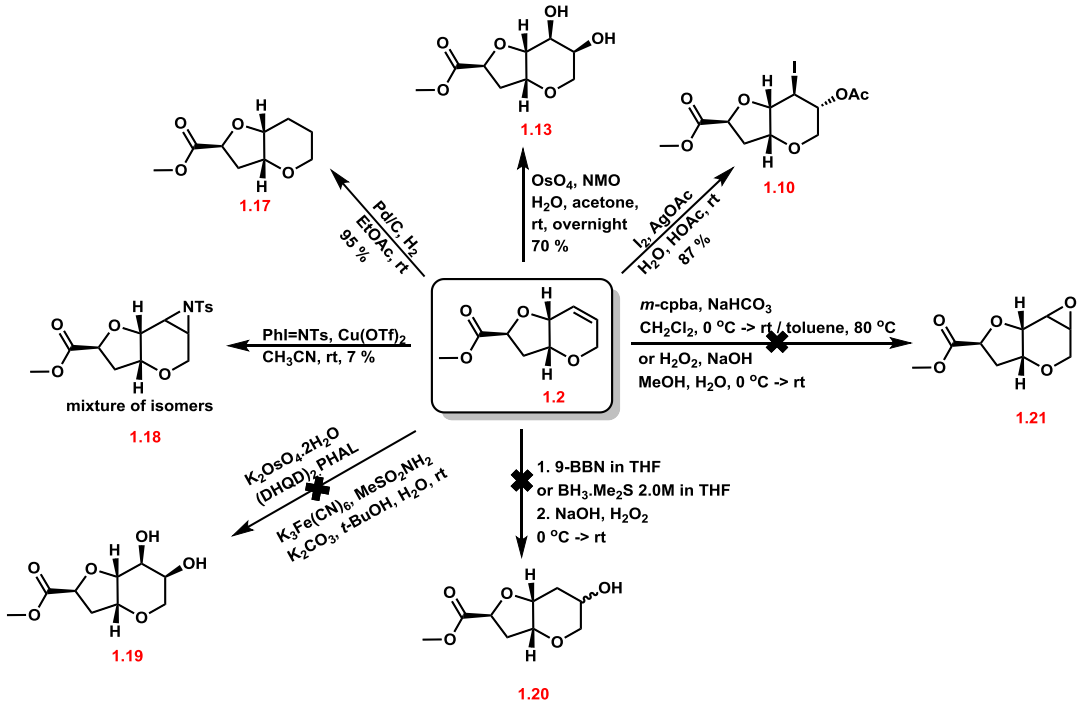

1.2.2. Structure determination by single-crystal X-ray diffraction

To confirm the stereochemistry of bicyclic system as well as the functional groups introduced at the double bond of **1.2**, single crystal of derivative **1.13a**, generated by the

monomesylation of diol **1.13** was obtained and analyzed by X-ray crystallography (Scheme 1.12 and Figure 1.7).

Scheme 1.12. Formation of monomesylated derivative **1.13a**

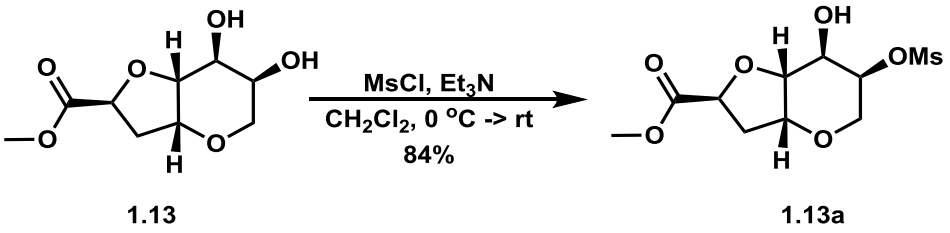

1.13 1.13a

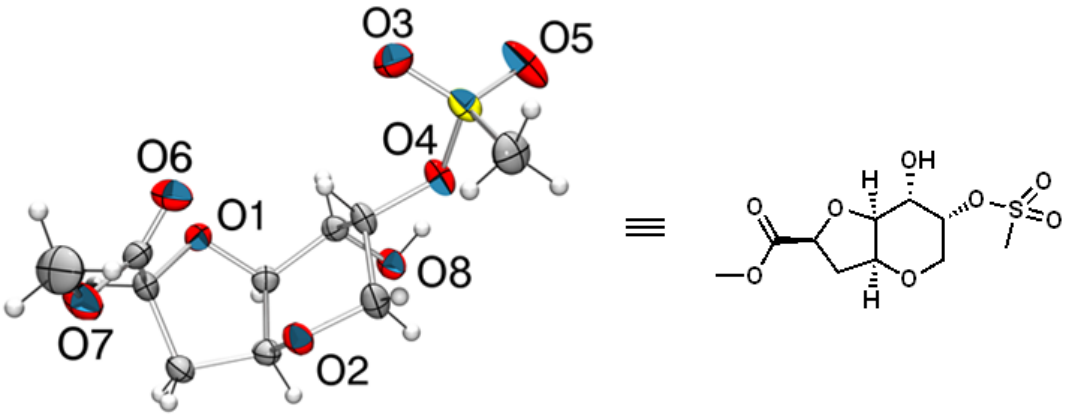

Figure 1.7. X-ray structure of monomesylated derivative **1.13a**

Crystal structure of **1.13a** revealed an inverted stereochemistry on the bicyclic system compared to the predicted structure based on chemistry and previous work. This could be explained by either the chemistry or the fact that single crystal X-ray crystallography technique could not give an unambiguous absolute configuration of system that has only one chiral center with small atoms. To confirm the absolute configuration, molecules with more than one chiral center, in which one of the chiral centers is already known, were prepared. The chiral sulfonyl chloride, (1S)-(+)-camphor-10-sulfonyl chloride was

used to make a derivative **1.22** from diol **1.13** (Scheme 1.13). Unfortunately, the single crystals of this derivative were not formed.

Scheme 1.13. Formation of derivative **1.22** to identify absolute stereochemistry

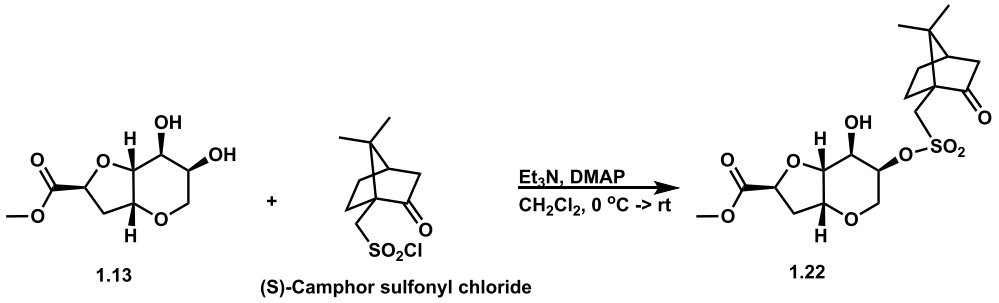

The stereochemistry of bicyclic system was further confirmed when a single crystal of derivative **1.25** with a heavy atom, bromine, was obtained. **1.25** was generated by the alkylation at C4 position.

Scheme 1.14. Formation of derivatives **1.25** and **1.25'** by alkylation at C4 position

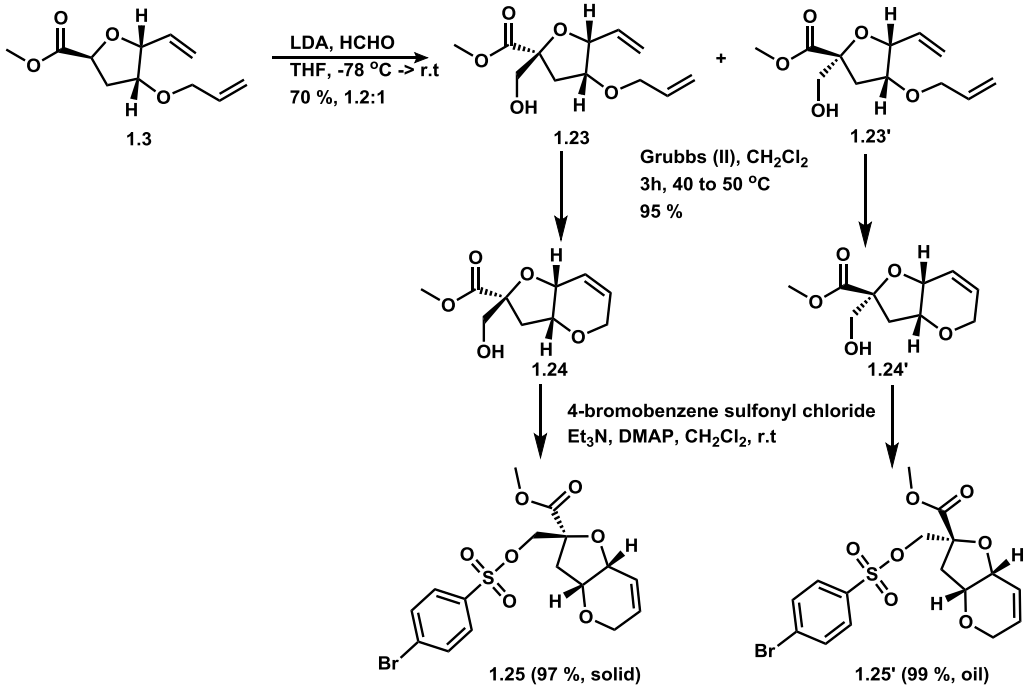

The alkylation was more efficient when it was performed before the metathesis ring closure step. Hence, the diene **1.3** was allowed to react with formaldehyde, giving a separable mixture of alkylation products **1.23** (less polar) and **1.23'** (more polar) in a 2:1 ratio. The mixture was separately carried through a sequence of metathesis and reaction with 4-bromobenzene sulfonyl chloride to generate derivatives **1.25** and **1.25'** in which a single crystal of the less polar alkylation product **1.25** was obtained and analyzed (Scheme 1.14).

Crystal structure of derivative **1.25** also revealed the opposite stereochemistry of bicyclic system compared to the desired dysiherbaine skeleton (Figure 1.8).

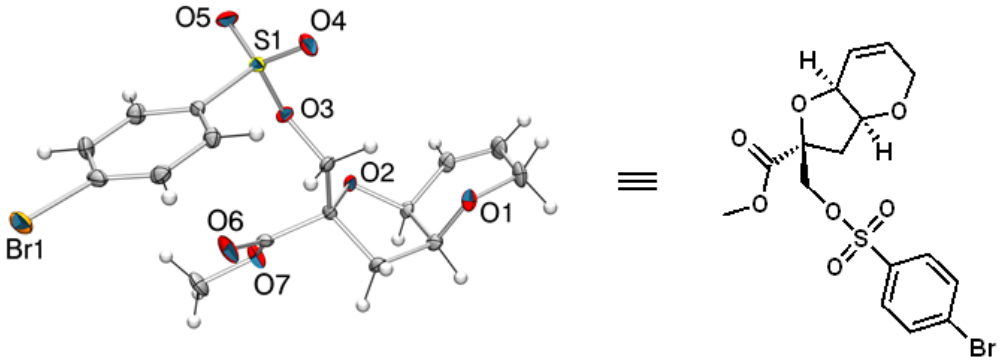

Figure 1.8. X-ray structure of derivative **1.25**

X-ray analysis of both derivatives **1.21** and **1.25** confirmed that the stereochemistry on bicyclic rings was the opposite of the desired product. Directed epoxidation by $VO(acac)_2$ and Pd-catalyzed ring opening of the epoxide to form the furan are the two steps where the stereochemistry can be lost (Scheme 1.15). The Pd-catalyzed cyclization of hydroxy epoxide is reported to occur through inversion,[35] resulting in a *cis*-fused bicyclic system which was observed in crystal structure of **1.21** and **1.25**.

Furthermore, this step will not effect on the stereochemistry of hydroxyl group in **1.9** or **1.9'** product, suggesting that the outcome stereochemistry of bicyclic ring depends mainly on the stereochemistry of the epoxide. Two possible products could be formed by the directed epoxidation of **1.5.** One is **1.4** that has the epoxide on the same side with the hydroxyl group and was predicted to be the major product. Further Pd-catalyzed reaction of **1.4** will provide product **1.9** with the desired stereochemistry on the bicyclic ring. However, the observed stereochemistry on the bicyclic rings by X-ray analysis matched product **1.9'**, suggesting that **1.4'** could possibly be the major product in epoxidation step.

Scheme 1.15. Possible steps involving in the inversion of stereochemistry

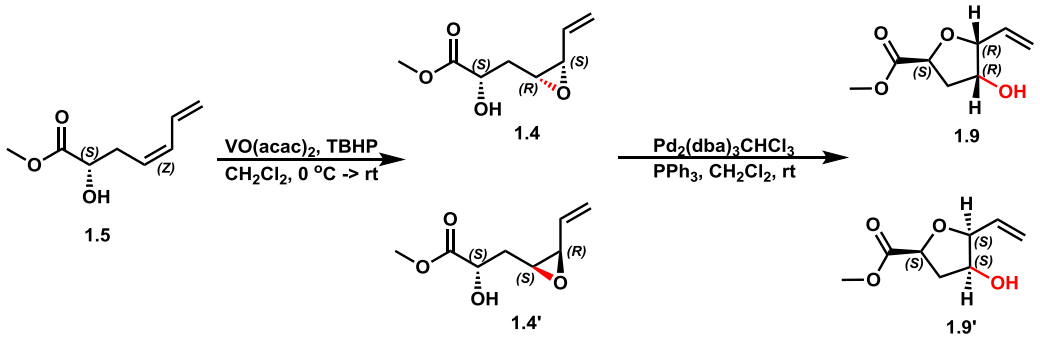

Scheme 1.16. Derivatives of epoxide **1.4** to clarify the stereochemistry

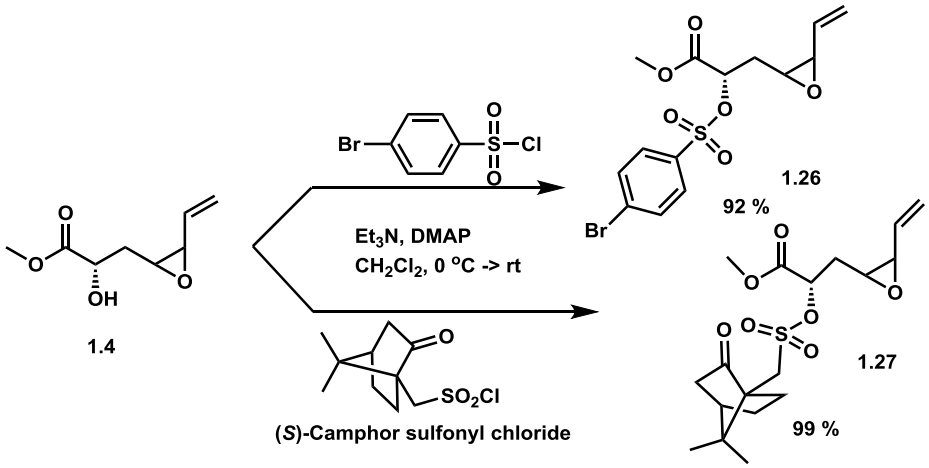

To clarify the stereochemistry in the directed epoxidation step, epoxide **1.4** was derivatized with 4-bromobenzene sulfonyl chloride and *(S)*-camphor sulfonyl chloride to generate derivatives **1.26** and **1.27**, respectively. Unfortunately, the mixture of diastereomers in both derivatives were not separable, preventing further studies to identify the stereochemistry of the epoxide.

Since we were not able to elucidate the stereochemistry of the directed epoxidation, based on X-ray analysis, we predicted using the other enantiomer of starting material for the total synthesis would provide the desired stereochemistry. Therefore, *(R)*-methyl glycidate was taken and carried through the same synthetic route as for the *(S)* enantiomer (Scheme 1.7 and 1.14). The less polar alkylation product at C4 was also derivatized with 4-bromobenzene sulfonyl chloride for X-ray crystallography study (Scheme 1.14). The single crystal of derivative **1.28** revealed that starting the synthesis with *(R)*-methyl glycidate provided the correct stereochemistry on a bicyclic system corresponding to the dysiherbaine skeleton. This could be due to the fact that the major product in the epoxidation step has the epoxide on the opposite side from the hydroxyl. We suspected that the methyl ester group in **1.4** may direct the epoxidation, rather than the hydroxyl group.

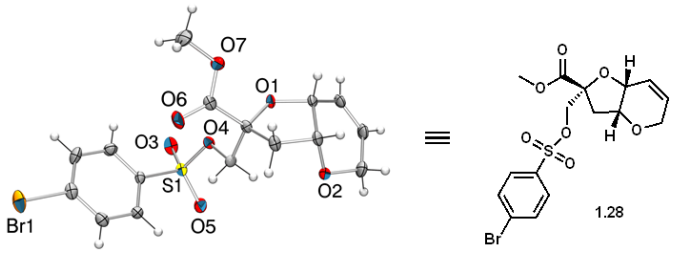

Figure 1.9. Crystal structure of derivative **1.28** generated from *(R)*-methyl glycidate

1.2.3. Installation of quaternary center at C4

To establish key intermediate **1.1**, the installation of amino acid side chain at C4 of intermediate **1.2** is necessary. Enolate type chemistry was explored as a method to achieve this step. It was expected that the steric environment of **1.2** would control the reaction to form the product with the desired stereochemistry, addition from the convex face. The deprotonation of acidic proton at C4 forms an anion that can potentially be used to react with the appropriate electrophiles to form the alkylation product. Previous work from our lab has found that the deprotonation step was more efficient when carried before the metathesis. Therefore, the diene **1.3** was deprotonated using LDA (Scheme 1.17).

Scheme 1.17. Installation of amino acid side chain at C4

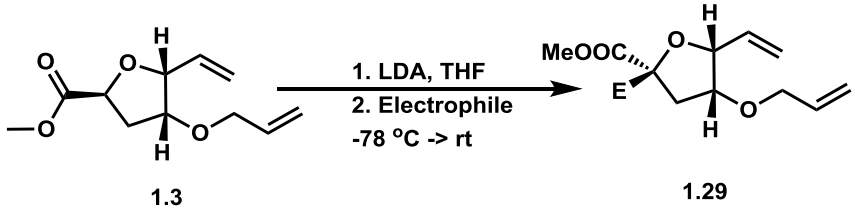

1.3 **1.29**

Various electrophiles (**1.30**-**1.34**, Figure 1.10) were used to react with the generated enolate, however, none of them provided the desired product. Reaction with **1.30** resulted in the elimination on the amino acid. Compounds **1.31** and **1.32** were then subjected to the reaction but in both cases there is no desired product formed. Another electrophile (**1.33**, known as Garner aldehyde) has been used by others with this system.[25] The desired product was detected by LC-MS but in low yield and in the presence of many by-products that were difficult to remove. Protected aziridine **1.34** in the presence of $TiCl_4$ was reacted with anion of **1.3**, with the hope that the release of ring strain of the

aziridine would accelerate its reaction with the anion. However, this reaction resulted in a decomposition and a mixture of products.

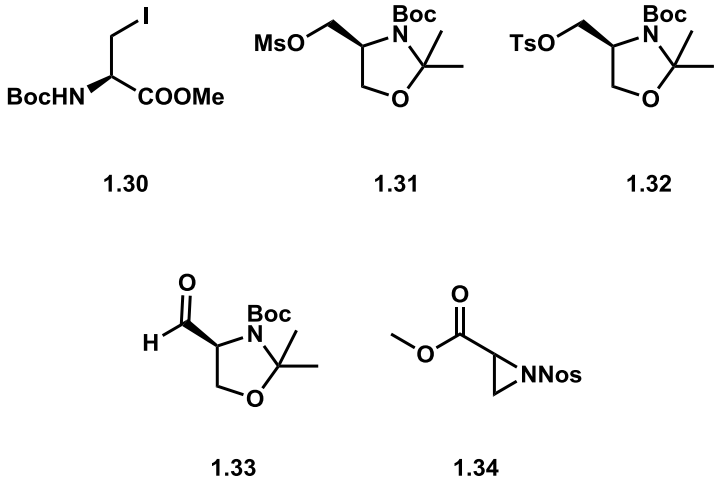

1.30 **1.31** **1.32**

1.33 **1.34**

Figure 1.10. Electrophiles used to examine in enolate chemistry

An alternative approach to install the amino acid side chain is by addition of formaldehyde followed by oxidation, Horner–Wadsworth–Emmon olefination and then asymmetric hydrogenation.[31] Formaldehyde was used as an electrophile to generate a mixture of diastereomeric alcohols that were easily separated by column chromatography. The major product **1.23** with the desired stereochemistry was subjected to ring-closing metathesis in high yield. The generated product **1.24** was oxidized and then converted to the amino acid side chain by Horner–Wadsworth–Emmon olefination (Scheme 1.18). Both Boc- and Cbz- protected products were prepared in good yield.

Scheme 1.18. Formation of the olefin intermediate

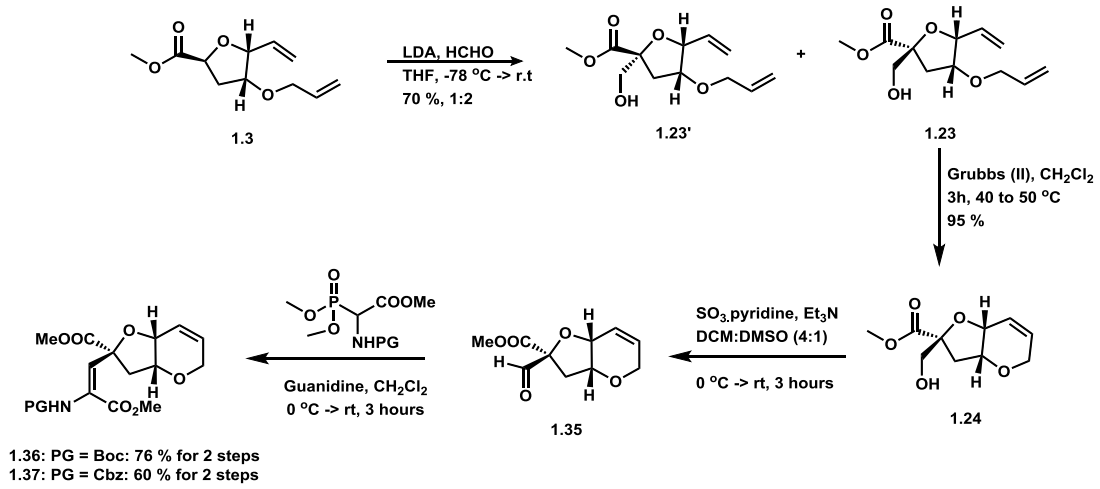

Asymmetric hydrogenation of unsaturated amino acid intermediates (**1.36** and **1.37**) were then used to form our key intermediate **1.1**. Following the optimized conditions reported in literature (Rh-DuPhos in THF, H_2 150 psi, 88 hours, RT) gave none of the desired product when the Boc- protected substrate (**1.36**) was utilized while the Cbz- compound **1.37** resulted in undesired product **1.38** from reduction of C8-C9 double bond, which we originally planned to functionalize to generate the desired analogs (Scheme 1.19). Changing the solvent from THF to methanol still resulted in the formation of **1.38**, however with slower reaction rate. Consequently, further study is required to control the selectivity of the hydrogenation reaction to achieve the key intermediate **1.1**.

Scheme 1.19. Asymmetric hydrogenation

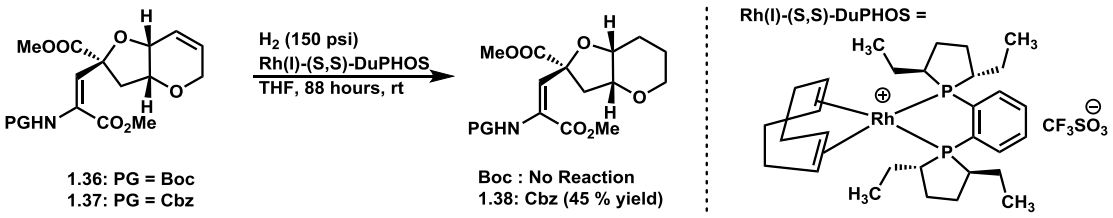

1.2.4. Addition of amino and hydroxyl groups at C8-C9

One of the remaining challenges in the synthesis of dysiherbaine is addition of the amino and hydroxyl groups at C8 and C9 with correct stereochemistry. Efforts to replace the iodide group in iodoacetate **1.10** by different nuclephiles (azide, amine, acetate) using various conditions were unsuccessful (Scheme 1.9). Mitsunobu reaction with different nucleophiles on dihydroxyl compound **1.13** to invert the stereochemistry was also fruitless (Scheme 1.10). The back-side attack at C8 position has proven to be difficult due to its steric and stereochemical issues.

Scheme 1.20. Approach to amino and hydroxyl groups at C8-C9

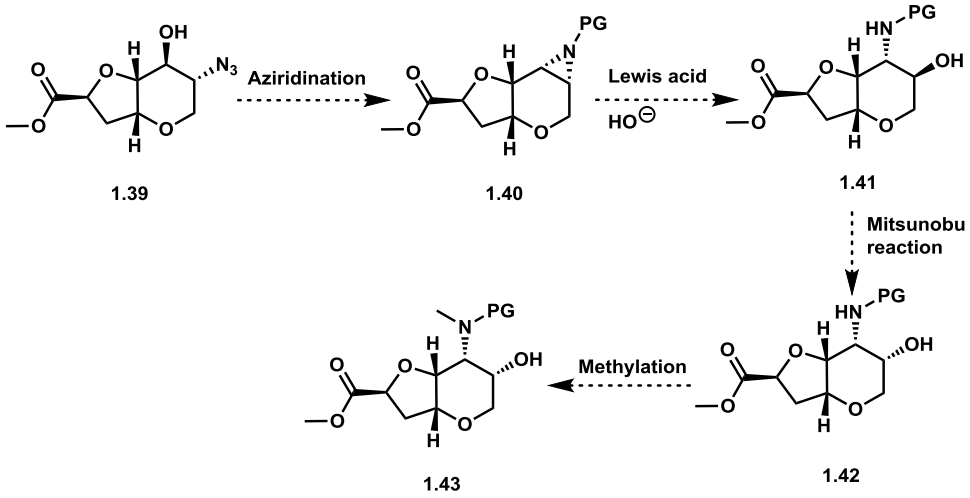

We envisaged that the use of an aziridine could overcome this problems. The strain of aziridine ring may facilitate opening by nucleophiles.[41-43] Such opening would provide the amine group at C8 in the α-position. The planned approach was to use azidoalcohol **1.39** to synthesize aziridine **1.40**. The attack of hydroxide nucleophile, would likely happen at C9 opening the aziridine ring to form **1.41**. A Mitsunobu reaction

would then be used to invert the stereochemistry of the hydroxyl group followed by the methylation of the protected amine group of **1.42** to provide the desired functionality at C8-C9 in DH with the correct stereochemistry (Scheme 1.20).

Scheme 1.21. Approach to azido alcohol

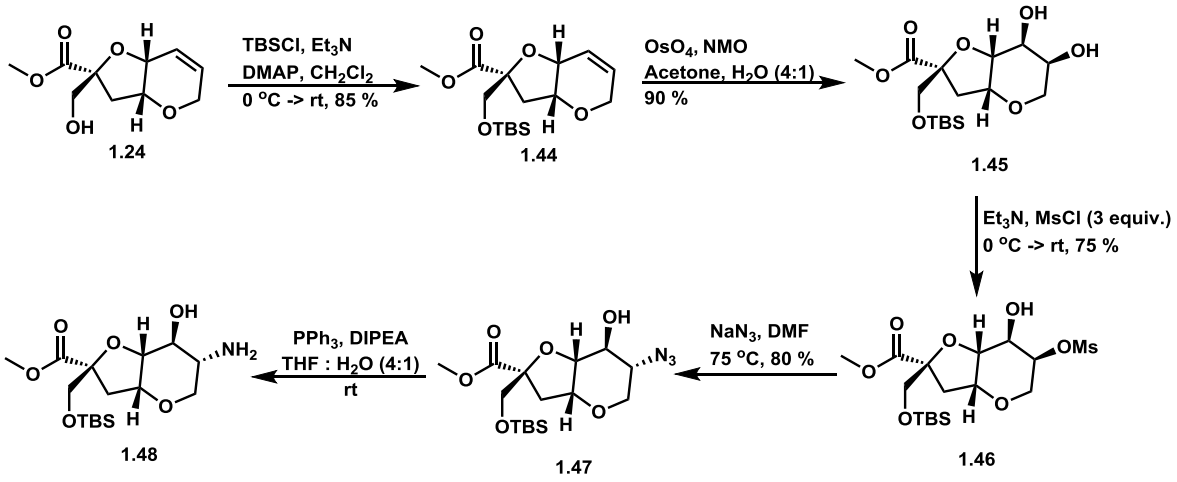

To access to DH, **1.24** was first protected by TBSCl. Dihydroxylation was then performed followed by mesylation and substitution to provide the azidoalcohol **1.47**. Treatment of **1.47** with PPh_3 and DIPEA did not provide the expected aziridine, instead, amino alcohol **1.48** with incorrect regiochemistry was generated. This could be possibly due to the strain of the bicyclic ring system. Activation of both hydroxyl groups by extra equivalents of MsCl was then attempted with the hope that the involvement of better leaving group would facilitate the generation of aziridine. Azidomesylate **1.50** was obtained in two steps from the diol **1.45** in high yield. Treatment of **1.50** with PPh_3 and DIPEA successfully provided aziridine **1.51**, which was protected with Boc_2O to facilitate the purification (Scheme 1.22).

Scheme 1.22. Approach to aziridine

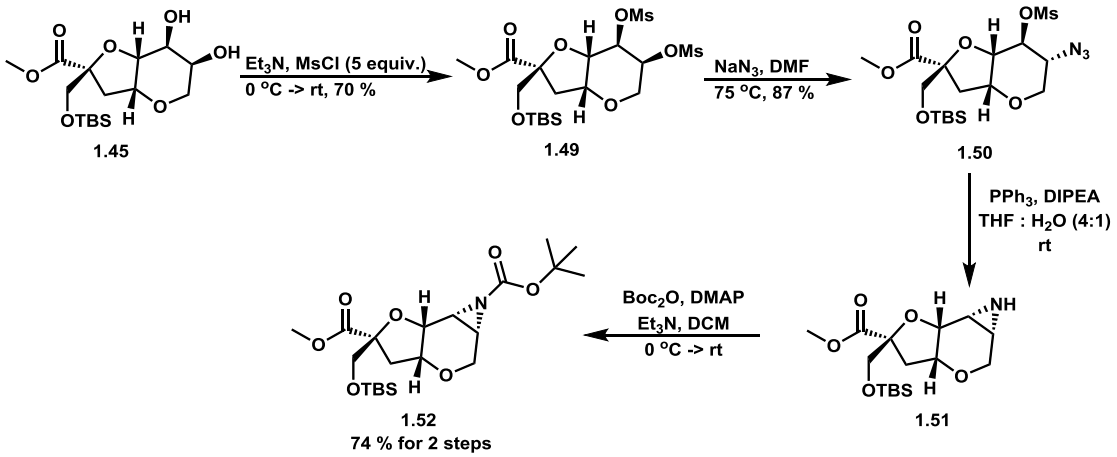

Scheme 1.23. Approach to aminohydroxyl group from aziridine

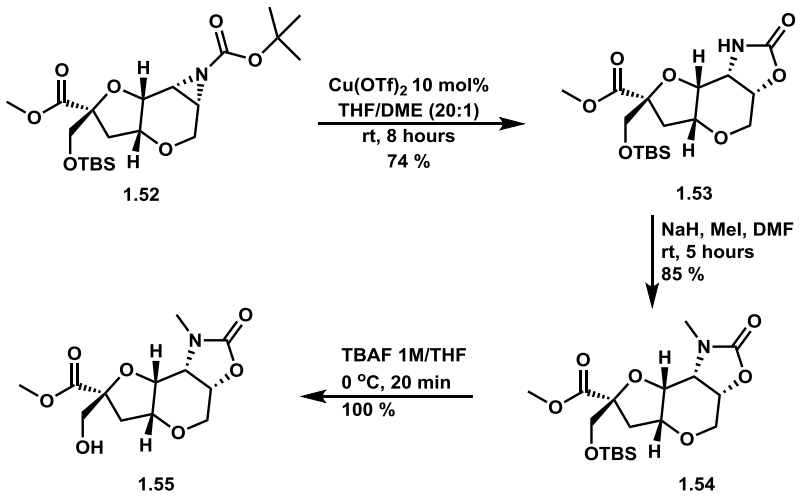

Our original strategy was to use an external nucleophile to open the aziridine ring (Scheme 1.20). However, we found that the ring opening and rearrangement of the Boc-protected aziridine catalyzed by Lewis acid was a more efficient method to install the oxygen.[44] Treatment of **1.52** with $Cu(OTf)_2$ in THF:DME (20:1) generated oxazolidinone with the desired regio- and stereo-chemistry confirmed by COSY an NOESY NMR spectroscopy. Methylation of oxazolidinone **1.53** with MeI/NaH successfully generated

1.54 from which TBS deprotection gave compound **1.55** to which we would then install the amino acid group. (Scheme 1.23).

1.2.5. Asymmetric hydrogenation and the completion of the total synthesis

The installation of amino acid side chain at C4 of compound **1.55** was the last key step to finish the synthesis of dysiherbaine. This was accomplished by oxidation followed by Horner–Wadsworth–Emmon olefination followed by asymmetric hydrogenation (Scheme 1.24). To access the substrate for asymmetric hydrogenation, the primary alcohol (**1.55**) was converted to an aldehyde by reaction with SO_3·pyridine in a mixture of CH_2Cl_2:DMSO (4:1). Olefination of that product (**1.56**) with *Z*-α-phosphonoglycine trimethyl ester (**1.57**) yielded unsaturated amino acid **1.58**, in 87% yield over two steps.[45]

Scheme 1.24. Approach to natural product target dysiherbaine

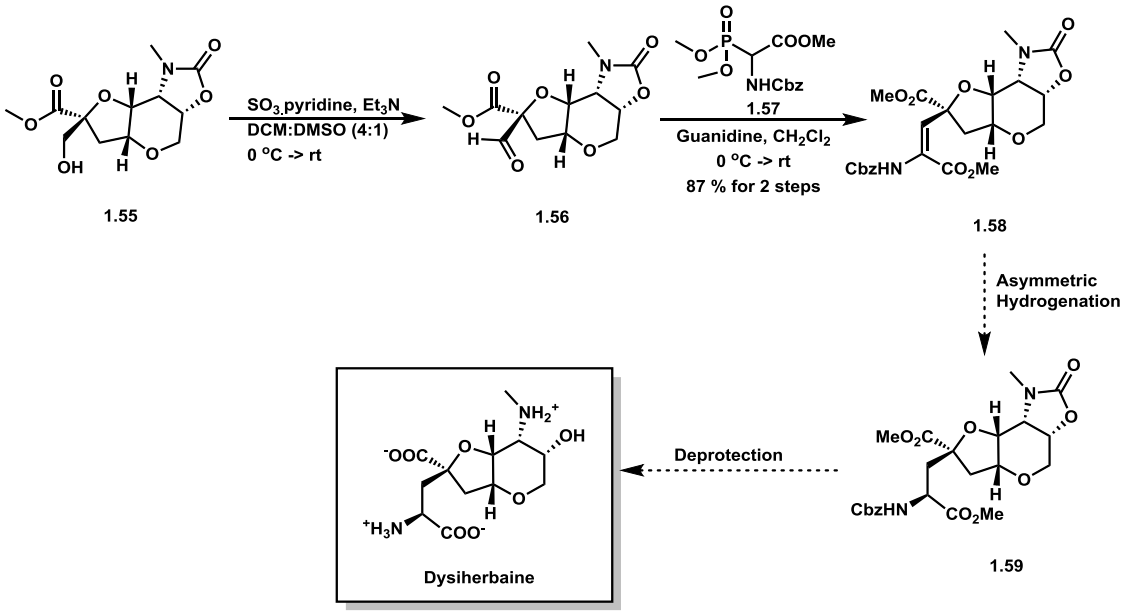

The asymmetric hydrogenation was conducted using optimal condition (Ru-DuPhos (5 mol%), H_2 (150 psi), THF) reported by Sasaki and coworkers in a previous synthesis of

DH.[31] However, a desired product was not detected (Table 1.4). Various conditions including increasing catalyst loading, H_2 pressure and changing solvent to methanol did not lead to the starting material being consumed (Table 1.4, entry 1-4).[41,45] When the reaction was run with 20 mol% of catalyst and 200 psi of H_2 in 5 days, mixture of enantiomeric hydrogenation products (**1.60** and **1.60'**) and their Cbz-deprotected adducts (**1.61** and **1.61'**) were observed (Table 1.4, entry 5 and Scheme 1.25).

Table 1.4. Asymmetric hydrogenation trials

Entry	Catalyst loading (mol %)	H_2 pressure (psi)	Solvent	Time (h)	Result
1	5	150	THF	88	No reaction
2	10	150	THF	88	No reaction
3	5	200	THF	88	No reaction
4	5	150	MeOH	88	No reaction
5	20	200	Distilled THF	120	**1.60:1.60'** (2:1) **1.61:1.61'** (1:1)
6	20	200	EtOH	88	**1.59** (91% yield)

Scheme 1.25. Asymmetric hydrogenation reaction producing undesired products

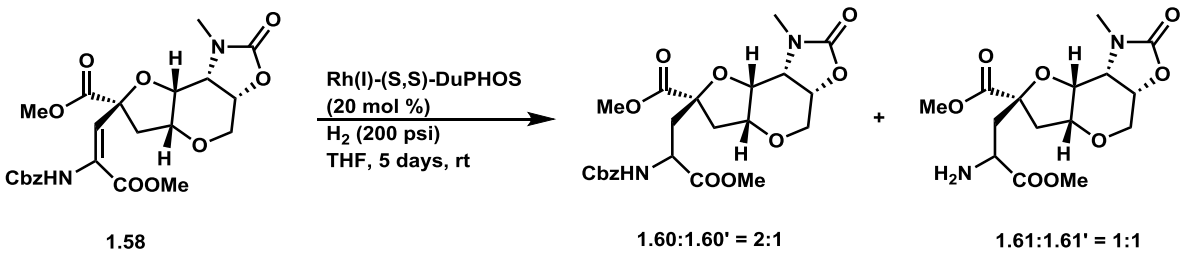

The racemic hydrogenation using Pd/C was also employed to evaluate the potential for diastereoselective control by substrate **1.58**. Surprisingly, when 10 mol% of Pd/C in MeOH was used, we observed formation of tetracyclic system resulting from a cascade reaction of hydrogenation, Cbz deprotection, and lactam formation. The products were generated as a mixture of diastereomers. Furthermore, we observed alkylation at the lactam nitrogen atom due to the reaction of solvents (i.e. *N*-methyl for MeOH and *N*-ethyl for EtOH, Scheme 1.26). The use of THF to avoid the alkylation resulted in the incomplete hydrogenation with a majority of starting material remaining.

Scheme 1.26. Non-asymmetric hydrogenation using Pd/C

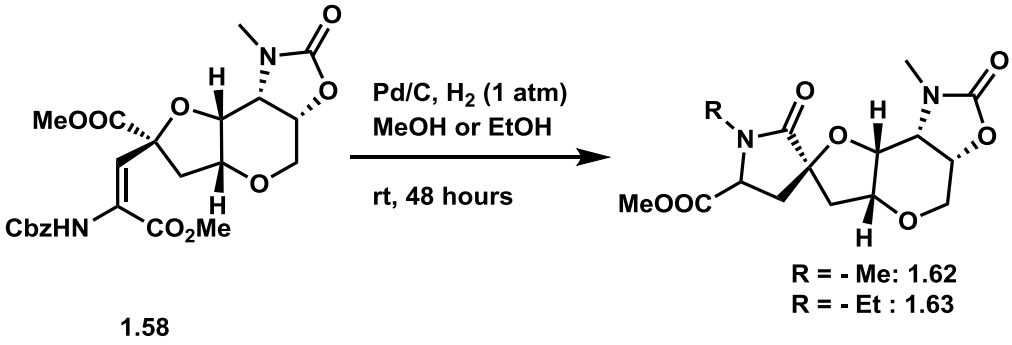

Ethanol seemed to be the most efficient solvent for non-asymmetric hydrogenation using Pd/C. Therefore, it was chosen as the solvent to reinvestigate the

asymmetric hydrogenation with Rh-DuPhos. Ultimately, **1.58** was successfully reduced, yielding the single diastereomer of **1.59** in high yield (Table 1.4, entry 6). The global deprotection of **1.59** was then performed by using NaOH 40% in MeOH. The reaction mixture was submitted to ion exchange column and reverse phase chromatography for purification. The ^{1}H and ^{13}C NMR spectra of the synthetic product match well to those of the natural product and synthesized dysiherbaine reported in literatures.[28-32]

1.3. CONCLUSION

In summary, we have successfully synthesized the natural product dysiherbaine using an approach that allows modification of functional groups at the biologically active center at a late stage of the total synthesis. This approach helps maximize access to potentially important analogs of dysiherbaine, while also providing a route to the parent compound. Although our proposed key intermediate **1.2** was not achieved due to the unselective hydrogenation, an alternative intermediate **1.24** could be used to diversify the functional moieties at C8-C9 pharmacoactive centers. To access dysiherbaine, the ring opening and rearrangement of the Boc-protected aziridine **1.52** catalyzed by $Cu(OTf)_2$ was efficiently used as a novel and stereoselective reaction to introduce the amino hydroxyl group at C8-C9. Furthermore, extensive studies on establishing working conditions for the asymmetric hydrogenation have been conducted to install the amino acid side chain at C4 center with the same stereochemistry as the natural product. The stereochemistry of the bicyclic system was also clarified by X-ray diffraction crystallography.

1.4. EXPERIMENTAL SECTION

1.4.1. General procedure.

Unless noted, all chemicals were purchased from Aldrich Chemical Co. or Acros Chemicals and used without further purification. Anhydrous solvents (toluene, CH_2Cl_2, THF, DMF) were obtained from a Pure Solv® solvent drying system by Innovative Technology. All reactions, unless otherwise noted, were carried out under N_2 in oven-dried glassware. Thin-layer chromatography (TLC) was performed on silica gel 60 F254 pre-coated plates (0.25 mm) from Silicycle and components were visualized by ultraviolet light (254 nm) and/or phosphomolybdic acid or *p*-anisaldehyde stain. Silicycle silica gel 230-400 (particle size 40-63 μm) mesh was used for all column chromatography. All the microwave reactions were performed on Biotage Initiator microwave instrument using Biotage microwave vials (0.5-2 mL, 2-5 mL and 10-20 mL). ^1H and ^{13}C NMR spectra were ecorded on JEOL ECX-400 NMR spectrometer (at 400 MHz and 100 MHz respectively) or JEOL ECA-500 NMR spectrometer (at 500 MHz and 125 MHz respectively) in $CDCl_3$, DMSO-d_6, CD_3OD, and D_2O. Chemical shifts were reported in ppm, multiplicities are indicated by s = singlet, d = doublet, t = triplet, q = quartet, sep = septet, dd = doublet of doublet, dt = doublet of triplet, m = multiplet, and br = broad resonance. Coupling constants 'J' were reported in Hz. Data for ^{13}C NMR were reported in terms of chemical shift. High-resolution mass spectral data were obtained from The University of Texas at Austin, Mass Spectrometry Facility, Austin, TX.

Methyl (2*S*,3a*R*,7a*R*)-2-(((*tert*-butyldimethylsilyl)oxy)methyl)-3,3a,5,7a-tetrahydro-2*H*-furo[3,2-*b*]pyran-2-carboxylate (1.44)

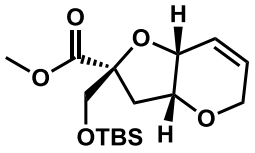

To a stirred solution of alcohol **1.24** (92 mg, 0.43 mmol, 1 equiv.) in 4.3 mL of dry CH_2Cl_2 was added, in 2 portions, triethylamine (0.3 mL, 2.15 mmol, 5 equiv.), DMAP (16 mg, 0.129 mmol, 0.3 equiv.) and TBSCl (129 mg, 0.86 mmol, 2 equiv.). The mixture was stirred at 0 ^oC for 5 min and then warmed up to room temperature and stirred for 48 hours. After completion, the reaction mixture was quenched with saturated $NaHCO_3$, concentrated under vacuum and then extracted with ethyl acetate (3 x 20 mL). The organic phases were combined and washed with brine, dried over anhydrous $MgSO_4$, filtered and concentrated to yield the crude product. The product was purified by column chromatography on silica gel using 20% EtOAc in hexane, 120 mg of product was obtained, 85% yield. ^1H NMR (400 MHz, $CDCl_3$) δ 6.08 (ddd, *J* = 10.5, 2.3, 2.3, 1H), 6.01 (ddd, *J* = 10.5, 3.7, 1.4 Hz, 1H), 4.17 (ddd, *J* = 5.0, 2.7, 2.3 Hz, 1H), 4.10 (ddd, *J* =16.5, 3.7, 1.0 Hz, 1H), 4.04 (dd, *J* = 4.1, 3.7 Hz, 1H), 4.00 (ddt, *J* = 17.0, 4.1, 2.3 Hz, 1H), 3.84 (d, *J* = 10.5 Hz, 1H), 3.71 (d, *J* = 8.7 Hz, 1H), 3.70 (s, 3H), 2.50 (d, *J* = 13.7 Hz, 1H), 2.39 (dd, *J* = 14.0, 5.0 Hz, 1H), 0.87 (s, 9H), 0.05 (s, 6H). ^{13}C NMR (101 MHz, $CDCl_3$) δ 173.7, 130.5, 122.8, 87.4, 75.6, 74.3, 67.1, 64.0, 52.4, 38.7, 25.9, 18.4, -5.3, -5.4. HRMS- ESI: m/z $[M + Na]^+$ calculated for $C_{16}H_{28}O_5Si$: 351.1604, measured 351.1601.

Methyl (2*S*,3a*R*,6*S*,7*S*,7a*R*)-2-(((*tert*-butyldimethylsilyl)oxy)methyl)-6,7-dihydroxyhexahydro-2*H*-furo[3,2-*b*]pyran-2-carboxylate (1.45)

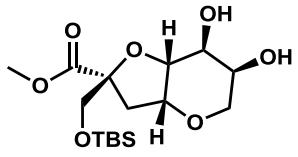

To a stirred solution of alkene **1.44** (1.7 g, 5.17 mmol, 1 equiv.) in 35 mL of acetone:water (4:1) was added NMO.H_2O (2 g, 15.51 mmol, 3 equiv.) and OsO_4 solution 2.5 wt. % in *t*-butanol (3.2 mL, 0.258 mmol, 0.05 equiv.) at 0 ^oC. The reaction was run for 12 hours at room temperature before quenched with $Na_2S_2O_3$. The mixture was concentrated under vacuum and extracted with ethyl acetate (3 x 40 mL). The organic phases were combined and washed with brine, dried over anhydrous $MgSO_4$, filtered and concentrated to yield crude product. The product was purified by column chromatography on silica gel using 90% EtOAc in hexane, 1.67 g of product was obtained, 90% yield. ^1H NMR (400 MHz, $CDCl_3$) δ 4.29 (dd, *J* = 3.2, 2.7 Hz, 1H), 4.16 (dd, *J* = 4.6, 1.8 Hz, 1H), 4.01 (dd, *J* = 2.8, 2.3 Hz, 1H), 3.99–3.95 (m, 1H), 3.88–3.81 (m, 2H), 3.74 (s, 3H), 3.63 (dd, *J* = 10.5, 4.6 Hz, 1H), 3.49 (dd, *J* = 10.5, 10.5 Hz, 1H), 2.38 (dd, *J* = 14.6, 5.0 Hz, 1H), 2.01 (d, *J* = 14.6 Hz, 1H), 0.84 (s, 9H), 0.03 (s, 3H), 0.02 (s, 3H). ^{13}C NMR (101 MHz, $CDCl_3$) δ 173.6, 87.2, 83.0, 73.4, 67.1, 64.4, 63.8, 52.4, 38.5, 25.9, 18.4, -5.3, -5.4. HRMS- ESI: m/z $[M + Na]^+$ calculated for $C_{16}H_{30}O_7Si$: 385.1659, measured 385.1655.

Methyl (2*S*,3a*R*,6*S*,7*R*,7a*S*)-2-(((*tert*-butyldimethylsilyl)oxy)methyl)-6,7-bis((methylsulfonyl)oxy)hexahydro-2*H*-furo[3,2-*b*]pyran-2-carboxylate (1.49)

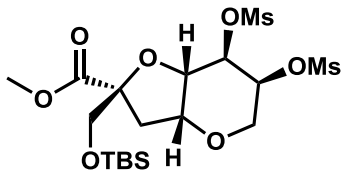

To a stirred solution of diol **1.45** (1.7 g, 4.74 mmol, 1 equiv.) in 47 mL of CH_2Cl_2 was added triethylamine (3.3 mL, 23.7 mmol, 5 equiv.) and MsCl (1.84 mL, 23.7 mmol, 5 equiv.) dropwise at 0 ^oC. The reaction was warmed to room temperature and run for 12 hours. After completion, the mixture was concentrated under vacuum, distributed into water and ethyl acetate, and extracted with ethyl acetate (3 x 40 mL). The organic layers were combined and washed with brine, dried over anhydrous $MgSO_4$, filtered and concentrated to yield crude product. The product was purified by column chromatography on silica gel using 40% EtOAc in hexane, 1.7 g of product was obtained, 70% yield. ^1H NMR (500 MHz, $CDCl_3$) δ 5.22 (dd, *J* = 4.6, 3.2 Hz, 1H), 5.18 (td, *J* = 5.7, 3.1 Hz, 1H), 4.3 (dt, *J* = 8.2, 3.2 Hz, 1H), 3.99 (dd, *J* = 12.1, 5.5 Hz, 1H), 3.87 (d, *J* = 10.7 Hz, 1H), 3.77 (dd, *J* = 12.1, 6.5 Hz, 1H), 3.73 (s, 3H), 3.66 (d, *J* = 10.7 Hz, 1H), 3.22 (s, 3H), 3.11 (s, 3H), 2.40 (d, *J* = 13.9 Hz, 1H), 2.22 (dd, *J* = 13.9, 4.4 Hz, 1H), 0.85 (s, 9H), 0.03 (s, 3H), 0.02 (s, 3H). ^{13}C NMR (126 MHz, $CDCl_3$) δ 173.1, 88.6, 81.1, 76.5, 75.5, 74.1, 66.7, 65.5, 52.5, 38.4, 38.3, 38.3, 25.8, 18.3, -5.3, -5.4. HRMS- ESI: m/z [M + Na]$^+$ calculated for $C_{18}H_{34}O_{11}S_2Si$: 541.1210, measured 541.1211.

Methyl (2*S*,3a*R*,6*R*,7*S*,7a*S*)-6-azido-2-(((*tert*-butyldimethylsilyl)oxy)methyl)-7-((methylsulfonyl)oxy)hexahydro-2*H*-furo[3,2-*b*]pyran-2-carboxylate (1.50)

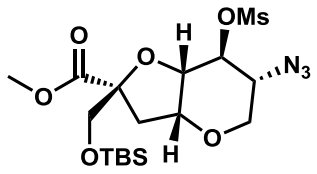

To a stirred solution of dimesylate **1.49** (2 g, 3.93 mmol, 1 equiv.) in 39 mL DMF was added NaN_3 (0.77 g, 11.8 mmol, 3 equiv.) at room temperature. The reaction was heated to 80 ^oC and run for 12 hours. After completion, the reaction was cooled to room temperature then water was added and the mixture was extracted with ethyl acetate (3 x 50 mL). The organic phases were combined and washed with brine, dried over anhydrous $MgSO_4$, filtered and concentrated to yield crude product. The product was purified by column chromatography on silica gel using 40% EtOAc in hexane, 1.6 g of product was obtained, 87% yield. ^1H NMR (500 MHz, $CDCl_3$) δ 4.92 (dd, *J* = 6.9, 5.3 Hz, 1H), 4.33 (ddd, *J* = 6.2, 4.3, 3.1 Hz, 1H), 4.15–4.12 (m, 1H), 3.87 (dd, *J* = 12.5, 4.8 Hz, 1H), 3.83 (d, *J* = 10.4 Hz, 1H), 3.77 (s, 3H), 3. 75 (dd, *J* = 12.4, 5.0 Hz, 1H), 3.69 (d, *J* = 10.4 Hz, 1H), 3.62 (dt, *J* = 6.8, 5.1 Hz, 1H), 3.20 (s, 3H), 2.54 (dd, *J* = 13.8, 2.9 Hz, 1H), 2.36 (dd, *J* = 13.9, 6.0 Hz, 1H), 0.86 (s, 9H), 0.04 (s, 6H). ^{13}C NMR (126 MHz, $CDCl_3$) δ 172.3, 87.8, 79.9, 78.2, 76.5, 67.1, 64.4, 56.4, 52.9, 38.7, 36.4, 25.8, 18.3, -5.3, -5.4. HRMS-ESI: m/z $[M + Na]^+$ calculated for $C_{17}H_{31}N_3O_8SSi$: 488.1499, measured 488.1501.

1-(*tert*-butyl) 5-methyl (1a*S*,3a*R*,5*S*,6a*R*,6b*R*)-5-(((*tert*-butyldimethylsilyl)oxy)methyl)hexahydrofuro[2',3':5,6]pyrano[3,4-*b*]azirine-1,5(2*H*)-dicarboxylate (1.52)

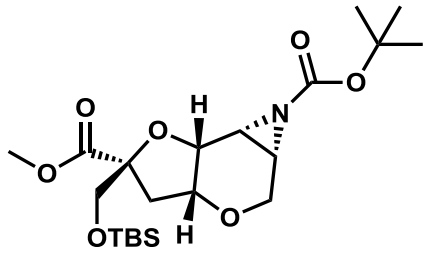

To a stirred solution of azidomesylate **1.50** (100 mg, 0.21 mmol, 1 equiv.) in 2.8 mL of THF and water (4:1) was added PPh_3 (197 mg, 0.75 mmol, 3.5 equiv.) and DIPEA (80 µL, 0.48 mmol, 2.3 equiv.) at room temperature. The reaction was run at the same temperature for 4 hours. After which, the solvents were removed under vacuum and ^{1}H-NMR of crude mixture was performed to confirm the azirdine. ^{1}H NMR (500 MHz, $CDCl_3$) δ 4.29 (dd, *J* = 6.1, 3.2 Hz, 1H), 3.95 (d, *J* = 12.3 Hz, 1H), 3.85 (d, *J* = 10.5 Hz, 1H), 3.71 (s, 3H), 3.68 – 3.60 (m, 4H), 2.44 (t, *J* = 5.6 Hz, 1H), 2.36 (dd, *J* = 14.0, 5.0 Hz, 1H), 2.25 (d, *J* = 14.0 Hz, 1H), 2.11 (d, *J* = 4.9 Hz, 1H).

To a stirred solution of above crude aziridine in CH_2Cl_2 (0.35 mL) was added triethylamine (76 µL, 0.55 mmol, 2.6 equiv.), Boc_2O (119 mg, 0.55 mmol, 2.6 equiv.) and few crystals of DMAP. The reaction was run at 0 ^oC for 30 min, then at room temperature for 12 hours. After completion, CH_2Cl_2 was removed under vacuum and the reaction mixture was distributed in water and ethyl acetate, extracted with ethyl acetate (3 x 20 mL). The organic phases were combined and washed with brine, dried over anhydrous $MgSO_4$, filtered and concentrated to yield crude product. The product was

purified by column chromatography on silica gel using 50% of EtOAc in hexane, 69 mg of product was obtained, 74% yield for 2 steps. ^{1}H NMR (500 MHz, $CDCl_3$) δ 4.27 (dd, *J* = 5.6, 4.8 Hz, 1H), 4.12 (d, *J* = 12.6 Hz, 1H), 3.85–3.82 (m, 1H), 3.81 (d, *J* = 10.3 Hz, 1H), 3.73–3.70 (m, 1H), 3.72 (s, 3H), 3.46 (dd, *J* = 12.6, 1.1 Hz, 1H), 3.01 (dd, *J* = 6.3, 5.7 Hz, 1H), 2.62 (d, *J* = 6.9 Hz, 1H), 2.48 (dd, *J* = 14.2, 1.7 Hz, 1H), 2.40 (dd, *J* = 14.2, 6.3 Hz, 1H), 1.44 (s, 9H), 0.86 (s, 9H), 0.04 (s, 6H). ^{13}C NMR (101 MHz, $CDCl_3$) δ 172.7, 161.9, 87.1, 81.2, 74.2, 67.6, 62.6, 52.4, 37.7, 35.3, 34.5, 28.0, 25.9, 18.3, -5.3, -5.4. HRMS- ESI: m/z $[M + Na]^+$ calculated for $C_{21}H_{37}NO_7Si$: 466.2237, measured 466.2240.

Methyl (3a*S*,5a*R*,7*S*,8a*R*,8b*R*)-7-(((*tert*-butyldimethylsilyl)oxy)methyl)-2-oxooctahydro-2*H*-furo[2',3':5,6]pyrano[4,3-*d*]oxazole-7-carboxylate (1.53)

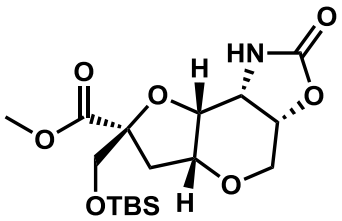

An oven-dried flask was charged with Boc protected aziridine **1.52** (287 mg, 0.65 mmol, 1 equiv.), THF (6.1 mL) and dimethoxylethane (0.3 mL). $Cu(OTf)_2$ (23 mg, 0.065 mmol, 0.1 equiv.) was added in one portion at room temperature. The reaction was run for 8 hours to full conversion. Afterwards, the solvents were removed under vacuum and the crude mixture was submitted to the column, eluting with 90% ethyl acetate in hexane on silica gel, 186 mg of product was obtained, 74% yield. ^{1}H NMR (500 MHz, $CDCl_3$) δ 5.95 (s, 1H), 4.60 (dd, *J* = 8.6, 1.1 Hz, 1H), 4.48 (dt, *J* = 13.2, 6.3 Hz, 1H), 4.35 (dd, *J* =

8.9, 5.2 Hz, 1H), 4.19 (dd, *J* = 6.3, 5.2 Hz, 1H), 4.00 (d, *J* = 13.6 Hz, 1H), 3.78–3.71 (m, 2H), 3.77 (s, 3H), 3.39 (dd, *J* = 13.6, 2.0 Hz, 1H), 2.54 (dd, *J* = 17.1, 9.8 Hz, 1H), 2.33 (dd, *J* = 13.1, 6.1 Hz, 1H), 0.87 (s, 9H), 0.05 (s, 3H), 0.04 (s, 3H). ^{13}C NMR (101 MHz, $CDCl_3$) δ 173.3, 158.6, 87.0, 77.3, 75.6, 71.9, 67.4, 66.8, 53.0, 51.0, 40.3, 25.9, 18.3, -5.3, -5.4. HRMS- ESI: m/z $[M + Na]^+$ calculated for $C_{17}H_{29}NO_7Si$: 410.1611, measured 410.1612.

Methyl (3a*S*,5a*R*,7*S*,8a*R*,8b*R*)-7-(((*tert*-butyldimethylsilyl)oxy)methyl)-1-methyl-2-oxooctahydro-2*H*-furo[2',3':5,6]pyrano[4,3-*d*]oxazole-7-carboxylate (1.54)

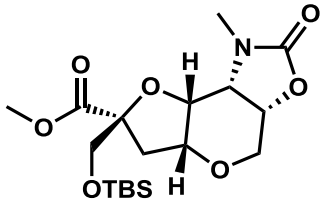

To a stirred solution of oxazolidinone **1.53** (152 mg, 0.39 mmol, 1 equiv.) in DMF (4.2 mL) NaH (24 mg, 0.6 mmol, 1.5 equiv.) was added at -10 ^oC. MeI (0.15 mL, 2.34 mmol, 6 equiv.) was subsequently added dropwise. The reaction was kept at -10 ^oC for 5 hours before quenching with saturated NH_4Cl. The mixture was then extracted with ethyl acetate (3 x 30 mL). The organic phases were combined and washed with brine, dried over anhydrous $MgSO_4$, filtered and concentrated to yield the crude product. The product was purified by column chromatography on silica gel using 4% of MeOH in CH_2Cl_2, 133 mg of product was obtained, 85% yield. ^{1}H NMR (500 MHz, $CDCl_3$) δ 4.26 (ddd, *J* = 7.4, 2.3,1.7 Hz, 1H), 4.21 (dd, *J* = 13.9, 1.1 Hz, 1H), 4.10 (dd, *J* = 5.6, 2.1 Hz, 1H), 3.95 (s, 1H), 3.81 (d, *J* = 10.4 Hz, 1H), 3.76 (dd, *J* = 7.0, 5.7 Hz, 1H), 3.72 (s, 3H), 3.66 (d, *J* = 10.4 Hz, 1H), 3.51 (dd, *J* = 13.8, 2.3 Hz, 1H), 2.98 (s, 3H), 2.60–2.50 (m, 2H), 0.87 (s,

9H), 0.04 (s, 3H), 0.03 (s, 3H). ^{13}C NMR (101 MHz, $CDCl_3$) δ 173.4, 159.3, 87.1, 76.1, 75.1, 68.6, 65.8, 64.5, 54.8, 52.5, 38.4, 30.3, 25.82, 18.2, -5.3, -5.4. HRMS- ESI: m/z [M + Na]$^+$ calculated for $C_{18}H_{31}NO_7Si$: 424.1768, measured 424.1770.

Methyl (3a*S*,5a*R*,7*S*,8a*R*,8b*R*)-7-(hydroxymethyl)-1-methyl-2-oxooctahydro-2*H*-furo[2',3':5,6]pyrano[4,3-*d*]oxazole-7-carboxylate (1.55)

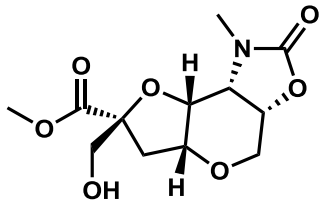

To a stirred solution of *N*-Methyl oxazolidinone **1.54** (165 mg, 0.4 mmol) in THF (5.3 mL) was added TBAF 1M in THF (0.6 mL) dropwise at 0 ^{o}C. The reaction was run at the same temperature for 30 min. After completion, THF was removed under vacuum and the crude mixture was submitted to column, eluting with 10% MeOH in EtOAc on silica gel, 114 mg of product was obtained, quantitative yield. ^{1}H NMR (500 MHz, CD_3OD) δ 4.31 (dt, *J* = 7.4, 1.7, 1H), 4.15 (dd, *J* = 5.7, 2.1 Hz, 1H), 4.08 (d, *J* = 14.0 Hz, 1H), 4.01–3.93 (m, 2H), 3.69 (d, *J* = 11.6 Hz, 1H), 3.64 (s, 3H), 3.58 (dd, *J* = 14.0, 2.1 Hz, 1H), 3.53 (d, *J* = 11.6 Hz, 1H), 2.97 (s, 3H), 2.50 (d, *J* = 13.7 Hz, 1H), 2.30 (dd, *J* = 13.5, 3.8 Hz, 1H). ^{13}C NMR (126 MHz, CD_3OD) δ 173.9, 160.6, 86.9, 75.5, 74.8, 69.8, 65.4, 63.9, 54.5, 51.2, 38.9, 29.1. HRMS- ESI: m/z [M + Na]$^+$ calculated for $C_{12}H_{17}NO_7$: 310.0903, measured 310.0907.

Methyl (3a*S*,5a*R*,7*S*,8a*R*,8b*R*)-7-((*E*)-2-(((benzyloxy)carbonyl)amino)-3-methoxy-3-oxoprop-1-en-1-yl)-1-methyl-2-oxooctahydro-2*H*-furo[2',3':5,6]pyrano[4,3-*d*]oxazole-7-carboxylate (1.58)

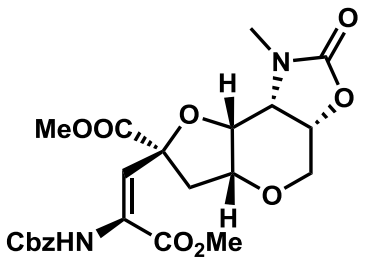

To a stirred solution of **1.55** (90 mg, 0.3 mmol) in CH_2Cl_2:DMSO (4:1, 0.083 M) at 0 ^oC was added triethylamine (0.22 mL, 1.56 mmol) and SO_3•pyridine complex (197 mg, 1.24 mmol). The resulting mixture was allowed to warm to room temperature over 3 hours. Upon completion, solvents were removed under vacuum and the crude mixture was carefully extracted with acetonitrile and brine. The combined organic extracts were dried over $MgSO_4$, filtered, and concentrated under reduced pressure to give a crude aldehyde.

To a stirred solution of the above aldehyde in CH_2Cl_2 (3.1 mL) at 0 ^oC were added $(MeO)_2P(O)CH(NHCbz)CO_2Me$ (308 mg, 0.93 mmol) and *N*,*N*,*N*',*N*'-tetramethylguanidine (0.16 mL, 1.24 mmol). The reaction mixture was stirred at room temperature for 3 hours and then quenched with saturated aqueous NH_4Cl. The mixture was extracted with $CHCl_3$ and the combined organic layers were washed with brine, dried over $MgSO_4$, filtered, and concentrated under reduced pressure. The resulting crude product was purified by flash chromatography, eluting with 1% MeOH/EtOAc. 128 mg (87%) of the desired product was obtained. ^1H NMR (500 MHz, $CDCl_3$) δ 7.68 (s, 1H), 7.41–7.28 (m, 5H), 6.10 (s, 1H), 5.18–5.11 (m, 2H), 4.25 (d, J = 6.9 Hz, 1H), 4.20 (d, J =

14.0 Hz, 1H), 4.15 (dd, *J* = 5.7, 2.1 Hz, 1H), 3.92 (t, *J* = 2.3 Hz, 1H), 3.78–3.75 (m, 1H), 3.74 (s, 6H), 3.50 (dd, *J* = 14.1, 2.1 Hz, 1H), 3.16 (d, *J* = 13.3 Hz, 1H), 2.91 (s, 3H), 2.23 (dd, *J* = 13.5, 3.6 Hz, 1H). ^{13}C NMR (126 MHz, $CDCl_3$) δ 172.9, 164.5, 158.8, 153.7, 135.9, 130.5, 128.6 (x2), 128.4 (x3), 126.4, 84.5, 75.2, 74.6, 68.3, 67.62, 64.7 54.4, 53.4, 52.8, 44.1, 30.2. HRMS- ESI: m/z [M + Na]$^+$ calculated for $C_{23}H_{26}N_2O_{10}$: 513.1485, measured 513.1492.

Methyl (3a*S*,5a*R*,7*R*,8a*R*,8b*R*)-7-((*S*)-2-(((benzyloxy)carbonyl)amino)-3-methoxy-3-oxopropyl)-1-methyl-2-oxooctahydro-2*H*-furo[2',3':5,6]pyrano[4,3-*d*]oxazole-7-carboxylate (1.59)

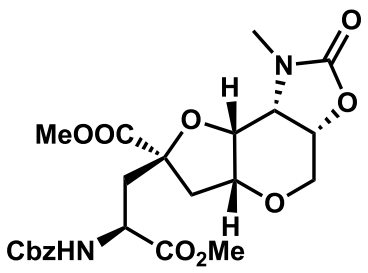

To a degassed mixture of **1.56** (22 mg, 0.045 mmol) in 0.9 mL of anhydrous ethanol (0.05 M) was added [Rh^I(COD)-(*S*,*S*)-EtDuPHOS]OTf (6.5 mg, 0.009 mmol). The mixture was degassed again before placing in a hydrogenation bomb and pressurized with hydrogen to an initial pressure of 200 psi. The reaction mixture was stirred at room temperature for 88 hours. The mixture was concentrated under reduced pressure. The resulting crude product was purified by flash chromatography, eluting with 4% MeOH/EtOAc. 20 mg of desired product was obtained, 91 % yield. ^{1}H NMR (500 MHz, $CDCl_3$) δ 7.40–7.28 (m, 5H), 5.63 (d, *J* = 7.2 Hz, 1H), 5.11 (s, 2H), 4.40–4.32 (m, 1H),

4.24 (d, *J* = 7.2 Hz, 1H), 4.19 (d, *J* = 14.0 Hz, 1H), 4.15 (d, *J* = 4.2 Hz, 1H), 3.88 (s, 1H), 3.78 (t, *J* = 6.4 Hz, 1H), 3.72 (s, 3H), 3.70 (s, 3H), 3.47 (dd, *J* = 13.9, 2.0 Hz, 1H), 2.94 (s, 3H), 2.83 (d, *J* = 13.3 Hz, 1H), 2.46 (dd, *J* = 14.7, 4.5 Hz, 1H), 2.15 (dd, *J* = 13.3, 3.7, 1H), 2.10 (dd, *J* = 14.2, 7.3, 1H). ^{13}C NMR (126 MHz, $CDCl_3$) δ 173.9, 172.1, 158.7, 155.9, 136.3, 128.6(x2), 128.2(x3), 84.8, 75.5, 74.9, 68.4, 67.2, 64.8, 54.4, 52.8, 52.7, 51.3, 43.7, 39.3, 30.3. HRMS- ESI: m/z $[M + Na]^+$ calculated for $C_{23}H_{28}N_2O_{10}$: 515.1642, measured 515.1648.

(–)-Dysiherbaine

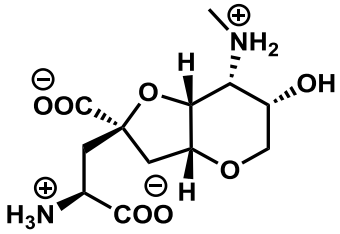

A solution of **1.59** (10 mg, 0.02 mmol) in MeOH (0.5 mL) and 40% NaOH aqueous (0.5 mL) was heated at 45 ºC for 17 hours. After cooling, the reaction mixture was directly submitted to ion exchange column (Amberlite IRC-86, H^+ form) using H_2O as an eluent. Ninhydrin positive fractions were combined and lyophilized. The residue was purified by reverse phase chromatography (Silicycle C18, 40-63 μm particle) using H_2O as eluent. Ninhydrin positive fractions were collected and lyophilized to afford 6.1 mg of (–)-dysiherbaine, 100% yield. ^{1}H NMR (500 MHz, D_2O) δ 4.27 (brm, 1H), 4.11 (brs, 1H), 3.84 (dd, *J* = 13.2, 2.3 Hz, 1H), 3.80 (m, 1H), 3.50–3.48 (m, 2H), 3.44 (dd, *J* = 11.5, 2.3 Hz, 1H), 2.70 (s, 3H), 2.55 (dd, *J* = 15.0, 2.3 Hz, 1H), 2.53 (d, *J* = 14.3 Hz, 1H), 2.12 (dd,

J = 14.3, 3.4 Hz, 1H), 1.88 (dd, *J* = 15.5, 12.0 Hz, 1H). ^{13}C NMR (126 MHz, D_2O) δ 180.0, 173.6, 88.4, 76.0, 74.8, 68.6, 62.1, 56.3, 53.4, 44.3, 39.1, 29.5. HRMS- ESI: m/z $[M + Na]^+$ calculated for $C_{12}H_{20}N_2O_7$: 327.1169, measured 327.1176.

Methyl (2*S*,3a*R*,6*R*,7S,7a*S*)-6-acetoxy-7-iodohexahydro-2*H*-furo[3,2-*b*]pyran-2-carboxylate (1.10)

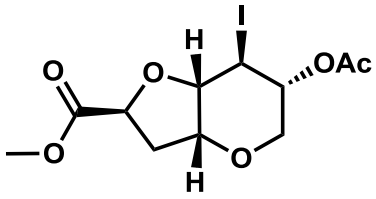

To a stirred solution of **1.2** (150 mg, 0.81 mmol) in 14 mL acetic acid was added H_2O (0.16 mL, 8.9 mmol), AgOAc (408 mg, 2.44 mmol). I_2 (310 mg, 1.22mmol) was ground to small powder and added in portions to the reaction mixture at room temperature. The reaction was run at same temperature for 4 hours. After completion, reaction mixture was filtered through celite and Et_2O was used to wash. The filtrate was extracted with Et_2O and H_2O (3 x 40 mL) and $NaHCO_3$ (2 x 10 mL). The organic layer was then dried with Na_2SO_4, filtered, and concentrated under reduced pressure. The resulting crude product was purified by flash chromatography, eluting with 50% EtOAc/Hexane. 262 mg (87%) of desired product was obtained. ^{1}H NMR (400 MHz, $CDCl_3$) δ 5.44–5.31 (m, 1H), 4.65 (dd, *J* = 9.8, 1.4 Hz, 1H), 4.30 (dd, *J* = 3.2, 1.9 Hz, 1H), 4.22 (dd, *J* = 10.9, 3.3 Hz, 1H), 4.04 (s, 1H), 3.90 (dd, *J* = 11.0, 4.6 Hz, 1H), 3.79 (s, 3H), 3.13 (dd, *J* = 10.8, 10.2 Hz, 1H), 2.70–2.57 (m, 1H), 2.44 (ddd, *J* = 13.5, 9.8, 3.5 Hz, 1H), 2.10 (s, 3H). ^{13}C NMR (101 MHz, $CDCl_3$) δ 172.8, 169.7, 83.2, 75.8, 75.3, 69.2, 67.8, 52.4, 39.2, 29.8, 26.3,

21.0. HRMS- ESI: m/z [M + Na]$^+$ calculated for $C_{11}H_{15}IO_6$: 392.9811, measured 392.9815.

Methyl (2*S*,3a*R*,6*S*,7*R*,7a*R*)-2-(((*tert*-butyldimethylsilyl)oxy)methyl)-7-hydroxy-6-((methylsulfonyl)oxy)hexahydro-2H-furo[3,2-*b*]pyran-2-carboxylate (1.46)

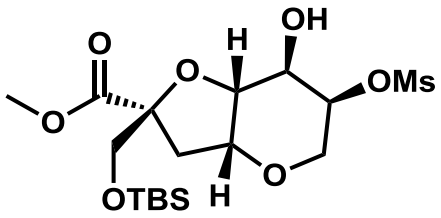

To a stirred solution of diol **1.45** (61 mg, 0.17 mmol, 1 equiv.) in 47 mL of CH_2Cl_2 was added triethylamine (70 µL, 0.51 mmol, 3 equiv.) and MsCl (40 µL, 0.51 mmol, 3 equiv.) dropwise at 0 ^oC. The reaction was warmed to room temperature and run for 12 hours. After completion, the mixture was concentrated under vacuum, distributed into water and ethyl acetate, extracted with ethyl acetate (3 x 20 mL). The organic layers were combined and washed with brine, dried over anhydrous $MgSO_4$, filtered, and concentrated to yield crude product. The crude product was purified by column chromatography on silica gel using 60% EtOAc in hexane, 56 mg of product was obtained, 75% yield. ^{1}H NMR (500 MHz, $CDCl_3$) δ 4.92 – 4.84 (m, 1H), 4.49 (dd, *J* = 3.4, 2.9 Hz, 1H), 4.21 (dd, *J* = 4.9, 1.9 Hz, 1H), 4.02 (t, *J* = 2.9 Hz, 1H), 3.85 (s, 2H), 3.82 – 3.78 (m, 2H), 3.74 (s, 3H), 3.07 (s, 3H), 2.42 (dd, *J* = 14.7, 5.1 Hz, 2H), 2.03 (d, *J* = 5.0 Hz, 1H), 0.85 (s, 9H), 0.04 (s, 3H), 0.04 (s, 3H). ^{13}C NMR (126 MHz, $CDCl_3$) δ 173.3, 86.7, 82.7, 75.1, 74.09, 68.0, 65.8, 62.1, 52.5, 38.5, 25.8, 18.3. HRMS- ESI: m/z [M + Na]$^+$ calculated for $C_{17}H_{32}O_9SSi$: 463.1434, measured 463.1431.

Methyl (2*S*,3a*R*,6*R*,7*S*,7a*R*)-6-azido-2-(((*tert*-butyldimethylsilyl)oxy)methyl)-7-hydroxyhexahydro-2*H*-furo[3,2-*b*]pyran-2-carboxylate (1.47)

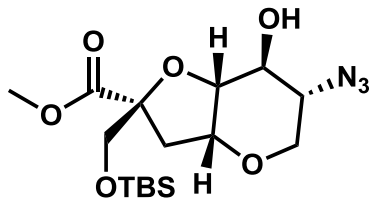

To a stirred solution of monomesylate **1.46** (41 mg, 0.093 mmol, 1 equiv.) in 1 mL DMF was added NaN_3 (18 mg, 0.28 mmol, 3 equiv.) at room temperature. The reaction was heated to 80 ºC and run for 12 hours. After completion, the reaction was cooled down to room temperature then water was added and the mixture was extracted with ethyl acetate (3x). The organic phases were combined and washed with brine, dried over anhydrous MgSO4, filtered, and concentrated to yield crude product. The crude product was purified by column chromatography on silica gel using 50% EtOAc in hexane, 29 mg of product was obtained, 80% yield. ^{1}H NMR (500 MHz, $CDCl_3$) δ 4.24 (ddd, *J* = 8.2, 6.0, 2.8 Hz, 2H), 3.98 (d, *J* = 9.9 Hz, 1H), 3.91 – 3.83 (m, 3H), 3.77 (dd, *J* = 12.5, 2.5 Hz, 1H), 3.73 (s, 3H), 2.43 (dd, *J* = 14.4, 5.7 Hz, 1H), 2.09 (dd, *J* = 14.5, 1.8 Hz, 1H), 0.85 (s, 9H), 0.05 (s, 3H), 0.03 (s, 3H). ^{13}C NMR (126 MHz, $CDCl_3$) δ 174.0, 86.9, 80.9, 77.4, 77.1, 76.9, 74.7, 67.79, 66.6, 63.7, 57.8, 52.5, 38.5, 25.8, 18.3. HRMS- ESI: m/z $[M + Na]^+$ calculated for $C_{16}H_{29}N_3O_6Si$: 410.1724, measured 410.1725.

Methyl (2*S*,3a*R*,6*R*,7*S*,7a*R*)-6-amino-2-(((*tert*-butyldimethylsilyl)oxy)methyl)-7-hydroxyhexahydro-2*H*-furo[3,2-*b*]pyran-2-carboxylate (1.48)

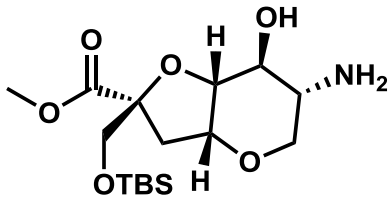

To a stirred solution of azido alcohol **1.47** (30 mg, 0.077 mmol, 1 equiv.) in 1 mL of THF and water (4:1) was added PPh_3 (71 mg, 0.27 mmol, 3.5 equiv.) and DIPEA (30 µL, 0.18 mmol, 2.3 equiv.) at room temperature. The reaction was run at the same temperature for 4 hours. After that, the solvents were removed under vacuum and NMR of crude mixture was performed to confirm the product. ^{1}H NMR (500 MHz, $CDCl_3$): δ 4.21 (dd, *J* = 4.9, 1.8 Hz, 1H), 4.14 (s, 1H), 3.99–3.89 (m, 3H), 3.87 (s, 1H), 3.75 (s, 3H), 3.65 (d, *J* = 11.7 Hz, 1H), 2.83 (s, 1H), 2.43 (dd, *J* = 14.5, 5.2 Hz, 1H), 2.11 (d, *J* = 14.5 Hz, 1H), 0.89 (s, 9H), 0.08 (s, 3H), 0.07 (s, 3H) (chemical shifts 7-8 ppm belong to PPh_3). ^{13}C NMR (126 MHz, $CDCl_3$) δ 173.7, 86.4, 81.8, 74.4, 67.7, 66.9, 66.7, 52.5, 50.62, 39.4, 25.9, 18.4 (chemical shifts 120-140 ppm belong to PPh_3).

Methyl (2*S*,3a*R*,7a*R*)-2-((*E*)-2-(((benzyloxy)carbonyl)amino)-3-methoxy-3-oxoprop-1-en-1-yl)-3,3a,5,7a-tetrahydro-2*H*-furo[3,2-*b*]pyran-2-carboxylate (1.37)

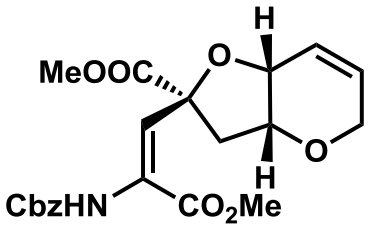

To a stirred solution of alcohol **1.24** (186 mg, 0.87 mmol) in 11 mL CH_2Cl_2:DMSO (4:1, 0.083 M) at 0 ℃ was added triethylamine (0.6 mL, 4.34 mmol) and SO_3**.**pyridine complex (554 mg, 3.48 mmol). The resulting mixture was allowed to warm to room temperature over 1 hour and quenched with saturated aqueous NH_4Cl (15 mL). The mixture was extracted with $CHCl_3$, and the combined organic extracts were washed with brine, dried over $MgSO_4$, filtered, and concentrated under reduced pressure to give a crude aldehyde as yellow oil.

To a stirred solution of the above aldehyde in CH_2Cl_2 (8.7 mL) at 0 ℃ were added $(MeO)_2P(O)CH(NHCbz)CO_2Me$ (865 mg, 2.61 mmol) and *N*,*N*,*N*',*N*'-tetramethylguanidine (0.4 mL, 3.48 mmol). The reaction mixture was stirred at room temperature for 3 hours and then quenched with saturated aqueous NH_4Cl. The mixture was extracted with $CHCl_3$ and the combined organic layers were washed with brine, dried over $MgSO_4$, filtered, and concentrated under reduced pressure. The resulting crude product was purified by flash chromatography, eluting with 50% EtOAc/Hexane. 217 mg (60%) of desired product was obtained over 2 steps. ^{1}H NMR (500 MHz, $CDCl_3$) δ 7.77 (s, 1H), 7.40–7.28 (m, 5H), 6.13–6.03 (m, 2H), 6.02 (s, 1H), 5.14 (dd, *J* = 17.2, 12.0 Hz, 2H), 4.19 (d, *J* = 3.0 Hz, 1H), 4.12–3.93 (m, 3H), 3.73 (s, 2H), 3.69 (s, 3H), 2.93 (d, *J* = 13.8 Hz, 1H), 2.32 (dd, *J* = 13.8, 4.8 Hz, 1H). ^{13}C NMR (126 MHz, $CDCl_3$) δ 172.6, 164.7, 153.7, 135.9, 131.0, 130.6, 128.6, 128.4, 128.3, 124.7, 122.0, 84.8, 74.5, 74.0, 67.6, 63.9, 53.1, 52.7, 44.2. HRMS- ESI: m/z $[M + Na]^+$ calculated for $C_{21}H_{23}NO_8$: 440.1322, measured : 440.1325.

Methyl (3a*S*,5a*R*,7*S*,8a*R*,8b*R*)-1'-ethyl-1-methyl-2,2'-dioxooctahydrospiro[furo[2',3':5,6]pyrano[4,3-*d*]oxazole-7,3'-pyrrolidine]-5'-carboxylate (1.63)

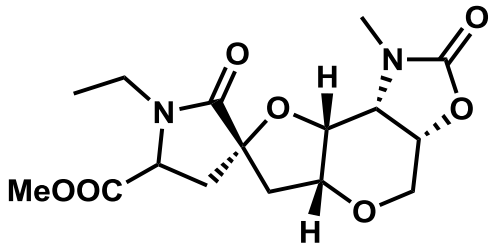

To a stirred solution of **1.56** (7 mg, 0.014 mmol) in anhydrous ethanol was added 10 mol% Pd/C (2 mg, 0.0014 mmol) at room temperature. The reaction was run under H_2 atmosphere for 48 hours. Upon completion, crude mixture was filtered through celite and solvent was removed under vacuum. Crude mixture was submitted to HPLC for purification, providing 2 mg of product (40% yield). ^{1}H NMR (500 MHz, CD_3OD) δ 4.57 (dt, *J* = 8.2, 5.2 Hz, 1H), 4.39 (dd, *J* = 8.6, 4.1 Hz, 1H), 4.34 (dd, *J* = 8.8, 3.9 Hz, 1H), 4.26 (dd, *J* = 12.7, 5.4 Hz, 1H), 4.14 (t, *J* = 4.3 Hz, 1H), 4.04 (dd, *J* = 8.2, 4.6 Hz, 1H), 3.77–3.72 (m, 4H), 3.61 (dq, *J* = 14.7, 7.4 Hz, 1H), 3.06 (dq, *J* = 14.3, 7.2 Hz, 1H), 2.89 (s, 3H), 2.48 (dd, *J* = 13.6, 8.6 Hz, 1H), 2.35–2.32 (m, 2H), 2.17 (dd, *J* = 13.3, 4.1 Hz, 1H), 1.09 (t, *J* = 7.2 Hz, 3H). ^{13}C NMR (101 MHz, CD_3OD) δ 173.3, 172.1, 160.0, 101.5, 82.9, 75.7, 73.3, 69.1, 63.2, 62.2, 57.8, 56.2, 54.5, 51.8, 42.7, 37.4, 37.2, 28.7, 11.0. HRMS- ESI: m/z $[M + Na]^+$ calculated for $C_{16}H_{22}N_2O_7$: 377.1325, measured 377.1329.

1.4.2. Crystallographic data.

Table 1.5. Crystal data and structure refinement of **1.13a**

Empirical formula	C10 H16 O8 S	
Formula weight	296.29	
Temperature	223(2) K	
Wavelength	0.71073 Å	
Crystal system	Orthorhombic	
Space group	P2(1)2(1)2(1)	
Unit cell dimensions	a = 8.2658(10) Å	α = 90°.
	b = 8.8356(11) Å	β = 90°.
	c = 17.8919(22) Å	γ = 90°.
Volume	1306.7(3) $Å^3$	
Z	4	
Density (calculated)	1.506 Mg/m^3	
Absorption coefficient	0.281 mm^{-1}	
F(000)	624	
Crystal size	0.40 x 0.35 x 0.30 mm^3	
Theta range for data collection	2.28 to 25.05°.	
Index ranges	-9<=h<=9, 0<=k<=10, 0<=l<=21	
Reflections collected	6640	
Independent reflections	2331 [R(int) = 0.0181]	
Completeness to theta = 25.05°	99.8%	
Absorption correction	Empirical	
Max. and min. transmission	0.9923 and 0.8185	
Refinement method	Full-matrix least-squares on F^2	
Data / restraints / parameters	2311 / 1 / 177	
Goodness-of-fit on F^2	1.082	
Final R indices [I>2sigma(I)]	R1 = 0.0237, wR2 = 0.0644	
R indices (all data)	R1 = 0.0246, wR2 = 0.0654	
Absolute structure parameter	-0.03(7)	
Extinction coefficient	0.0084(18)	
Largest diff. peak and hole	0.221 and -0.201 $e.Å^{-3}$	

Table 1.6. Crystal data and structure refinement of **1.25**

Empirical formula	C16 H17 Br O7 S	
Formula weight	433.27	
Temperature	113(2) K	
Wavelength	1.54178 Å	
Crystal system	Monoclinic	
Space group	P2(1)	
Unit cell dimensions	a = 9.3426(2) Å	α = 90°.
	b = 10.4443(2) Å	β = 115.2830(6)°.
	c = 10.0312(2) Å	γ = 90°.
Volume	885.05(3) $Å^3$	
Z	2	
Density (calculated)	1.626 Mg/m^3	
Absorption coefficient	4.598 mm^{-1}	
F(000)	440	
Crystal size	0.40 x 0.30 x 0.20 mm^3	
Theta range for data collection	4.88 to 70.21°.	
Index ranges	-11<=h<=9, -10<=k<=11, 0<=l<=11	
Reflections collected	5932	
Independent reflections	2568 [R(int) = 0.0225]	
Completeness to theta = 70.21°	92.4%	
Absorption correction	Empirical	
Max. and min. transmission	0.7533 and 0.4663	
Refinement method	Full-matrix least-squares on F^2	
Data / restraints / parameters	2564 / 1 / 227	
Goodness-of-fit on F^2	1.096	
Final R indices [I>2sigma(I)]	R1 = 0.0194, wR2 = 0.0466	
R indices (all data)	R1 = 0.0195, wR2 = 0.0468	
Absolute structure parameter	0.027(12)	
Extinction coefficient	0.0093(5)	
Largest diff. peak and hole	0.225 and -0.367 e.$Å^{-3}$	

Table 1.7. Crystal data and structure refinement of **1.28**

Empirical formula	C16 H17 Br O7 S	
Formula weight	433.27	
Temperature	123(2) K	
Wavelength	1.54178 Å	
Crystal system	Monoclinic	
Space group	P2(1)	
Unit cell dimensions	a = 9.3496(4) Å	α = 90°.
	b = 10.4621(5) Å	β = 115.240(1)°.
	c = 10.0359(4) Å	γ = 90°.
Volume	887.95(7) $Å^3$	
Z	2	
Density (calculated)	1.620 Mg/m^3	
Absorption coefficient	4.583 mm^{-1}	
F(000)	440	
Crystal size	0.40 x 0.30 x 0.25 mm^3	
Theta range for data collection	5.23 to 66.67°.	
Index ranges	-10<=h<=10, -12<=k<=10, 0<=l<=11	
Reflections collected	5903	
Independent reflections	2425 [R(int) = 0.0236]	
Completeness to theta = 66.67°	97.6%	
Absorption correction	Empirical	
Max. and min. transmission	0.7528 and 0.5187	
Refinement method	Full-matrix least-squares on F^2	
Data / restraints / parameters	2423 / 1 / 228	
Goodness-of-fit on F^2	1.047	
Final R indices [I>2sigma(I)]	R1 = 0.0190, wR2 = 0.0461	
R indices (all data)	R1 = 0.0190, wR2 = 0.0461	
Absolute structure parameter	0.039(12)	
Extinction coefficient	0.0088(6)	
Largest diff. peak and hole	0.327 and -0.278 e.$Å^{-3}$	

REFERENCES

(1) Sahai, S. *European Archives of Psychiatry and Clinical Neuroscience* **1990**, *240*, 121.

(2) Sprengel, R. In *Neuroscience in the 21st Century*; Pfaff, D., Ed.; Springer New York: 2013, p 59.

(3) Niswender, C. M.; Conn, P. J. *Annual Review of Pharmacology and Toxicology* **2010**, *50*, 295.

(4) Cortese, B. M.; Phan, K. L. *CNS Spectrums* **2005**, *10*, 820.

(5) Traynelis, S. F.; Wollmuth, L. P.; McBain, C. J.; Menniti, F. S.; Vance, K. M.; Ogden, K. K.; Hansen, K. B.; Yuan, H.; Myers, S. J.; Dingledine, R. *Pharmacological Reviews* **2010**, *62*, 405.

(6) Sobolevsky, A. I.; Rosconi, M. P.; Gouaux, E. *Nature* **2009**, *462*, 745.

(7) Furukawa, H.; Singh, S. K.; Mancusso, R.; Gouaux, E. *Nature* **2005**, *438*, 185.

(8) Vicini, S.; Wang, J. F.; Li, J. H.; Zhu, W. J.; Wang, Y. H.; Luo, J. H.; Wolfe, B. B.; Grayson, D. R. *Functional and Pharmacological Differences Between RecombinantN-Methyl-d-Aspartate Receptors*, 1998; Vol. 79.

(9) Tsuzuki, K.; Lambolez, B.; Rossier, J.; Ozawa, S. *Journal of Neurochemistry* **2001**, *77*, 1650.

(10) Isaac, J. T. R.; Ashby, M. C.; McBain, C. J. *Neuron* **2007**, *54*, 859.

(11) Fernandes, H. B.; Catches, J. S.; Petralia, R. S.; Copits, B. A.; Xu, J.; Russell, T. A.; Swanson, G. T.; Contractor, A. *Neuron* **2009**, *63*, 818.

(12) Pinheiro, P. S.; Perrais, D.; Coussen, F.; Barhanin, J.; Bettler, B.; Mann, J. R.; Malva, J. O.; Heinemann, S. F.; Mulle, C. *Proceedings of the National Academy of Sciences of the United States of America* **2007**, *104*, 12181.

(13) Burnashev, N.; Villarroel, A.; Sakmann, B. *The Journal of Physiology* **1996**, *496*, 165.

(14) Ferraguti, F.; Shigemoto, R. *Cell Tissue Res* **2006**, *326*, 483.

(15) Enz, R. *Frontiers in Molecular Neuroscience* **2012**, *5*, 52.

(16) Jingami, H.; Nakanishi, S.; Morikawa, K. *Current Opinion in Neurobiology* **2003**, *13*, 271.

(17) Kew, J. C.; Kemp, J. *Psychopharmacology* **2005**, *179*, 4.

(18) Sakai, R.; Kamiya, H.; Murata, M.; Shimamoto, K. *Journal of the American Chemical Society* **1997**, *119*, 4112.

(19) Sakai, R.; Swanson, G. T.; Shimamoto, K.; Green, T.; Contractor, A.; Ghetti, A.; Tamura-Horikawa, Y.; Oiwa, C.; Kamiya, H. *Journal of Pharmacology and Experimental Therapeutics* **2001**, *296*, 650.

(20) Swanson, G. T.; Green, T.; Sakai, R.; Contractor, A.; Che, W.; Kamiya, H.; Heinemann, S. F. *Neuron*, **2002**, *34*, 589.

(21) Sakai, R.; Koike, T.; Sasaki, M.; Shimamoto, K.; Oiwa, C.; Yano, A.; Suzuki, K.; Tachibana, K.; Kamiya, H. *Organic Letters* **2001**, *3*, 1479.

(22) Sanders, J. M.; Ito, K.; Settimo, L.; Pentikäinen, O. T.; Shoji, M.; Sasaki, M.; Johnson, M. S.; Sakai, R.; Swanson, G. T. *Journal of Pharmacology and Experimental Therapeutics* **2005**, *314*, 1068.

(23) Shoji, M.; Akiyama, N.; Tsubone, K.; Lash, L. L.; Sanders, J. M.; Swanson, G. T.; Sakai, R.; Shimamoto, K.; Oikawa, M.; Sasaki, M. *The Journal of Organic Chemistry* **2006**, *71*, 5208.

(24) Lash, L. L.; Sanders, J. M.; Akiyama, N.; Shoji, M.; Postila, P.; Pentikäinen, O. T.; Sasaki, M.; Sakai, R.; Swanson, G. T. *Journal of Pharmacology and Experimental Therapeutics* **2008**, *324*, 484.

(25) Sasaki, M.; Maruyama, T.; Sakai, R.; Tachibana, K. *Tetrahedron Letters* **1999**, *40*, 3195.

(26) Frydenvang, K.; Lash, L. L.; Naur, P.; Postila, P. A.; Pickering, D. S.; Smith, C. M.; Gajhede, M.; Sasaki, M.; Sakai, R.; Pentikaïnen, O. T.; Swanson, G. T.; Kastrup, J. S. *The Journal of Biological Chemistry* **2009**, *284*, 14219.

(27) Cachet, X.; Poree, F.-H. *RSC Advances* **2013**, *3*, 12466.

(28) Snider, B. B.; Hawryluk, N. A. *Organic Letters* **2000**, *2*, 635.

(29) Masaki, H.; Maeyama, J.; Kamada, K.; Esumi, T.; Iwabuchi, Y.; Hatakeyama, S. *Journal of the American Chemical Society* **2000**, *122*, 5216.

(30) Phillips, D.; Chamberlin, A. R. *The Journal of Organic Chemistry* **2002**, *67*, 3194.

(31) Sasaki, M.; Tsubone, K.; Aoki, K.; Akiyama, N.; Shoji, M.; Oikawa, M.; Sakai, R.; Shimamoto, K. *The Journal of Organic Chemistry* **2008**, *73*, 264.

(32) Celindro, N. C.; Kim, T. W.; Kang, S. H. *Chemical Communications* **2012**, *48*, 6295.

(33) Schaus, S. E.; Brandes, B. D.; Larrow, J. F.; Tokunaga, M.; Hansen, K. B.; Gould, A. E.; Furrow, M. E.; Jacobsen, E. N. *Journal of the American Chemical Society* **2002**, *124*, 1307.

(34) Khrimian, A.; Klun, J. A.; Hijji, Y.; Baranchikov, Y. N.; Pet'ko, V. M.; Mastro, V. C.; Kramer, M. H. *Journal of Agricultural and Food Chemistry* **2002**, *50*, 6366.

(35) Suzuki, T.; Sato, O.; Hirama, M. *Tetrahedron Letters* **1990**, *31*, 4747.

(36) Brimble, M. A.; Nairn, M. R. *The Journal of Organic Chemistry* **1996**, *61*, 4801.

(37) Woodward, R. B.; Brutcher, F. V. *Journal of the American Chemical Society* **1958**, *80*, 209.

(38) Cambie, R. C.; Chambers, D.; Lindsay, B. G.; Rutledge, P. S.; Woodgate, P. D. *Journal of the Chemical Society, Perkin Transactions 1* **1980**, 822.

(39) Macdonald, T. L.; Narasimhan, N.; Burka, L. T. *Journal of the American Chemical Society* **1980**, *102*, 7760.

(40) Martin, S. F.; Dodge, J. A. *Tetrahedron Letters* **1991**, *32*, 3017.

(41) Schwardt, O.; Koliwer-Brandl, H.; Zimmerli, R.; Mesch, S.; Rossato, G.; Spreafico, M.; Vedani, A.; Kelm, S.; Ernst, B. *Bioorganic & Medicinal Chemistry* **2010**, *18*, 7239.

(42) Takeuchi, H.; Shiobara, Y.; Mitani, M.; Koyama, K. *Journal of the Chemical Society, Chemical Communications* **1985**, 1251.

(43) Bhanu Prasad, B. A.; Sekar, G.; Singh, V. K. *Tetrahedron Letters* **2000**, *41*, 4677.

(44) Ferraris, D.; Drury, W. J.; Cox, C.; Lectka, T. *The Journal of Organic Chemistry* **1998**, *63*, 4568.

(45) Burk, M. J.; Allen, J. G.; Kiesman, W. F. *Journal of the American Chemical Society* **1998**, *120*, 657.

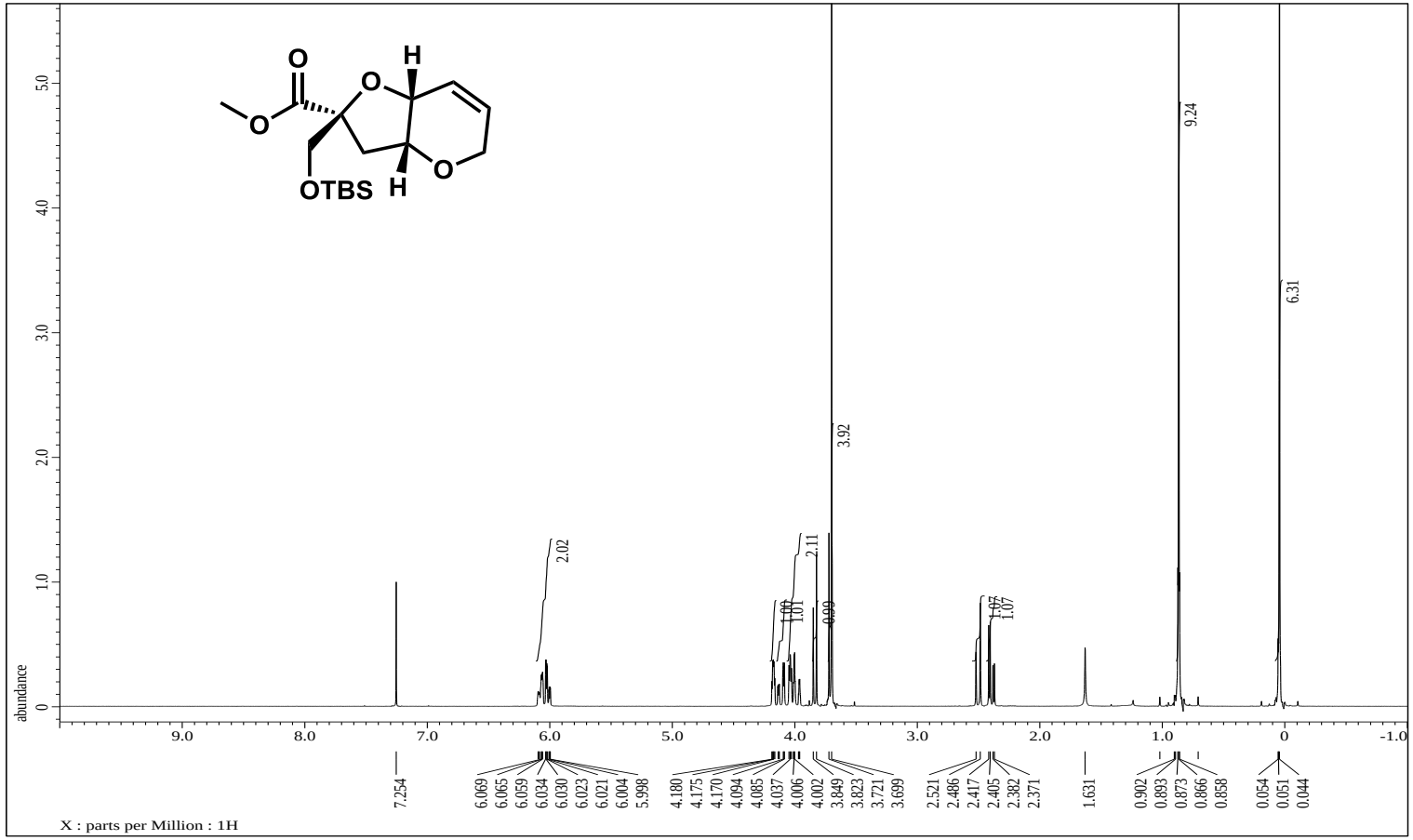

Figure 1.11. ^{1}H NMR (400 MHz, $CDCl_3$) of Methyl (2*S*,3a*R*,7a*R*)-2-(((*tert*-butyldimethylsilyl)oxy)methyl)-3,3a,5,7a-tetrahydro-2*H*-furo[3,2-*b*]pyran-2-carboxylate (**1.44**)

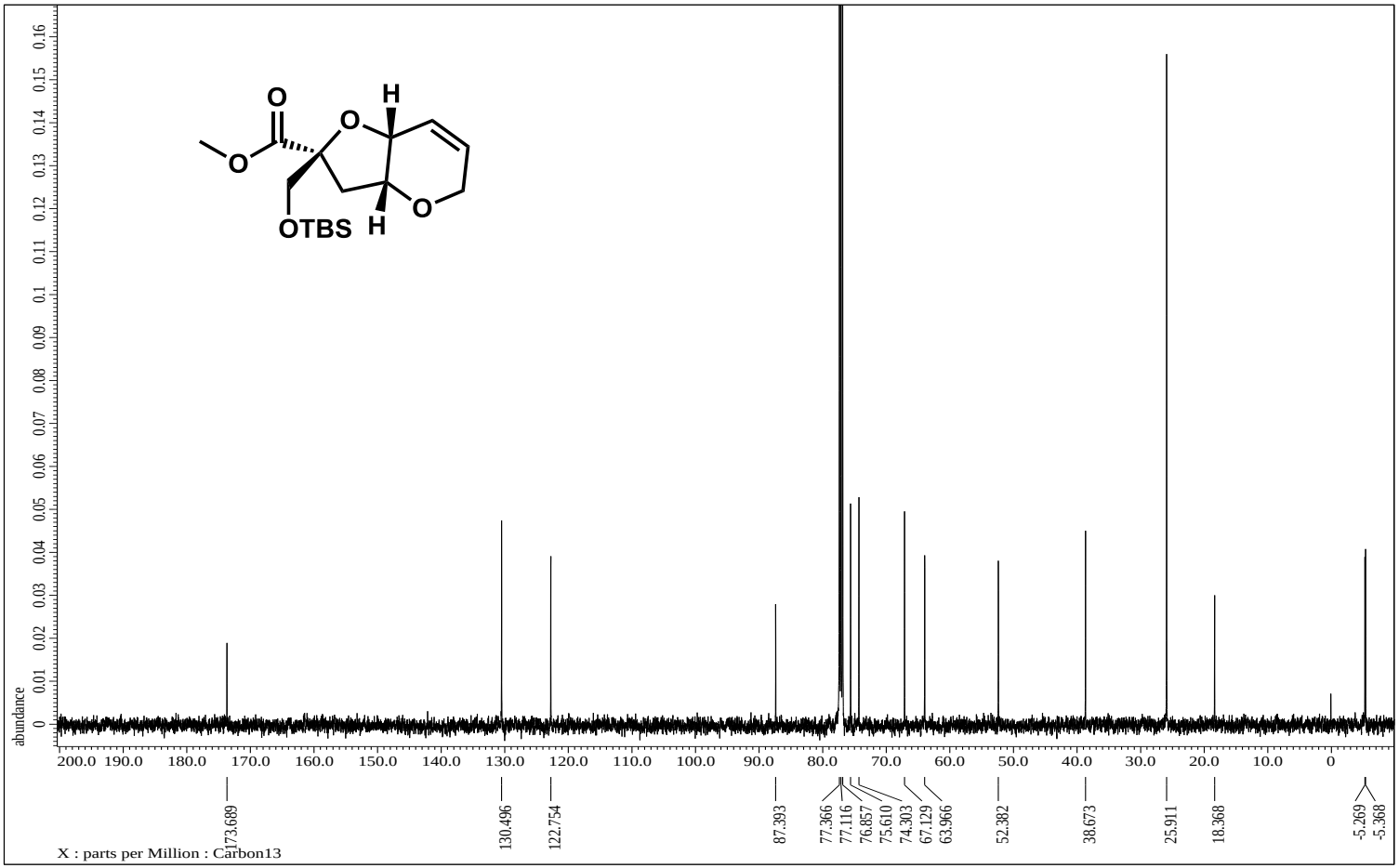

Figure 1.12. ^{13}C NMR (101 MHz, $CDCl_3$) of Methyl (2*S*,3a*R*,7a*R*)-2-(((*tert*-butyldimethylsilyl)oxy)methyl)-3,3a,5,7a-tetrahydro-2*H*-furo[3,2-*b*]pyran-2-carboxylate (**1.44**)

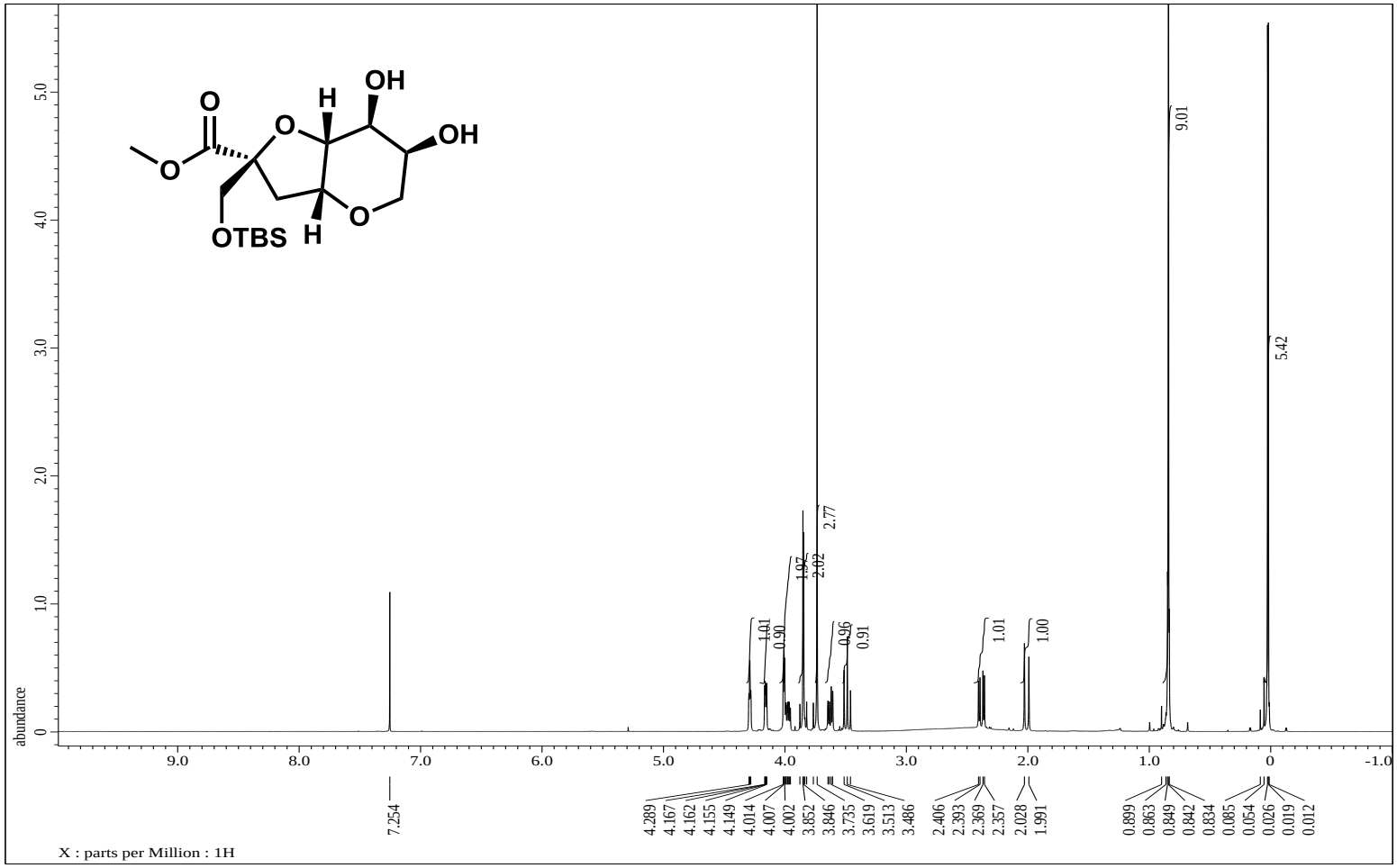

Figure 1.13. ^{1}H NMR (400 MHz, $CDCl_3$) of Methyl (2*S*,3a*R*,6*S*,7*S*,7a*R*)-2-(((*tert*-butyldimethylsilyl)oxy)methyl)-6,7-dihydroxyhexahydro-2*H*-furo[3,2-*b*]pyran-2-carboxylate (**1.45**)

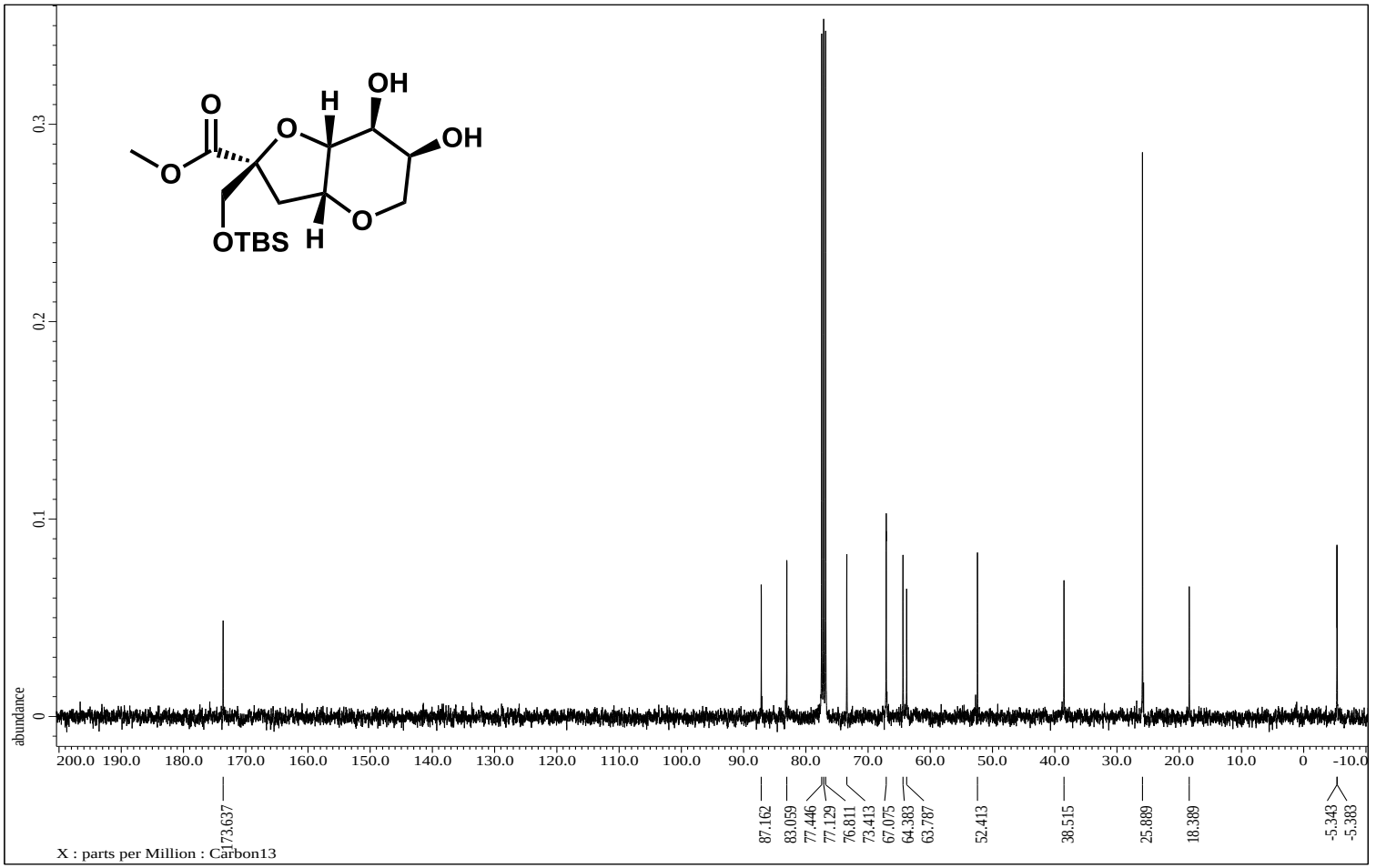

Figure 1.14. ^{13}C NMR (101 MHz, $CDCl_3$) of Methyl (2*S*,3a*R*,6*S*,7*S*,7a*R*)-2-(((*tert*-butyldimethylsilyl)oxy)methyl)-6,7-dihydroxyhexahydro-2*H*-furo[3,2-*b*]pyran-2-carboxylate (**1.45**)

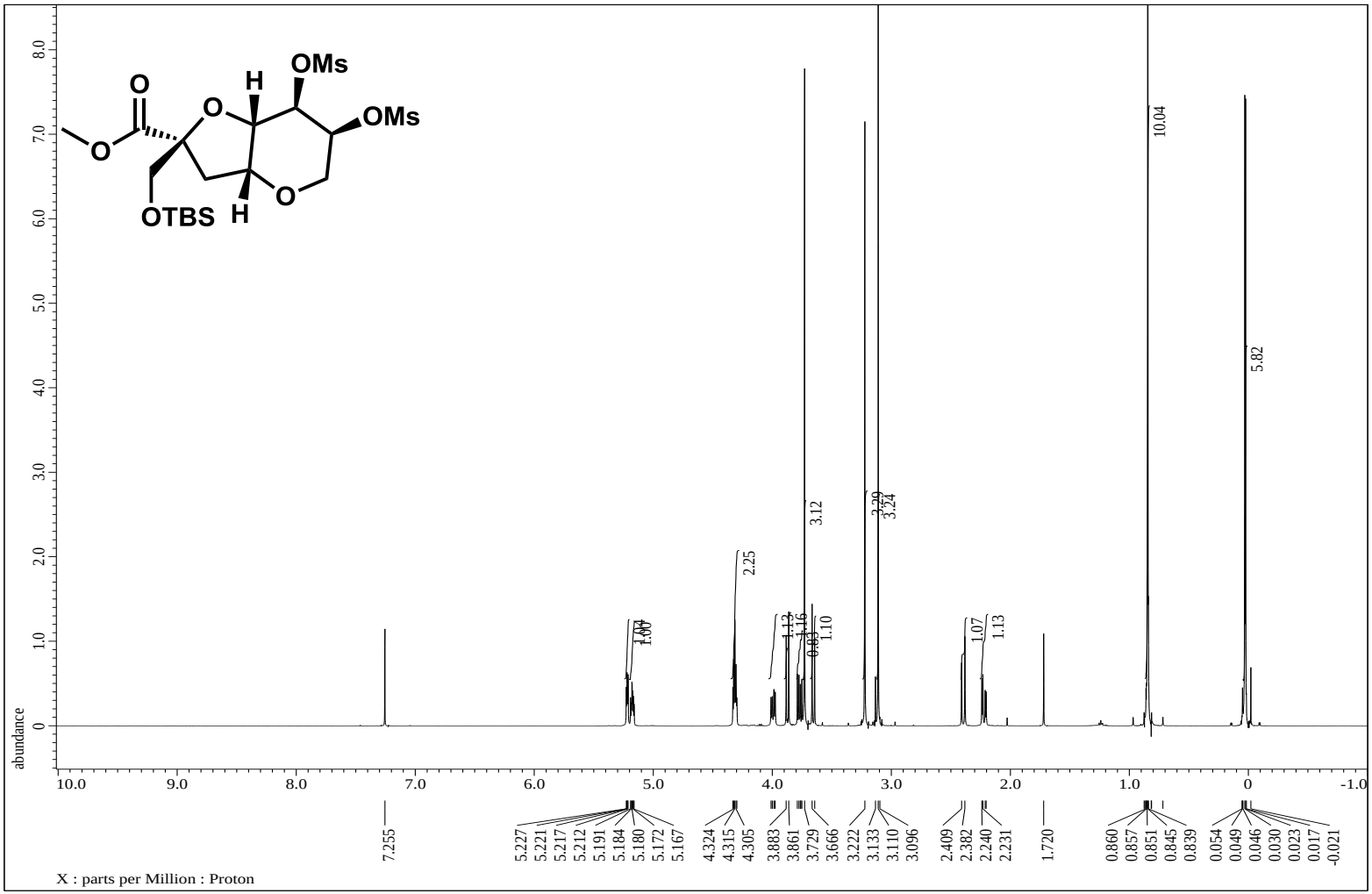

Figure 1.15. ^{1}H NMR (500 MHz, $CDCl_3$) of Methyl (2*S*,3a*R*,6*S*,7*R*,7a*S*)-2-(((*tert*-butyldimethylsilyl)oxy)methyl)-6,7-bis((methylsulfonyl)oxy)hexahydro-2*H*-furo[3,2-*b*]pyran-2-carboxylate (**1.49**)

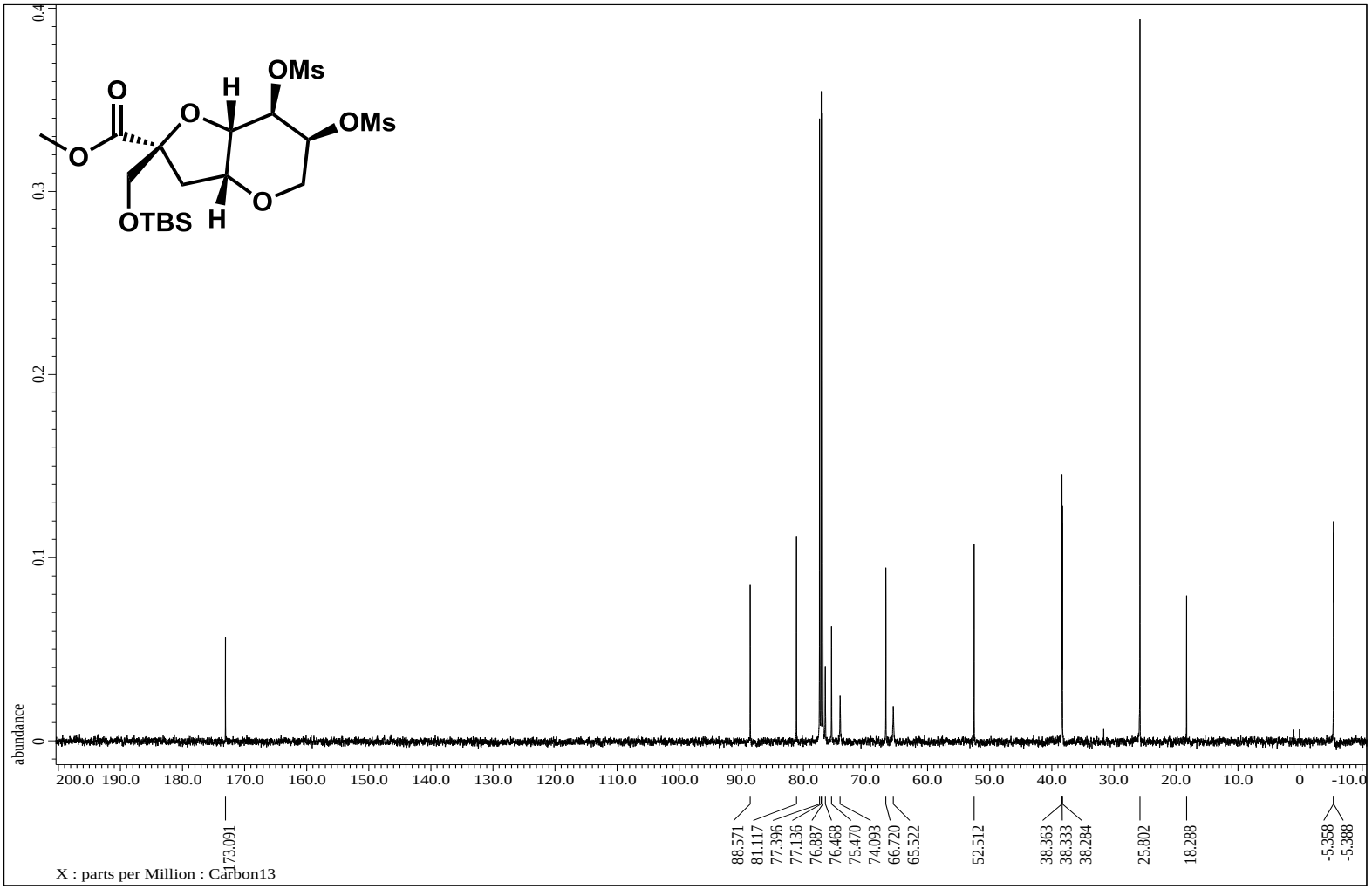

Figure 1.16. ^{13}C NMR (126 MHz, $CDCl_3$) of Methyl (2*S*,3a*R*,6*S*,7*R*,7a*S*)-2-(((*tert*-butyldimethylsilyl)oxy)methyl)-6,7-bis((methylsulfonyl)oxy)hexahydro-2*H*-furo[3,2-*b*]pyran-2-carboxylate (**1.49**)

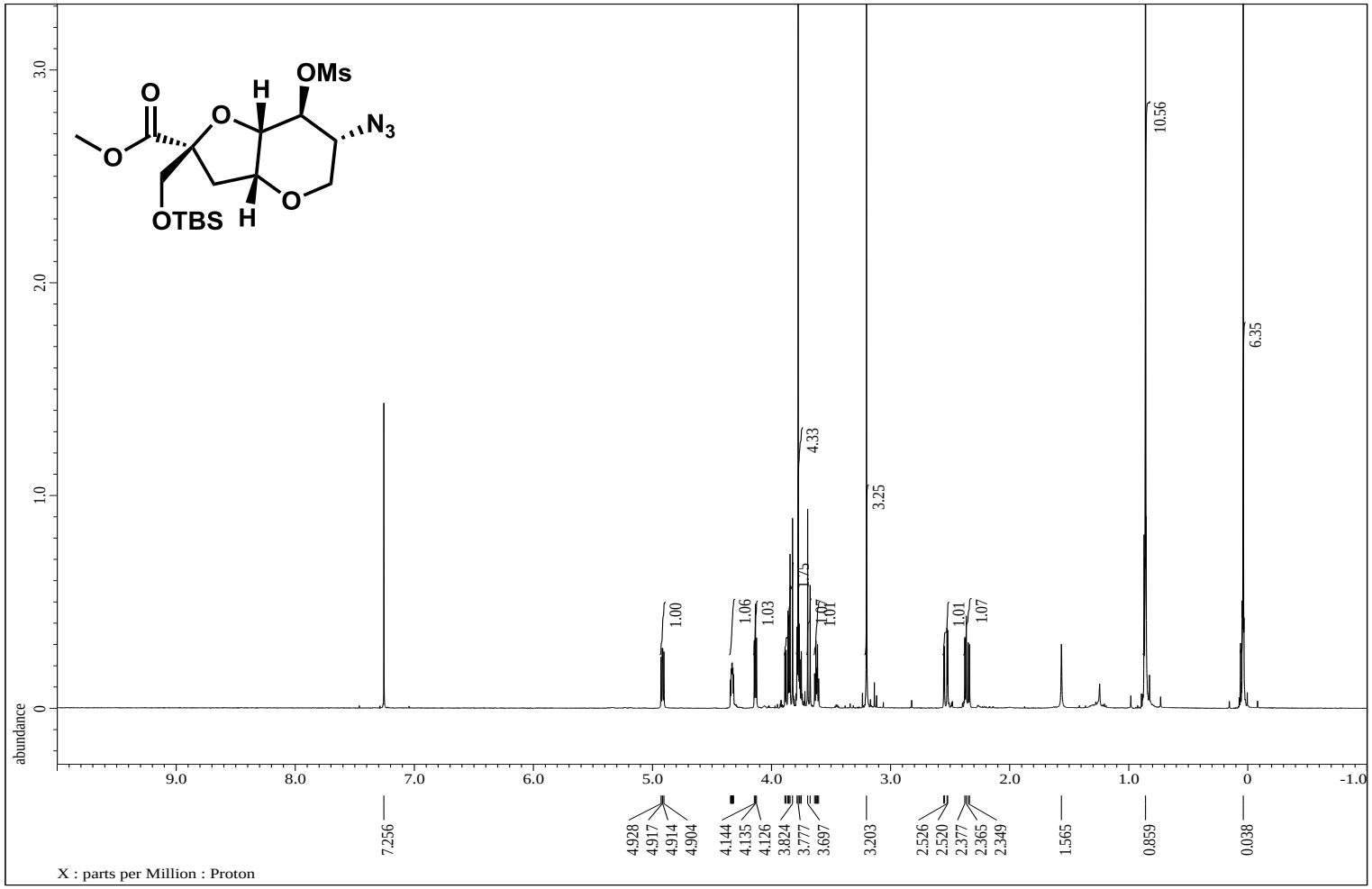

Figure 1.17. ^{1}H NMR (500 MHz, $CDCl_3$) of Methyl (2*S*,3a*R*,6*R*,7*S*,7a*S*)-6-azido-2-(((*tert*-butyldimethylsilyl)oxy)methyl)-7-((methylsulfonyl)oxy)hexahydro-2*H*-furo[3,2-*b*]pyran-2-carboxylate (**1.50**)

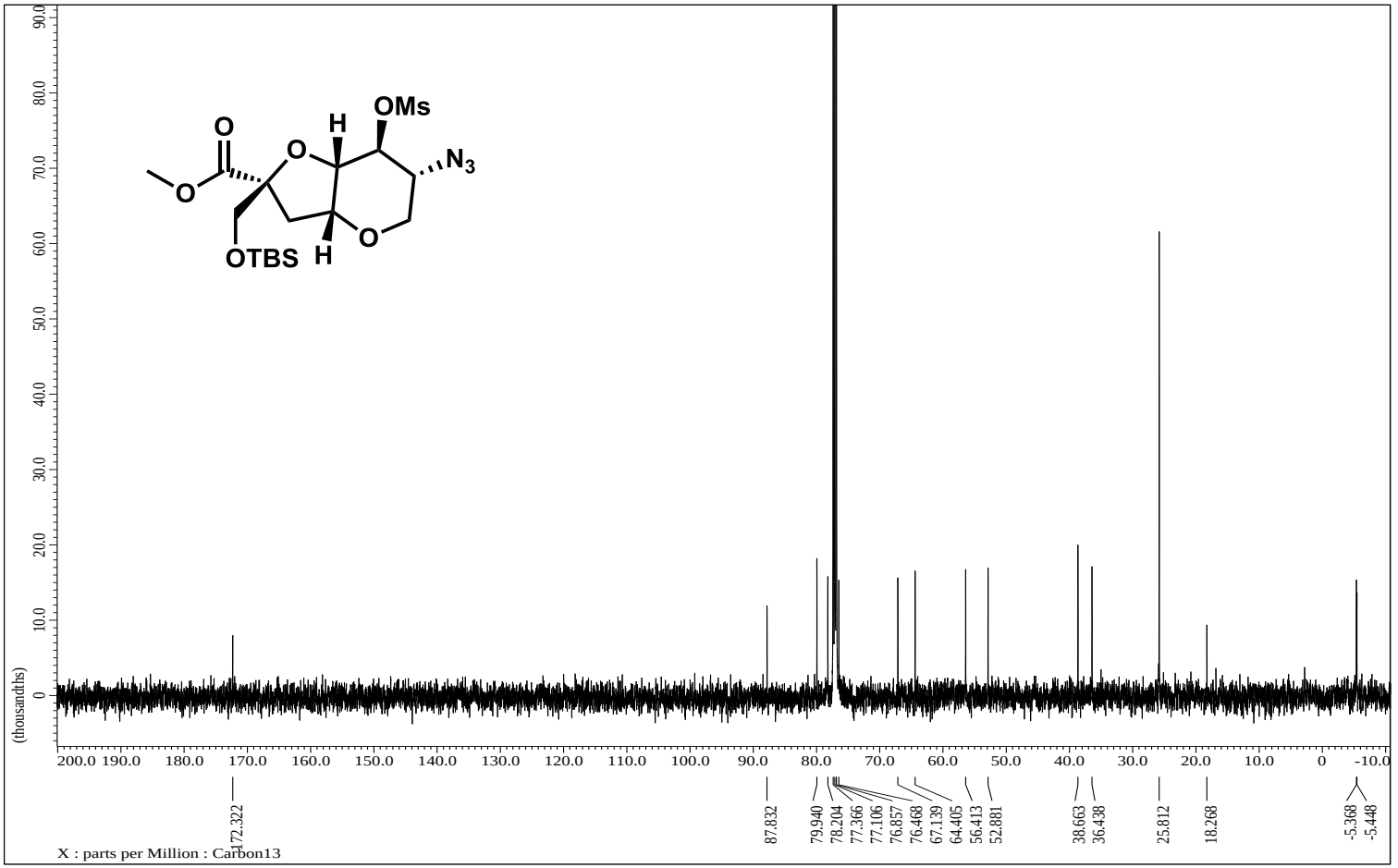

Figure 1.18. ^{13}C NMR (126 MHz, $CDCl_3$) of Methyl (2*S*,3a*R*,6*R*,7*S*,7a*S*)-6-azido-2-(((*tert*-butyldimethylsilyl)oxy)methyl)-7-((methylsulfonyl)oxy)hexahydro-2*H*-furo[3,2-*b*]pyran-2-carboxylate (**1.50**)

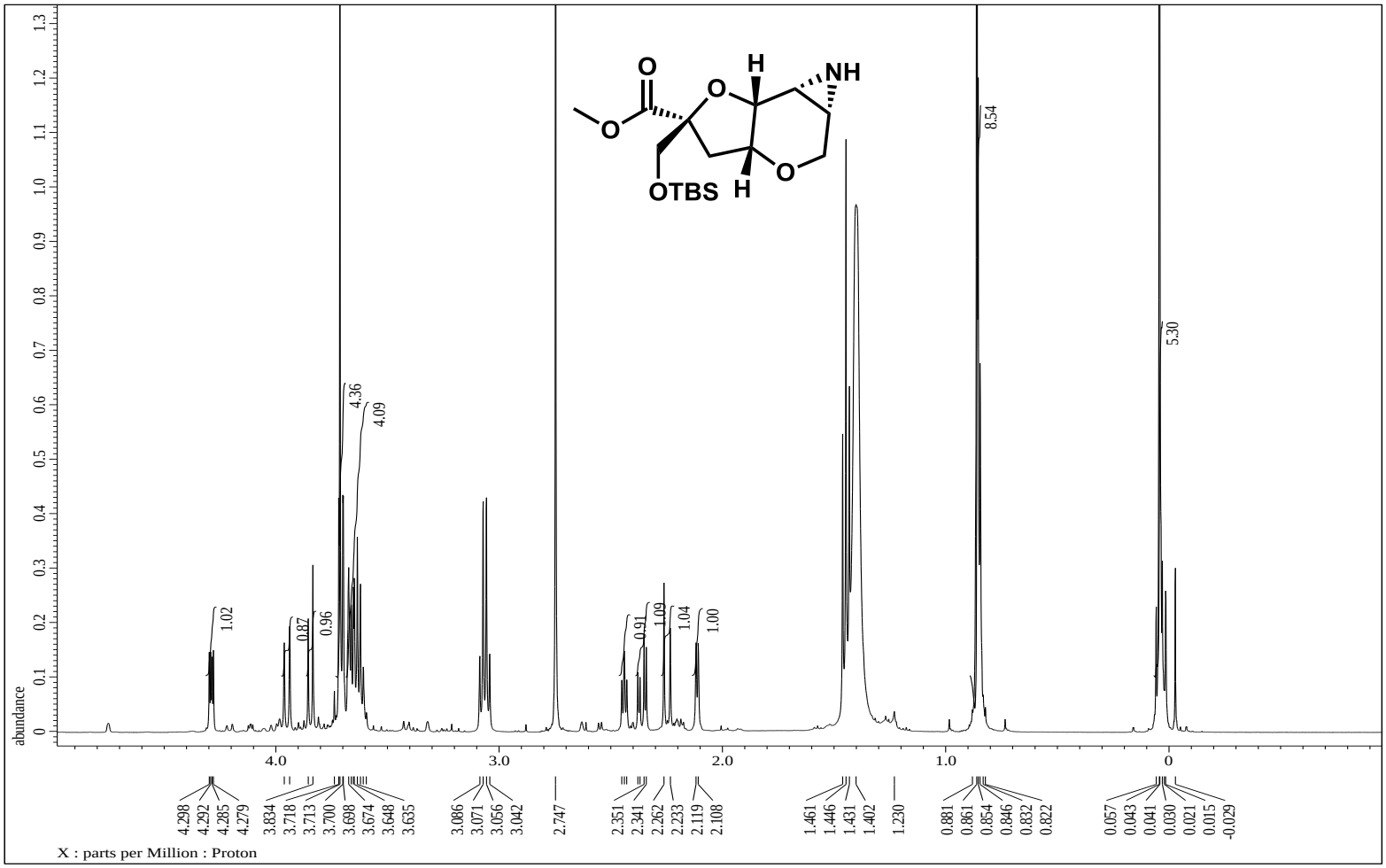

Figure 1.19. Crude ^{1}H NMR (500 MHz, $CDCl_3$) of Methyl (1a*S*,3a*R*,5*S*,6a*R*,6b*R*)-5-(((*tert*-butyldimethylsilyl)oxy)methyl)octahydrofuro[2',3':5,6]pyrano[3,4-*b*]azirine-5-carboxylate (**1.51**)

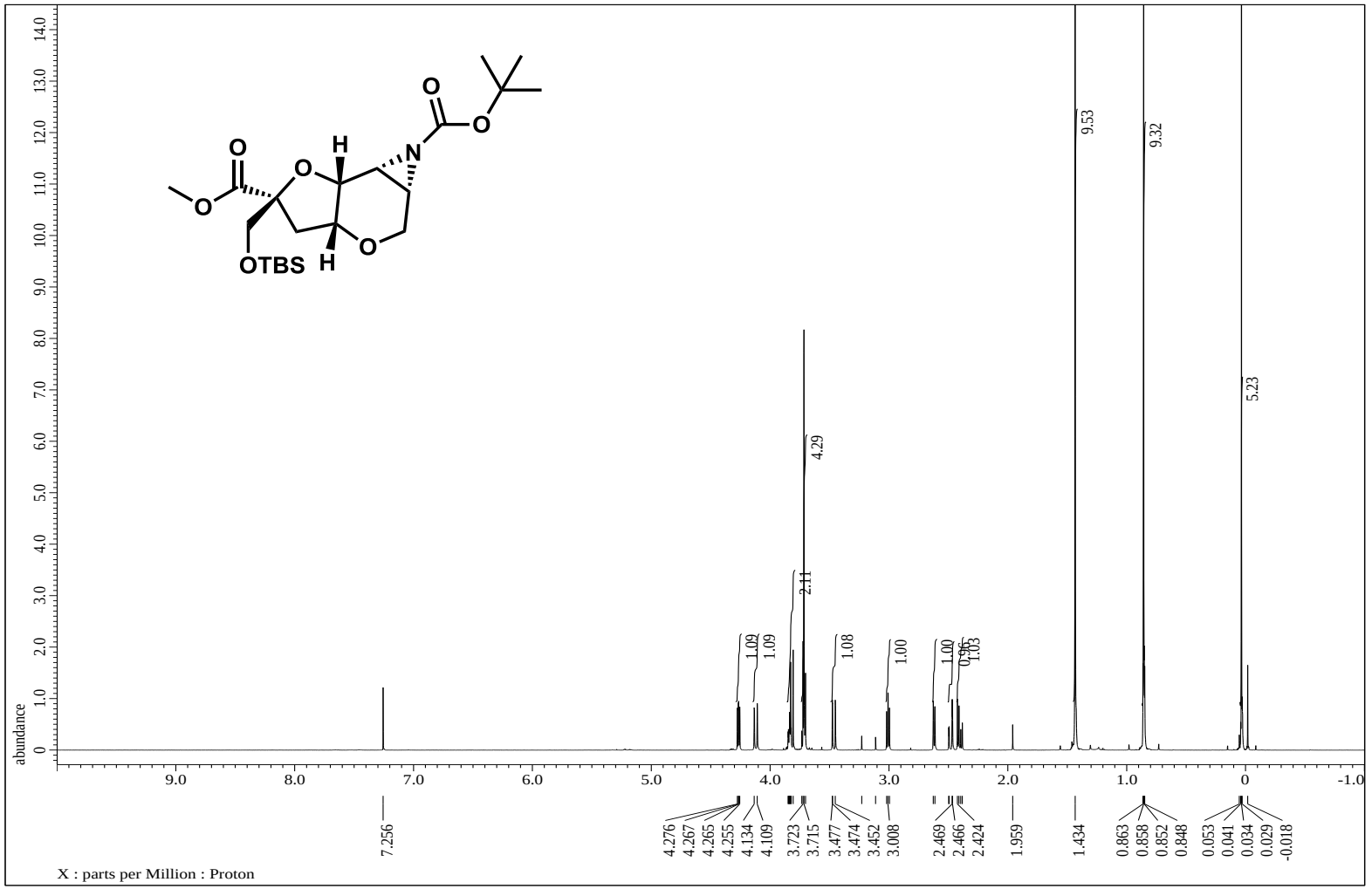

Figure 1.20. ^{1}H NMR (500 MHz, $CDCl_3$) of 1-(*tert*-butyl) 5-methyl (1a*S*,3a*R*,5*S*,6a*R*,6b*R*)-5-(((*tert*-butyldimethylsilyl)oxy)methyl)hexahydrofuro[2',3':5,6]pyrano[3,4-*b*]azirine-1,5(2*H*)-dicarboxylate (**1.52**)

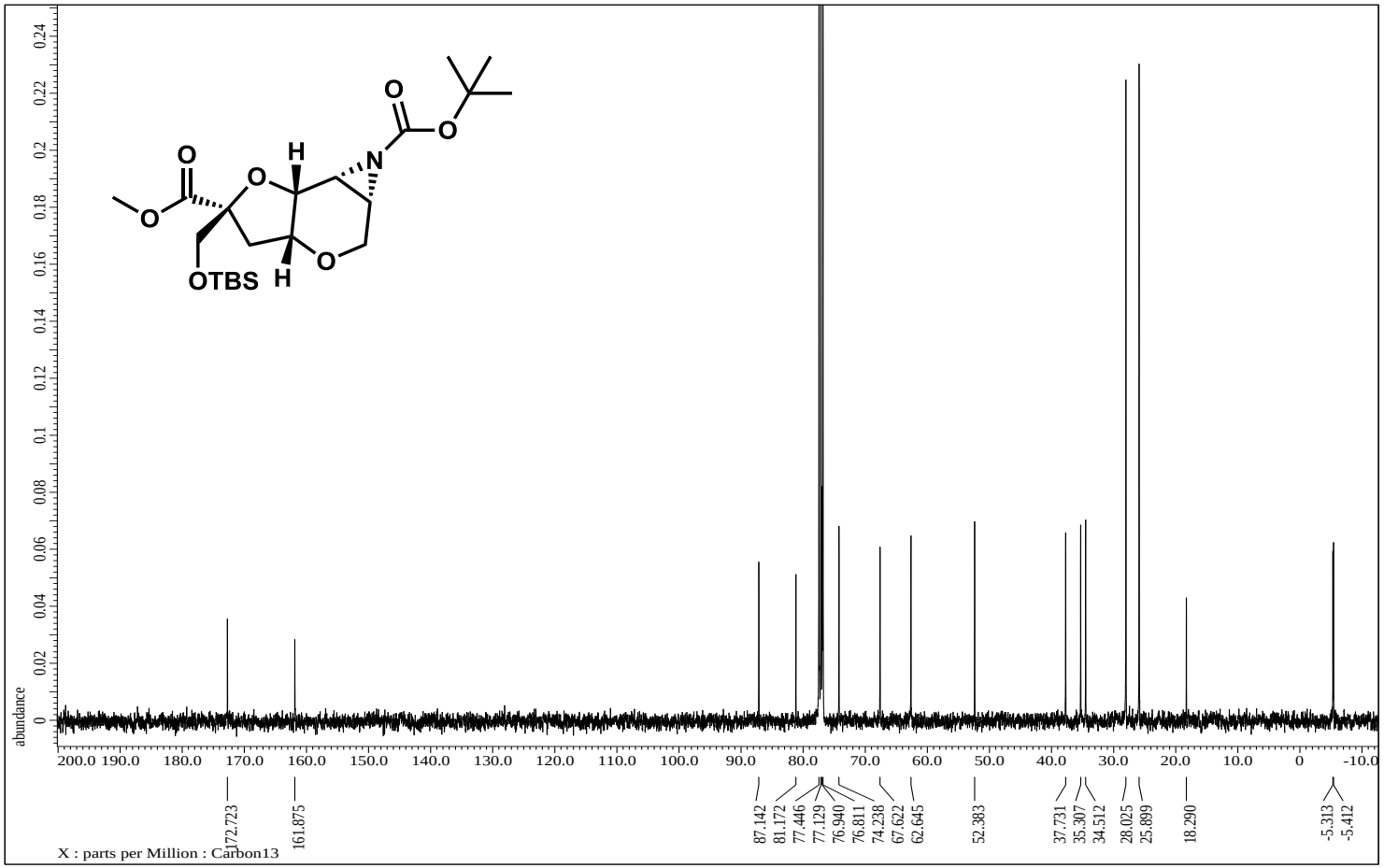

Figure 1.21. ^{13}C NMR (126 MHz, $CDCl_3$) of 1-(*tert*-butyl) 5-methyl (1a*S*,3a*R*,5*S*,6a*R*,6b*R*)-5-(((*tert*-butyldimethylsilyl)oxy)methyl)hexahydrofuro[2',3':5,6]pyrano[3,4-*b*]azirine-1,5(2*H*)-dicarboxylate (**1.52**)

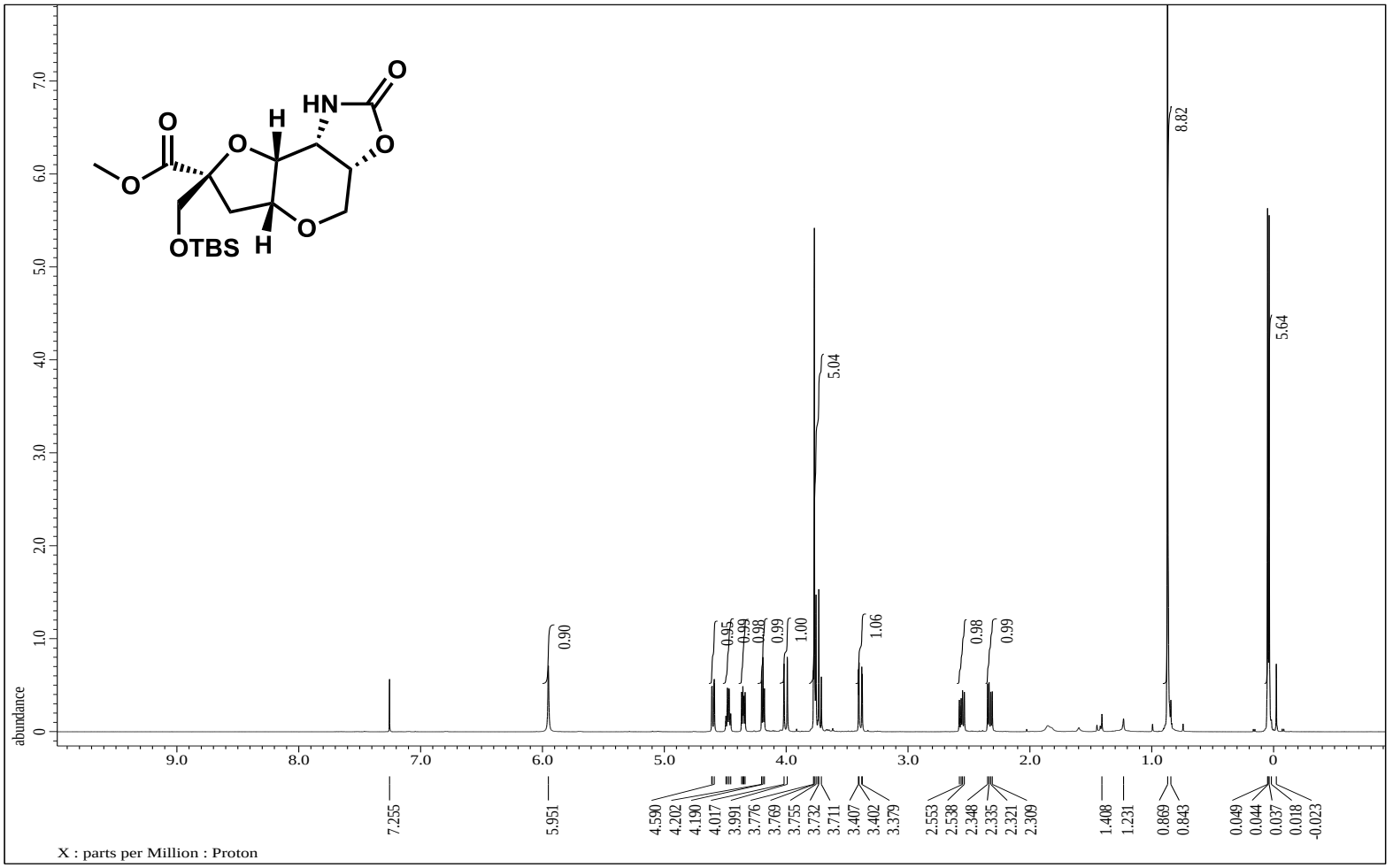

Figure 1.22. ^{1}H NMR (500 MHz, $CDCl_3$) of Methyl (3a*S*,5a*R*,7*S*,8a*R*,8b*R*)-7-(((*tert*-butyldimethylsilyl)oxy)methyl)-2-oxooctahydro-2*H*-furo[2',3':5,6]pyrano[4,3-*d*]oxazole-7-carboxylate (**1.53**)

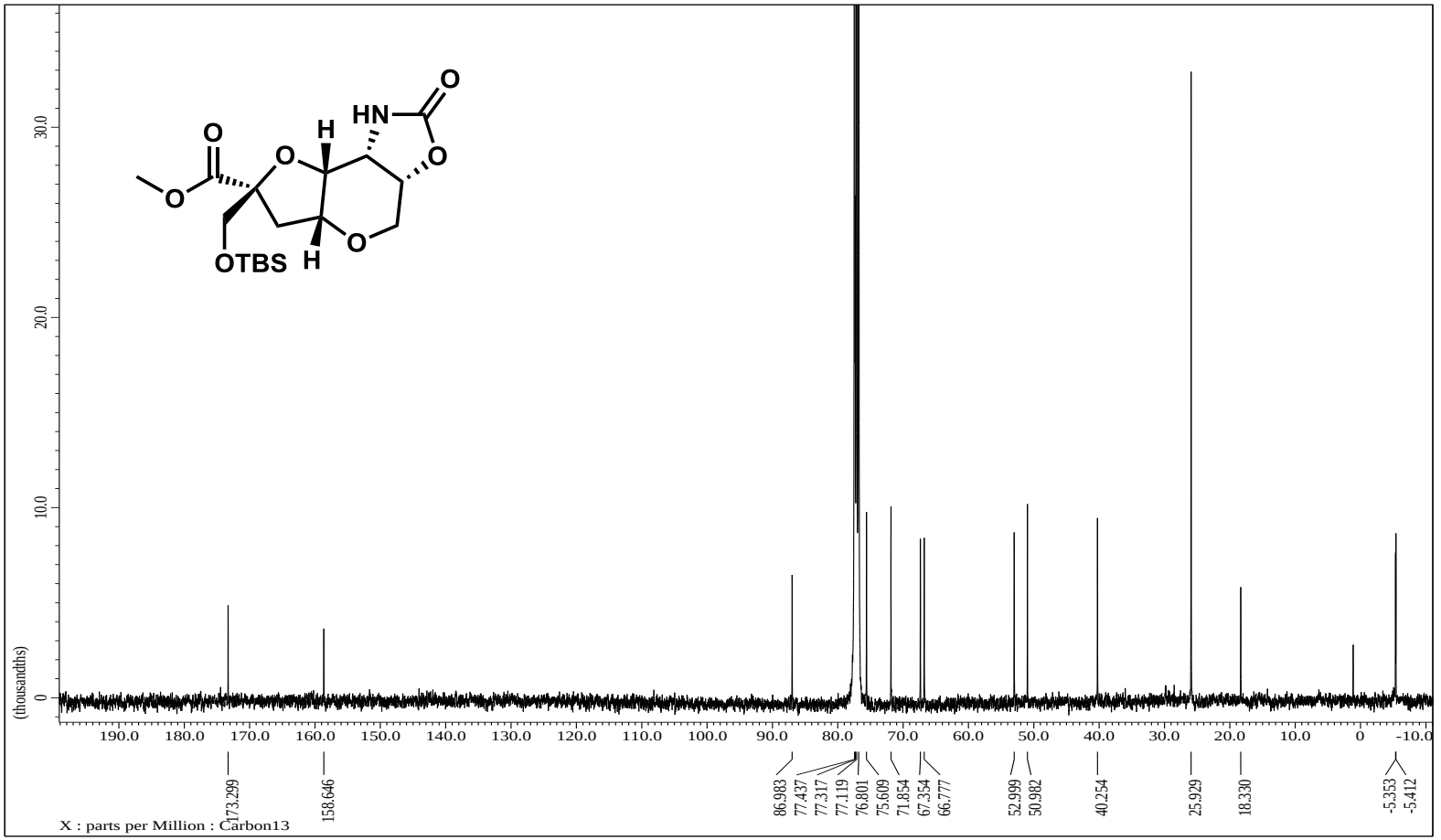

Figure 1.23. ^{13}C NMR (126 MHz, $CDCl_3$) of Methyl (3a*S*,5a*R*,7*S*,8a*R*,8b*R*)-7-(((*tert*-butyldimethylsilyl)oxy)methyl)-2-oxooctahydro-2*H*-furo[2',3':5,6]pyrano[4,3-*d*]oxazole-7-carboxylate (**1.53**)

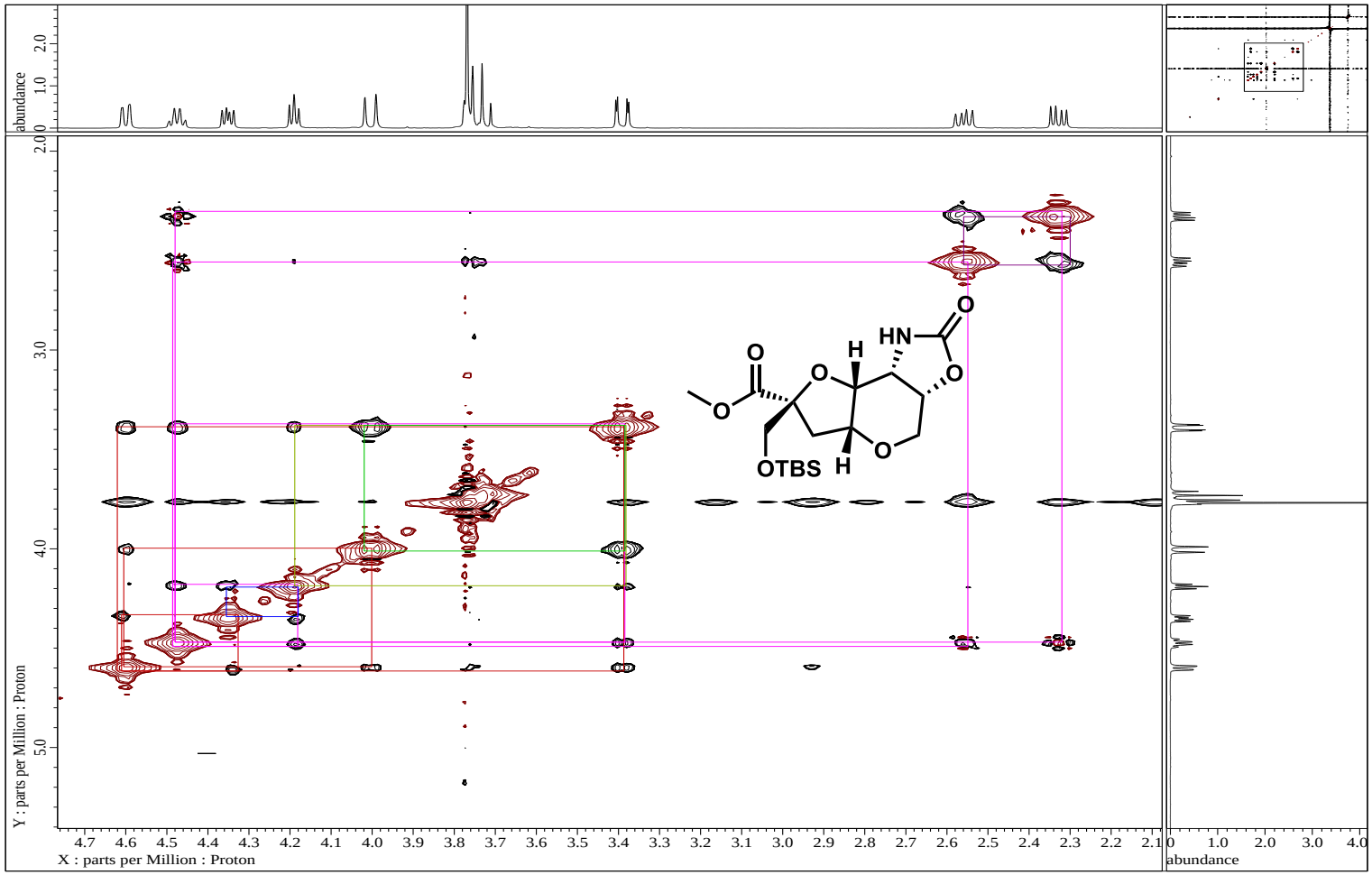

Figure 1.24. NOESY NMR (500 MHz, $CDCl_3$) of Methyl (3a*S*,5a*R*,7*S*,8a*R*,8b*R*)-7-(((*tert*-butyldimethylsilyl)oxy)methyl)-2-oxooctahydro-2*H*-furo[2',3':5,6]pyrano[4,3-*d*]oxazole-7-carboxylate (**1.53**)

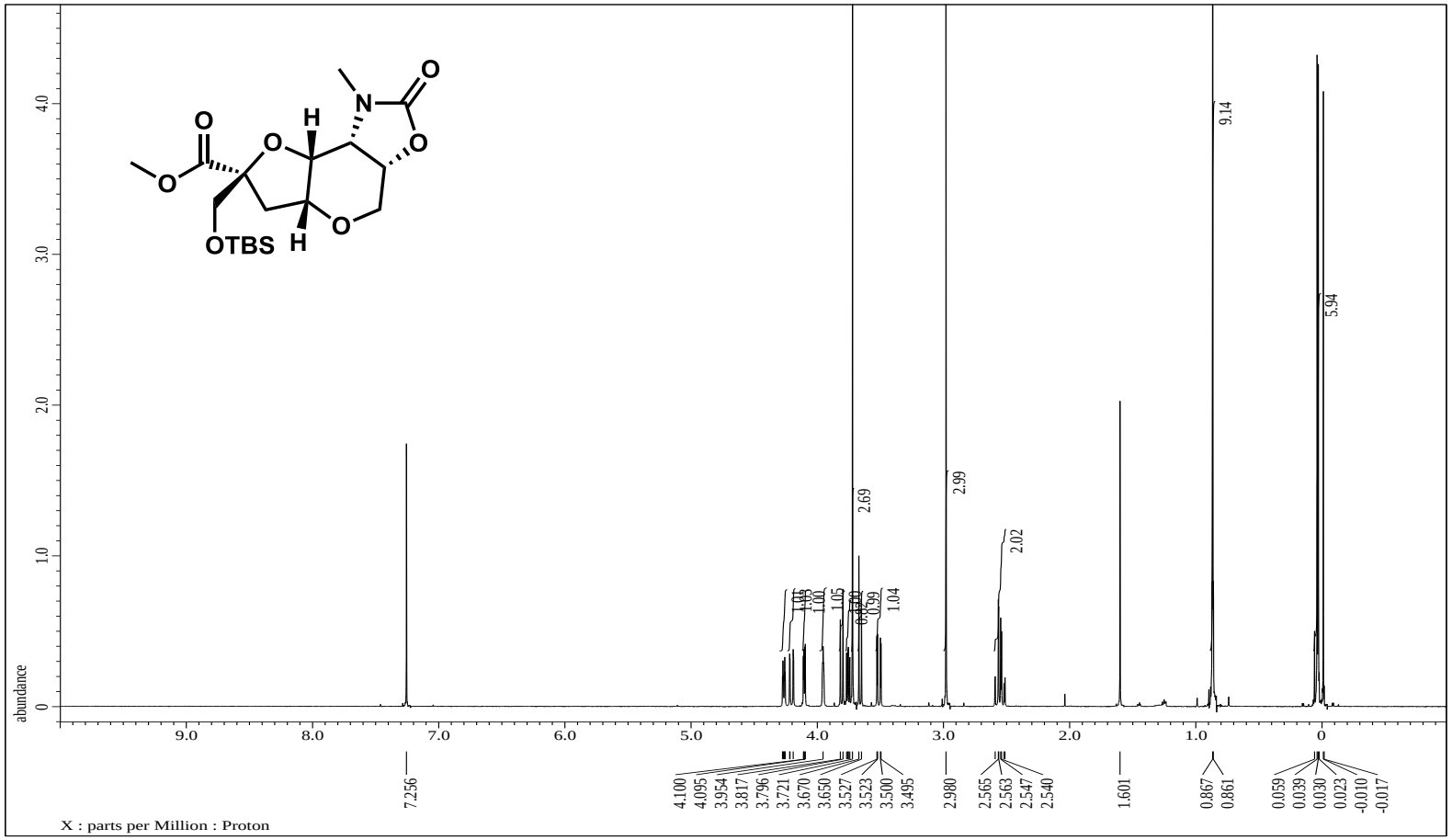

Figure 1.25. ^{1}H NMR (500 MHz, $CDCl_3$) of Methyl (3a*S*,5a*R*,7*S*,8a*R*,8b*R*)-7-(((*tert*-butyldimethylsilyl)oxy)methyl)-1-methyl-2-oxooctahydro-2*H*-furo[2',3':5,6]pyrano[4,3-*d*]oxazole-7-carboxylate (**1.54**)

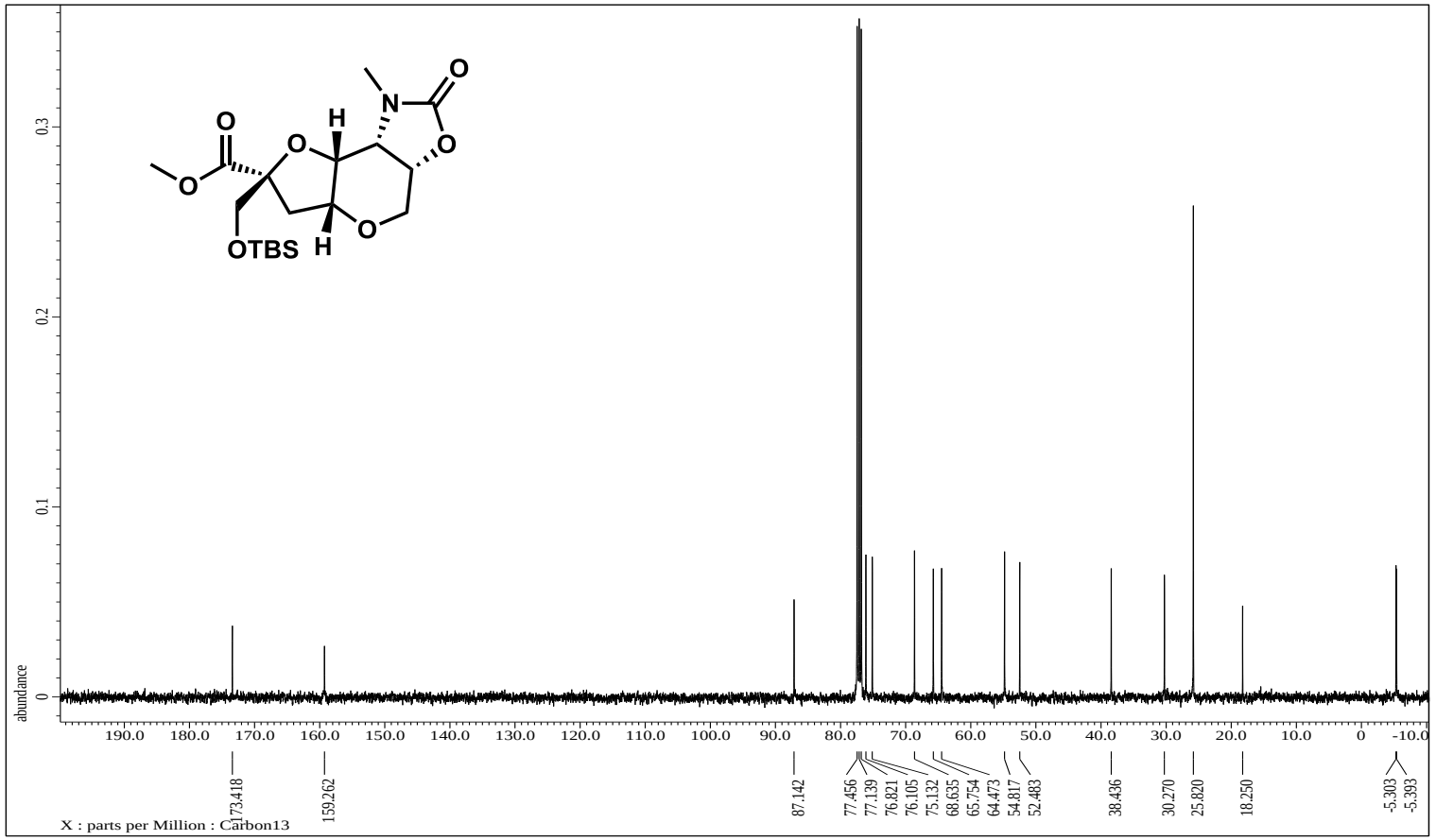

Figure 1.26. ^{13}C NMR (101 MHz, $CDCl_3$) of Methyl (3a*S*,5a*R*,7*S*,8a*R*,8b*R*)-7-(((*tert*-butyldimethylsilyl)oxy)methyl)-1-methyl-2-oxooctahydro-2*H*-furo[2',3':5,6]pyrano[4,3-*d*]oxazole-7-carboxylate (**1.54**)

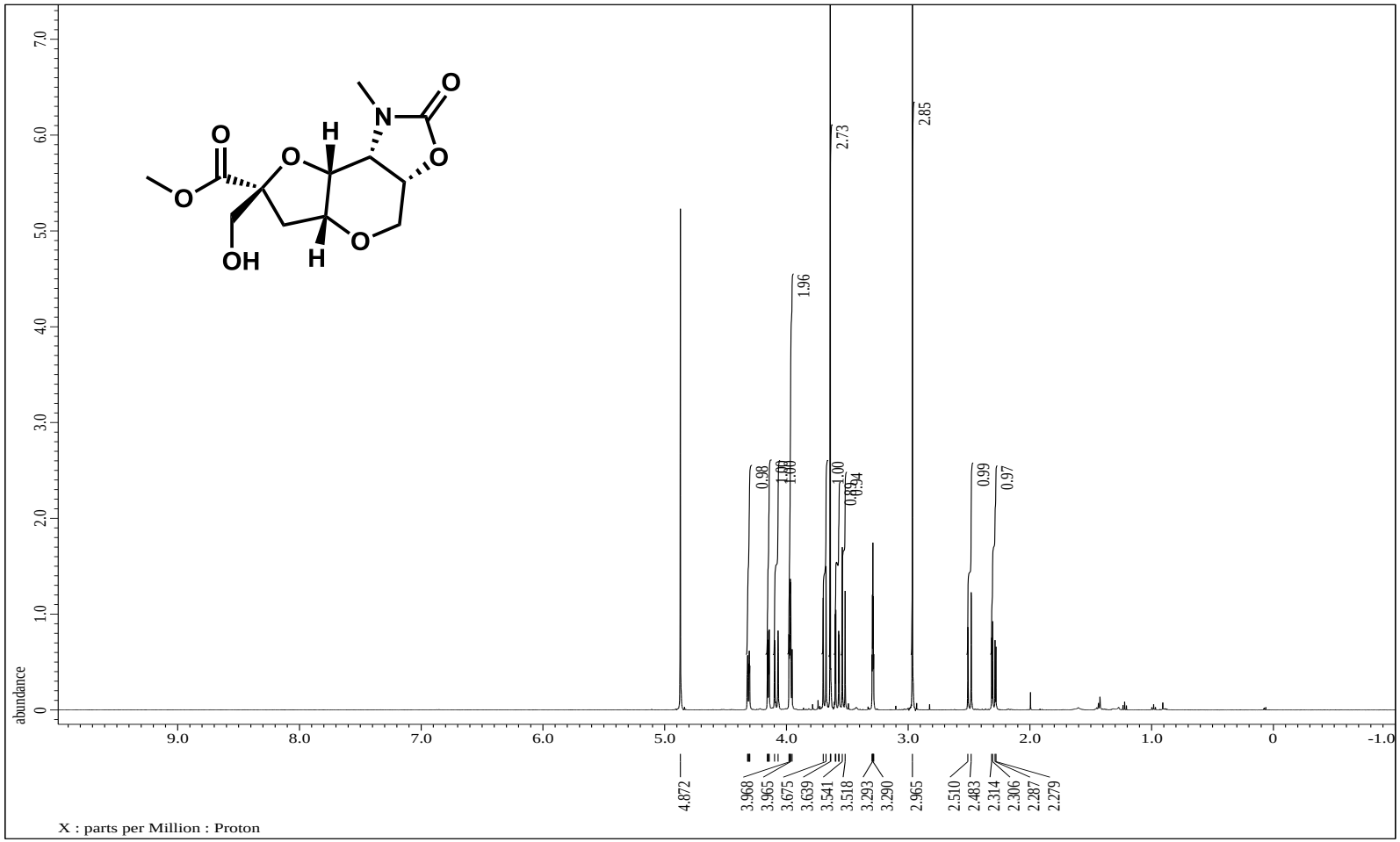

Figure 1.27. ^{1}H NMR (500 MHz, CD_3OD) of Methyl (3a*S*,5a*R*,7*S*,8a*R*,8b*R*)-7-(hydroxymethyl)-1-methyl-2-oxooctahydro-2*H*-furo[2',3':5,6]pyrano[4,3-*d*]oxazole-7-carboxylate (**1.55**)

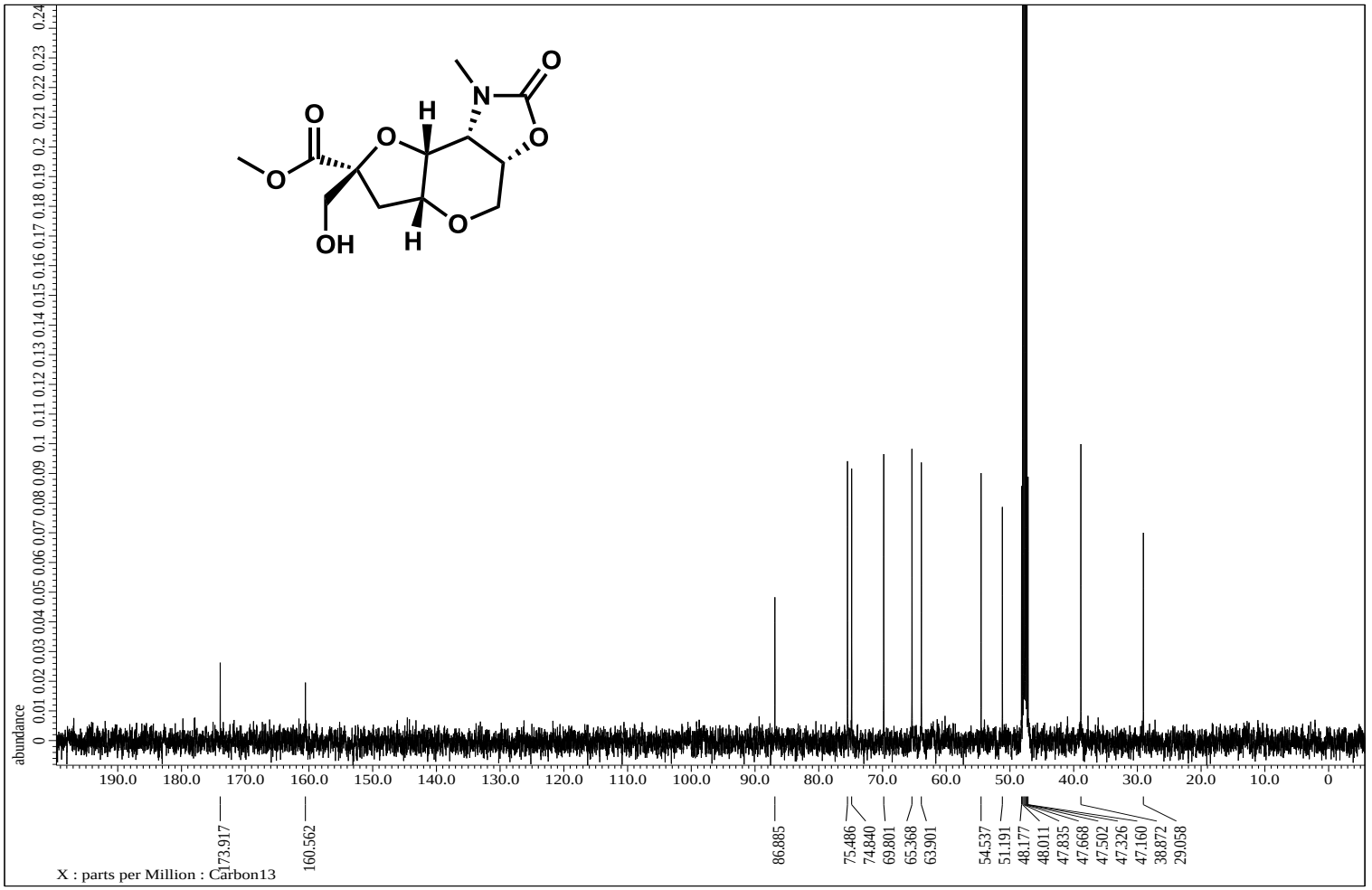

Figure 1.28. ^{13}C NMR (101 MHz, CD_3OD) of Methyl (3a*S*,5a*R*,7*S*,8a*R*,8b*R*)-7-(hydroxymethyl)-1-methyl-2-oxooctahydro-2*H*-furo[2',3':5,6]pyrano[4,3-*d*]oxazole-7-carboxylate (**1.55**)

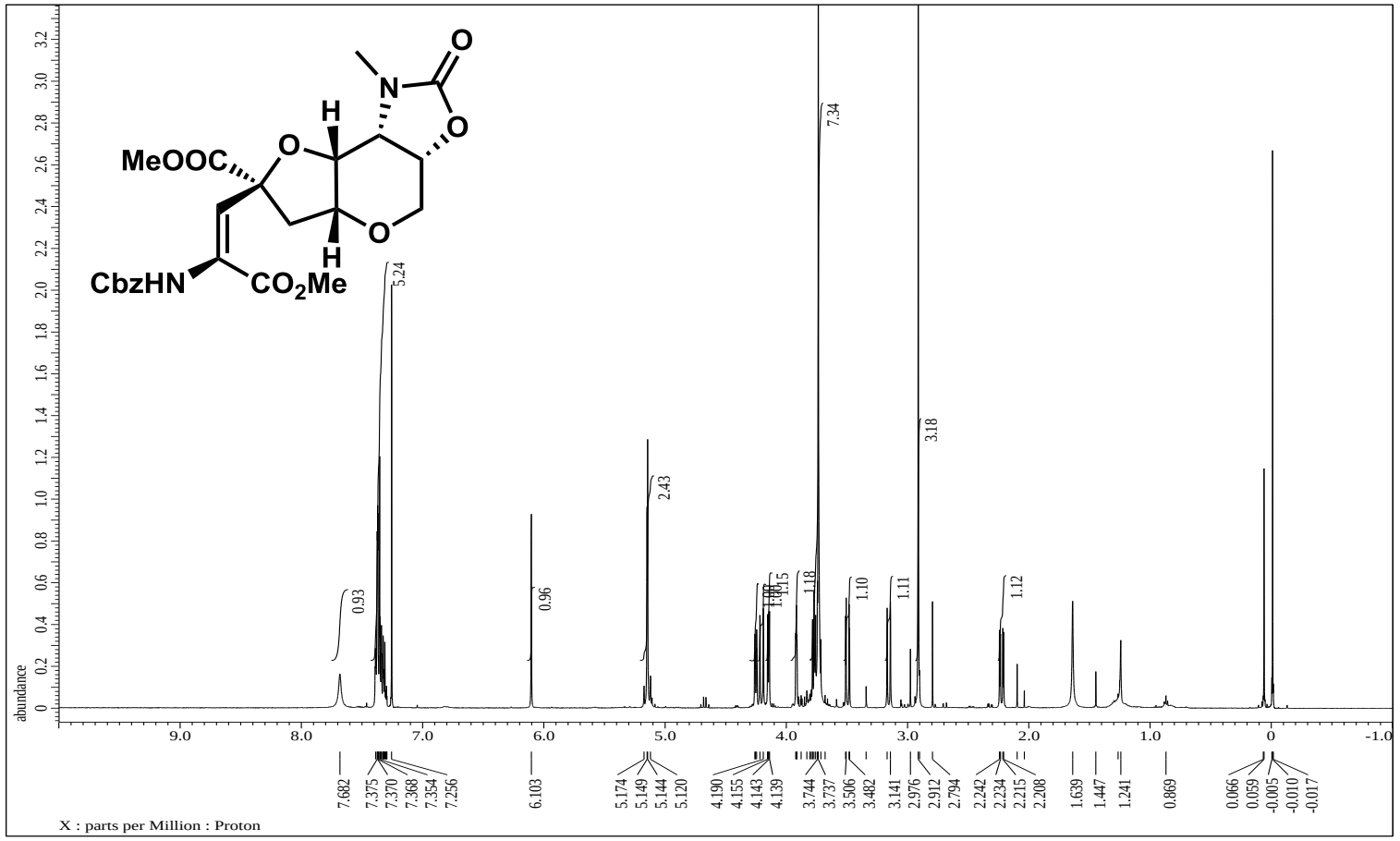

Figure 1.29. ^{1}H NMR (500 MHz, $CDCl_3$) of Methyl (3a*S*,5a*R*,7*S*,8a*R*,8b*R*)-7-((*E*)-2-(((benzyloxy)carbonyl)amino)-3-methoxy-3-oxoprop-1-en-1-yl)-1-methyl-2-oxooctahydro-2*H*-furo[2',3':5,6]pyrano[4,3-*d*]oxazole-7-carboxylate (**1.58**)

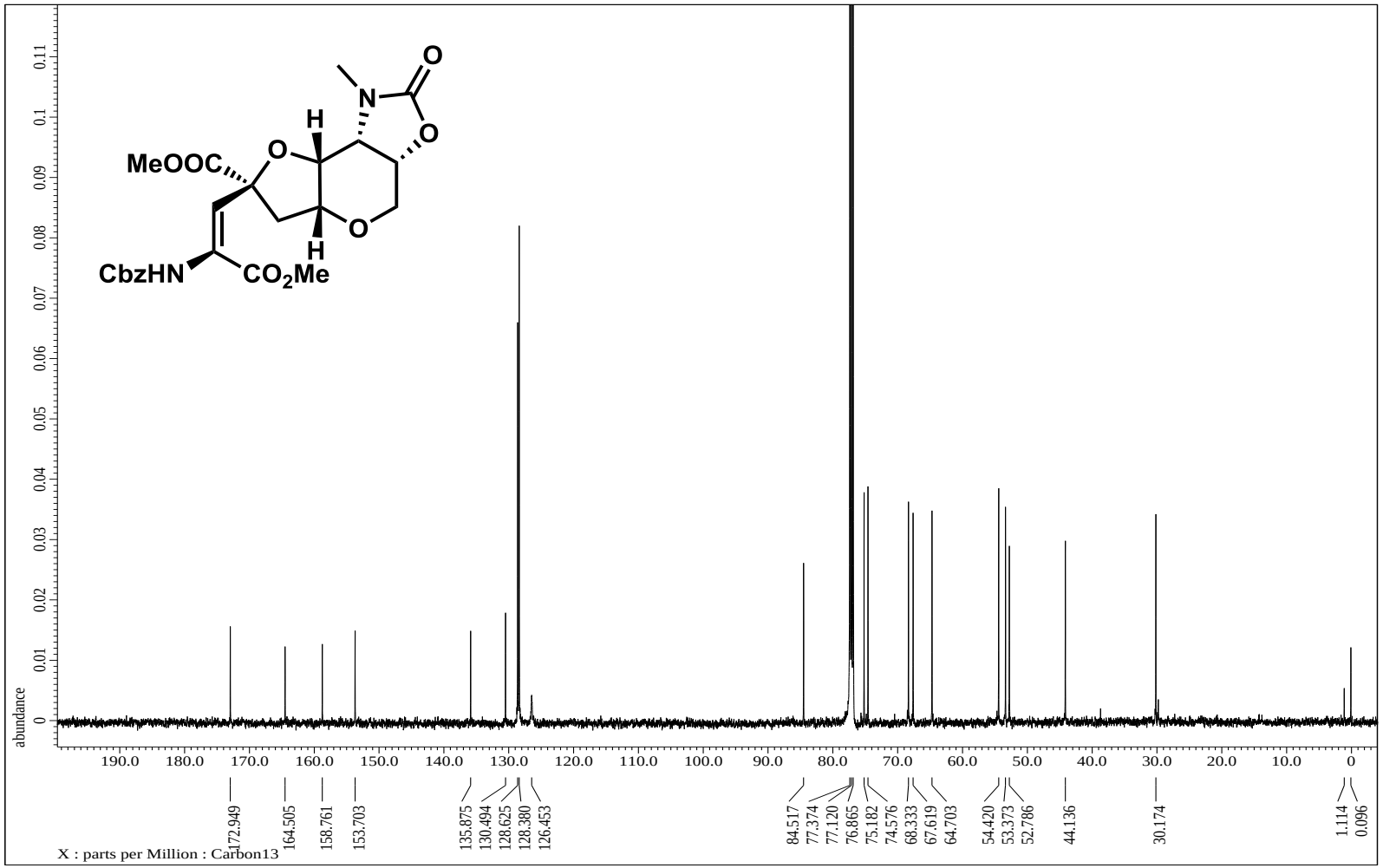

Figure 1.30. ^{13}C NMR (126 MHz, $CDCl_3$) of Methyl (3a*S*,5a*R*,7*S*,8a*R*,8b*R*)-7-((*E*)-2-(((benzyloxy)carbonyl)amino)-3-methoxy-3-oxoprop-1-en-1-yl)-1-methyl-2-oxooctahydro-2*H*-furo[2',3':5,6]pyrano[4,3-*d*]oxazole-7-carboxylate (**1.58**)

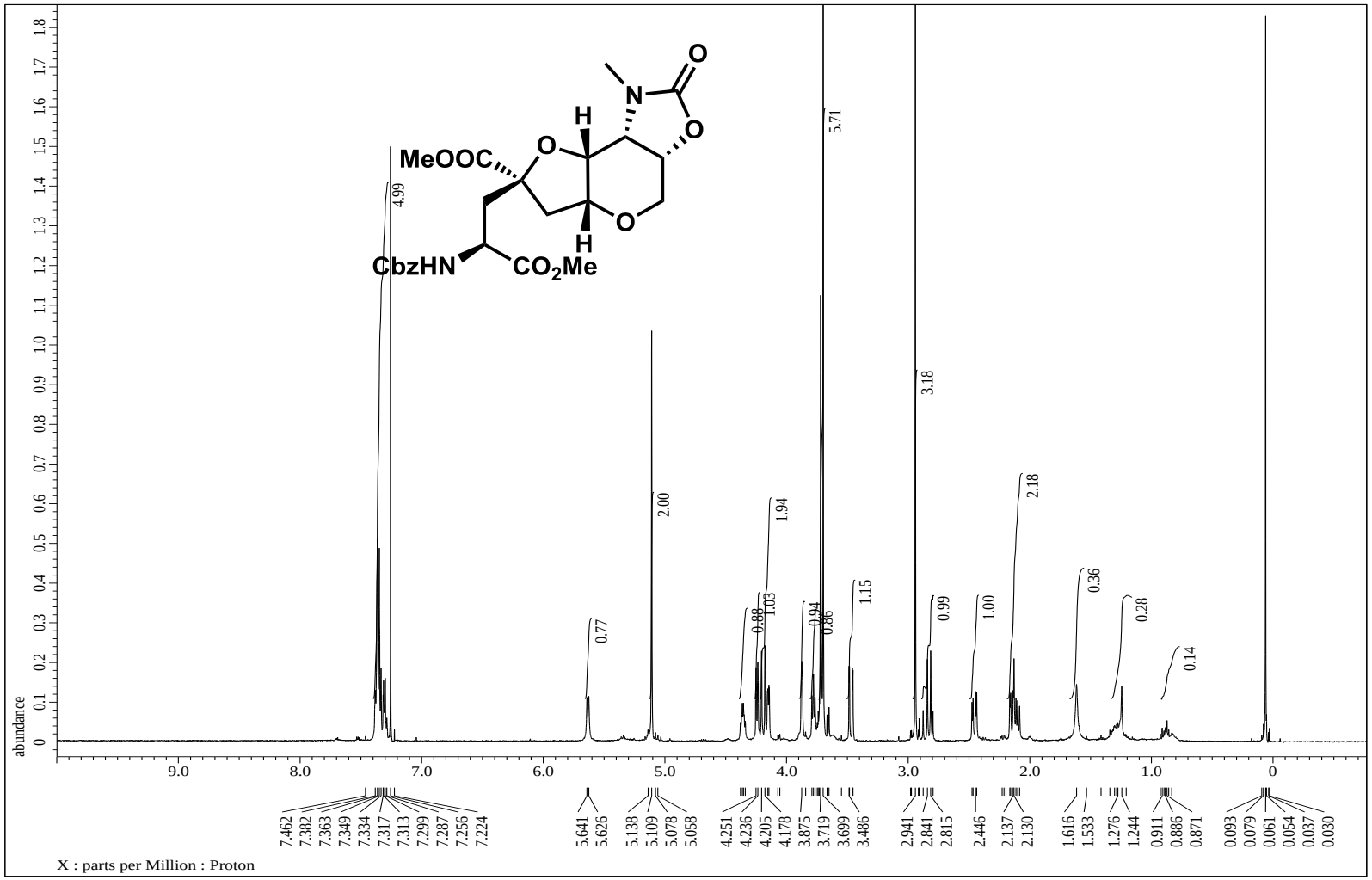

Figure 1.31. ^{1}H NMR (500 MHz, $CDCl_3$) of Methyl (3a*S*,5a*R*,7*R*,8a*R*,8b*R*)-7-((*S*)-2-(((benzyloxy)carbonyl)amino)-3-methoxy-3-oxopropyl)-1-methyl-2-oxooctahydro-2*H*-furo[2',3':5,6]pyrano[4,3-*d*]oxazole-7-carboxylate (**1.59**)

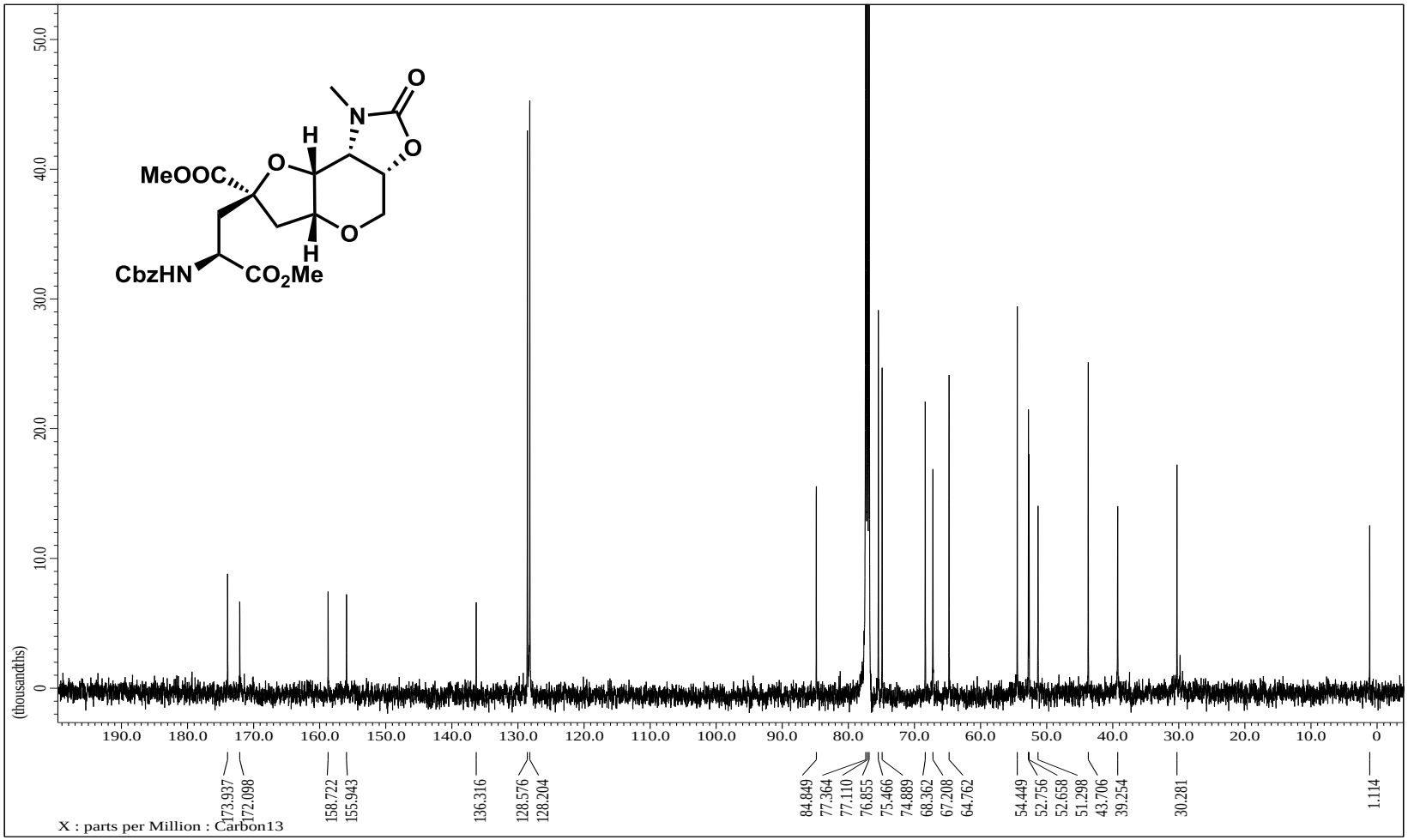

Figure 1.32. ^{13}C NMR (126 MHz, $CDCl_3$) of Methyl (3a*S*,5a*R*,7*R*,8a*R*,8b*R*)-7-((*S*)-2-(((benzyloxy)carbonyl)amino)-3-methoxy-3-oxopropyl)-1-methyl-2-oxooctahydro-2*H*-furo[2',3':5,6]pyrano[4,3-*d*]oxazole-7-carboxylate (**1.59**)

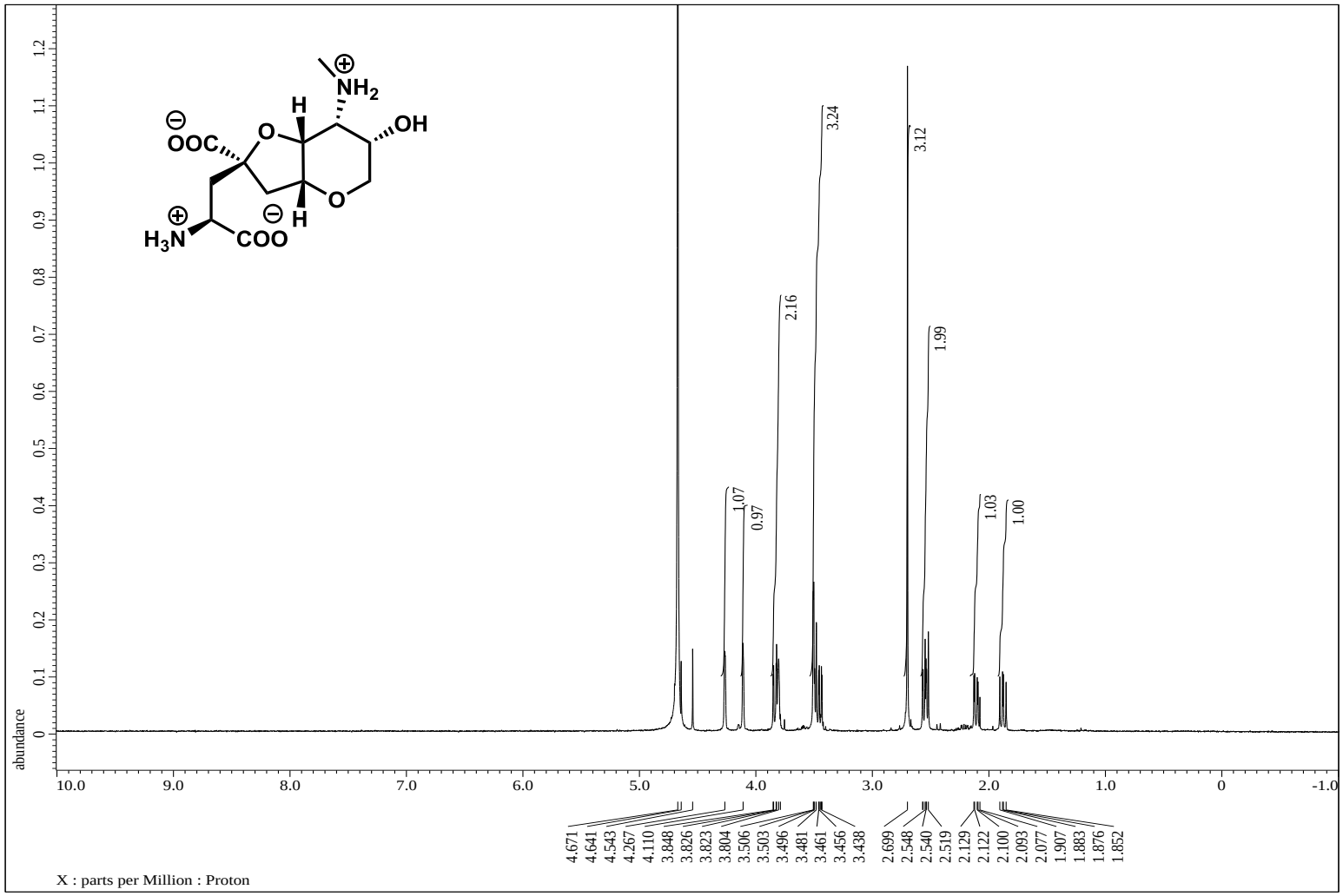

Figure 1.33. ^{1}H NMR (500 MHz, D_2O) of (–)-Dysiherbaine

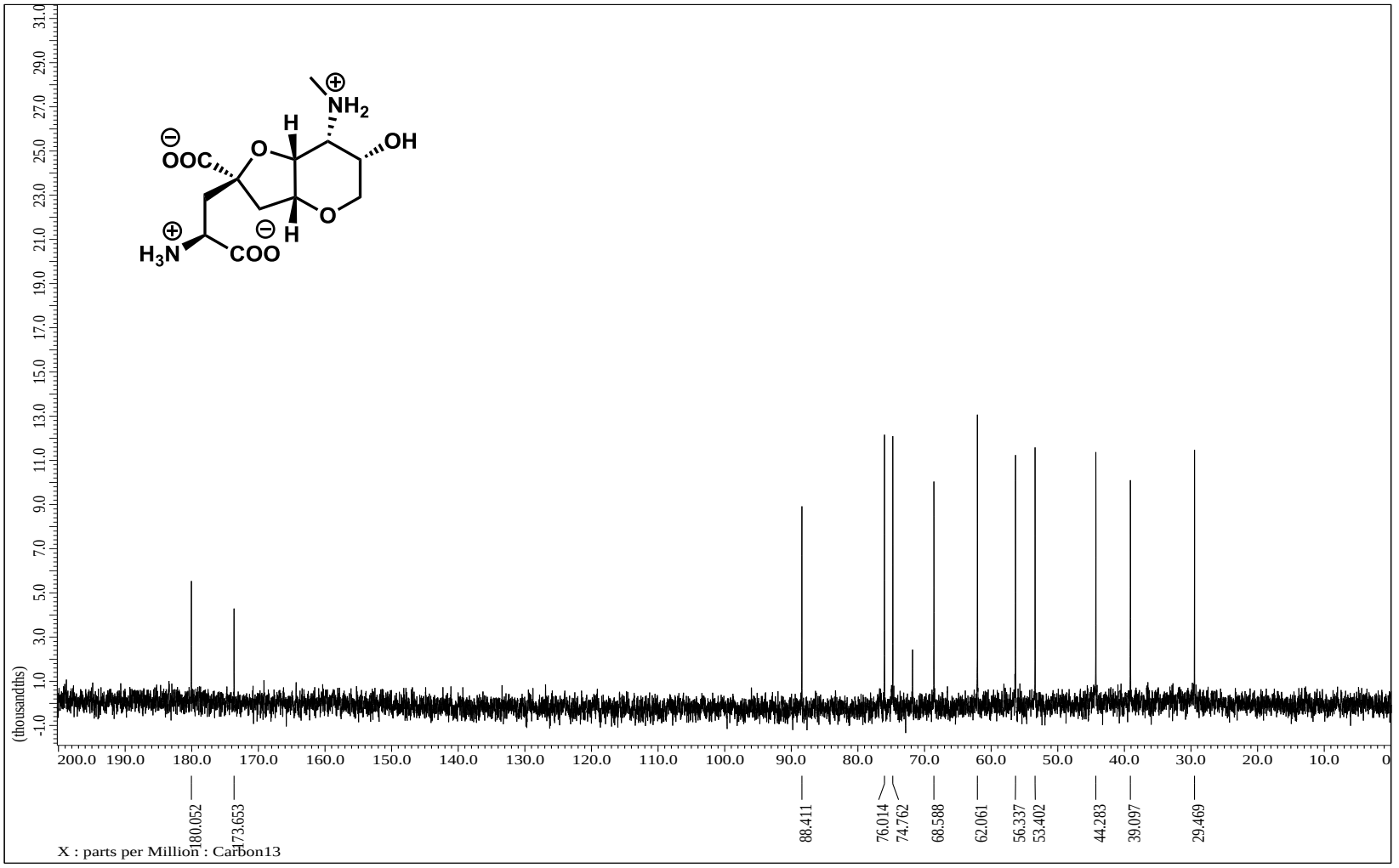

Figure 1.34. ^{13}C NMR (126 MHz, D_2O) of (–)-Dysiherbaine

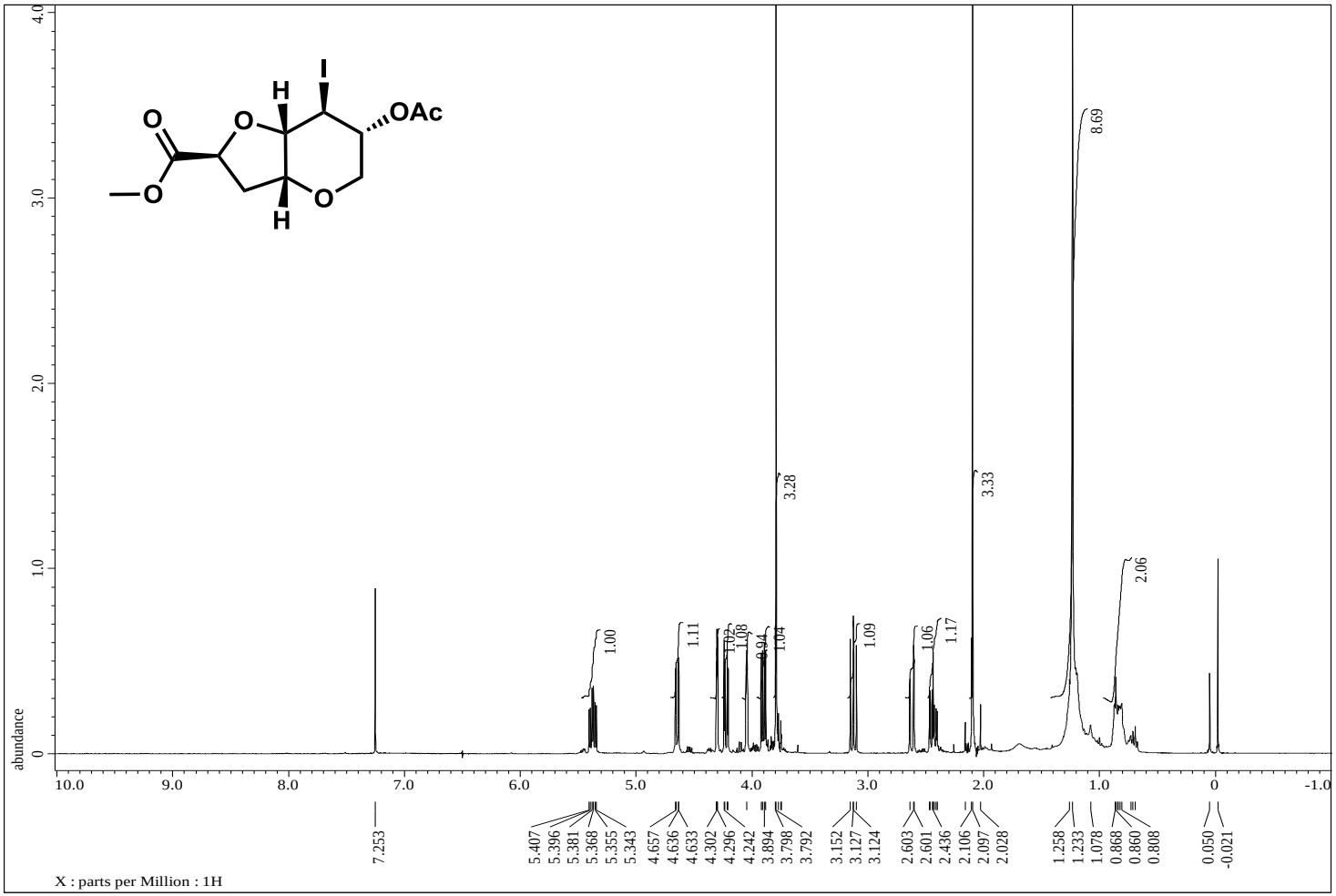

Figure 1.35. ^{1}H NMR (400 MHz, $CDCl_3$) of Methyl (2*S*,3a*R*,6*R*,7S,7a*S*)-6-acetoxy-7-iodohexahydro-2*H*-furo[3,2-*b*]pyran-2-carboxylate (**1.10**)

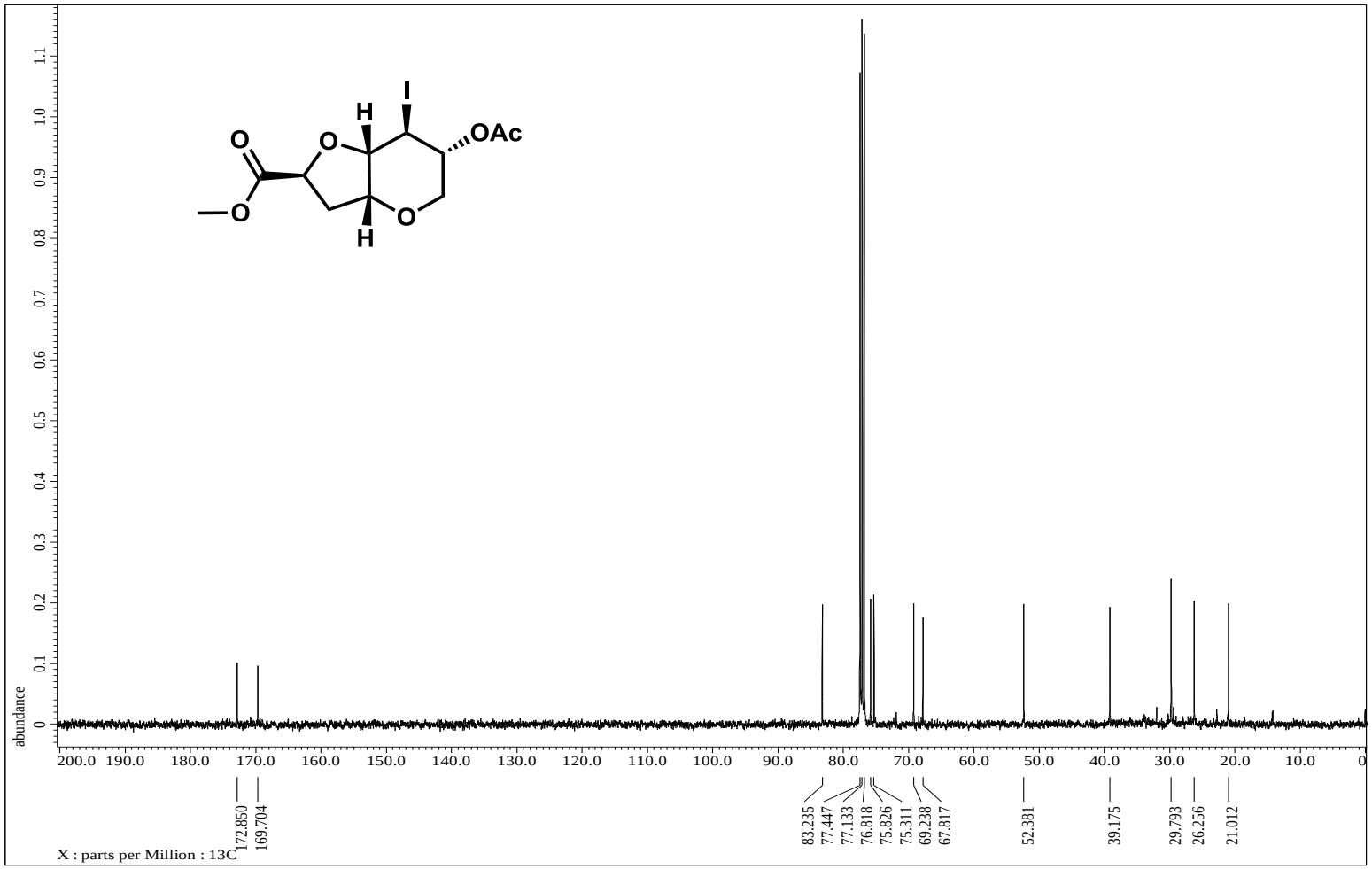

Figure 1.36. ^{13}C NMR (101 MHz, $CDCl_3$) of Methyl (2*S*,3a*R*,6*R*,7S,7a*S*)-6-acetoxy-7-iodohexahydro-2*H*-furo[3,2-*b*]pyran-2-carboxylate (**1.10**)

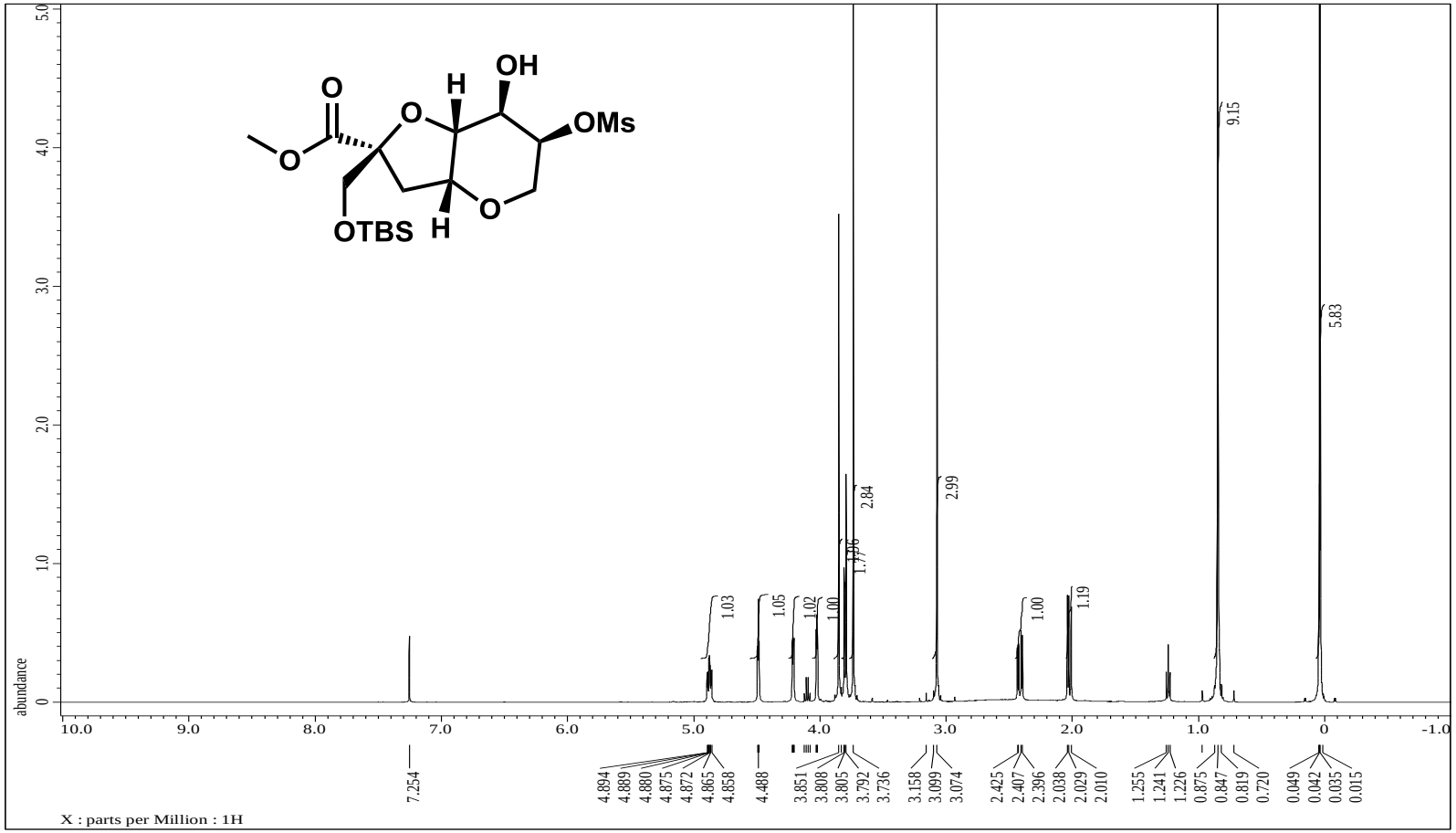

Figure 1.37. ^{1}H NMR (500 MHz, $CDCl_3$) of Methyl (2*S*,3a*R*,6*S*,7*R*,7a*R*)-2-(((*tert*-butyldimethylsilyl)oxy)methyl)-7-hydroxy-6-((methylsulfonyl)oxy)hexahydro-2H-furo[3,2-*b*]pyran-2-carboxylate (**1.46**)

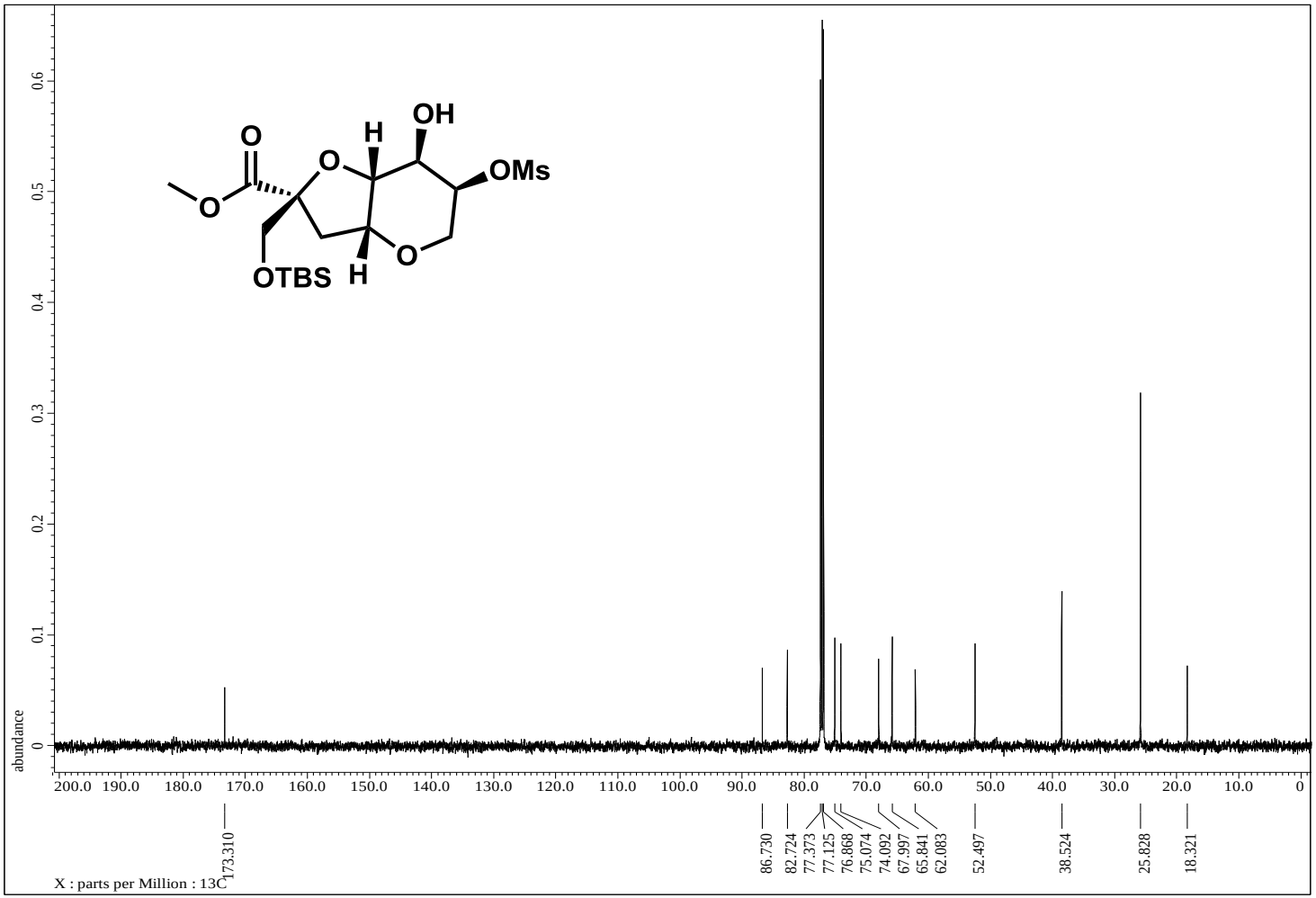

Figure 1.38. ^{13}C NMR (126 MHz, $CDCl_3$) of Methyl (2*S*,3a*R*,6*S*,7*R*,7a*R*)-2-(((*tert*-butyldimethylsilyl)oxy)methyl)-7-hydroxy-6-((methylsulfonyl)oxy)hexahydro-2H-furo[3,2-*b*]pyran-2-carboxylate (**1.46**)

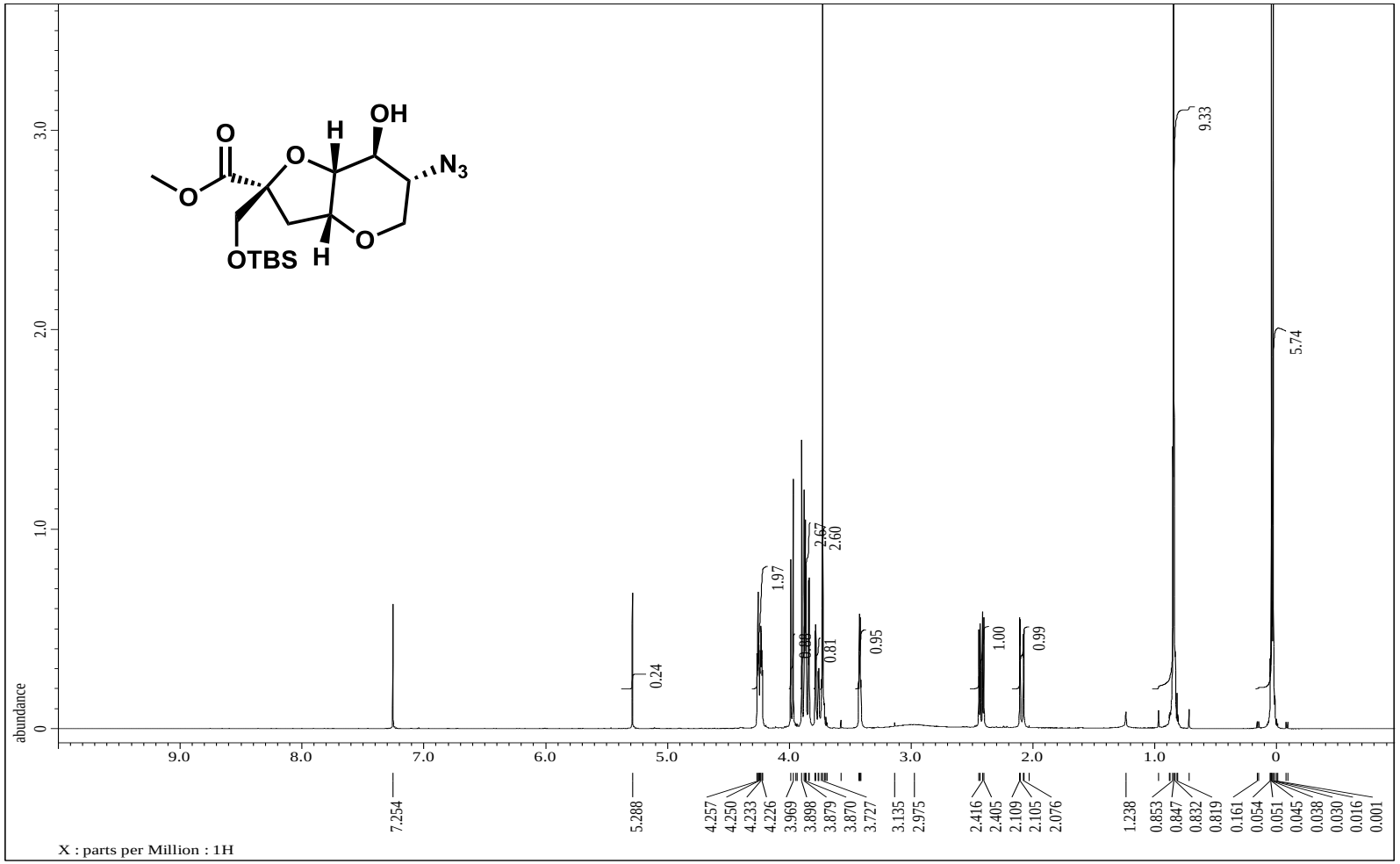

Figure 1.39. ^{1}H NMR (500 MHz, $CDCl_3$) of Methyl (2*S*,3a*R*,6*R*,7*S*,7a*R*)-6-azido-2-(((*tert*-butyldimethylsilyl)oxy)methyl)-7-hydroxyhexahydro-2*H*-furo[3,2-*b*]pyran-2-carboxylate (**1.47**)

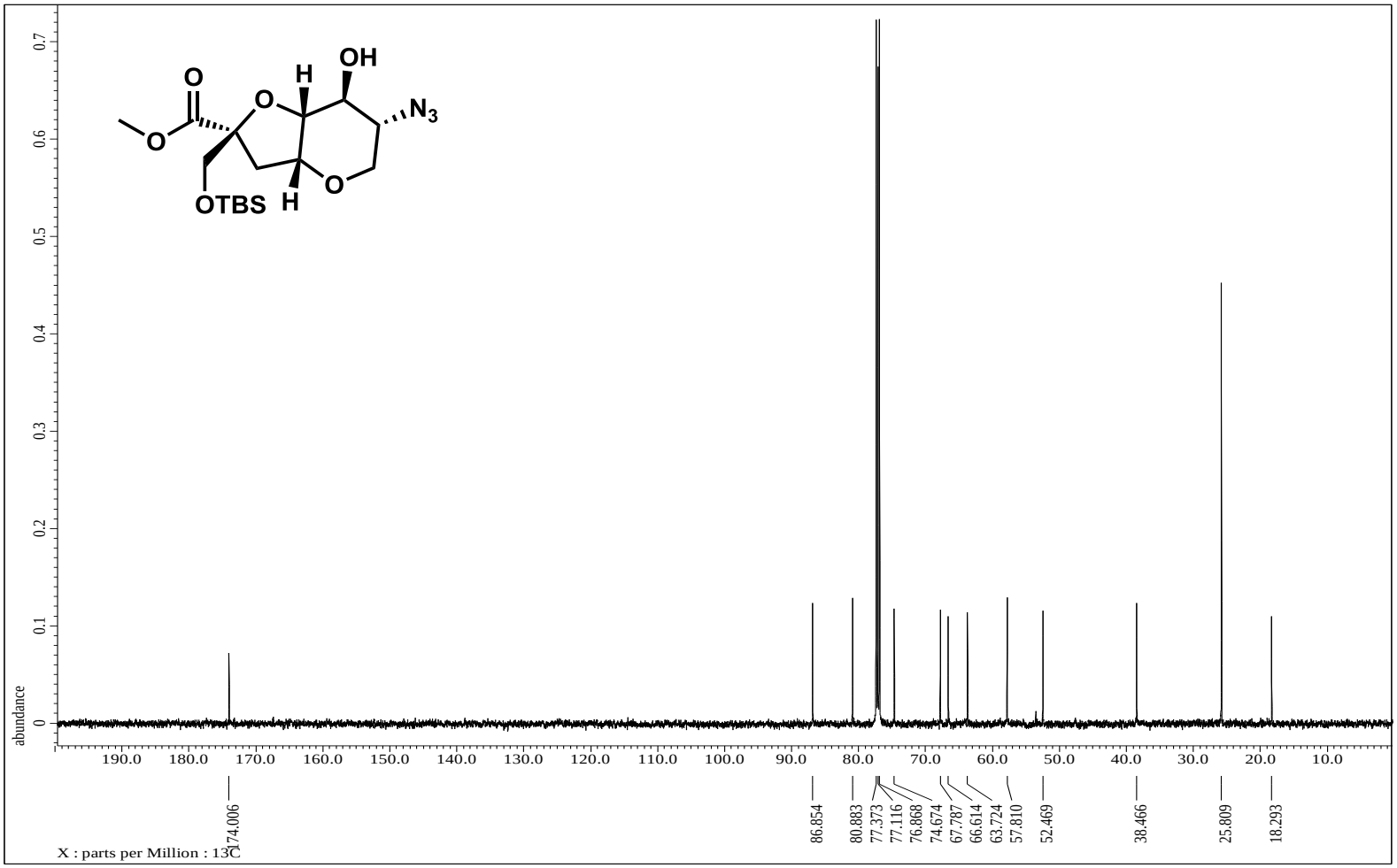

Figure 1.40. ^{13}C NMR (126 MHz, $CDCl_3$) of Methyl (2*S*,3a*R*,6*R*,7*S*,7a*R*)-6-azido-2-(((*tert*-butyldimethylsilyl)oxy)methyl)-7-hydroxyhexahydro-2*H*-furo[3,2-*b*]pyran-2-carboxylate (**1.47**)

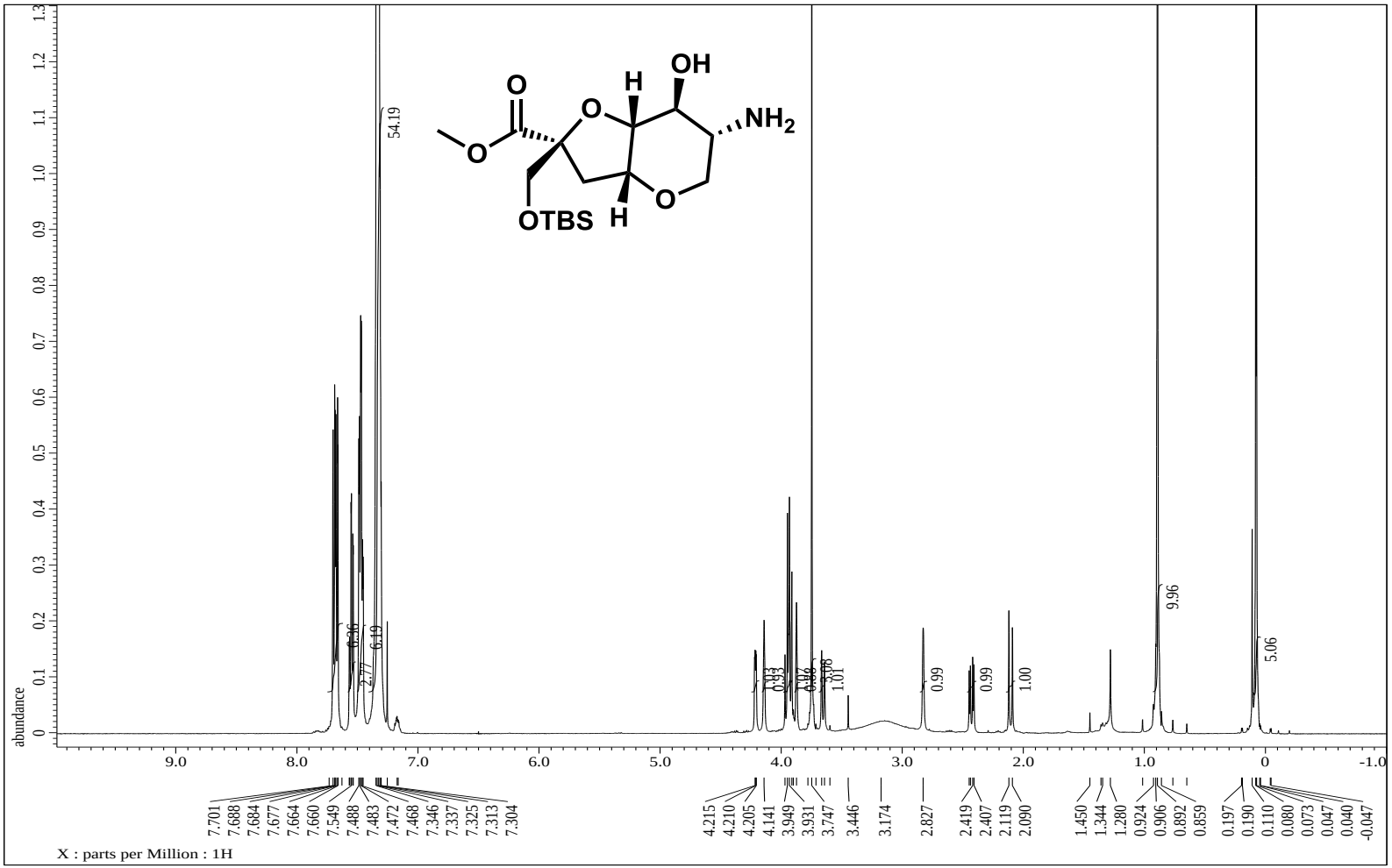

Figure 1.41. ^{1}H NMR (500 MHz, $CDCl_3$) of Methyl (2*S*,3a*R*,6*R*,7*S*,7a*R*)-6-amino-2-(((*tert*-butyldimethylsilyl)oxy)methyl)-7-hydroxyhexahydro-2*H*-furo[3,2-*b*]pyran-2-carboxylate (**1.48**)

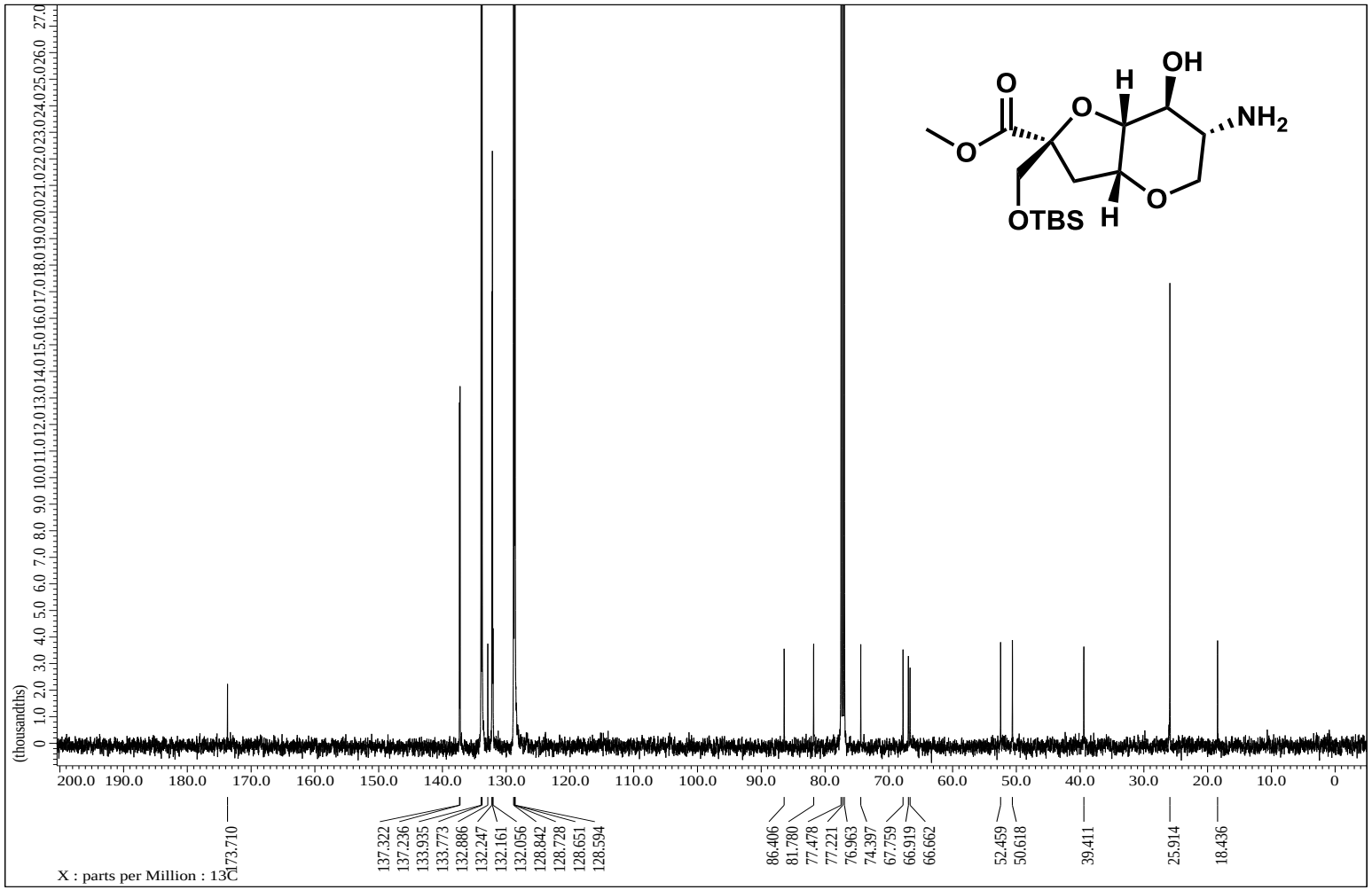

Figure 1.42. ^{13}C NMR (126 MHz, $CDCl_3$) of Methyl (2*S*,3a*R*,6*R*,7*S*,7a*R*)-6-amino-2-(((*tert*-butyldimethylsilyl)oxy)methyl)-7-hydroxyhexahydro-2*H*-furo[3,2-*b*]pyran-2-carboxylate (**1.48**)

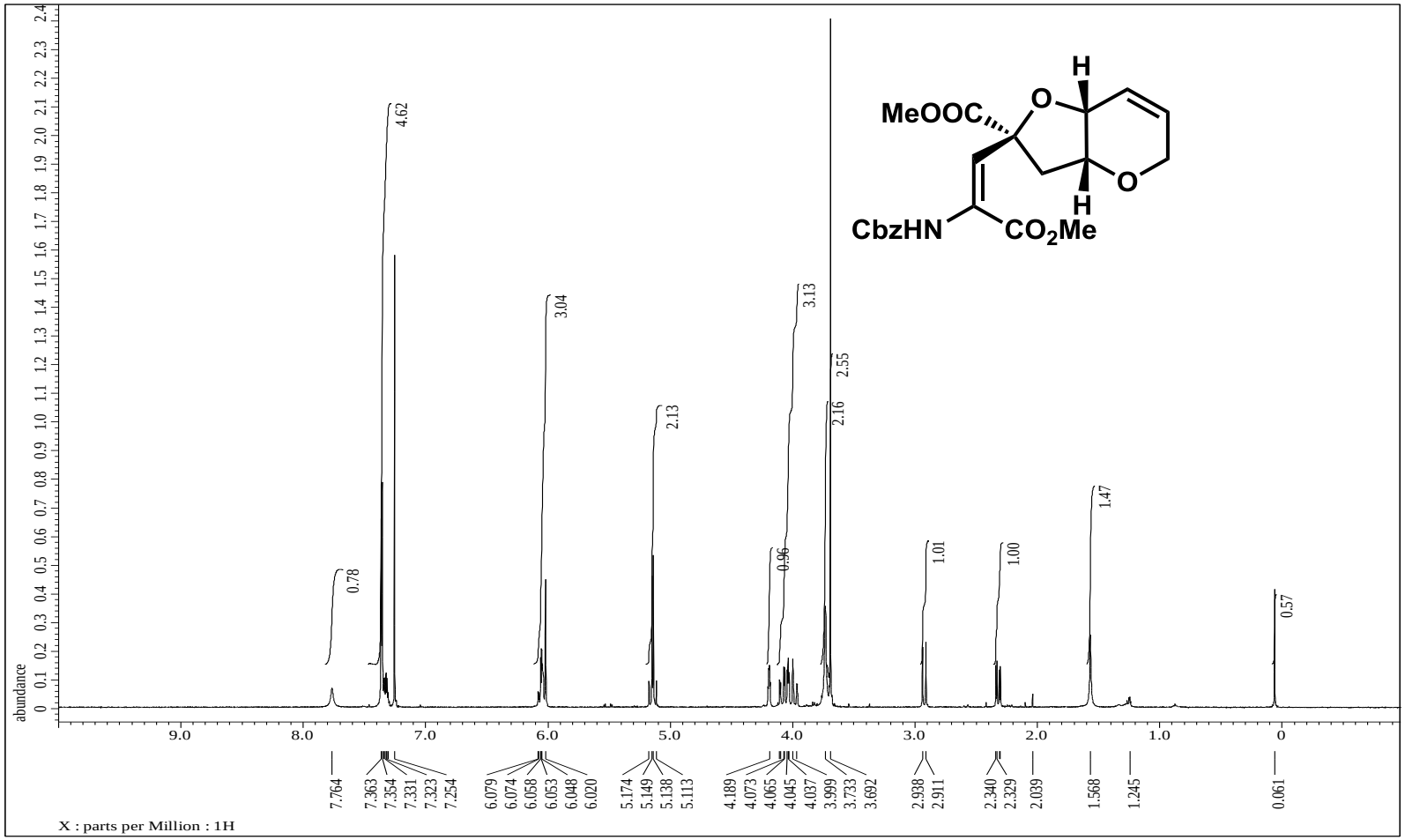

Figure 1.43. ^{1}H NMR (500 MHz, $CDCl_3$) of Methyl (2*S*,3a*R*,7a*R*)-2-((*E*)-2-(((benzyloxy)carbonyl)amino)-3-methoxy-3-oxoprop-1-en-1-yl)-3,3a,5,7a-tetrahydro-2*H*-furo[3,2-*b*]pyran-2-carboxylate (**1.37**)

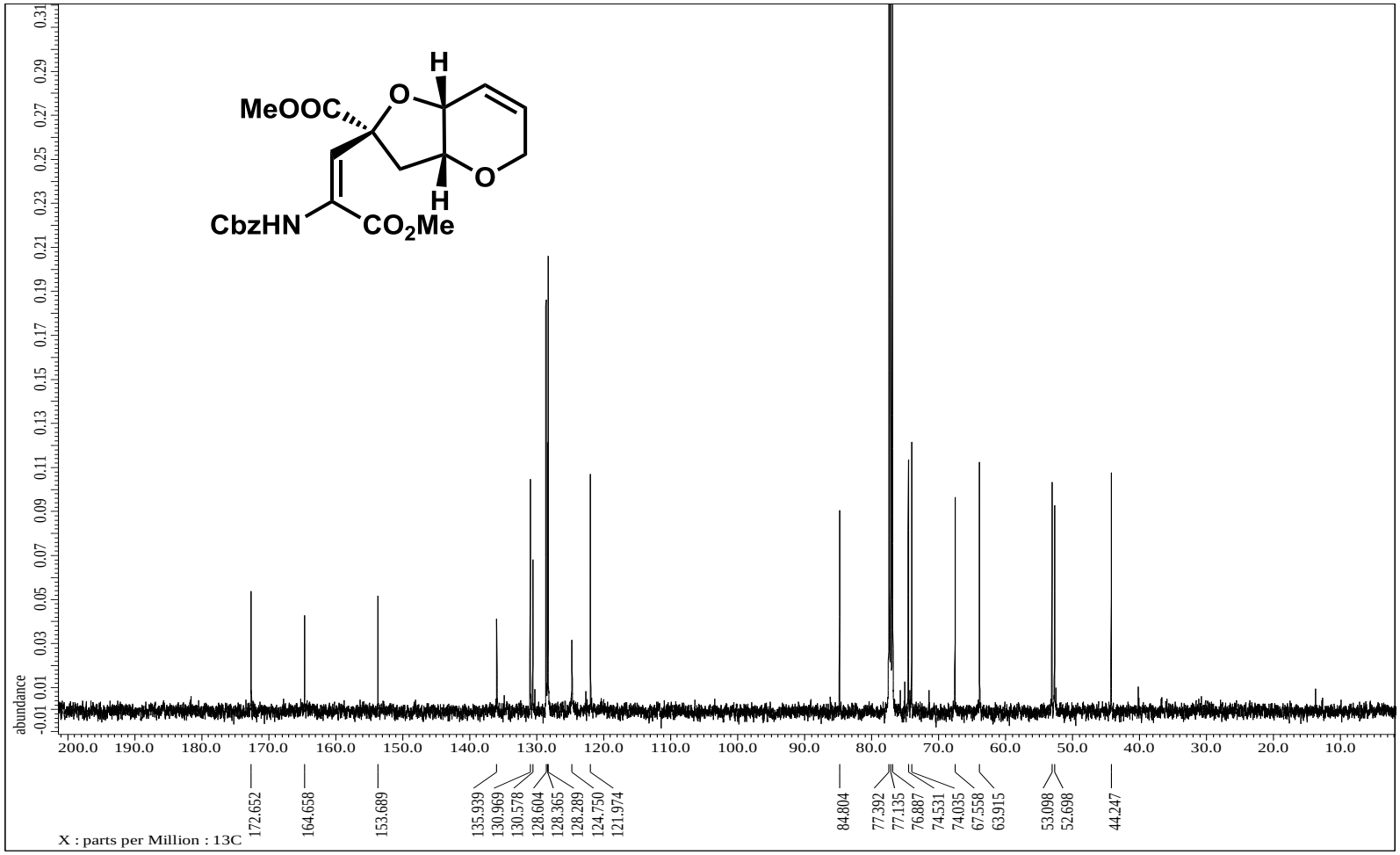

Figure 1.44. ^{13}C NMR (126 MHz, $CDCl_3$) of Methyl (2*S*,3a*R*,7a*R*)-2-((*E*)-2-(((benzyloxy)carbonyl)amino)-3-methoxy-3-oxoprop-1-en-1-yl)-3,3a,5,7a-tetrahydro-2*H*-furo[3,2-*b*]pyran-2-carboxylate (**1.37**)

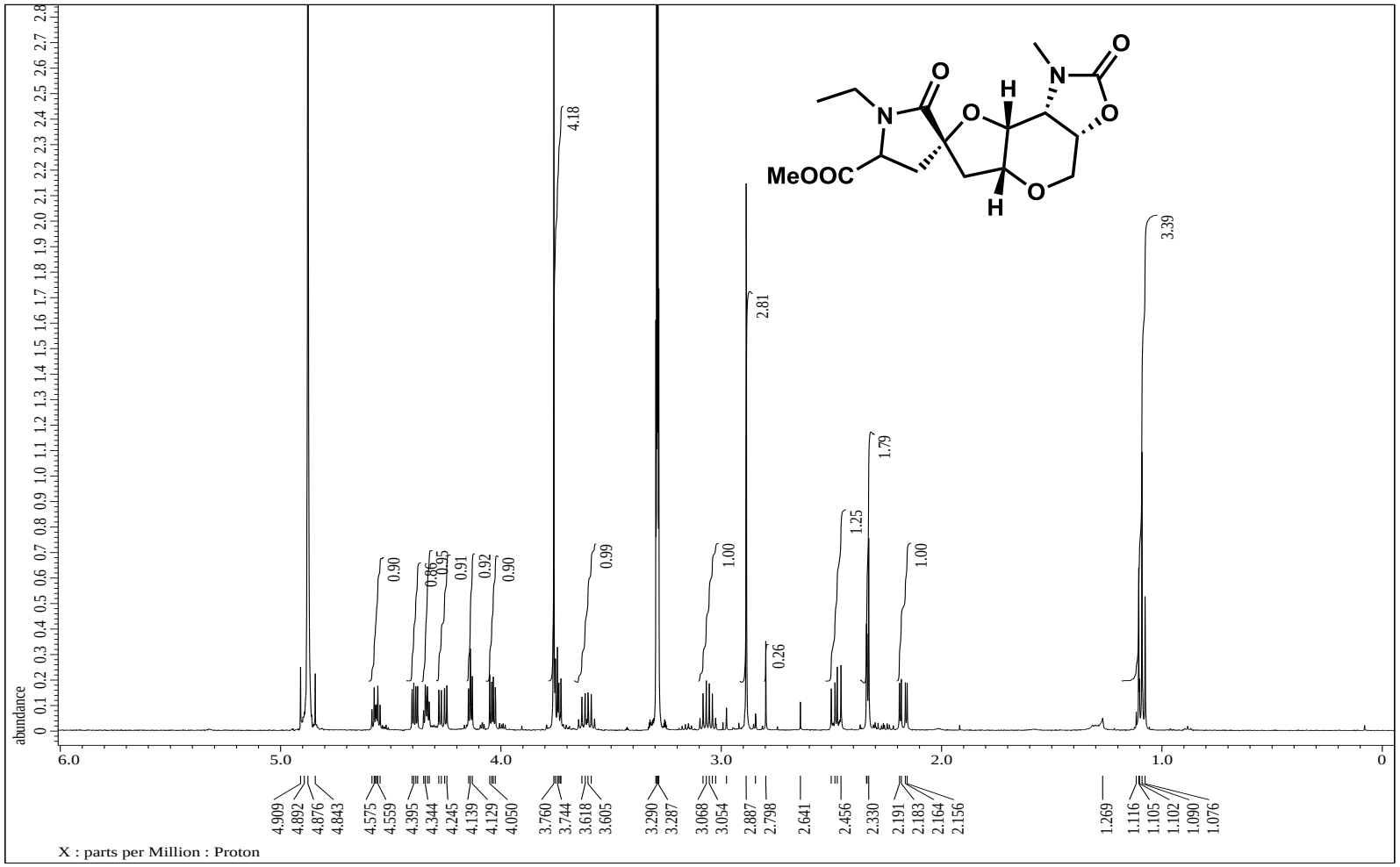

Figure 1.45. ^{1}H NMR (500 MHz, $CDCl_3$) of Methyl (3a*S*,5a*R*,7*S*,8a*R*,8b*R*)-1'-ethyl-1-methyl-2,2'-dioxooctahydrospiro[furo[2',3':5,6]pyrano[4,3-*d*]oxazole-7,3'-pyrrolidine]-5'-carboxylate (**1.63**)

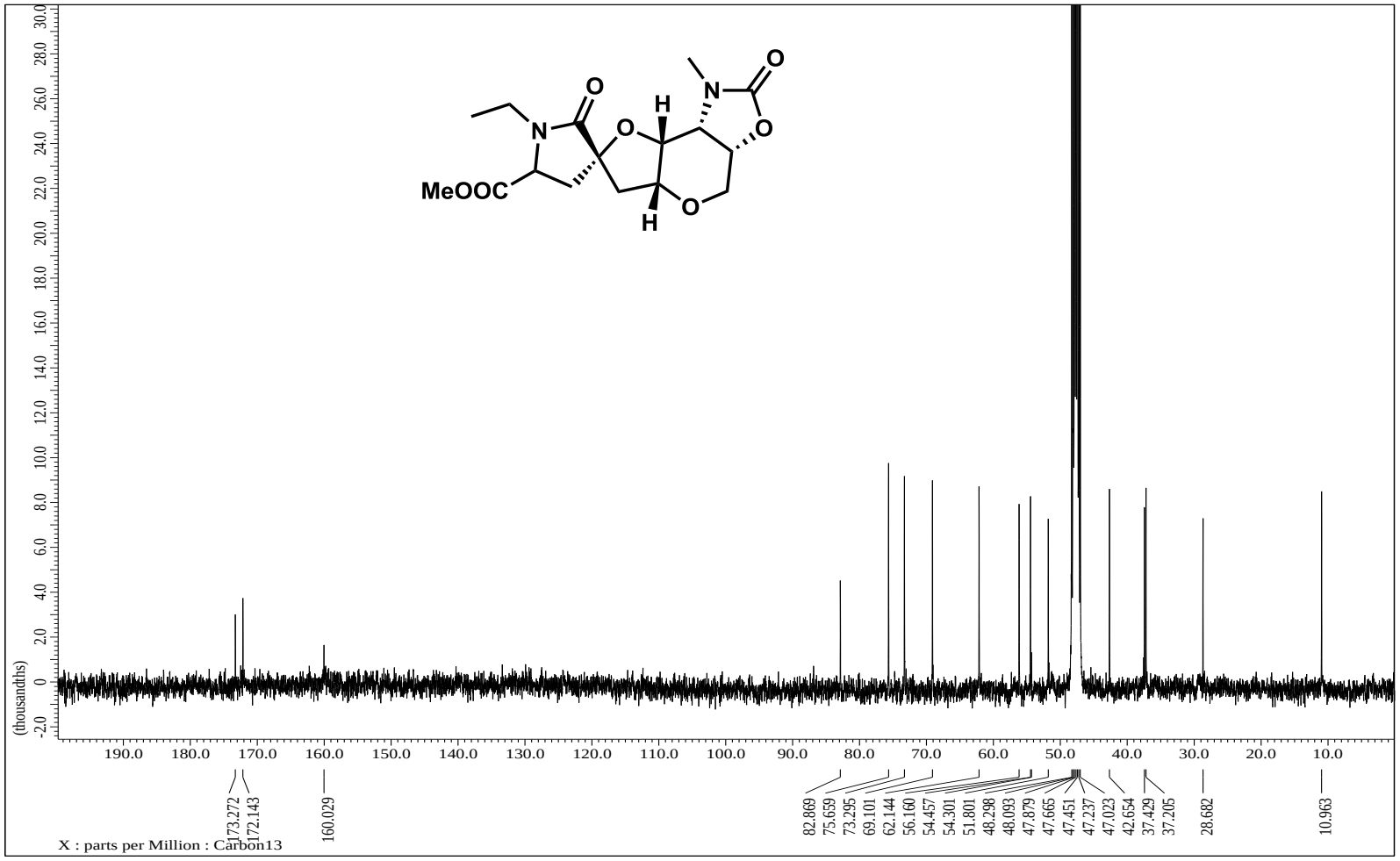

Figure 1.46. ^{13}C NMR (126 MHz, $CDCl_3$) of Methyl (3a*S*,5a*R*,7*S*,8a*R*,8b*R*)-1'-ethyl-1-methyl-2,2'-dioxooctahydrospiro[furo[2',3':5,6]pyrano[4,3-*d*]oxazole-7,3'-pyrrolidine]-5'-carboxylate (**1.63**)

Chapter 2: Separase Inhibitors (Sepin) for Breast Cancer Therapy

2.1. INTRODUCTION

In recent years, breast cancer (BC) has become one of the most common types of cancer in humans, in terms of both new cases and cancer death rates in females. Although there has been tremendous progress in early diagnosis and treatment of breast cancer, treatment options for advanced, metastatic, highly heterogeneous, and refractory breast cancer tumors are extremely limited, contributing to most of the breast cancer-related deaths in the USA and around the world.[1] Therefore, the discovery of new targets and drugs for the treatment of breast cancer is an urgent and essential clinical challenge.

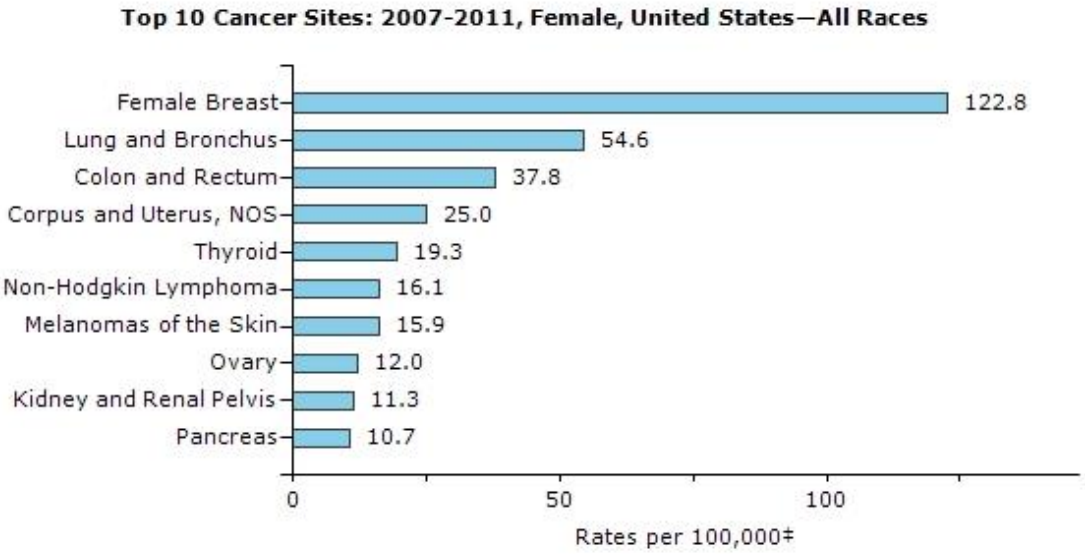

Figure 2.1. Cancer statistics showing the death rate in female of top ten cancers in the US during 2007-2011 period from http://apps.nccd.cdc.gov/uscs/toptencancers.aspx

2.1.1. Separase - an overexpressed enzyme in human cancers

A majority of highly aggressive breast tumor cells have an abnormal chromosome number, a phenotype known as aneuploidy.[2,3] Although aneuploidy is a well-established feature of advanced breast cancer, surprisingly the aneuploidy status and its underlying mechanisms have not been well exploited for therapy and as a means to circumvent tumor heterogeneity.

Separase is a cysteine protease that plays a crucial role in the separation of sister chromatids into two daughter cells during metaphase to anaphase by hydrolyzing its substrate cohensin.[4] Recent studies found that separase is overexpressed and mislocalized in a number of human tumors, including breast, prostate, and osteosarcoma. Separase is overexpressed in more than 60% of breast cancers, 50% of triple-negative breast cancer (TNBC), and 65% of Luminal-B breast cancer tumors.[5,6] In addition, the conditional overexpression of separase in mouse mammary glands induces not only aneuploidy but also mammary tumorigenesis. Therefore, the modulation of separase enzymatic activity could constitute a new therapeutic strategy for targeting resistant, separase-overexpressing aneuploid tumors, particularly the hard-to-treat TNBC. Targeting separase can also provide an effective novel approach to develop new anticancer drugs for breast cancer therapy.

2.1.2. Preliminary studies of separase inhibitor (sepin) by high throughput screening (HTS)

While structural information of separase is still unavailable, high throughput screening (HTS) has been used to search for potential separase inhibitors (sepin's). The screening results from a 14,400-compound library has provided 5 active compounds in

which 2,2-dimethyl-5-nitro-2*H*-benzimidazole-1,3-dioxide (sepin1.1, Figure 2.2) exhibited the highest activity toward inhibiting separase with a half-maximal inhibitory concentration (IC_{50}) of 15μM.[7] Further studies showed that sepin1.1 inhibits the growth of separase-overexpressing human TNBC xenografts in mice in a separase-dependent manner, and has no appreciable effect on TNBC tumors with low-separase expression, suggesting that the specificity and efficacy of this compound in targeting tumors is due to separase overexpression. Targeting separase by sepin1.1 also results in high level of apoptosis. These results suggest that inhibition of separase represents a new line of therapy to treat breast and other tumors addicted to separase overexpression.[7]

2.1.3. Scope of this project

In this project, we focus on structural modification of sepin1.1, the most active separase inhibitor from the HTS, to determine the SAR of this molecule and to find more active inhibitors. The structural modification of sepin1.1 will be systematically conducted on three regions of its skeleton: the $-NO_2$ substituent at the C5 position, the heterocycle attached to the benzene ring, and the C2 position of carbon between the two nitrogen atoms (Figure 2.2). These modified analogs will provide a unique tool for SAR study.

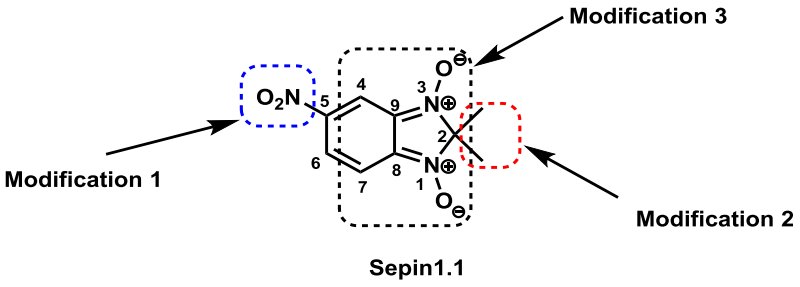

Figure 2.2. Structure of sepin1.1 with domains marked for structural modification.

2.2. RESULT AND DISCUSSION

2.2.1. Chemistry

2.2.1.1. Validation of the lead compound

Structure of sepin1.1 was reported by the library source (Maybridge) as 2,2-dimethyl-5-nitro-2*H*-benzimidazole. The approach to synthesize this compound starts with the condensation of diamine (**2.1**) with acetone in acidic conditions to generate benzimidazoline (**2.2**) which is further oxidized by MnO_2 to give the final product, *2H*-benzimidazole (**2.3**) (Scheme 2.1).[8,9]

Scheme 2.1. A synthetic route to 2,2-dimethyl-5-nitro-2*H*-benzimidazol

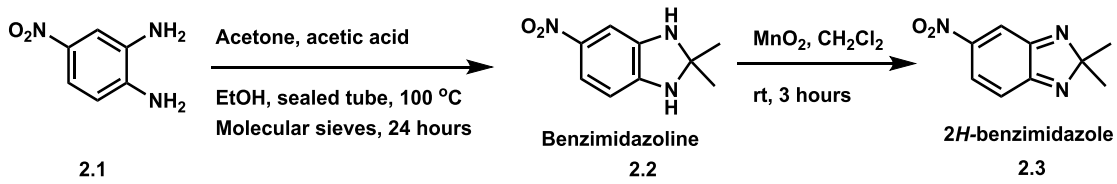

Our extensive efforts to purify the final product proved that it is unstable. The compound did not survive through column chromatography even though different absorbents such as alumina (basic, neutral), KP-NH were used. We were able to recrystallize the molecule from diethyl ether however the pure product decomposed to a complex mixture after standing at room temperature for a couple of days. The instability of the lead compound prompted us to reinvestigate its structure.

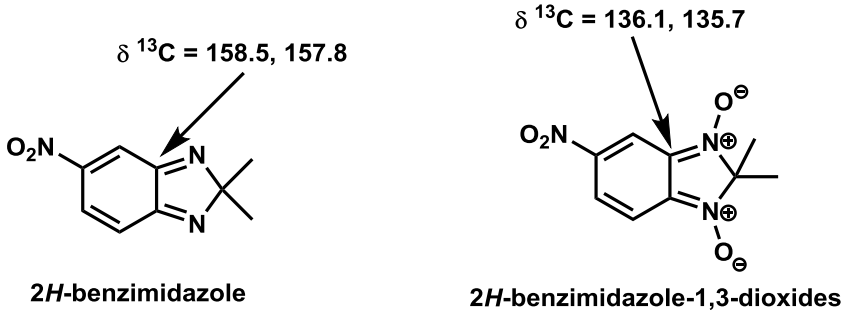

Figure 2.3. Difference in ^{13}C-chemical shifts of *2H*-benzimidazole and *2H*-benzimidazole-1,3-dioxide.

Compared to the sample used in the HTS, the compound we synthesized based on the reported structure has significant differences in ^{13}C-NMR chemical shifts, particularly at carbons connected to the nitrogens. The synthesized sample has chemical shifts at 158.50 and 157.76 ppm, while the molecule used in the HTS has chemical shifts at 136.09 and 135.66 ppm. Compared to the known structure in literature, we confirmed that the correct structure of sepin1.1 is 2,2-dimethyl-5-nitro-2*H*-benzimidazole-1,3-dioxide (as shown in Figure 2.2 and 2.3).[10] The shift of carbon signals in C=N bonds to a higher field in the correct structure is due to the additional electron density provided by two oxygen atoms bonded directly to the nitrogens.[10]

The identification of the correct structure allowed us to access the synthesis of sepin1.1 and a series of analogs. The analogs were generated by systematically modifying three main regions on sepin1.1's skeleton: the -NO_2 group, the dimethyl group, and the ring system (Figure 2.2). The general route being taken to sepin1.1 and its analogs starts with acid[11] (method 1) or base[12] (method 2) catalyzed cyclization of nitroaniline **2.4** to give benzofuroxans **2.5**. Reaction of benzofuroxan **2.5** with an alcohol in the presence of sulfuric acid (method A) provides the 2*H*-benzimidazole-1,3-dioxides derivatives.[10]

Alternatively, reaction of **2.5** with nitro alkanes in the presence of pyridine (method B) also provides the desired products (Scheme 2.3).[13-15] The selective method in each reaction mainly depends on the substituent **X** on the nitroaniline **2.4.**

Scheme 2.3. General synthetic route to access to sepin1.1 and its analogs

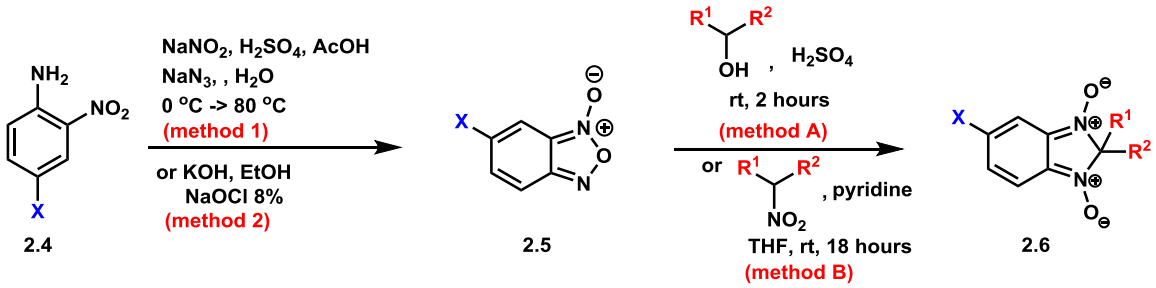

2.2.1.2. Modification of the NO_2 group

The modification of the NO_2 group can be achieved by using different nitroanilines **2.4** as starting materials. Various functional groups were chosen to replace the NO_2 group either due to their similarity in electronic properties or to provide diverse analogs for SAR study. The selective condition to generate benzofuroxan **2.5** depends mainly on the functional group **X** on nitroaniline. Particularly, carboxylic acid and bromo groups (entry 1 and 3, Table 2.1) proceeded under basic conditions while the fluoro, trifluoromethyl, and trifluoromethylsulfonyl groups (entry 5, 6, and 7, Table 2.1) required the acidic method.[16] Benzofuroxan bearing a hydroxyl group could not be obtained using either set of conditions (entry 8, Table 2.1). However, when the nitroaniline bearing a fluorine group was cyclized under basic conditions, the substitution of fluorine group by an ethoxy group took place (entry 4, Table 2.1), providing an analog containing an electron-donating group. Furthermore, benzofuroxan bearing a methyl ester group (entry

2, Table 2.1) was successfully generated by esterification of its corresponding carboxylic acid.[17] The selective condition for the second step in the synthesis of analogs also depends on the functional group **X**. Generally, the use of alcohol and sulfuric acid is preferred when **X** is an electron-withdrawing group while the use of nitroalkane and pyridine is favored when **X** is an electron-donating group. The method used and the yield for each nitroaniline substrate were summarized and shown in Table 2.1.

To diversify the lead compound, well-established chemistry such as the Suzuki coupling reaction or Click reaction were used because of the high yield and generality of these reactions. The bromine-substituted analog was synthesized not only as an example for replacing the $-NO_2$ group but also because further modification by the Suzuki reaction will make other derivatives accessible. Simple phenylboronic acid was chosen to perform this chemistry. A mixture of decomposed products was observed when the reaction was performed with Pd(dppf)Cl_2 catalyst in microwave reactor at 150 ^oC for 15 minutes.[18,19] When the reaction temperature was decreased to 100 ^oC, three products (**2.8**, **2.9**, **2.10**) in which the oxygens of N-O groups were reduced were obtained (Scheme 2.4), suggesting that the starting material is sensitive to both reducing agents and temperature. Switching the catalyst to a Pd(NHC) complex and lowering the reaction temperature[20] allowed the generation of the desired product **2.11** in 31% yield. It is the first successful Suzuki reaction on *2H*-benzimidazole-1,3-dioxide substrate as we know of.[21]

Table 2.1. The used methods (in parenthesis) and the yield for the analogs generated by modification of the NO_2 group.

Entry	SM	Benzofuroxan	Yield	*2H*-Benzimidazole-1,3-dioxides	Yield
1.	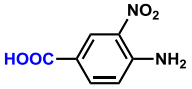	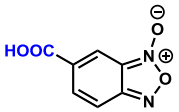 (2)	72 %	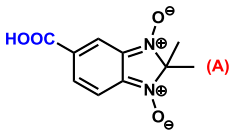 (A)	31 %
2.	–	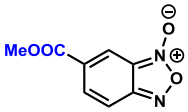		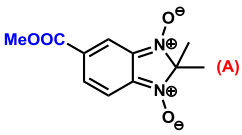 (A)	56 %
3.	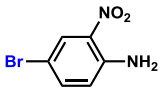	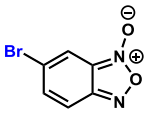 (2)	85 %	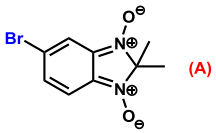 (A)	71 %
4.	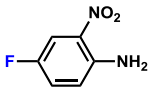	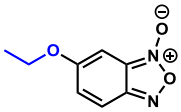 (2)	86 %	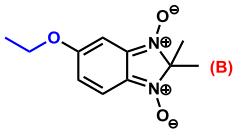 (B)	38 %
5.	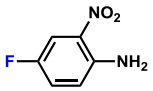	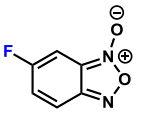 (1)	66 %	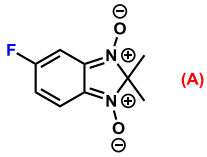 (A)	77 %
6.	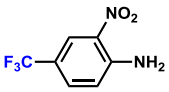	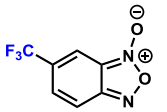 (1)	78 %	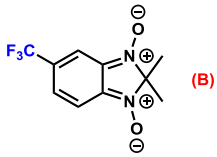 (B)	49 %
7.	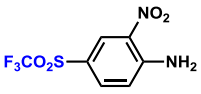	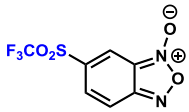 (1)	78 %	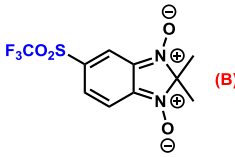 (B)	49 %
8.	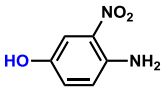	N.R (1,2)			

Scheme 2.4. Suzuki reaction of bromine-substituted analog

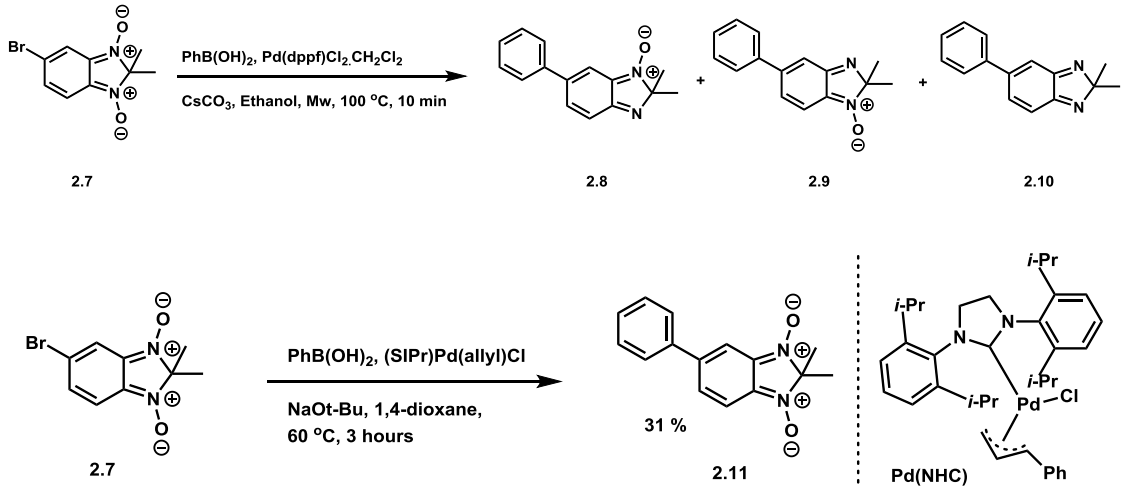

Scheme 2.5. Oxidation of deoxygenated mixtures by *m*-CPBA

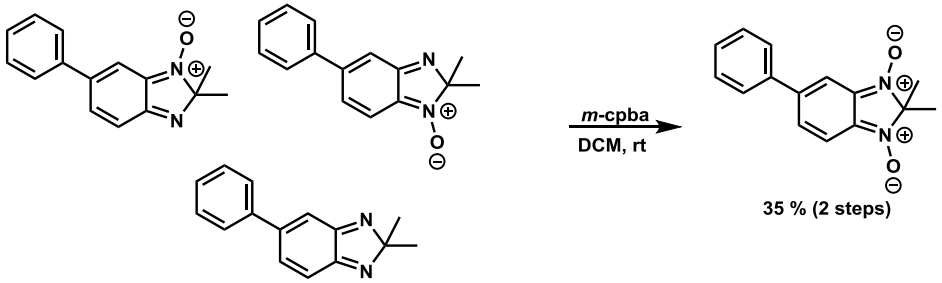

Furthermore, the mixture of deoxygenated products can be oxidized back by using excess *m*-CPBA in 35 % yield for 2 steps (Scheme 2.5).[22]

The analog-bearing fluorine **2.12** was also used for further modification by reacting it with different nucleophiles (Scheme 2.6). The azide analog **2.13** was successfully generated by reacting with NaN_3 in MeOH, and this analog was then subjected to the Click reaction with an alkyne.[23] Unfortunately, the Click reaction did not work well on this type of substrate. In most of cases, the starting material was recovered or the deoxygenated products were observed. Furthermore, the azide adduct is not stable when stored over a number of days.

Scheme 2.6. Nucleophilic substitutions on the fluorine analog.

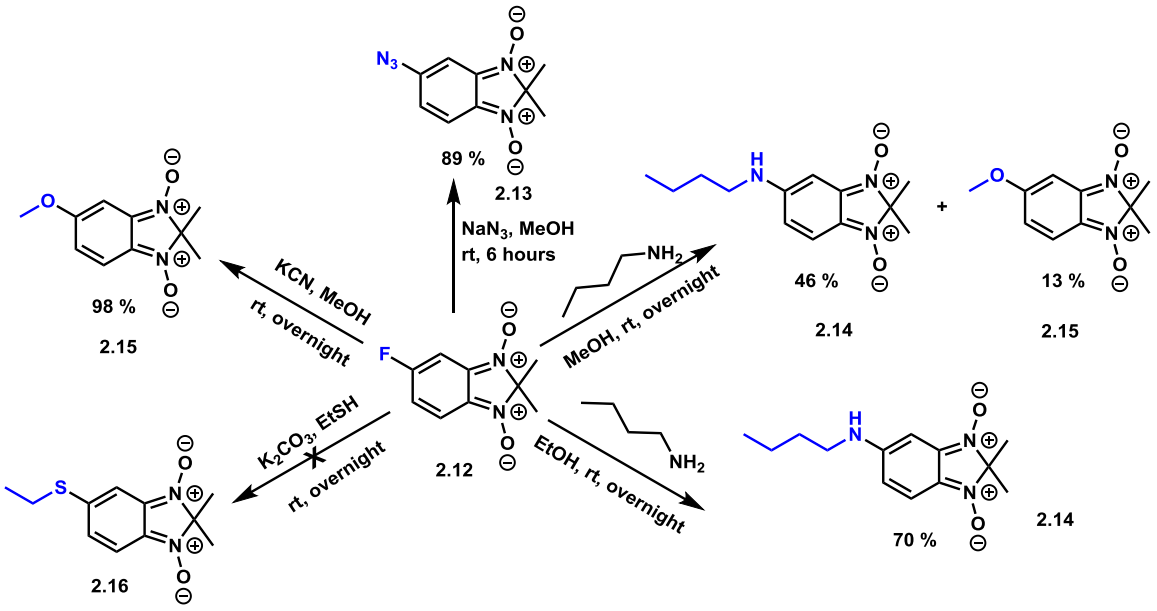

A primary amine was also used to replace fluorine to generate the amine analog. The reaction in MeOH provided a mixture of products in which the product **2.15** resulted from replacement of –F group by –OMe one with 13% yield. Changing solvent to EtOH provided the desired product **2.14** in high yield. Interestingly, the reaction with KCN in MeOH did not give the desired product, instead methoxylated product **2.15** was formed as a single product in high yield. The ethanethiol also failed to replace the fluorine.

By modifying the $–NO_2$ group, ten analogs carrying different functional groups including carboxylic acid, ester, fluorine, bromine, ethoxyl, phenyl, amine, trifluoro, and trifluorosulfonyl have been successfully synthesized and were tested to determine the effect of this position on the enzyme separase. Their structures along with their names were summarized below (Figure 2.4).

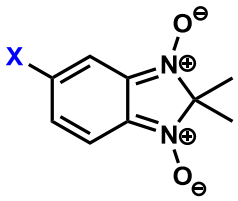

Compound	X	Yield(%)
Sepin1.1	NO_2	74
Sepin1.2	COOH	31
Sepin1.3	$COOCH_3$	56
Sepin1.4	OEt	38
Sepin1.5	CF_3	49
Sepin1.6	SO_2CF_3	42
Sepin1.7	F	77
Sepin1.8	$NH(C_4H_9)$	70
Sepin1.9	Br	71
Sepin1.10	C_6H_5	31

Figure 2.4. Ten analogs obtained by replacing of NO_2 group

2.2.1.3. Modification of dimethyl group

The modification of the dimethyl group was obtained by using different alcohols in the last step of preparing sepin1.1 while keeping other modification positions, such as nitro group, unchanged (Scheme 2.7).

Scheme 2.7. General synthetic modification of dimethyl group

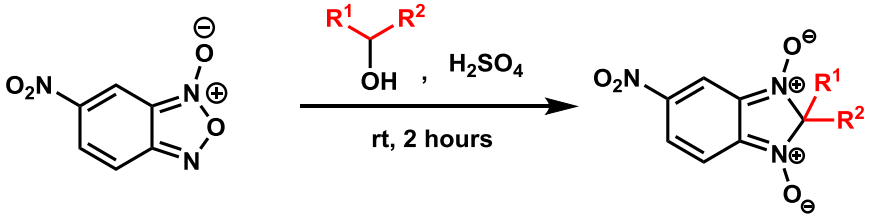

The reaction for this last step occurs through the formation of carbocation from the alcohol under acidic condition (Scheme 2.8).[10] The product depends on the rearrangement of the carbocation. For instance, the use of 1-butanol provided the methyl ethyl substituted analog (entry 1, Table 2.2). When 1-pentanol was used, a mixture of inseparable products resulted from the rearrangement was obtained (entry 2, Table 2.2). However, when the hydrocarbon chain was extended to 1-hexanol, we were able to

separate the mixture of products with 1.5 to 1 ratio (entry 3, Table 2.2). Cyclopentanol and cyclohexanol were also successfully used in the reaction (entry 4 and 5, Table 2.2).

Table 2.2. The analogs generated by the modification of dimethyl group

Entry	Alcohol	2*H*-Benzimidazole-1,3-dioxide	Yield
1.	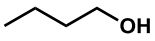	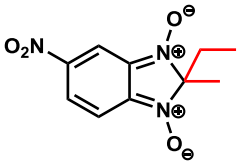	63 %
2.	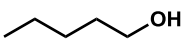	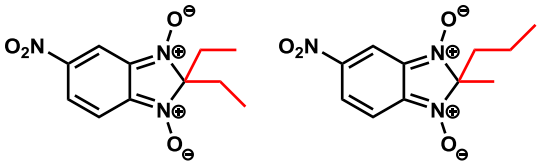	43 %
3.	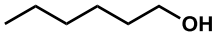	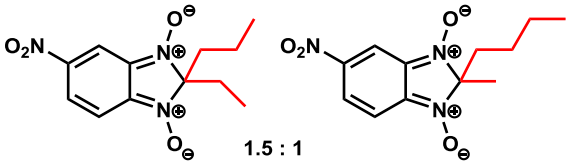 1.5 : 1	35 %
4.	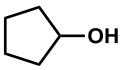	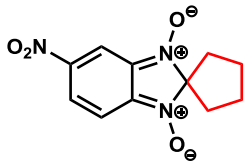	63 %
5.	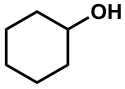	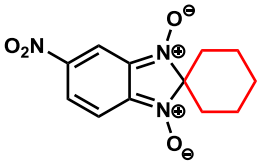	43 %

Reaction conditions: bezofuroxan (1 equiv.), alcohol (1.7 equiv.), H_2SO_4, rt, 2 hours

Scheme 2.8. Proposed mechanism for the generation of 2*H*-benzimidazole-1,3-dioxide

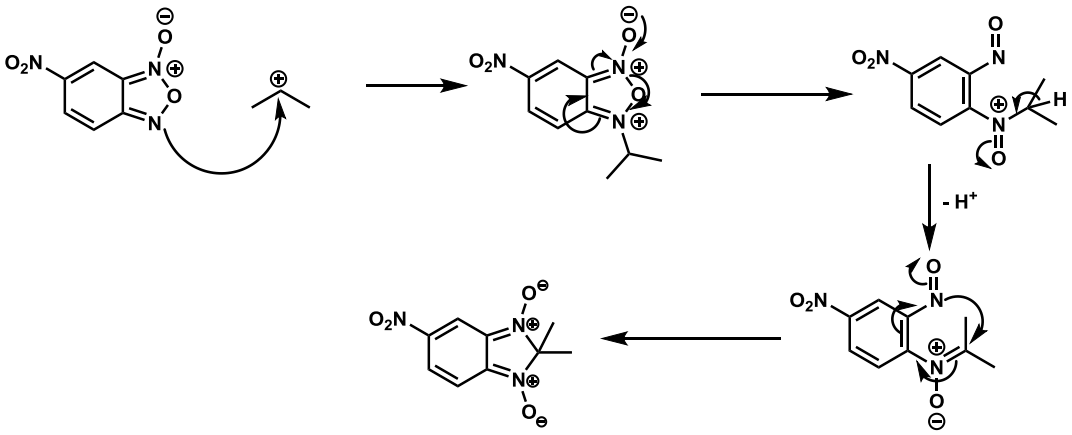

Due to the harsh conditions when using sulfuric acid as reaction solvent, the scope of alcohol substrates is limited. Only saturated hydrocarbon chains can be used to replace the dimethyl group. The installation of other functional groups including alkene, alkyne, alcohol and amine into this position has been challenging (Figure 2.5). Different reaction conditions such as using other acids ($Bi(OTf)_3$, $HClO_4$, TfOH, HCl, and toluenesulfonic acid)[24,25] were also attempted to avoid the use of sulfuric acid but was not successful.

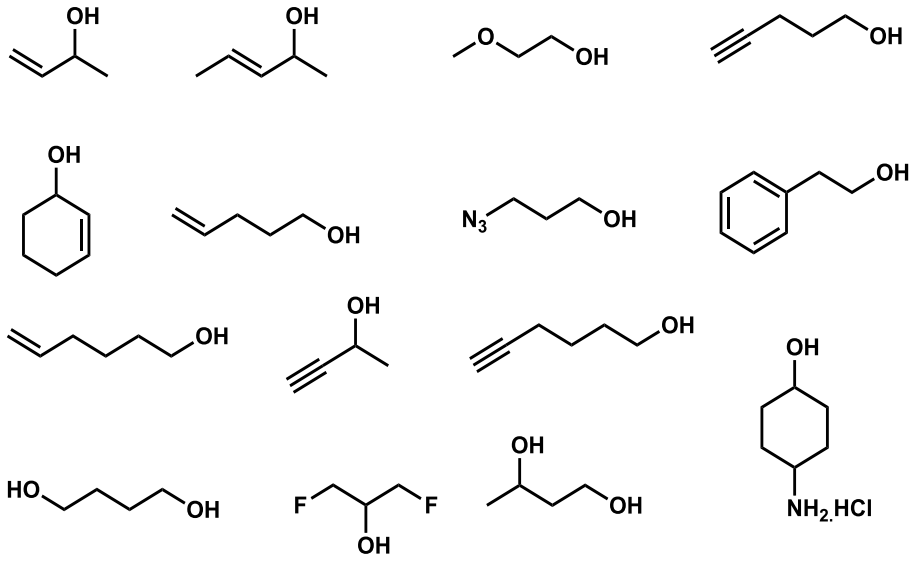

Figure 2.5. List of unsuccessful alcohol substrates in the reaction

In order to further diversify at the dimethyl position, the installation of other functional groups at this site is necessary. While searching for alcohol substrates which can tolerate in the reaction conditions, we found that the diol **2.17** reacts but generates the dehydrated product **2.20**. To prevent the dehydration, substrate **2.18** which carries a carboxylic acid group in place of the hydroxyl group in the diol **2.17** was used. Unfortunately, that reaction provides an inseparable mixture of products due to the carbocation rearrangement under reaction condition. In order to avoid rearrangement products, substrate **2.19** was used and the desired product (**2.22**) was successfully formed, providing the first analog with a functional group at dimethyl position (Scheme 2.9). This analog will be useful not only for SAR study but also to provide more diverse analogs through functionalization of the acid.

Scheme 2.9. Scope of alcohol substrates in modification of dimethyl group

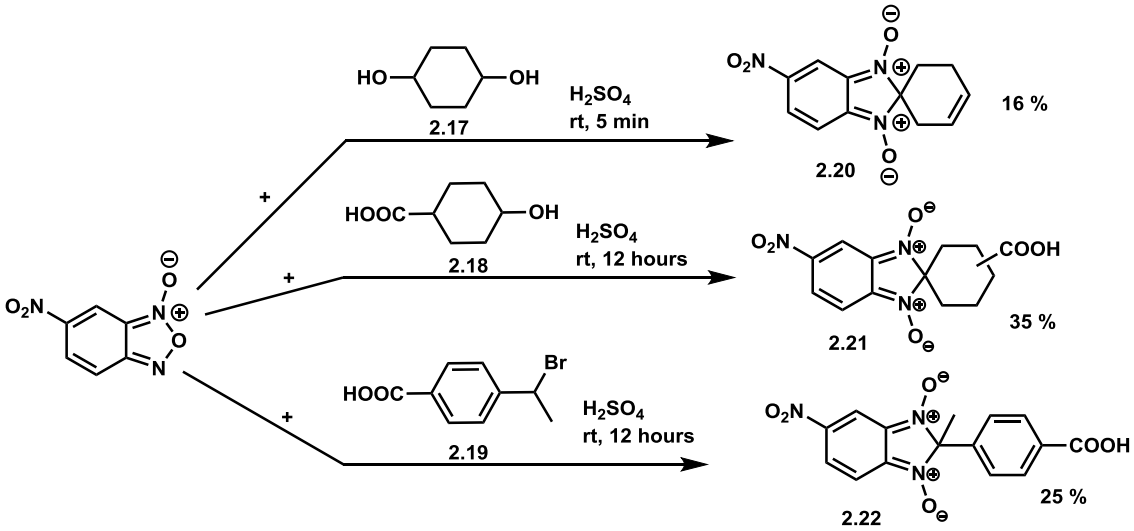

By modifying the dimethyl group, six different compounds that have alkyl chains, spiro-derivatives, and aryl chains have been synthesized and were used to determine the

effect of this position on the inhibitory activity on separase. The summary of their structures along with their names is shown in Figure 2.6.

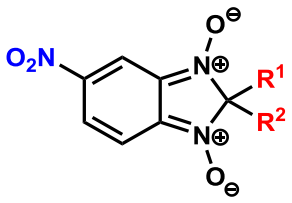

Compound	R^1	R^2	Yield(%)
Sepin1.11	CH_3	C_2H_5	63
Sepin1.12	C_2H_5	C_3H_7	21
Sepin1.13	CH_3	C_4H_9	14
Sepin1.14	CH_3	PhCOOH	25
Sepin1.15		$-(CH_2)_4-$	63
Sepin1.16		$-(CH_2)_5-$	43

Figure 2.6. Six analogs generated by the modification of dimethyl group

2.2.1.4. Other modifications

Further modification of sepin1.1 was taken on the ring system. Sepin1.17 and sepin1.18 were generated from their corresponding benzofuroxan using sulfuric acid and *iso*-propanol.[10] Sepin1.19 was formed by the bromination of sepin1.1 at the *meta*-position of the nitro group.[26] The precursor to synthesize sepin1.1, 5-nitrobenzofuroxan (sepin 1.20) and its reduced form (sepin1.21) were also studied in the bioassay to determine their inhibitory activities toward separase.[27] By using benzofuroxan as starting material, the quinoxaline-1,4-dioxide (sepin 1.22) was also synthesized and tested due to its potential bioactivity in anticancer, antibacteria, and antifungal (Scheme 2.10).[28-30]

Scheme 2.10. Other modifications

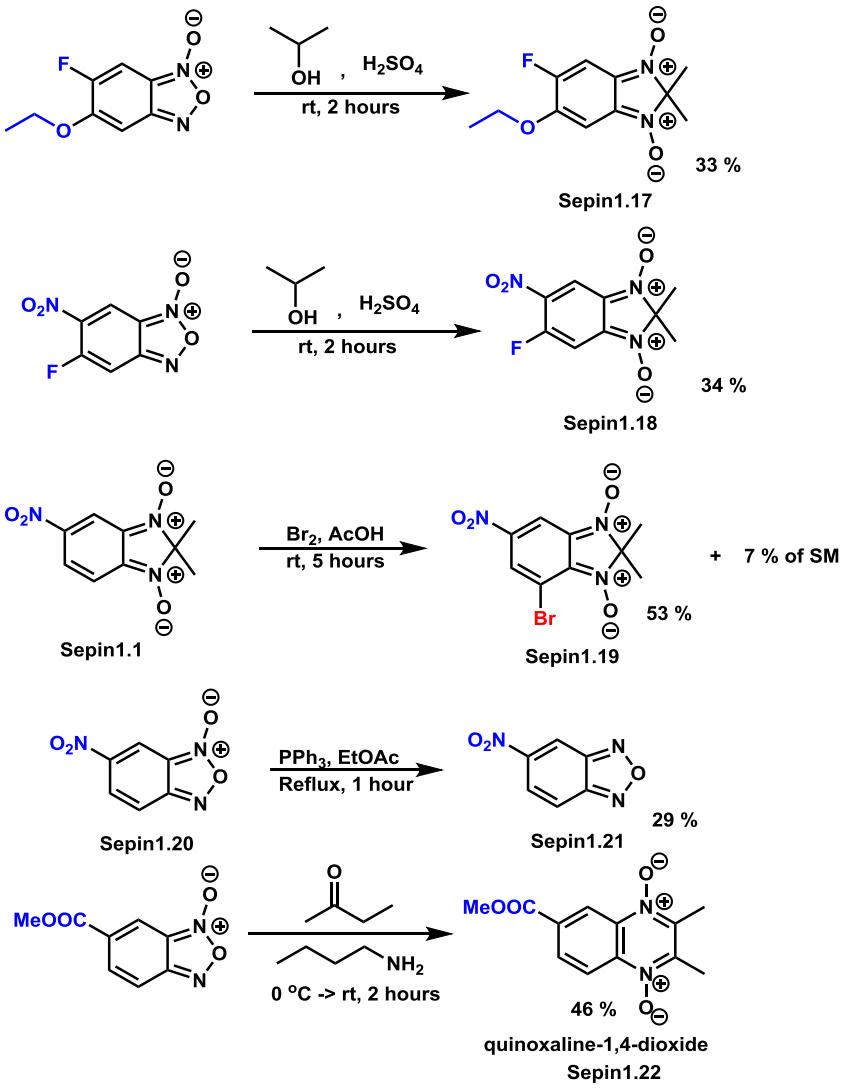

2.2.2. Structure determination

The molecular structure of sepin derivatives was successfully confirmed by single-crystal X-ray diffraction. Crystal structure of compounds with functional modification at the nitro group, the dimethyl group, and other positions on the heterocyclic ring are presented in Figure 2.7, 2.8, and 2.9, respectively. To our knowledge, these structures are the first examples of isolated 2*H*-benzimidazole-1,3-

dioxides derivatives that have been analyzed using single-crystal X-ray diffraction. To date, the only available structure of 2*H*-benzimidazole-1,3-dioxide characterized by X-ray diffraction was reported by Keller *et al.* in which the molecule is co-crystallized with $H[AuCl_4]$.[31] For all sepin structures reported in our work, the bond distance of C4-C5 and C6-C7 bonds in the benzene ring are significantly shorter than the C9-C4, C5-C6, C7-C8, and C8-C9 bonds (see notation in Figure 2.7.A and selected bond lengths in Table 2.3), suggesting a C-C double bond as drawn in Figure 2.2. Interestingly, although this difference in the bond lengths of C-C bonds of the benzene ring was also observed in other 2*H*-benzimidazole derivatives,[22] there is very little variation for aromatic C-C bonds in the 2*H*-benzimidazole-1,3-dioxide reported by Keller *et al.*, which may be due to the interaction of the molecule with the $[AuCl_4]^-$ anion.[31]

Table 2.3. Selected bond lengths of some sepin compounds

	Sepin1.2	**Sepin1.4**	**Sepin1.14**	**Sepin1.15**	**Sepin1.17**	**Sepin1.19**
Bond Length (Å)						
C9-C4	1.414(2)	1.412(4)	1.413(4)	1.406(2)	1.419(3)	1.401(6)
C4-C5	1.364(2)	1.358(4)	1.368(5)	1.361(2)	1.346(3)	1.357(6)
C5-C6	1.451(2)	1.454(4)	1.417(5)	1.427(2)	1.453(3)	1.423(6)
C6-C7	1.357(2)	1.352(4)	1.358(5)	1.363(2)	1.362(3)	1.371(6)
C7-C8	1.417(2)	1.422(4)	1.414(4)	1.420(2)	1.422(3)	1.422(6)
C8-C9	1.432(4)	1.432(4)	1.423(4)	1.423(2)	1.435(3)	1.441 (6)
N1-O1	1.3048(14)	1.291(3)	1.279(3)	1.2656(16)	1.287(2)	1.278(4)
N2-O2	1.2712(15)	1.296(3)	1.268(3)	1.2834(16)	1.288(2)	1.275(4)
C8-N1	1.3253(19)	1.332(4)	1.330(4)	1.3384(19)	1.338(3)	1.338(5)
C9-N3	1.3326(18)	1.341(4)	1.339(4)	1.3436(19)	1.333(3)	1.338(5)

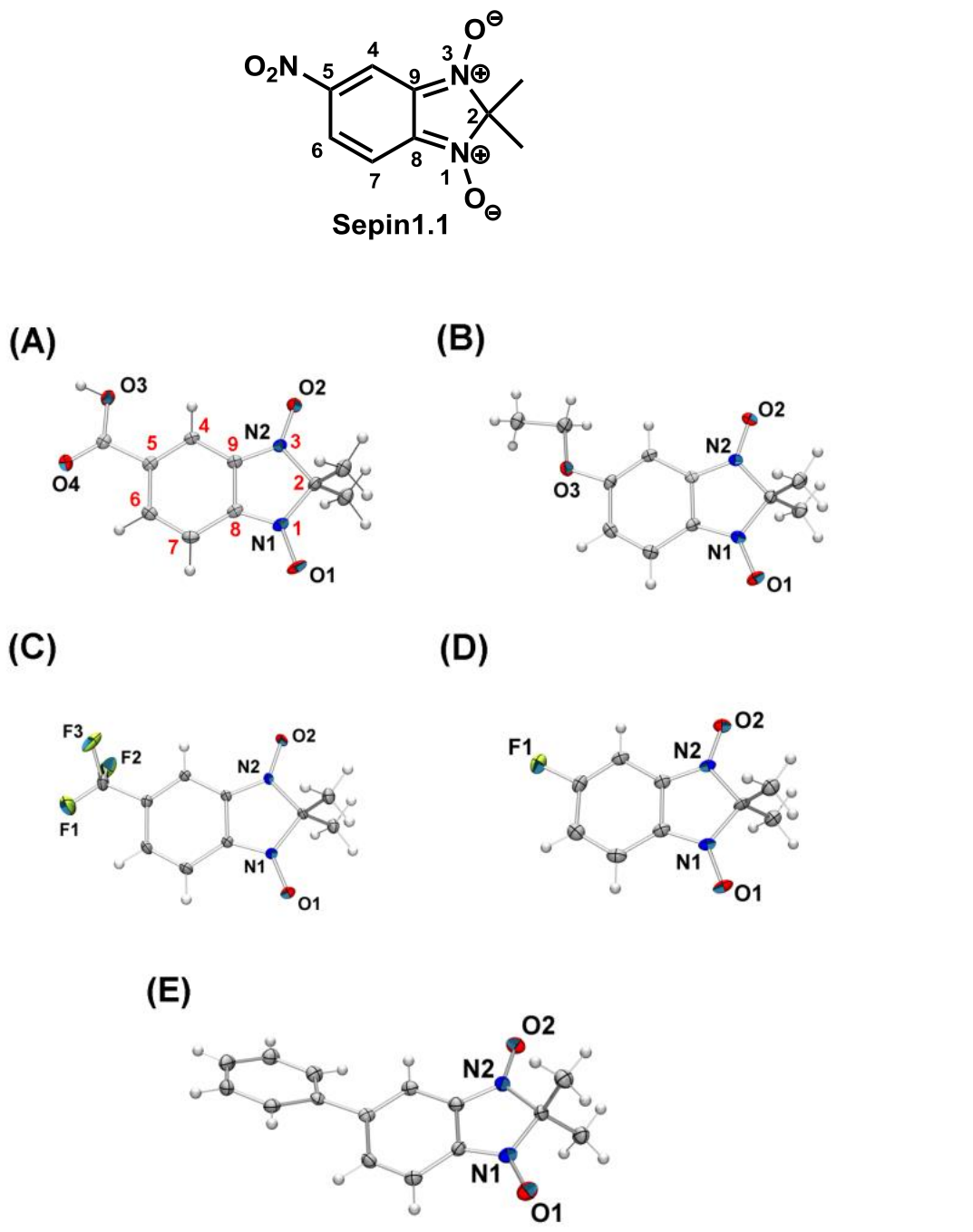

Figure 2.7. ORTEP diagram of (A) sepin1.2, (B) sepin1.4, (C) sepin1.5, (D) sepin1.7, and (E) sepin1.10.

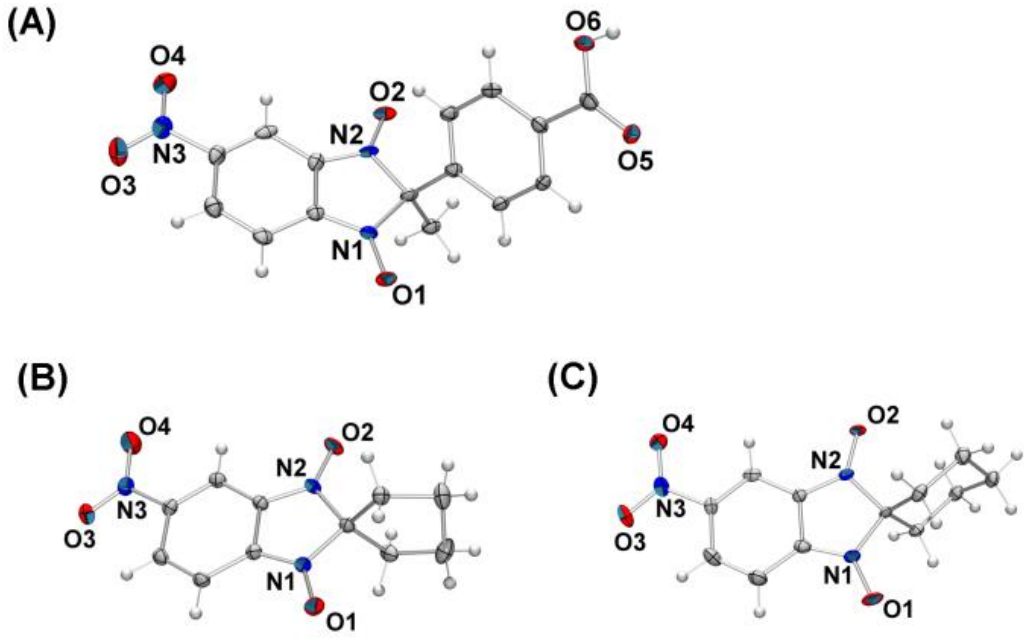

Figure 2.8. ORTEP diagram of (A) sepin1.14, (B) sepin1.15, and (C) sepin1.16.

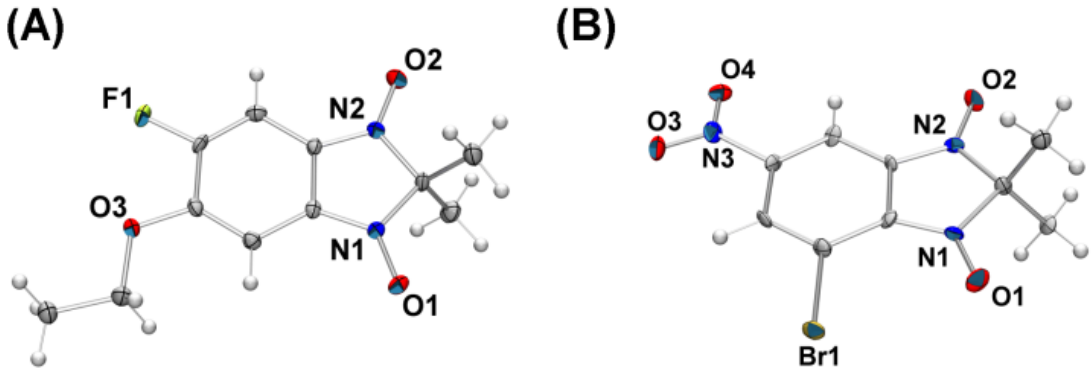

Figure 2.9. ORTEP diagram of (A) sepin1.17 and (B) sepin1.19.

2.2.3. Biological Activity

Biological study of sepin1.1 analogs was performed in collaboration with Prof. Debananda Pati's laboratory in Baylor College of Medicine. The separase enzymatic activity was measured by fluorogenic assay (Scheme 2.11).[32]

Scheme 2.11. Fluorogenic assay to measure separase activity.

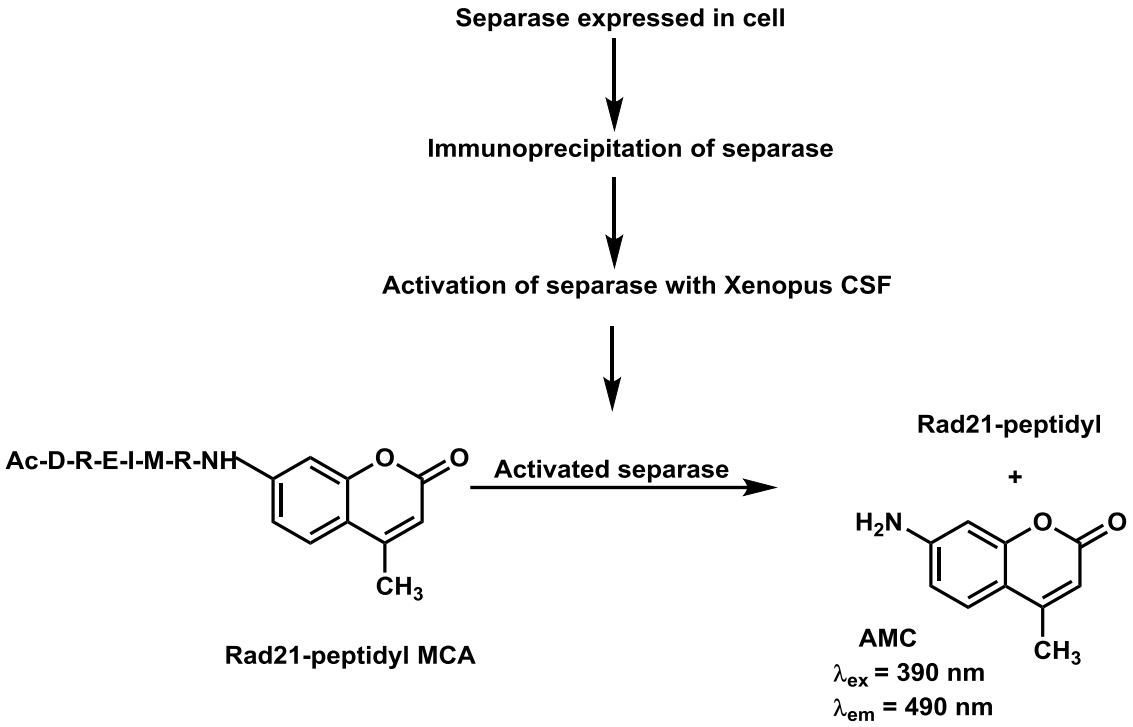

Briefly, separase was expressed in 293T cells and immunoprecipitated from growing cells by using immunoglobulin G (IgG)-conjugated Sepharose 6. Xenopus CSF extracted from frog eggs was then used to activate separase by degrading its inhibitor, securin. To test the inhibitory activity, sepin analogs were mixed with activated separase, followed by the addition of the enzyme substrate Rad21-MCA peptide (Ac-Asp-Arg-Glu-Ile-Nle-Arg-MCA). In the presence of separase, Rad21-MCA peptide is cleaved and a free coumaric acid (AMC) which is fluorescence active is released and measured at λ_{ex} =

390 nm and λ_{em} = 490 nm. By monitoring the fluorescent intensity of the free AMC formed, the inhibitory activity was determined. The better the inhibitor is, the lower the fluorescent intensity that will be observed. The concentration of sepin analogs to inhibit 50% of separase activity (IC_{50}) was calculated and presented in Table 2.4. For compounds that have low activity (IC_{50} > highest tested concentration), the inhibitory activity at 100 µM of those compounds were used to discuss the structure-activity relationship.

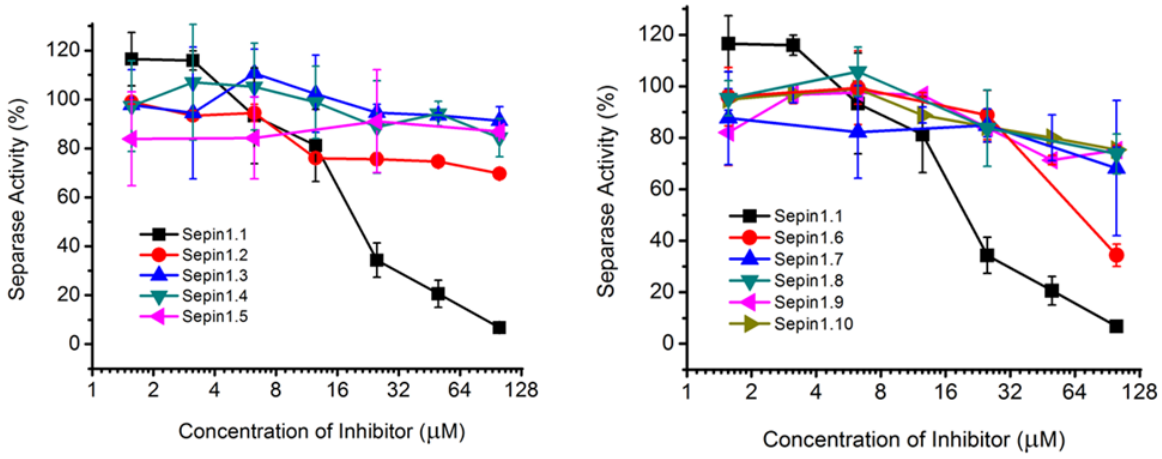

Figure 2.10. Inhibitory activity toward separase enzyme of analogs by $-NO_2$ modification

As mentioned earlier, sepin1.1 exhibits an inhibitory activity toward separase with an IC_{50} of 15 µM. Based on the structure of this lead compound, functional modifications have been made at the C5 position, bearing the nitro group, the C2 position that has the dimethyl chain, and the substituents on the heterocyclic ring.

Figure 2.10 illustrates the inhibitory activity of sepin analogs in which the nitro group has been replaced by other functional groups. The results revealed that the

replacement of the NO_2 group significantly reduces the inhibitory activity of sepin derivatives compared to the lead compound sepin1.1. All versions in which the nitro group has been replaced (sepin1.2-1.10) were less active suggesting that the presence of the NO_2 group is crucial for the inhibition toward separase enzyme. The derivative with a (trifluoromethyl)sulfonyl group in place of the nitro (sepin1.6), which inhibits 65.6 % separase enzyme at 100 μM concentration, was the most active among those molecules. The inhibitory activity toward separase seems to increase with the strength of the electron withdrawing group (-NO_2 > -SO_2CF_3 > -COOH > -F > -Br > -C_6H_5 > -$COOCH_3$ > -$NH(C_4H_9)$ > -CF_3 > -OEt). Derivatives that have functional groups with an electron-donating characteristic (-OEt, -$NH(C_4H_9)$ in sepin1.4 and sepin1.8, respectively) or weakly-electron-withdrawing effect (-COOH, -$COOCH_3$, -CF_3, -F, -Br, and -C_6H_5 in sepin1.2, sepin1.3, sepin1.5, sepin1.7, sepin1.9, and sepin1.10, respectively) show low inhibitory activity toward separase. Although derivatives with stronger electron-withdrawing groups such as -SO_2CF_3 in sepin1.6 reveals higher biological activity, the separase inhibition caused by these compounds still lower than that of sepin1.1 with –NO_2 group.

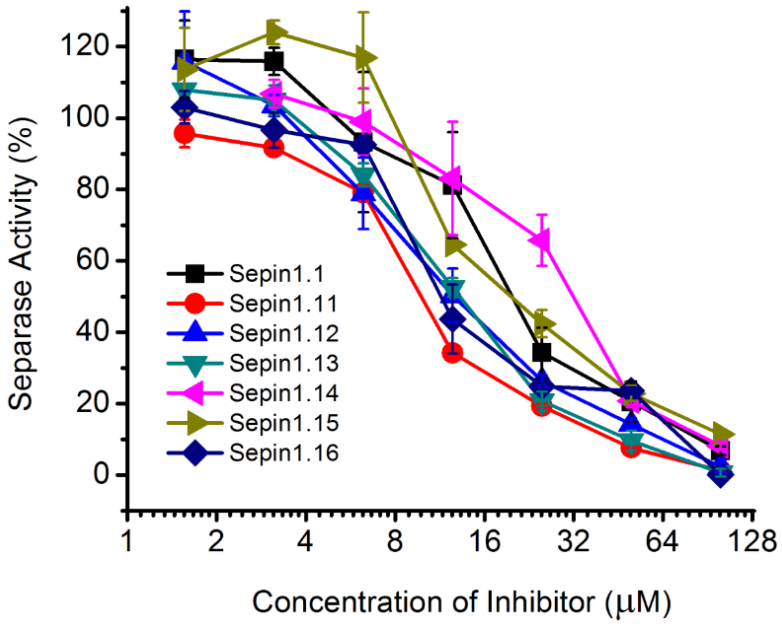

Figure 2.11. Inhibitory activity toward separase enzyme of analogs by dimethyl modification

Sepin analogs in which the dimethyl group at the C2 position have been modified to other alkyl chains show a moderate effect on the inhibitory activity of separase. The derivative in which one of the methyl groups is replaced by an ethyl group, the activity of the resulted compound (sepin1.11) increases 1.4 fold compared to sepin1.1. Modifying the methyl groups to propyl (sepin1.12), butyl (sepin1.13) or spiro-alkane (sepin1.15 and sepin1.16) did not change the inhibitory activity significantly although some improvement was observed (Figure 2.11 and Table 2.4). The results suggest that this position could be used to attach a photo-labeling moiety, which could be used to study the binding site of the inhibitor to separase enzyme. Sepin1.14, which has a –COOH group at the para position of a phenyl group attached to C2 position has been successfully synthesized and its inhibitory activity toward separase is comparable to the lead

compound with an IC_{50} of 16.86 μM. Further modification on the carboxylic acid group of this compound may provide a tool for photoaffinity labeling studies.

Structural modification of the substituent at other aromatic positions on the 6-member ring resulted in a dramatic change in separase inhibition with both increasing and decreasing activity.

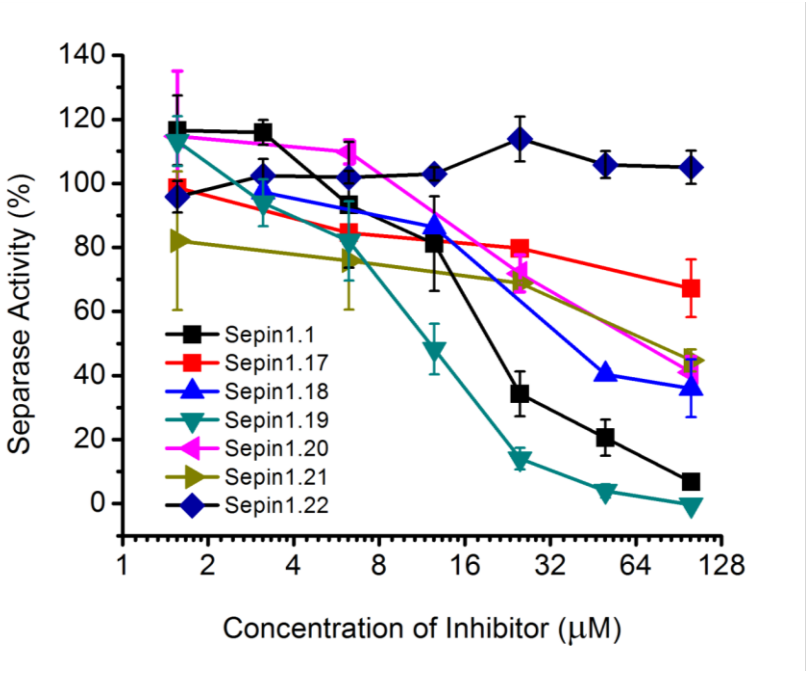

Figure 2.12. Inhibitory activity toward separase enzyme of analogs by other modifications

Derivative with fluorine and ethoxy groups at C5 and C6, respectively (sepin1.17) exhibits very low inhibitory activity. Sepin analog that has a fluorine atom substituted at C6 of sepin1.1 (sepin1.18) shows higher activity, however, only about a half of that of sepin1.1. Sepin1.20, which is the precursor of sepin1.1 and its reductive form (sepin1.21), showed moderate inhibitory activity toward separase, but was not comparable to sepin1.1. Interestingly, the brominated derivative of sepin1.1 with a

bromine atom at C7 (sepin1.19) shows a 1.6 fold lower in IC_{50} (10.21 µM) compared to that of sepin1.1. This was the derivative with best activity toward separase enzyme we have synthesized (Figure 2.12 and Table 2.4).

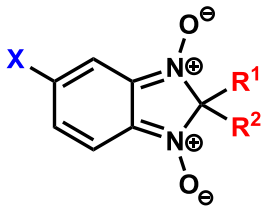

Table 2.4. Separase inhibitory results

Compound	X	R^1	R^2	IC_{50} (µM)	Inhibitory activity at 100 µM (%)
Sepin1.1	$-NO_2$	$-CH_3$	$-CH_3$	16.73	87.8
Sepin1.2	-COOH	$-CH_3$	$-CH_3$	-	30.3
Sepin1.3	$-COOCH_3$	$-CH_3$	$-CH_3$	-	8.7
Sepin1.4	$-OC_2H_5$	$-CH_3$	$-CH_3$	-	15.6
Sepin1.5	$-CF_3$	$-CH_3$	$-CH_3$	-	13.1
Sepin1.6	$-SO_2CF_3$	$-CH_3$	$-CH_3$	-	65.6
Sepin1.7	-F	$-CH_3$	$-CH_3$	-	31.8
Sepin1.8	$-NH(C_4H_9)$	$-CH_3$	$-CH_3$	-	26.3
Sepin1.9	-Br	$-CH_3$	$-CH_3$	-	24.8
Sepin1.10	$-C_6H_5$	$-CH_3$	$-CH_3$	-	24.6
Sepin1.11	$-NO_2$	$-CH_3$	$-C_2H_5$	12.08	98.8
Sepin1.12	$-NO_2$	$-C_2H_5$	$-C_3H_7$	11.69	97.7
Sepin1.13	$-NO_2$	$-CH_3$	$-C_4H_9$	12.65	99.4
Sepin1.14	$-NO_2$	$-CH_3$	$-C_6H_4$(*p*-COOH)	16.86	91.8
Sepin1.15	$-NO_2$		$-(CH_2)_4-$	16.77	88.6
Sepin1.16	$-NO_2$		$-(CH_2)_5-$	14.19	99.9
Sepin1.17[a]	-F; $-OC_2H_5$ (*o*)	$-CH_3$	$-CH_3$	-	32.8
Sepin1.18[a]	$-NO_2$; -F (*o*)	$-CH_3$	$-CH_3$	33.56	64.0
Sepin1.19[a]	$-NO_2$; -Br (*m*)	$-CH_3$	$-CH_3$	10.21	100
Sepin1.20[b]	$-NO_2$	-	-	53.04	59.0
Sepin1.21[b]	$-NO_2$	-	-	-	55.3
Sepin1.22[c]	-COOMe	-	-	-	0

[a] The first group is at C5 position, the position for the second group is given in parenthesis and relative to the first group (*o*: ortho; *m*: meta). [b] These molecules are the precursors to sepin1.1. [c] See Scheme 2.10 for chemical structures.

2.2.4. DFT calculations

To better understand the structure-activity relationship of sepin analogs, DFT calculations have been performed to explore the distribution of electron density on these molecules, which may give insight to help understand the biological activity of the tested compounds. The atomic coordinates from the crystal structure of these molecules (when available) were used as starting geometry for structural optimization using B3LYP/6-31G* methodology. Figure 2.11 shows the electrostatic potential surface mapping of selected derivative and the Mulliken charges of the atoms on the 2*H*-benzimidazole-1,3-dioxide ring skeleton. When comparing the calculation results and the inhibitory activity toward separase enzyme, we observed a correlation between the charges on the 5-member ring and the activity of sepin analogs. Derivatives that have more positive charge on the 5-member ring, especially the charge on the two nitrogens of the N-O groups, seem to possess better activity as separase inhibitors. This charge distribution is dependent on the substituent group on the 6-member ring, particularly at C5. This is consistent with our preliminary speculation of the dependence of biological activity on the strength of electron withdrawing effect mentioned earlier. Additionally, the activity of sepin analogs also depends on the charge of the two oxygen atoms. The more negative charge on these two oxygen atoms, the better the activity of the compound, suggesting that the nitrogen and oxygen atoms associated with the oxide bond on the 2*H*-benzimidazole-1,3-dioxide could be the sites that bind to the separase enzyme. The results also correlate with the much lower activity of sepin1.18 compared to sepin1.1 and sepin1.19, although substituents on sepin1.18 have more electron-withdrawing

characteristics. Highly active analogs have significant more negative charge on the two oxygens than derivatives with low activity.

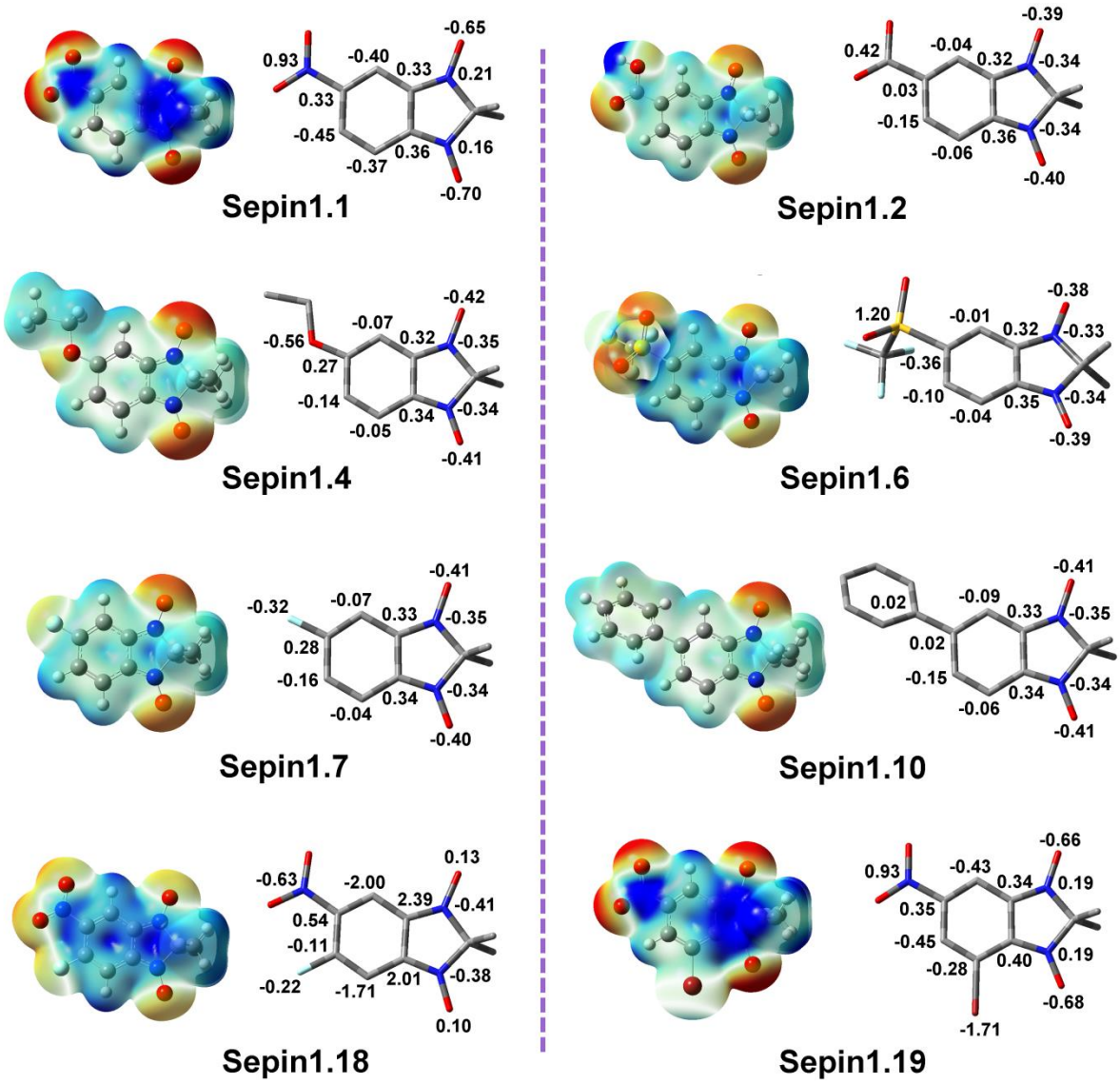

Figure 2.13. Eletrostatic potential surface mapping of selected sepin derivatives and Mulliken charges on selected atoms (carbon: grey, oxygen: red, nitrogen: blue, fluorine: cyan, sulfur: yellow, bromine: brown) on the 2*H*-benzimidazole-1,3-dioxides skeleton of these molecules. Surface mappings are plotted at 0.004 e/au^3 constant electron density and 0.004 isodensity value using the same scale for charges with the most positive potential in deepest blue color and most negative potential in deepest red color).

2.3. CONCLUSION

The synthesis, structural information, and structure-activity relationship of a novel class of separase inhibitors have been studied. Various analogs of sepin1.1 were synthesized by modifying three main positions on the structure of the molecule. The bioassay on the sepin analogs toward the inhibition of separase enzyme revealed that the substituent at C5 of the 2*H*-benzimidazole-1,3-dioxide skeleton affect on the inhibitory activity toward separase. Of these analogs the NO_2 group as in the lead compound is essential for the activity. Modification at the C2 shows a moderate effect on the biological activity of those compounds, suggesting that derivatives from this group could be used to help identify the actual active site in enzyme by photoaffinity labeling studies, which will assist substantially in the search for stronger inhibitors. Changing the substituents at other positions on 2*H*-benzimidazole-1,3-dioxide or the skeleton of the molecule dramatically affects the separase inhibition of sepin analogs. The sepin derivative with highest activity was found to be the bromine-substituted C7 on sepin1.1 skeleton. DFT calculation supports the correlation between the charges on the oxide nitrogen and oxygen atoms and the activity toward separase, suggesting that the oxide moieties on sepin's skeleton could possibly be the binding site to separase enzyme.

2.4. EXPERIMENTAL SECTION

2.4.1. General procedures

Unless noted, all reagents were purchased from Aldrich or Acros and used without further purification. Thin-layer chromatography (TLC) was performed on silica gel 60 F254pre-coated plates (0.25 mm) from Silicycle and components were visualized

by ultraviolet light (254 nm) and/or phosphomolybdic acid or *p*-anisaldehyde stain. Silicycle silica gel 230-400 (particle size 40-63 µm) mesh was used for all column chromatography. All the microwave reactions were performed on Biotage Initiator microwave instrument using Biotage microwave vials (0.5-2 mL, 2-5 mL and 10-20 mL). ^{1}H and ^{13}C NMR spectra were ecorded on JEOL ECX-400 NMR spectrometer (at 400 MHz and 100 MHz respectively) or JEOL ECA-500 NMR spectrometer (at 500 MHz and 125 MHz respectively) in $CDCl_3$, DMSO-d_6 and CD_3OD. Chemical shifts were reported in ppm, multiplicities are indicated by s = singlet, d = doublet, t = triplet, q = quartet, sep = septet, dd = doublet of doublet, dt = doublet of triplet, m = multiplet, and br = broad resonance. Coupling constants 'J' were reported in Hz. Data for ^{13}C NMR were reported in terms of chemical shift. High-resolution mass spectral data were obtained from The University of Texas at Austin, Mass Spectrometry Facility, Austin, TX.

2,2-dimethyl-5-nitro-*2H*-benzimidazol-1,3-dioxide (sepin1.1)

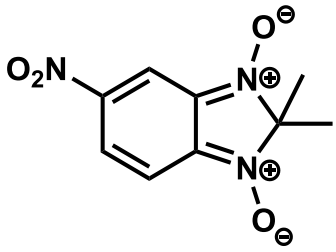

To a stirred solution of 1 mmol 5-nitrobenzofuroxan (181 mg) in concentrated sulfuric acid (2 mL) 1.7 mmol 2-propanol (102 mg, 0.13 mL) was added dropwise at room temperature. The reaction mixture was stirred for 2 hours before it was poured into ice-water and extracted with chloroform (3 x 20 mL). The organic layer was dried over $MgSO_4$ and evaporated. The crude mixture was purified by column chromatography on a

silica gel (1% MeOH in $CHCl_3$), obtained 165 mg of dark violet solid. Yield = 74%. ^{1}H NMR (400 MHz, $CDCl_3$) δ 8.18 (s, 1H), 7.58 (d, *J* = 10.1 Hz, 1H), 7.35 (d, *J* = 10.1 Hz, 1H), 1.72 (s, 6H). ^{13}C NMR (101 MHz, $CDCl_3$) δ 149.5, 136.1, 135.7, 123.9, 117.7, 113.9, 99.9, 24.6. HRMS (CI+) m/z calculated for $C_9H_9N_3O_4$ *m/z* 223.0593 ($[M]^+$), found 223.0594 ($[M]^+$).

2,2-dimethyl-*2H*-benzimidazol-1,3-dioxide-5-carboxylic acid (sepin1.2)

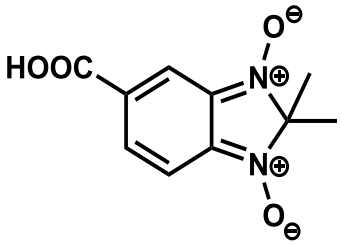

Sepin1.2 was prepared in a similar procedure for sepin1.1 using benzofuroxan-5-carboxylic acid (180 mg, 1 mmol). Column chromatography on a silica gel (20% MeOH in EtOAc) afforded a dark violet solid (69 mg, 31%). ^{1}H NMR (400 MHz, DMSO-d_6) δ 7.53 (s, 1H), 7.42 (d, *J* = 9.6 Hz, 1H), 7.08 (d, *J* = 9.6 Hz, 1H), 1.52 (s, 6H). ^{13}C NMR (101 MHz, DMSO-d_6) δ 167.2, 141.1, 137.0, 136.6, 132.8, 115.6, 114.7, 97.4, 24.1. HRMS (CI+) m/z calculated for $C_{10}H_{10}N_2O_4$ *m/z* 222.0641 ($[M]^+$), found 222.0641 ($[M]^+$).

Methyl 2,2-dimethyl-*2H*-benzimidazol-1,3-dioxide-5-carboxylate (sepin1.3).

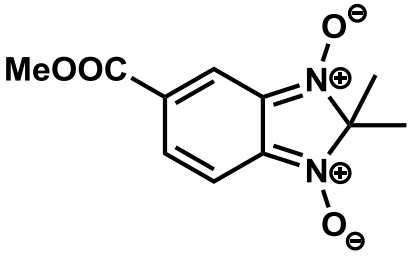

Sepin1.3 was prepared in a similar procedure for sepin1.1 using Methyl benzofuroxan-5-carboxylate (194 mg, 1 mmol). Column chromatography on a silica gel (50% EtOAc in hexanes) afforded a dark violet solid (132 mg, 56%). ^{1}H NMR (500 MHz, $CDCl_3$) δ 7.94 (t, *J* = 1.1 Hz, 1H), 7.42 (dd, *J* = 9.7, 1.1 Hz, 1H), 7.25 (dd, *J* = 9.7, 1.2 Hz, 1H), 3.90 (s, 3H), 1.70 (s, 6H). ^{13}C NMR (126 MHz, $CDCl_3$) δ 164.8, 136.6, 132.6, 129.9, 119.0, 116.1, 98.5, 53.0, 24.4. HRMS (CI+) m/z calculated for $C_{11}H_{12}N_2O_4$ *m/z* 236.0797 ($[M]^+$), found 236.0797 ($[M]^+$).

5-ethoxy-2,2-dimethyl-*2H*-benzimidazol-1,3-dioxide (sepin1.4)

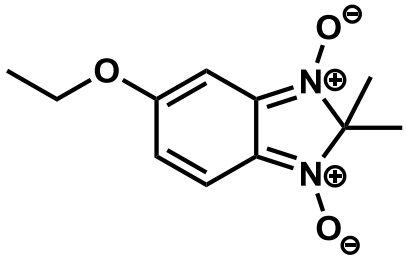

To a stirred solution of 1 mmol 5-ethoxybenzofuroxan (180 mg) in THF (10 mL) was added 2-nitropropane (1.2 mmol) and piperidine (1.2 mmol). The reaction mixture was stirred at room temperature for 24 hours. The solvent was then removed under vacuum and the crude mixture was purified by column chromatography (5% MeOH in EtOAc), afforded 84 mg of a dark violet solid. Yield = 38%. ^{1}H NMR (400 MHz, $CDCl_3$) δ 7.15 (d, *J* = 9.7, 1H), 6.62 (dd, *J* = 9.7, 1.4 Hz, 1H), 6.34 (d, *J* = 1.4 Hz, 1H), 4.01 (q, *J* = 6.9 Hz, 2H), 1.69 (s, 6H), 1.42 (t, *J* = 7.5 Hz, 3H). ^{13}C NMR (101 MHz, $CDCl_3$) δ 161.3, 136.5, 134.2, 129.3, 116.6, 97.5, 90.6, 64.9, 24.2, 14.3. HRMS (CI+) m/z calculated for $C_{11}H_{14}N_2O_3$ *m/z* 222.1004 ($[M]^+$), found 222.1006 ($[M]^+$).

2,2-dimethyl-5-(trifluoromethyl)-*2H*-benzimidazol-1,3-dioxide (sepin1.5)

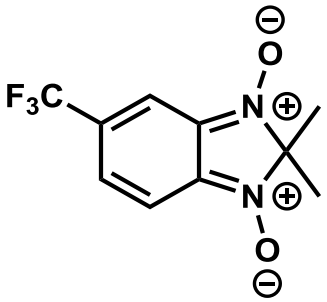

Sepin1.5 was prepared in a similar procedure for sepin1.4 using 5-trifluoromethylbenzofuroxan (204 mg, 1 mmol). Column chromatography on a silica gel (50% EtOAc in hexanes) afforded a red solid (120 mg, 49%). ^{1}H NMR (400 MHz, $CDCl_3$) δ 7.56 (dd, J = 2.6, 1.3 Hz, 1H), 7.36 – 7.32 (m, 1H), 6.97 (d, J = 9.7 Hz, 1H), 1.71 (s, 6H). ^{13}C NMR (101 MHz, $CDCl_3$) δ 136.2, 135.5, 132.6 (d, $J_{C\text{-}F}$ = 32.7 Hz), 126.2 (d, $J_{C\text{-}F}$ = 3.4 Hz), 123.9, 117.5, 114.7 (d, $J_{C\text{-}F}$ = 5.9 Hz), 98.8, 24.4. ^{19}F NMR (471 MHz, $CDCl_3$) δ -65.74 (s). HRMS (CI+) m/z calculated for $C_{10}H_9F_3N_2O_2$ *m/z* 246.0616 ($[M]^+$), found 246.0621 ($[M]^+$).

2,2-dimethyl-5-(trifluoromethylsulfonyl)-*2H*-benzimidazol-1,3-dioxide (sepin1.6)

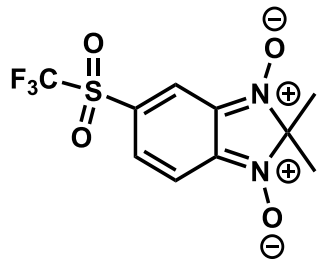

Sepin1.6 was prepared in a similar procedure for sepin1.1 using 5-trifluoromethylsulfonylbenzofuroxan (268 mg, 1 mmol). Column chromatography on a silica gel (30% EtOAc in hexanes) afforded a dark violet solid (130 mg, 42%). ^{1}H NMR

(500 MHz, $CDCl_3$) δ 8.02 (s, 1H), 7.42 (d, *J* = 9.74, 1H), 7.18 (d, *J* = 9.74 Hz, 1H), 1.73 (s, 6H). ^{13}C NMR (126 MHz, $CDCl_3$) δ 136.4, 135.9, 134.6, 126.7, 123.7, 120.6, 118.6, 100.0, 24.6. ^{19}F NMR (471 MHz, $CDCl_3$) δ -77.24 (s). HRMS (CI+) m/z calculated for $C_{10}H_9F_3N_2O_4S$ *m/z* 310.0235 ($[M]^+$), found 310.0237 ($[M]^+$).

5-fluoro-2,2-dimethyl-*2H*-benzimidazol-1,3-dioxide (sepin1.7)

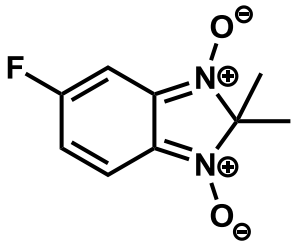

Sepin1.7 was prepared in a similar procedure for sepin1.1 using 5-fluorobenzofuroxan (154 mg, 1 mmol). Column chromatography on a silica gel (70% EtOAc in hexanes) afforded a red solid (151 mg, 77%). ^1H NMR (500 MHz, $CDCl_3$) δ 7.56 (d, *J* = 1.1 Hz, 1H), 7.36 – 7.32 (m, 1H), 6.97 (d, *J* = 9.7 Hz, 1H), 1.71 (s, 6H). ^{13}C NMR (126 MHz, $CDCl_3$) δ 163.8 (d, $J_{C\text{-}F}$ = 264.0 Hz), 135.6, 134.6, 124.1 (d, $J_{C\text{-}F}$ = 35.4 Hz), 118.0 (d, $J_{C\text{-}F}$ = 7.1 Hz), 99.2 (d, $J_{C\text{-}F}$ = 30.8 Hz), 98.2, 24.3. ^{19}F NMR (471 MHz, $CDCl_3$) δ -103.71 (td, *J* = 7.2, 5.6 Hz). HRMS (CI+) m/z calculated for $C_9H_9FN_2O_2$ *m/z* 196.0648 ($[M]^+$), found 196.0647 ($[M]^+$).

5-(butylamino)-2,2-dimethyl-*2H*-benzimidazol-1,3-dioxide (sepin1.8)

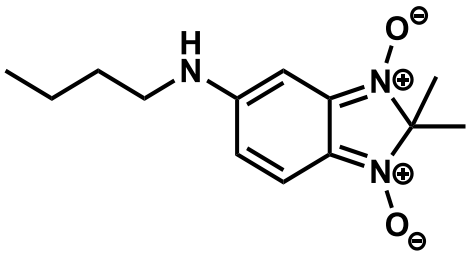

Starting material sepin1.7 (50 mg, 0.25 mmol) was dissolved in EtOH (2 mL), then *n*-butylamine (31 µL, 0.31 mmol) was added dropwise at room temperature. The reaction was run for 24 hours. Solvent was removed under vacuum and the mixture was submitted to flask chromatography, eluted by 5% MeOH in CH_2Cl_2, afforded 44 mg of a green solid, 70% yield. ^{1}H NMR (500 MHz, $CDCl_3$) δ 7.06 (d, *J* = 9.7 Hz, 1H), 6.51 (dd, *J* = 9.7, 1.6 Hz, 1H), 5.77 (d, *J* = 1.6 Hz, 1H), 5.03 (s, 1H), 3.11 (td, *J* = 7.2, 5.5 Hz, 2H), 1.67 (s, 6H), 1.63 – 1.56 (m, 2H), 1.37 (dq, *J* = 14.7, 7.4 Hz, 2H), 0.91 (t, *J* = 7.4 Hz, 3H). ^{13}C NMR (126 MHz, $CDCl_3$) δ 148.9, 136.9, 134.0, 129.5, 116.3, 96.54, 83.3, 43.5, 30.6, 24.0, 20.3, 13.8. HRMS (CI+) m/z calculated for $C_{13}H_{19}N_3O_2$ *m/z* 249.1477 ($[M]^+$), found 249.1483 ($[M]^+$).

5-bromo-2,2-dimethyl-*2H*-benzimidazol-1,3-dioxide (sepin1.9).

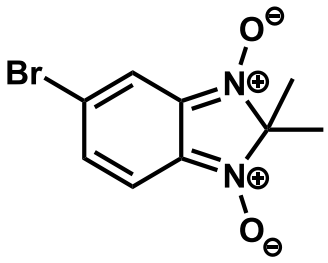

Sepin1.9 was prepared in a similar procedure for sepin1.1 using 5-bromobenzofuroxan (215 mg, 1 mmol). Column chromatography on a silica gel (2% MeOH in $CHCl_3$) afforded a dark violet solid (182 mg, 71%). ^{1}H NMR (400 MHz, $CDCl_3$) δ 7.46 (d, *J* = 1.2 Hz, 1H), 7.08 (dd, *J* = 9.7, 1.2 Hz, 1H), 6.93 (dd, *J* = 9.7, 1.2 Hz, 1H), 1.67 (s, 6H). ^{13}C NMR (101 MHz, $CDCl_3$) δ 136.4, 134.9, 134.8, 126.1, 118.0, 116.8, 97.9, 24.3. HRMS (CI+) m/z calculated for $C_9H_9BrN_2O_2$ *m/z* 255.9847 ($[M]^+$), found 255.9846 ($[M]^+$).

2,2-dimethyl-5-phenyl-*2H*-benzimidazol-1,3-dioxide (sepin1.10).

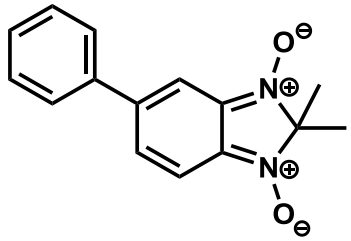

In an oven-dried flask sepin1.9 (50 mg, 0.19 mmol), $PhB(OH)_2$ (28.5 mg, 0.23 mmol), (SIPr)Pd(allyl)Cl (6.3 mg, 0.0097 mmol) and NaO*t*-Bu (56 mg, 0.58 mmol) was dissolved in 1,4-dioxane (0.5 mL). The reaction was run at 60 ºC for 12 hours. Upon completion, the solvent was removed under vacuum and the mixture was distributed into water and chloroform, then extracted with chloroform (3 x 30 mL). The organic phases were dried over $MgSO_4$ and evaporated before submitting to flask chromatography, eluting with 50% EtOAc in hexane, 15 mg of dark violet solid was obtained, 31% yield. ^{1}H NMR (400 MHz, $CDCl_3$) δ 7.57 – 7.54 (m, 2H), 7.48 – 7.42 (m, 3H), 7.38 (s, 1H), 7.31 (dd, *J* = 9.7, 0.6 Hz, 1H), 7.25 – 7.24 (m, 1H), 1.73 (s, 6H). ^{13}C NMR (101 MHz, $CDCl_3$) δ 143.6, 138.0, 136.9, 135.9, 132.2, 129.4, 129.3, 126.6, 116.1, 112.0, 97.6, 24.3. HRMS (CI+) m/z calculated for $C_{15}H_{14}N_2O_2$ *m/z* 254.1055 ($[M]^+$), found 254.1054 ($[M]^+$).

2-ethyl-2-methyl-5-nitro-*2H*-benzimidazol-1,3-dioxide (sepin1.11)

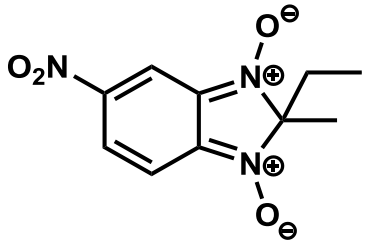

Sepin1.11 was prepared in a similar procedure for sepin1.1 using 5-nitrobenzofuroxan (181 mg, 1 mmol) and *n*-butanol (126 mg, 0.16 mL, 1.7 mmol). Column chromatography on a silica gel (2% MeOH in $CHCl_3$) afforded a dark violet solid (149 mg, 63%). ^1H NMR (400 MHz, $CDCl_3$) δ 8.18 (s, 1H), 7.58 (dd, *J* = 10.1, 1.6 Hz, 1H), 7.36 (d, *J* = 10.1 Hz, 1H), 2.19 (q, *J* = 7.3 Hz, 2H), 1.70 (s, 3H), 0.72 (t, *J* = 7.3 Hz, 3H). ^{13}C NMR (101 MHz, $CDCl_3$) δ 149.5, 137.2, 136.7, 123.8, 117.3, 113.6, 103.2, 31.5, 24.2, 6.4. HRMS (CI+) m/z calculated for $C_{10}H_{11}N_3O_4$ *m/z* 237.0750 ($[M]^+$), found 237.0749 ($[M]^+$).

2-ethyl-5-nitro-2-propyl-*2H*-benzimidazol-1,3-dioxide (sepin1.12)

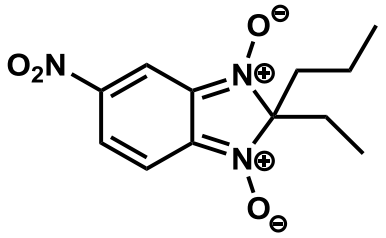

Sepin1.12 was prepared in a similar procedure for sepin1.1 using 5-nitrobenzofuroxan (181 mg, 1 mmol) and *n*-hexanol (174 mg, 0.21 mL, 1.7 mmol). Column chromatography on a silica gel (30% EtOAc in hexanes) afforded a dark violet solid (56 mg, 21%). ^1H NMR (500 MHz, $CDCl_3$) δ 8.17 (dd, *J* = 1.6, 1.1 Hz, 1H), 7.57 (dd, *J* = 10.1, 1.7 Hz, 1H), 7.35 (dd, *J* = 10.1, 1.0 Hz, 1H), 2.16 (q, *J* = 7.3 Hz, 2H), 2.11 – 2.07 (m, 2H), 1.10 – 1.00 (m, 2H), 0.85 (t, *J* = 7.3 Hz, 3H), 0.70 (t, *J* = 7.3 Hz, 3H). ^{13}C NMR (126 MHz, $CDCl_3$) δ 149.4, 138.1, 137.7, 123.8, 117.0, 113.2, 106.5, 39.6, 31.6, 15.2, 13.3, 6.2. HRMS (CI+) m/z calculated for $C_{12}H_{15}N_3O_4$ *m/z* 265.1063 ($[M]^+$), found 265.1057 ($[M]^+$).

2-butyl-2-methyl-5-nitro-*2H*-benzimidazol-1,3-dioxide (sepin1.13)

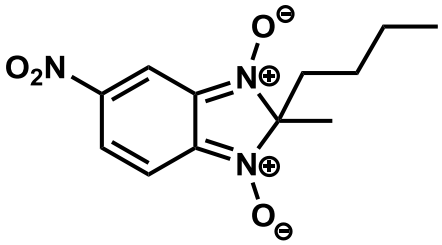

Sepin1.13 was prepared in a similar procedure for sepin1.1 using 5-nitrobenzofuroxan (181 mg, 1 mmol) and *n*-hexanol (174 mg, 0.21 mL, 1.7 mmol). Column chromatography on a silica gel (30% EtOAc in hexanes) afforded a dark violet solid (37 mg, 14%). ^{1}H NMR (500 MHz, $CDCl_3$) δ 8.18 (dd, *J* = 1.6, 1.1 Hz, 1H), 7.58 (dd, *J* = 10.1, 1.7 Hz, 1H), 7.35 (dd, *J* = 10.1, 1.0 Hz, 1H), 2.15 – 2.08 (m, 2H), 1.69 (s, 3H), 1.26 (dt, *J* = 14.7, 7.4 Hz, 2H), 1.04 – 0.95 (m, 2H), 0.83 (t, *J* = 7.4 Hz, 3H). ^{13}C NMR (126 MHz, $CDCl_3$) δ 149.5, 137.0, 136.6, 123.8, 117.3, 113.6, 102.9, 37.6, 24.6, 23.8, 21.9, 13.7. HRMS (CI+) m/z calculated for $C_{12}H_{15}N_3O_4$ *m/z* 265.1063 ($[M]^+$), found 265.1057 ($[M]^+$).

2-(4-caboxyphenyl)-2-methyl-5-nitro-*2H*-benzimidazol-1,3-dioxide (sepin1.14)

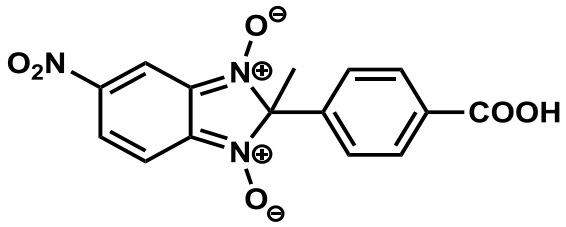

Sepin 1.14 was prepared in a similar procedure for sepin1.1 using 5-nitrobenzofuroxan (181 mg, 1 mmol) and 4-(1-bromoethyl)benzoic acid (160 mg, 0.7 mmol). The product was purified by HPLC affording a dark violet solid (82 mg, 25%). ^{1}H NMR (600 MHz, DMSO-d_6) δ 13.25 (s, 1H), 8.05 (s, 1H), 7.97 (d, *J* = 8.5 Hz, 2H), 7.59 – 7.56 (m, 3H),

7.44 (d, J = 10.1 Hz, 1H), 2.07 (s, 3H). ^{13}C NMR (151 MHz, DMSO-d_6) δ 167.0, 150.2, 137.4, 137.4, 137.2, 133.2, 130.4, 127.5, 125.0, 118.2, 114.3, 101.2, 23.6. HRMS (CI+) m/z calculated for $C_{15}H_{11}N_3O_6$ *m/z* 329.0605 ($[M]^+$), found 329.0592 ($[M]^+$).

5-nitro-2-spirocyclopentane-*2H*-benzimidazol-1,3-dioxide (sepin1.15)

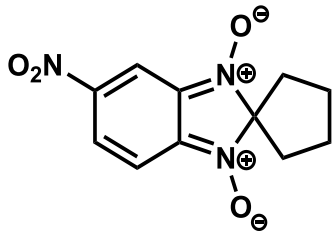

Sepin1.15 was prepared in a similar procedure for sepin1.1 using 5-nitrobenzofuroxan (181 mg, 1 mmol) and cyclopentanol (146 mg, 0.15 mL, 1.7 mmol). Column chromatography on a silica gel (50% EtOAc in hexanes) afforded a dark violet solid (157 mg, 63%). ^{1}H NMR (500 MHz, $CDCl_3$) δ 8.15 (d, J = 1.0 Hz, 1H), 7.56 (dd, J = 10.1, 1.5 Hz, 1H), 7.32 (d, J = 10.0 Hz, 1H), 2.37 – 2.26 (m, 4H), 2.15 – 2.06 (m, 4H). ^{13}C NMR (126 MHz, $CDCl_3$) δ 149.4, 136.4, 135.9, 123.6, 117.4, 113.7, 107.9, 40.7, 26.8. HRMS (CI+) m/z calculated for $C_{11}H_{11}N_3O_4$ *m/z* 249.0750 ($[M]^+$), found 249.0750 ($[M]^+$).

5-nitro-2-spirocyclohexane-*2H*-benzimidazol-1,3-dioxide (sepin1.16)

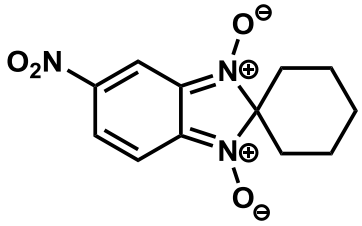

Sepin1.16 was prepared in a similar procedure for sepin1.1 using 5-nitrobenzofuroxan (181 mg, 1 mmol) and cyclohexanol (170 mg, 0.18 mL, 1.7 mmol). Column chromatography on a silica gel (20% EtOAc in hexanes) afforded a dark violet solid (113 mg, 43%). ^{1}H NMR (500 MHz, $CDCl_3$) δ 8.20 (s, 1H), 7.60 (dd, *J* = 10.0, 1.6 Hz, 1H), 7.37 (dd, *J* = 10.0 Hz, 1H), 2.04 – 1.88 (m, 8H), 1.71 – 1.58 (m, 2H). ^{13}C NMR (101 MHz, $CDCl_3$) δ 149.2, 136.1, 135.7, 123.5, 117.5, 113.8, 100.6, 34.1, 23.5, 19.0. HRMS (CI+) m/z calculated for $C_{12}H_{13}N_3O_4$ *m/z* 263.0906 ($[M]^+$), found 263.0911 ($[M]^+$).

5-ethoxy-6-fluoro-2,2-dimethyl-*2H*-benzimidazol-1,3-dioxide (sepin1.17)

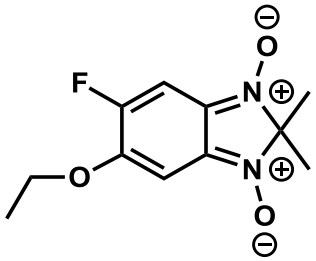

Sepin1.17 was prepared in a similar procedure for sepin1.1 using 5-ethoxyl-6-fluorobenzofuroxan (198 mg, 1 mmol). Column chromatography on a silica gel (3% MeOH in EtOAc) afforded a red solid (79 mg, 33%). ^{1}H NMR (500 MHz, $CDCl_3$) δ 6.91 – 6.86 (dd, *J* = 8.59 Hz, 1H), 6.46 (dd, *J* = 8.02 Hz, 1H), 4.08 (q, *J* = 7.0 Hz, 2H), 1.68 (s, 6H), 1.47 (t, *J* = 7.0 Hz, 3H). ^{13}C NMR (126 MHz, $CDCl_3$) δ 157.8 (d, $J_{C\text{-}F}$ = 272.9 Hz),

153.1 (d, $J_{C\text{-}F}$ = 20.8 Hz), 133.8, 132.2, 99.4 (d, $J_{C\text{-}F}$ = 27.9 Hz), 97.4, 92.9, 65.9, 24.1, 14.2. ^{19}F NMR (471 MHz, $CDCl_3$) δ -116.85 (t, *J* = 8.2 Hz). HRMS (CI+) m/z calculated for $C_{11}H_{13}FN_2O_3$ *m/z* 240.0910 ($[M]^+$), found 240.0912 ($[M]^+$).

5-fluoro-2,2-dimethyl-6-nitro-*2H*-benzimidazol-1,3-dioxide (sepin1.19)

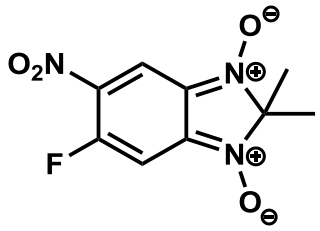

Sepin1.19 was prepared in a similar procedure for sepin1.1 using 5-nitro-6-fluorobenzofuroxan (200 mg, 1 mmol). Column chromatography on a silica gel (30% EtOAc in hexanes) afforded a red solid (82 mg, 34%). ^{1}H NMR (500 MHz, $CDCl_3$) δ 7.99 (d, *J* = 7.4 Hz, 1H), 7.08 (d, *J* = 8.6 Hz, 1H), 1.71 (s, 6H). ^{13}C NMR (126 MHz, $CDCl_3$) δ 154.7 (d, $J_{C\text{-}F}$ = 275.7 Hz), 142.5 (d, $J_{C\text{-}F}$ = 21.52 Hz), 134.06, 132.8, 116.0 (d, $J_{C\text{-}F}$ = 4.4 Hz), 102.9 (d, $J_{C\text{-}F}$ = 31.1 Hz), 99.9, 24.5. ^{19}F NMR (471 MHz, $CDCl_3$) δ -114.48, -114.49, -114.51. HRMS (CI+) m/z calculated for $C_9H_8FN_3O_4$ *m/z* 241.0499 ($[M]^+$), found 241.0500 ($[M]^+$).

4-bromo-2,2-dimethyl-6-nitro-*2H*-benzimidazol-1,3-dioxide (sepin1.18)

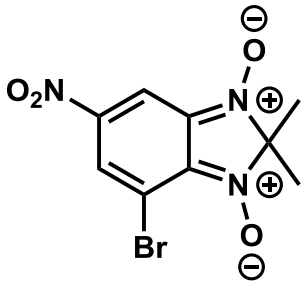

Starting material sepin1.1 (100 mg, 0.45 mmol) was dissolved in acetic acid (4.5 mL), then Br_2 (50 µL, 0.9 mmol) was added slowly. The reaction was run in 5 hours at room temperature before pouring into the ice-water, extracting with chloroform. The crude mixture was purified by flask chromatography, eluting with 30% EtOAc in hexane, obtain 72 mg of product as a dark violet solid, 53% yield. ^{1}H NMR (400 MHz, $CDCl_3$) δ 8.22 (d, *J* = 2.1 Hz, 1H), 7.85 (d, *J* = 2.1 Hz, 1H), 1.70 (s, 6H). ^{13}C NMR (101 MHz, $CDCl_3$) δ 148.5, 136.6, 133.6, 127.1, 112.4, 111.5, 100.5, 24.9. HRMS (CI+) m/z calculated for $C_9H_8BrN_3O_4$ *m/z* 300.9698 ($[M]^+$), found 300.9703 ($[M]^+$).

2,3-dimethyl-6-(methoxycarbonyl)quinoxaline-1,4-dioxide (sepin1.22)

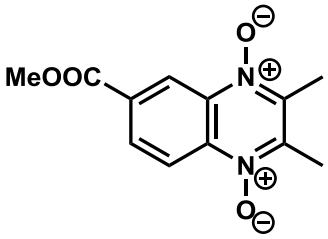

An oven-dried flask was added 5-nitrobenzofuroxane (150 mg, 0.77 mmol), 2-butanone (0.4 mL, 4.33 mmol) and *n*-butylamine (0.1 mL, 0.93 mmol) at 0 ^{o}C. The reaction was run in 2 hours at room temperature and stand for overnight. Chloroform (3 x 20 mL) was used to extract and the crude solid mixture was washed with diethylether, filtered to obtain a pure product, yellow solid. ^{1}H NMR (400 MHz, DMSO-d_6) δ 8.89 (d, *J* = 1.7 Hz, 1H), 8.51 (d, *J* = 9.0 Hz, 1H), 8.27 (dd, *J* = 8.9, 1.8 Hz, 1H), 3.93 (s, 3H), 2.58 (s, 6H). ^{13}C NMR (101 MHz, DMSO-d_6) δ 165.3, 144.0, 143.1, 138.5, 136.3, 131.9, 130.6, 121.8, 121.3, 53.5, 15.2, 15.1. HRMS (CI+) m/z calculated for $C_{12}H_{12}N_2O_4$ *m/z* 248.0797 ($[M]^+$), found 248.0797 ($[M]^+$).

2,2-dimethyl-5-nitro-*2H*-benzimidazole.diethylether

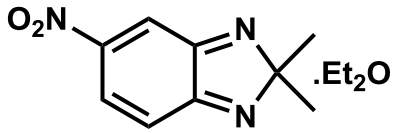

^{1}H NMR (400 MHz, $CDCl_3$) δ 8.27 – 8.19 (m, 1H), 7.74 (dd, *J* = 10.1, 1.7 Hz, 1H), 7.41 (d, *J* = 10.1 Hz, 1H), 1.59 (s, 6H). ^{13}C NMR (101 MHz, $CDCl_3$) δ 158.50, 157.76, 152.77, 127.99, 127.90, 124.26, 108.63, 77.44, 77.12, 76.81, 21.38.

2.4.2 Crystallography data

Table 2.5. Crystal data and structure refinement of **sepin1.2**

Empirical formula	C10 H14 N2 O6	
Formula weight	258.23	
Temperature	100(2) K	
Wavelength	0.71073 Å	
Crystal system	Triclinic	
Space group	P -1	
Unit cell dimensions	a = 6.7290(10) Å	α = 89.389(3)°.
	b = 7.4900(10) Å	β = 75.196(3)°.
	c = 12.5230(10) Å	γ = 73.782(2)°.
Volume	584.67(13) $Å^3$	
Z	2	
Density (calculated)	1.467 Mg/m^3	
Absorption coefficient	0.122 mm^{-1}	
F(000)	272	
Crystal size	0.330 x 0.140 x 0.120 mm^3	
Theta range for data collection	3.665 to 24.994°.	
Index ranges	-7<=h<=7, -8<=k<=8, -14<=l<=14	
Reflections collected	14595	
Independent reflections	2047 [R(int) = 0.0412]	
Completeness to theta = 25.242°	97.5 %	
Refinement method	Full-matrix least-squares on F^2	
Data / restraints / parameters	2047 / 0 / 182	
Goodness-of-fit on F^2	1.014	
Final R indices [I>2sigma(I)]	R1 = 0.0327, wR2 = 0.0903	
R indices (all data)	R1 = 0.0395, wR2 = 0.0975	
Largest diff. peak and hole	0.237 and -0.215 $e.Å^{-3}$	

Table 2.6. Crystal data and structure refinement of **sepin1.4**

Empirical formula	C11 H14 N2 O3	
Formula weight	222.24	
Temperature	100(2) K	
Wavelength	0.71073 Å	
Crystal system	Monoclinic	
Space group	P 21/c	
Unit cell dimensions	a = 9.742 Å	α = 90°.
	b = 14.507 Å	β = 109.44°.
	c = 8.032 Å	γ = 90°.
Volume	1070.4 $Å^3$	
Z	4	
Density (calculated)	1.379 Mg/m^3	
Absorption coefficient	0.102 mm^{-1}	
F(000)	472	
Crystal size	0.19 x 0.16 x 0.08 mm^3	
Theta range for data collection	3.034 to 27.444°.	
Index ranges	-9<=h<=12, -18<=k<=13, -10<=l<=10	
Reflections collected	8350	
Independent reflections	2439 [R(int) = 0.1086]	
Completeness to theta = 25.242°	99.8 %	
Refinement method	Full-matrix least-squares on F^2	
Data / restraints / parameters	2439 / 0 / 148	
Goodness-of-fit on F^2	1.072	
Final R indices [I>2sigma(I)]	R1 = 0.0841, wR2 = 0.1395	
R indices (all data)	R1 = 0.1508, wR2 = 0.1626	
Largest diff. peak and hole	0.312 and -0.380 $e.Å^{-3}$	

Table 2.7. Crystal data and structure refinement of **sepin1.5**

Empirical formula	C10 H9 F3 N2 O2	
Formula weight	246.19	
Temperature	100(2) K	
Wavelength	0.71073 Å	
Crystal system	Monoclinic	
Space group	P 21/m	
Unit cell dimensions	a = 7.986 Å	α = 90°.
	b = 7.760 Å	β = 97.61°.
	c = 8.334 Å	γ = 90°.
Volume	511.9 $Å^3$	
Z	4	
Density (calculated)	1.597 Mg/m^3	
Absorption coefficient	0.148 mm^{-1}	
F(000)	252	
Crystal size	0.190 x 0.180 x 0.040 mm^3	
Theta range for data collection	3.320 to 27.471°.	
Index ranges	-10<=h<=10, -10<=k<=10, -10<=l<=10	
Reflections collected	9900	
Independent reflections	1256 [R(int) = 0.0347]	
Completeness to theta = 25.242°	99.8 %	
Refinement method	Full-matrix least-squares on F^2	
Data / restraints / parameters	1256 / 40 / 125	
Goodness-of-fit on F^2	1.136	
Final R indices [I>2sigma(I)]	R1 = 0.0408, wR2 = 0.0951	
R indices (all data)	R1 = 0.0463, wR2 = 0.0973	
Largest diff. peak and hole	0.344 and -0.298 $e.Å^{-3}$	

Table 2.8. Crystal data and structure refinement of **sepin1.7**

Empirical formula	C9 H9 F N2 O2	
Formula weight	196.18	
Temperature	100(2) K	
Wavelength	0.71073 Å	
Crystal system	Orthorhombic	
Space group	C m c a	
Unit cell dimensions	a = 6.863 Å	α = 90°.
	b = 16.492 Å	β = 90°.
	c = 15.582 Å	γ = 90°.
Volume	1763.6 $Å^3$	
Z	8	
Density (calculated)	1.478 Mg/m^3	
Absorption coefficient	0.120 mm^{-1}	
F(000)	816	
Crystal size	0.140 x 0.120 x 0.030 mm^3	
Theta range for data collection	2.470 to 27.445°.	
Index ranges	-8<=h<=8, -21<=k<=21, -20<=l<=20	
Reflections collected	15840	
Independent reflections	1096 [R(int) = 0.0796]	
Completeness to theta = 25.242°	100.0 %	
Refinement method	Full-matrix least-squares on F^2	
Data / restraints / parameters	1096 / 0 / 83	
Goodness-of-fit on F^2	1.285	
Final R indices [I>2sigma(I)]	R1 = 0.0697, wR2 = 0.1662	
R indices (all data)	R1 = 0.0731, wR2 = 0.1686	
Largest diff. peak and hole	0.464 and -0.308 $e.Å^{-3}$	

Table 2.9. Crystal data and structure refinement of **sepin1.10**

Empirical formula	C15 H14 N2 O2	
Formula weight	254.28	
Temperature	100(2) K	
Wavelength	0.71073 Å	
Crystal system	Monoclinic	
Space group	P 21/c	
Unit cell dimensions	a = 12.333 Å	α = 90°.
	b = 10.462 Å	β = 107.36°.
	c = 10.060 Å	γ = 90°.
Volume	1238.9 $Å^3$	
Z	4	
Density (calculated)	1.363 Mg/m^3	
Absorption coefficient	0.092 mm^{-1}	
F(000)	536	
Crystal size	0.170 x 0.160 x 0.110 mm^3	
Theta range for data collection	3.016 to 27.516°.	
Index ranges	-16<=h<=15, -13<=k<=13, -13<=l<=13	
Reflections collected	19799	
Independent reflections	2835 [R(int) = 0.0581]	
Completeness to theta = 25.242°	99.9 %	
Refinement method	Full-matrix least-squares on F^2	
Data / restraints / parameters	2835 / 0 / 174	
Goodness-of-fit on F^2	1.075	
Final R indices [I>2sigma(I)]	R1 = 0.0476, wR2 = 0.0937	
R indices (all data)	R1 = 0.0648, wR2 = 0.1005	
Largest diff. peak and hole	0.304 and -0.219 $e.Å^{-3}$	

Table 2.10. Crystal data and structure refinement of **sepin1.14**

Empirical formula	C15 H11 N3 O6	
Formula weight	329.27	
Temperature	100(2) K	
Wavelength	0.71073 Å	
Crystal system	Triclinic	
Space group	P -1	
Unit cell dimensions	a = 6.098 Å	α = 101.37°.
	b = 7.853 Å	β = 97.64°.
	c = 14.648 Å	γ = 95.20°.
Volume	676.6 $Å^3$	
Z	2	
Density (calculated)	1.616 Mg/m^3	
Absorption coefficient	0.128 mm^{-1}	
F(000)	340	
Crystal size	0.120 x 0.120 x 0.040 mm^3	
Theta range for data collection	3.285 to 27.482°.	
Index ranges	-7<=h<=7, -10<=k<=10, -17<=l<=19	
Reflections collected	11057	
Independent reflections	3091 [R(int) = 0.0749]	
Completeness to theta = 25.242°	99.8 %	
Refinement method	Full-matrix least-squares on F^2	
Data / restraints / parameters	3091 / 0 / 219	
Goodness-of-fit on F^2	1.112	
Final R indices [I>2sigma(I)]	R1 = 0.0791, wR2 = 0.1441	
R indices (all data)	R1 = 0.1194, wR2 = 0.1601	
Largest diff. peak and hole	0.404 and -0.357 $e.Å^{-3}$	

Table 2.11. Crystal data and structure refinement of **sepin1.15**

Empirical formula	C11 H11 N3 O4	
Formula weight	249.23	
Temperature	100(2) K	
Wavelength	0.71073 Å	
Crystal system	Monoclinic	
Space group	P 21/n	
Unit cell dimensions	a = 8.716 Å	α = 90°.
	b = 5.696 Å	β = 96.55°.
	c = 21.744 Å	γ = 90°.
Volume	1072.5 $Å^3$	
Z	4	
Density (calculated)	1.544 Mg/m^3	
Absorption coefficient	0.120 mm^{-1}	
F(000)	520	
Crystal size	0.240 x 0.180 x 0.070 mm^3	
Theta range for data collection	3.467 to 27.460°.	
Index ranges	-11<=h<=11, -7<=k<=7, -26<=l<=28	
Reflections collected	10838	
Independent reflections	2445 [R(int) = 0.0416]	
Completeness to theta = 25.242°	99.8 %	
Refinement method	Full-matrix least-squares on F^2	
Data / restraints / parameters	2445 / 0 / 163	
Goodness-of-fit on F^2	1.083	
Final R indices [I>2sigma(I)]	R1 = 0.0450, wR2 = 0.0967	
R indices (all data)	R1 = 0.0600, wR2 = 0.1038	
Largest diff. peak and hole	0.209 and -0.285 $e.Å^{-3}$	

Table 2.12. Crystal data and structure refinement of **sepin1.16**

Empirical formula	C12 H13 N3 O4	
Formula weight	263.25	
Temperature	100(2) K	
Wavelength	0.71073 Å	
Crystal system	Monoclinic	
Space group	P 21/c	
Unit cell dimensions	a = 8.790 Å	α = 90°.
	b = 13.710 Å	β = 94.45°.
	c = 9.595 Å	γ = 90°.
Volume	1152.8 $Å^3$	
Z	4	
Density (calculated)	1.517 Mg/m^3	
Absorption coefficient	0.116 mm^{-1}	
F(000)	552	
Crystal size	0.140 x 0.120 x 0.020 mm^3	
Theta range for data collection	3.373 to 27.496°.	
Index ranges	-11<=h<=11, -17<=k<=17, -12<=l<=12	
Reflections collected	18170	
Independent reflections	2647 [R(int) = 0.1001]	
Completeness to theta = 25.242°	99.8 %	
Refinement method	Full-matrix least-squares on F^2	
Data / restraints / parameters	2647 / 0 / 172	
Goodness-of-fit on F^2	1.174	
Final R indices [I>2sigma(I)]	R1 = 0.0915, wR2 = 0.1602	
R indices (all data)	R1 = 0.1255, wR2 = 0.1725	
Largest diff. peak and hole	0.359 and -0.360 $e.Å^{-3}$	

Table 2.13. Crystal data and structure refinement of **sepin1.18**

Empirical formula	C11 H13 F N2 O3	
Formula weight	240.23	
Temperature	100(2) K	
Wavelength	0.71073 Å	
Crystal system	Monoclinic	
Space group	P 21/c	
Unit cell dimensions	a = 9.854 Å	α = 90°.
	b = 14.409 Å	β = 108.74°.
	c = 7.968 Å	γ = 90°.
Volume	1071.4 $Å^3$	
Z	4	
Density (calculated)	1.489 Mg/m^3	
Absorption coefficient	0.121 mm^{-1}	
F(000)	504	
Crystal size	0.240 x 0.180 x 0.110 mm^3	
Theta range for data collection	3.047 to 24.998°.	
Index ranges	-11<=h<=11, -17<=k<=15, -9<=l<=9	
Reflections collected	9133	
Independent reflections	1890 [R(int) = 0.0520]	
Completeness to theta = 25.242°	97.2 %	
Refinement method	Full-matrix least-squares on F^2	
Data / restraints / parameters	1890 / 0 / 157	
Goodness-of-fit on F^2	1.078	
Final R indices [I>2sigma(I)]	R1 = 0.0436, wR2 = 0.0883	
R indices (all data)	R1 = 0.0586, wR2 = 0.0939	
Largest diff. peak and hole	0.207 and -0.233 $e.Å^{-3}$	

Table 2.14. Crystal data and structure refinement of **sepin1.19**

Empirical formula	C9 H8 Br N3 O4	
Formula weight	302.09	
Temperature	100(2) K	
Wavelength	0.71073 Å	
Crystal system	Orthorhombic	
Space group	P n a 21	
Unit cell dimensions	a = 16.999 Å	α = 90°.
	b = 6.653 Å	β = 90°.
	c = 9.495 Å	γ = 90°.
Volume	1073.8 $Å^3$	
Z	4	
Density (calculated)	1.869 Mg/m^3	
Absorption coefficient	3.836 mm^{-1}	
F(000)	600	
Crystal size	0.300 x 0.200 x 0.070 mm^3	
Theta range for data collection	2.396 to 27.534°.	
Index ranges	-22<=h<=22, -7<=k<=8, -8<=l<=12	
Reflections collected	5323	
Independent reflections	2003 [R(int) = 0.0580]	
Completeness to theta = 25.242°	99.8 %	
Refinement method	Full-matrix least-squares on F^2	
Data / restraints / parameters	2003 / 1 / 156	
Goodness-of-fit on F^2	0.897	
Final R indices [I>2sigma(I)]	R1 = 0.0330, wR2 = 0.0620	
R indices (all data)	R1 = 0.0406, wR2 = 0.0638	
Absolute structure parameter	0.096(16)	
Largest diff. peak and hole	0.550 and -0.514 $e.Å^{-3}$	

REFERENCES

(1) Torre, L. A.; Bray, F.; Siegel, R. L.; Ferlay, J.; Lortet-Tieulent, J.; Jemal, A. *CA: A Cancer Journal for Clinicians* **2015**, *65*, 87.

(2) Holland, A. J.; Cleveland, D. W. *Nat Rev Mol Cell Biol* **2009**, *10*, 478.

(3) Holland, A. J.; Cleveland, D. W. *EMBO reports* **2012**, *13*, 501.

(4) Uhlmann, F. *Secured Cutting: Controlling Separase at the Metaphase to Anaphase Transition*, *EMBO reports* **2001**, *2*, 487-492.

(5) Zhang, N.; Ge, G.; Meyer, R.; Sethi, S.; Basu, D.; Pradhan, S.; Zhao, Y.-J.; Li, X.-N.; Cai, W.-W.; El-Naggar, A. K.; Baladandayuthapani, V.; Kittrell, F. S.; Rao, P. H.; Medina, D.; Pati, D. *Proceedings of the National Academy of Sciences* **2008**, *105*, 13033.

(6) Meyer, R.; Fofanov, V.; Panigrahi, A.; Merchant, F.; Zhang, N.; Pati, D. *Clinical Cancer Research* **2009**, *15*, 2703.

(7) Zhang, N.; Scorsone, K.; Ge, G.; Kaffes, C. C.; Dobrolecki, L. E.; Mukherjee, M.; Lewis, M. T.; Berg, S.; Stephan, C. C.; Pati, D. *Journal of Biomolecular Screening* **2014**, *19*, 878.

(8) Song, S.; Kim, J.; Shim, J.; Kim, J.; Hoon Lee, B.; Jin, Y.; Kim, I.; Lee, K.; Suh, H. *Solar Energy Materials and Solar Cells* **2012**, *98*, 323.

(9) Hazelton, J. C.; Iddon, B.; Redhouse, A. D.; Suschitzky, H. *Tetrahedron* **1995**, *51*, 5597.

(10) Samsonov, V. A.; Volodarskii, L. B.; Shamirzaeva, V. *Chem Heterocycl Compd* **1994**, *30*, 460.

(11) Gaughran, R. J.; Picard, J. P.; Kaufman, J. V. R. *Journal of the American Chemical Society* **1954**, *76*, 2233.

(12) Dyall, L. *Australian Journal of Chemistry* **1984**, *37*, 2013.

(13) Boiani, M.; Boiani, L.; Merlino, A.; Hernández, P.; Chidichimo, A.; Cazzulo, J. J.; Cerecetto, H.; González, M. *European Journal of Medicinal Chemistry* **2009**, *44*, 4426.

(14) Boiani, M.; Boiani, L.; Denicola, A.; Torres de Ortiz, S.; Serna, E.; Vera de Bilbao, N.; Sanabria, L.; Yaluff, G.; Nakayama, H.; Rojas de Arias, A.; Vega, C.; Rolan, M.; Gómez-Barrio, A.; Cerecetto, H.; González, M. *Journal of Medicinal Chemistry* **2006**, *49*, 3215.

(15) Merlino, A.; Benitez, D.; Campillo, N. E.; Paez, J. A.; Tinoco, L. W.; Gonzalez, M.; Cerecetto, H. *MedChemComm* **2012**, *3*, 90.

(16) Leyva, S.; Castanedo, V. c.; Leyva, E. *Journal of Fluorine Chemistry* **2003**, *121*, 171.

(17) Haroun, M.; Helissey, P.; Giorgi-Renault, S. *Synthetic Communications* **2001**, *31*, 2329.

(18) Agarkov, A.; Gilbertson, S. R. *Journal of Combinatorial Chemistry* **2008**, *10*, 655.

(19) Gong, Y.; He, W. *Organic Letters* **2002**, *4*, 3803.

(20) Navarro, O.; Kaur, H.; Mahjoor, P.; Nolan, S. P. *The Journal of Organic Chemistry* **2004**, *69*, 3173.

(21) Aguirre, G.; Boiani, L.; Cerecetto, H.; Di Maio, R.; González, M.; Porcal, W.; Denicola, A.; Möller, M.; Thomson, L.; Tórtora, V. *Bioorganic & Medicinal Chemistry* **2005**, *13*, 6324.

(22) Kaftory, M.; Shteiman, V.; Botoshansky, M. *Acta Crystallographica Section C* **2002**, *58*, o183.

(23) Key, J. A.; Cairo, C. W. *Dyes and Pigments* **2011**, *88*, 95.

(24) Qin, H.; Yamagiwa, N.; Matsunaga, S.; Shibasaki, M. *Angewandte Chemie International Edition* **2007**, *46*, 409.

(25) Liu, P. N.; Dang, L.; Wang, Q. W.; Zhao, S. L.; Xia, F.; Ren, Y. J.; Gong, X. Q.; Chen, J. Q. *The Journal of Organic Chemistry* **2010**, *75*, 5017.

(26) Samsonov, V. A.; Gatilov, Y. V.; Savel'ev, V. A. *Russian Journal of Organic Chemistry* **2013**, *49*, 1208.

(27) Ghosh, P. B.; Ternai, B.; Whitehouse, M. W. *Journal of Medicinal Chemistry* **1972**, *15*, 255.

(28) Duque-Montaño, B. E.; Gómez-Caro, L. C.; Sanchez-Sanchez, M.; Monge, A.; Hernández-Baltazar, E.; Rivera, G.; Torres-Angeles, O. *Bioorganic & Medicinal Chemistry* **2013**, *21*, 4550.

(29) Ochal, Z.; Bretner, M.; Wolinowska, R.; Tyski, S. *Medicinal Chemistry* **2013**, *9*, 1129.

(30) Torres, E.; Moreno-Viguri, E.; Galiano, S.; Devarapally, G.; Crawford, P. W.; Azqueta, A.; Arbillaga, L.; Varela, J.; Birriel, E.; Di Maio, R.; Cerecetto, H.; González, M.; Aldana, I.; Monge, A.; Pérez-Silanes, S. *European Journal of Medicinal Chemistry* **2013**, *66*, 324.

(31) Keller, H. J.; Leichtert, I.; Uhlmann, G.; Weiss, J. *Chemische Berichte* **1977**, *110*, 1684.

(32) Basu, D.; Zhang, N.; Panigrahi, A. K.; Horton, T. M.; Pati, D. *Analytical Biochemistry* **2009**, *392*, 133.

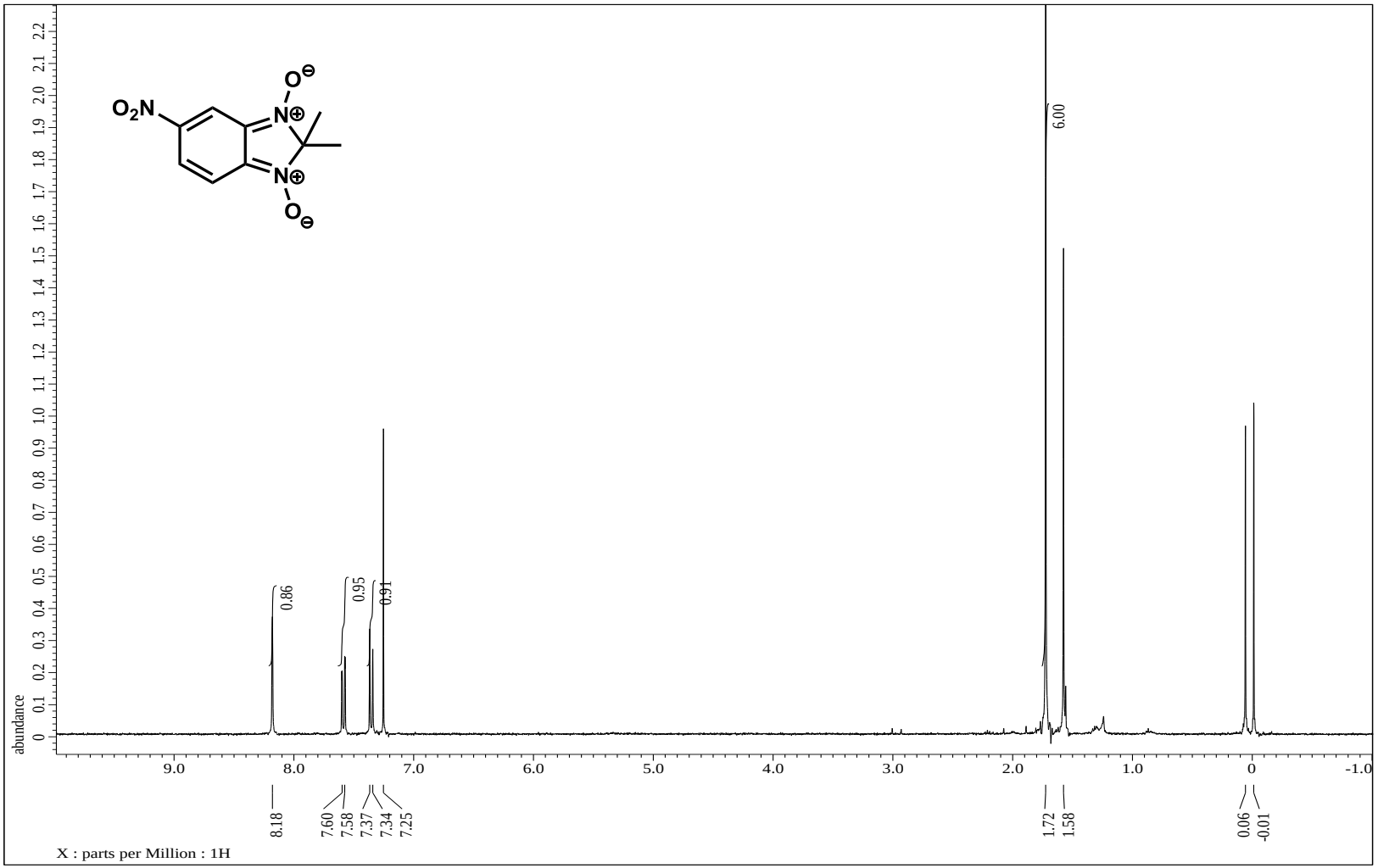

Figure 2.14. ^{1}H NMR (400 MHz, $CDCl_3$) of 2,2-dimethyl-5-nitro-*2H*-benzimidazol-1,3-dioxide (sepin1.1)

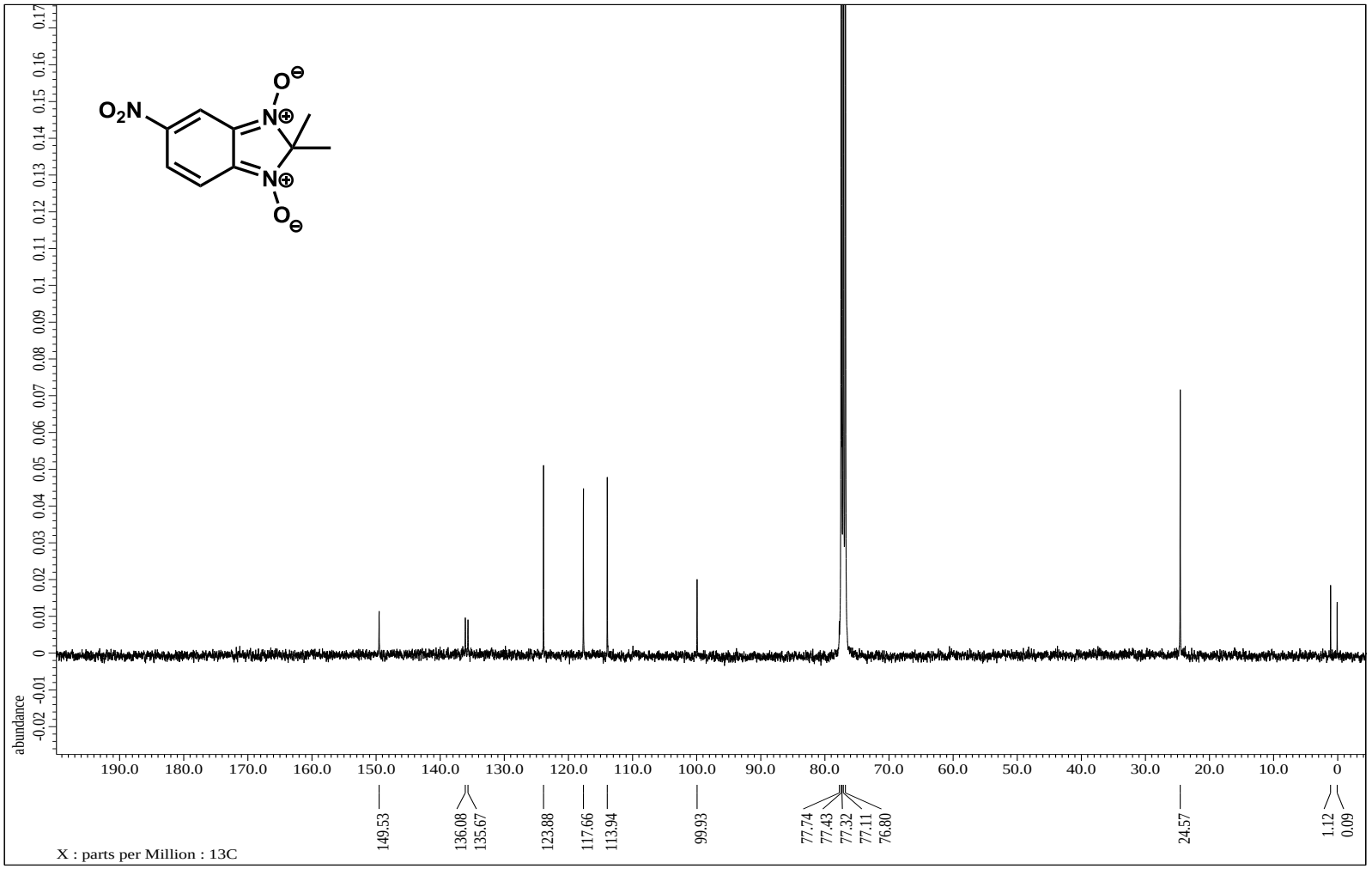

Figure 2.15. ^{13}C NMR (101 MHz, $CDCl_3$) of 2,2-dimethyl-5-nitro-*2H*-benzimidazol-1,3-dioxide (sepin1.1)

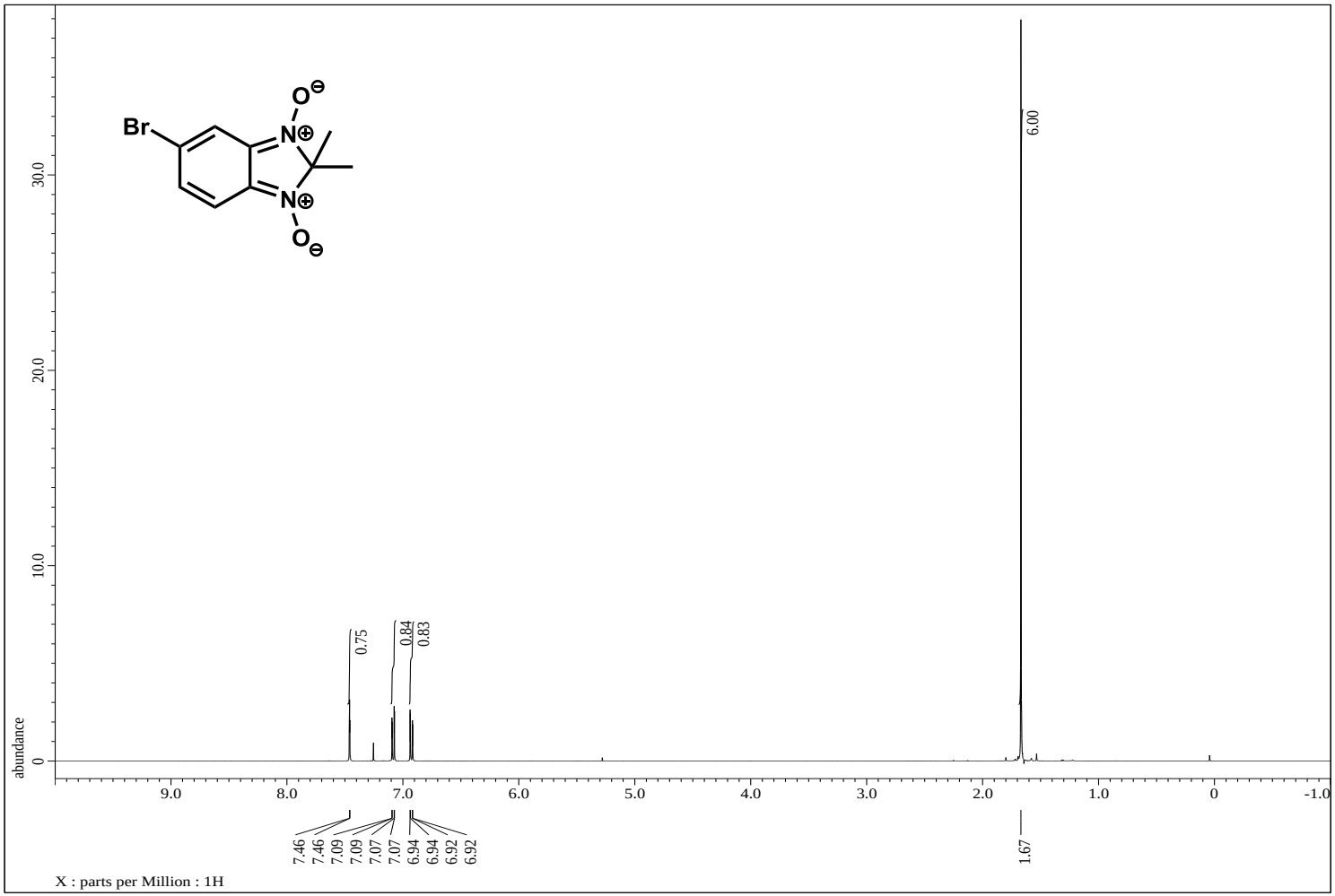

Figure 2.16. ^{1}H NMR (400 MHz, $CDCl_3$) of 5-bromo-2,2-dimethyl-*2H*-benzimidazol-1,3-dioxide (sepin1.9)

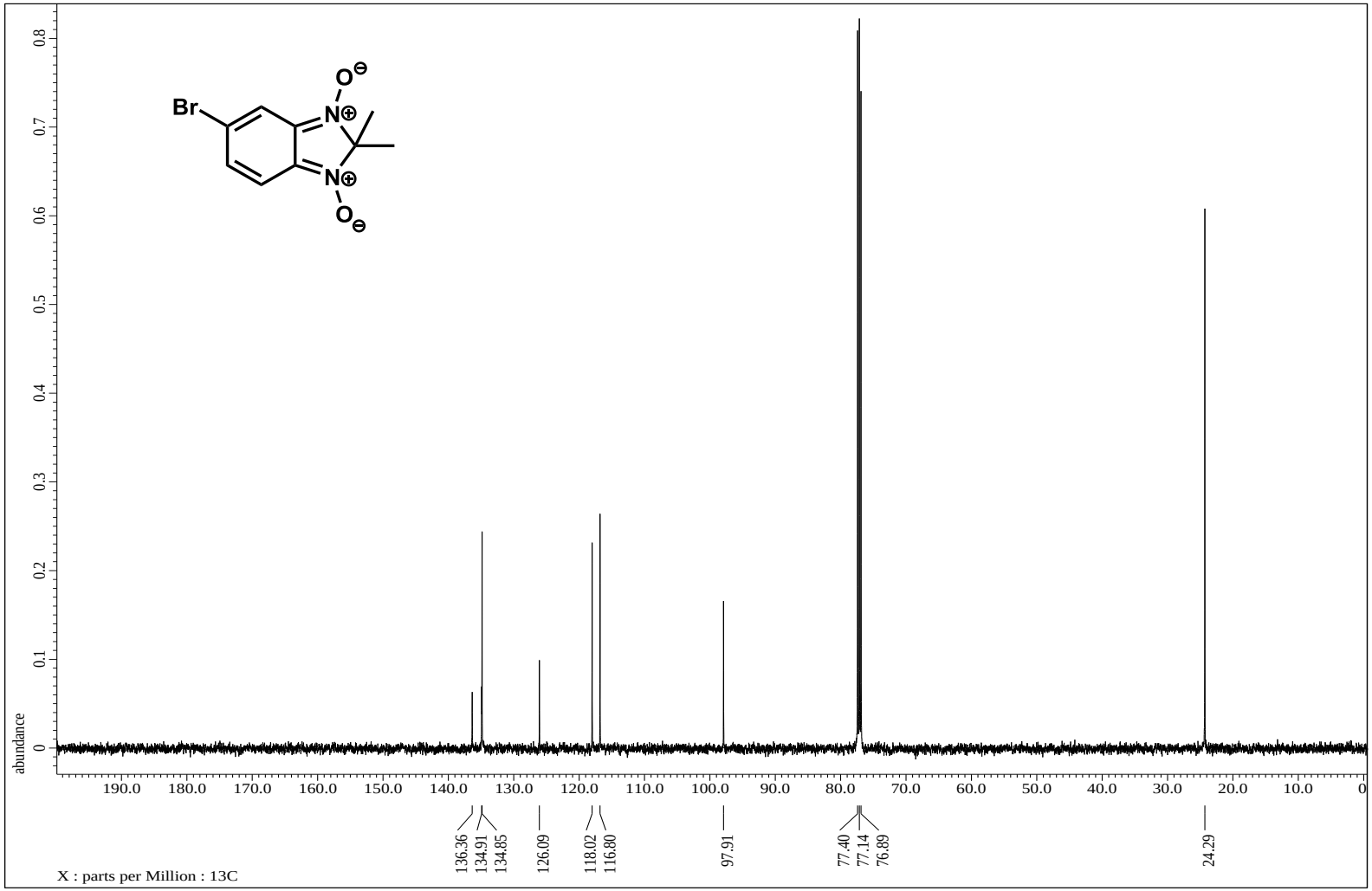

Figure 2.17. ^{13}C NMR (101 MHz, $CDCl_3$) of 5-bromo-2,2-dimethyl-*2H*-benzimidazol-1,3-dioxide (sepin1.9)

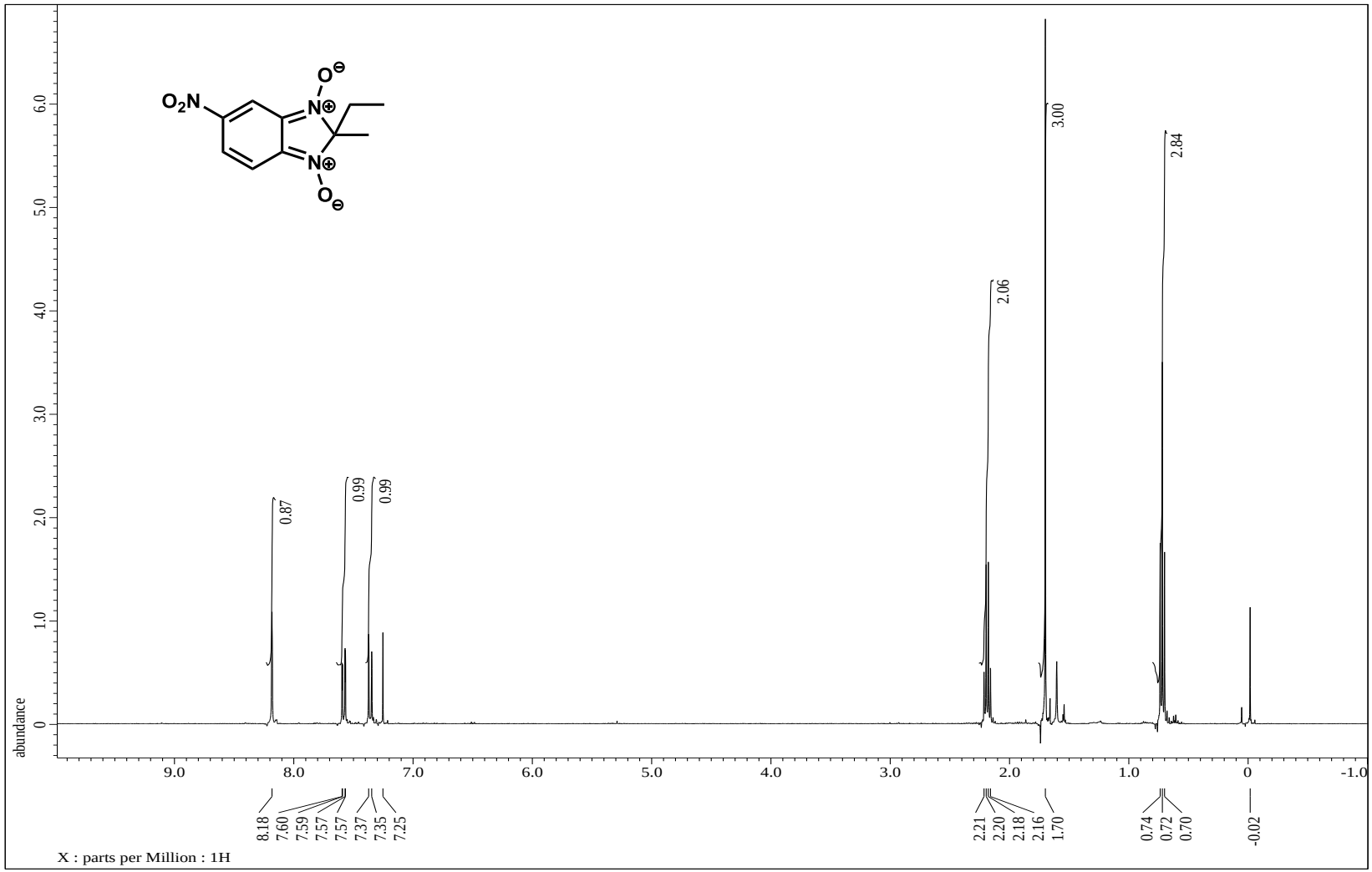

Figure 2.18. ^{1}H NMR (400 MHz, $CDCl_3$) of 2-ethyl-2-methyl-5-nitro-*2H*-benzimidazol-1,3-dioxide (sepin1.11)

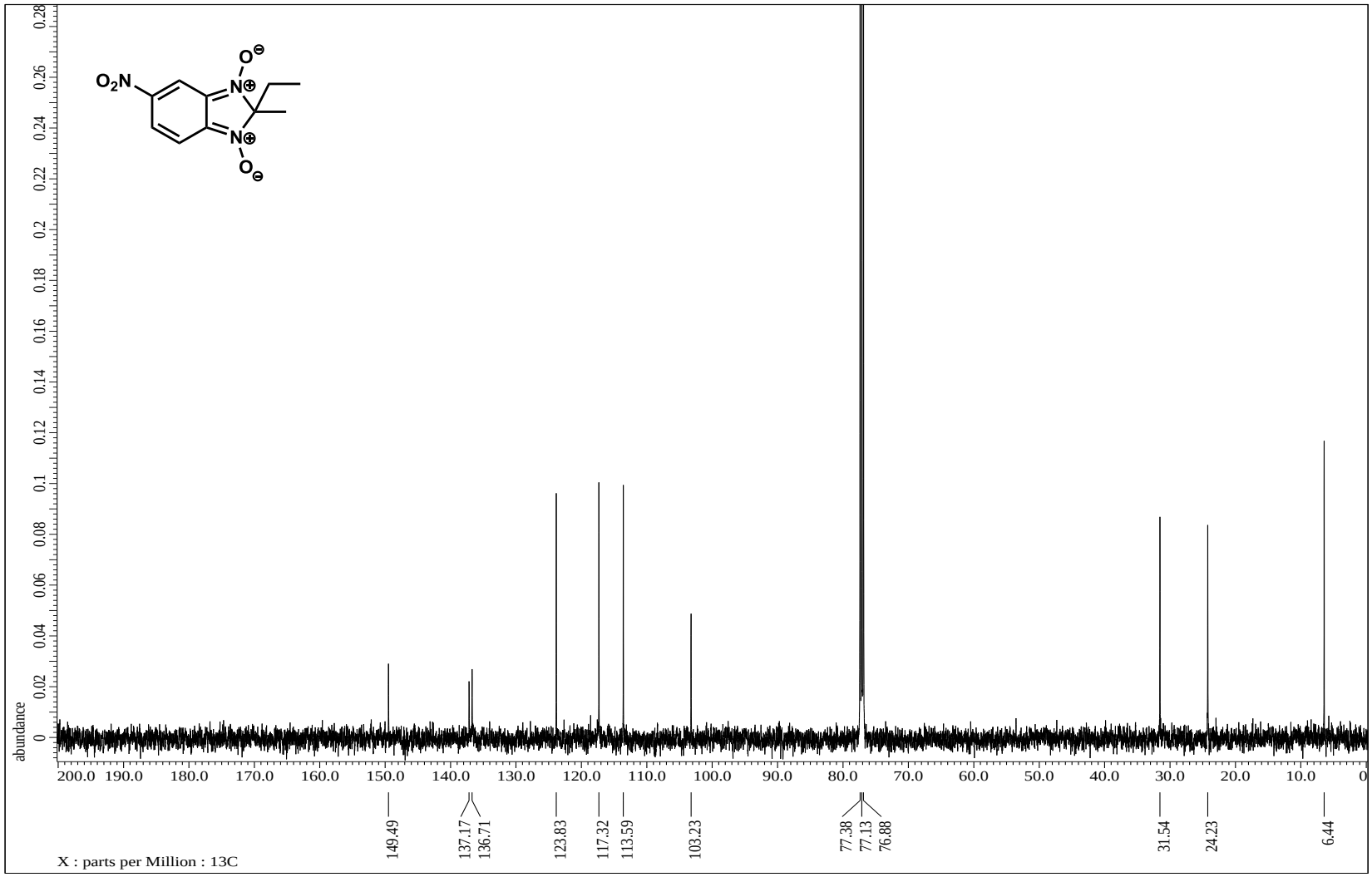

Figure 2.19. ^{13}C NMR (101 MHz, $CDCl_3$) of 2-ethyl-2-methyl-5-nitro-*2H*-benzimidazol-1,3-dioxide (sepin1.11)

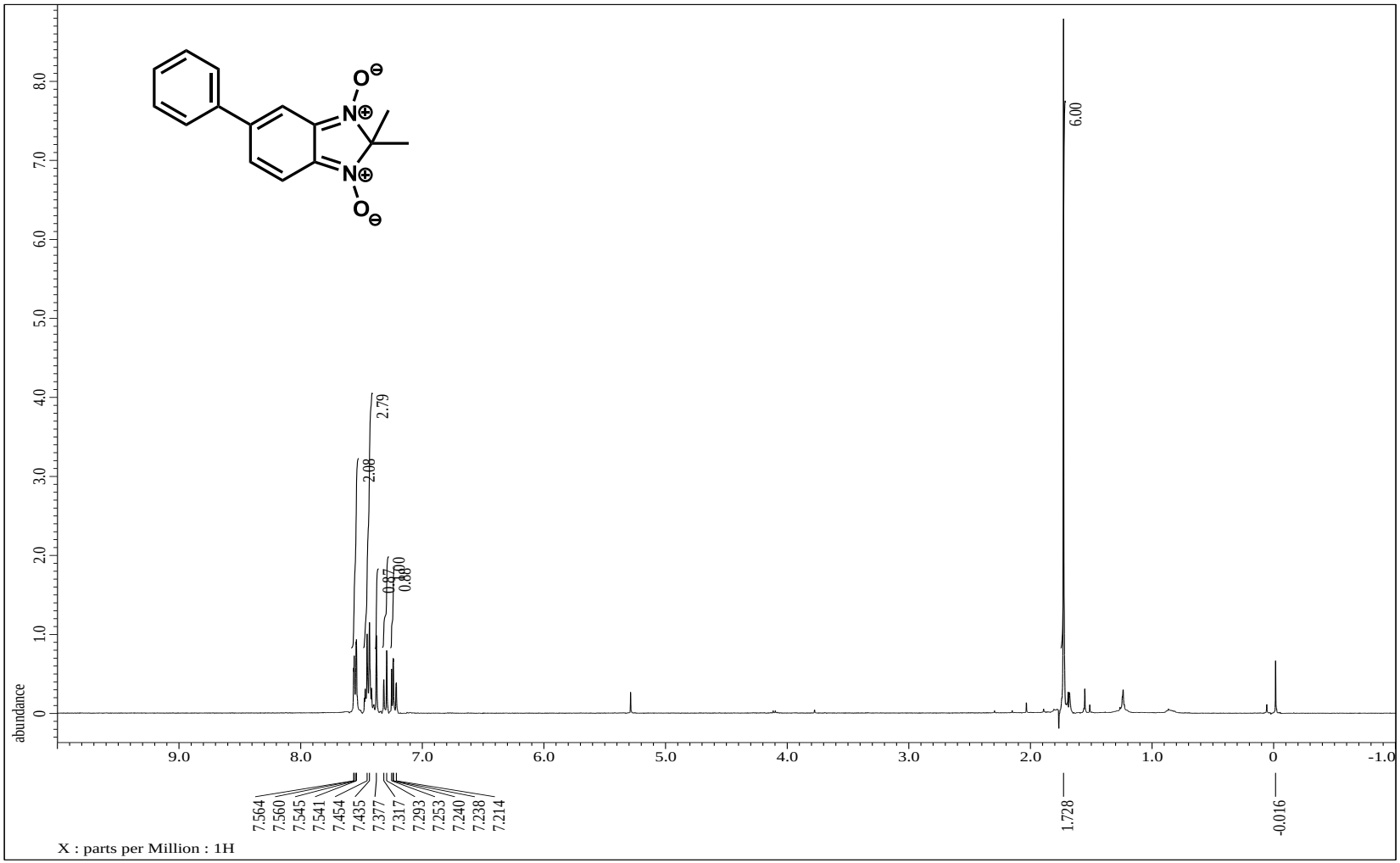

Figure 2.20. ^{1}H NMR (400 MHz, $CDCl_3$) of 2,2-dimethyl-5-phenyl-*2H*-benzimidazol-1,3-dioxide (sepin1.10)

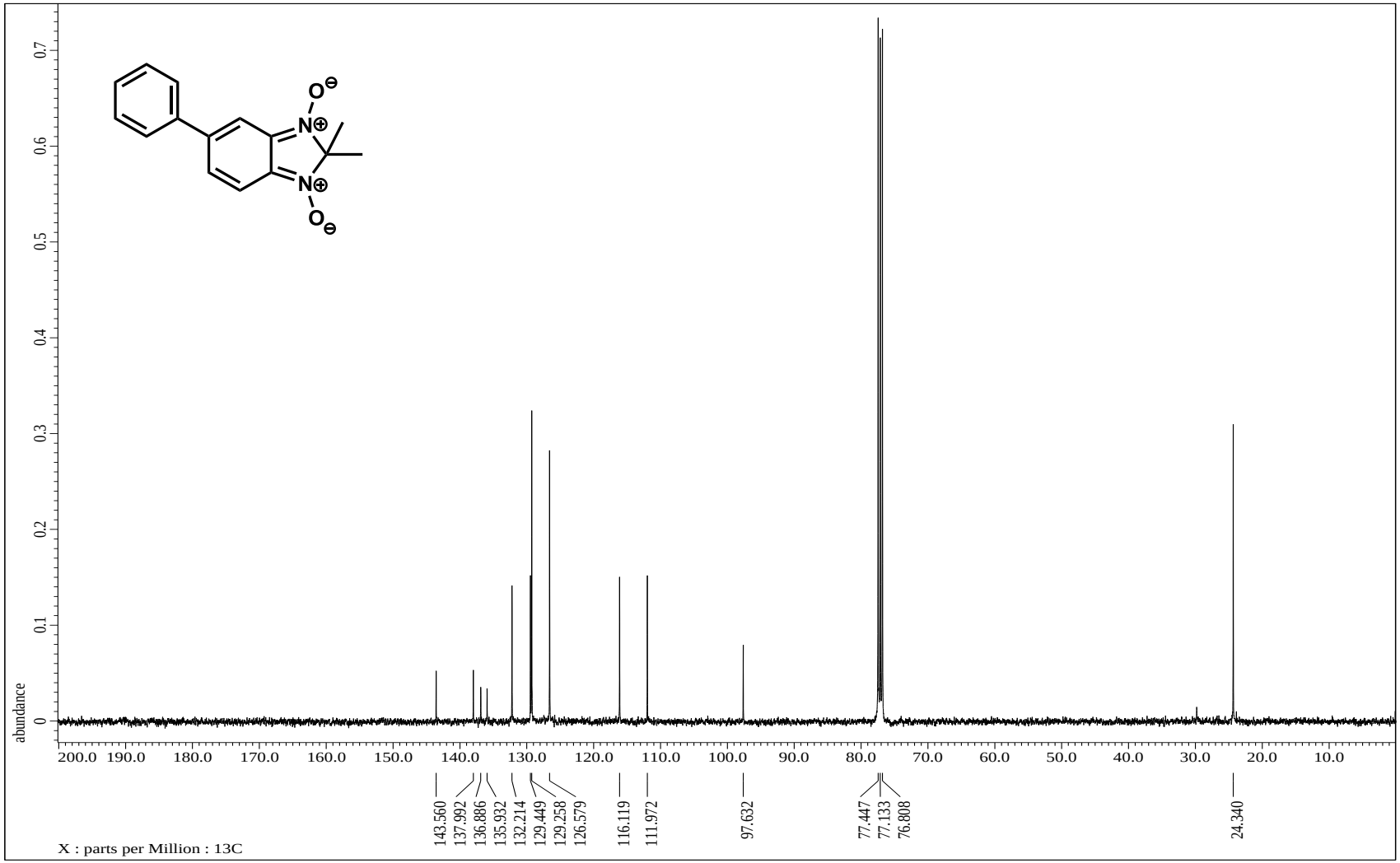

Figure 2.21. ^{13}C NMR (101 MHz, $CDCl_3$) of 2,2-dimethyl-5-phenyl-*2H*-benzimidazol-1,3-dioxide (sepin1.10)

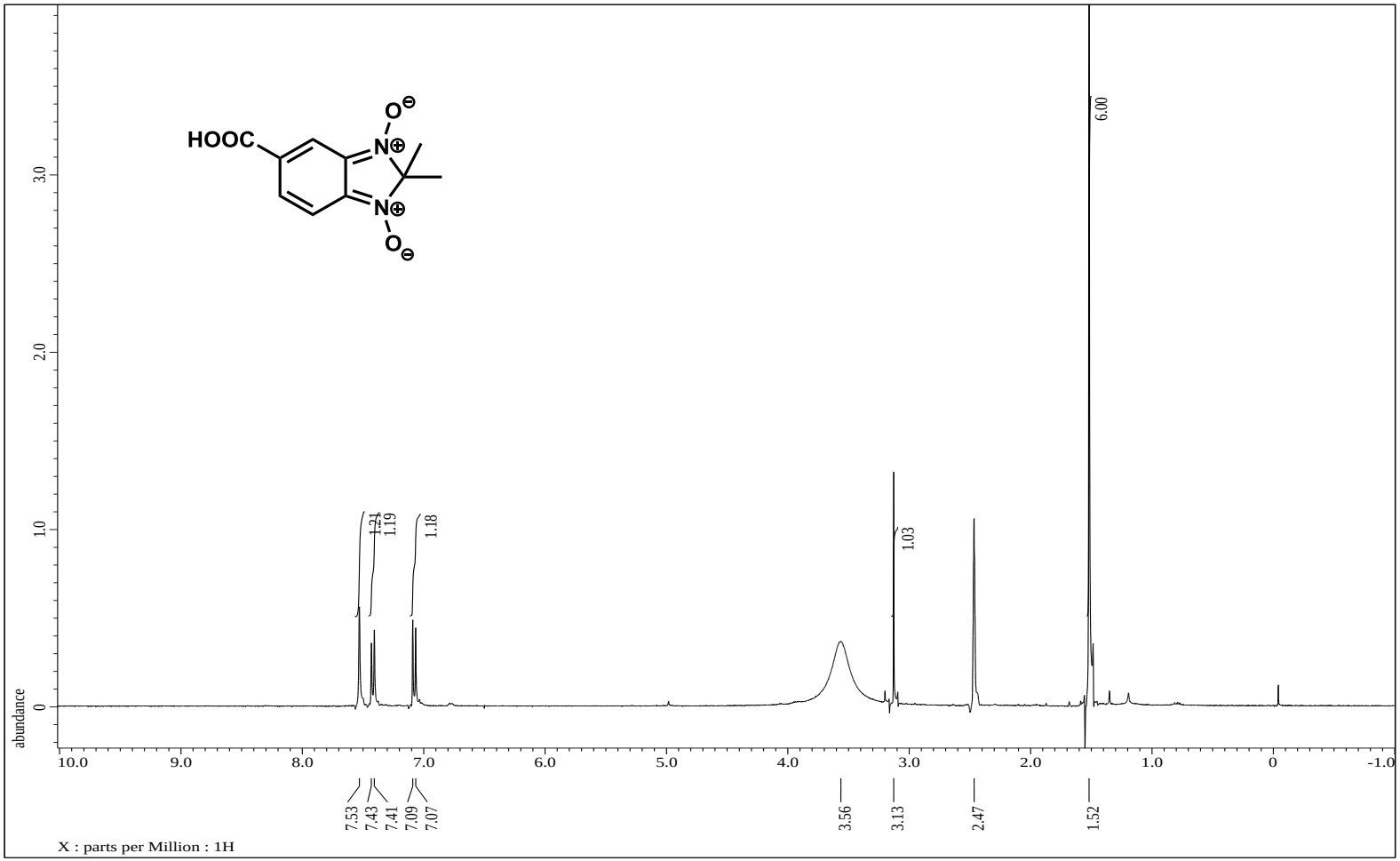

Figure 2.22. ^{1}H NMR (400 MHz, DMSO-d_6) of 2,2-dimethyl-*2H*-benzimidazol-1,3-dioxide-5-carboxylic acid (sepin1.2)

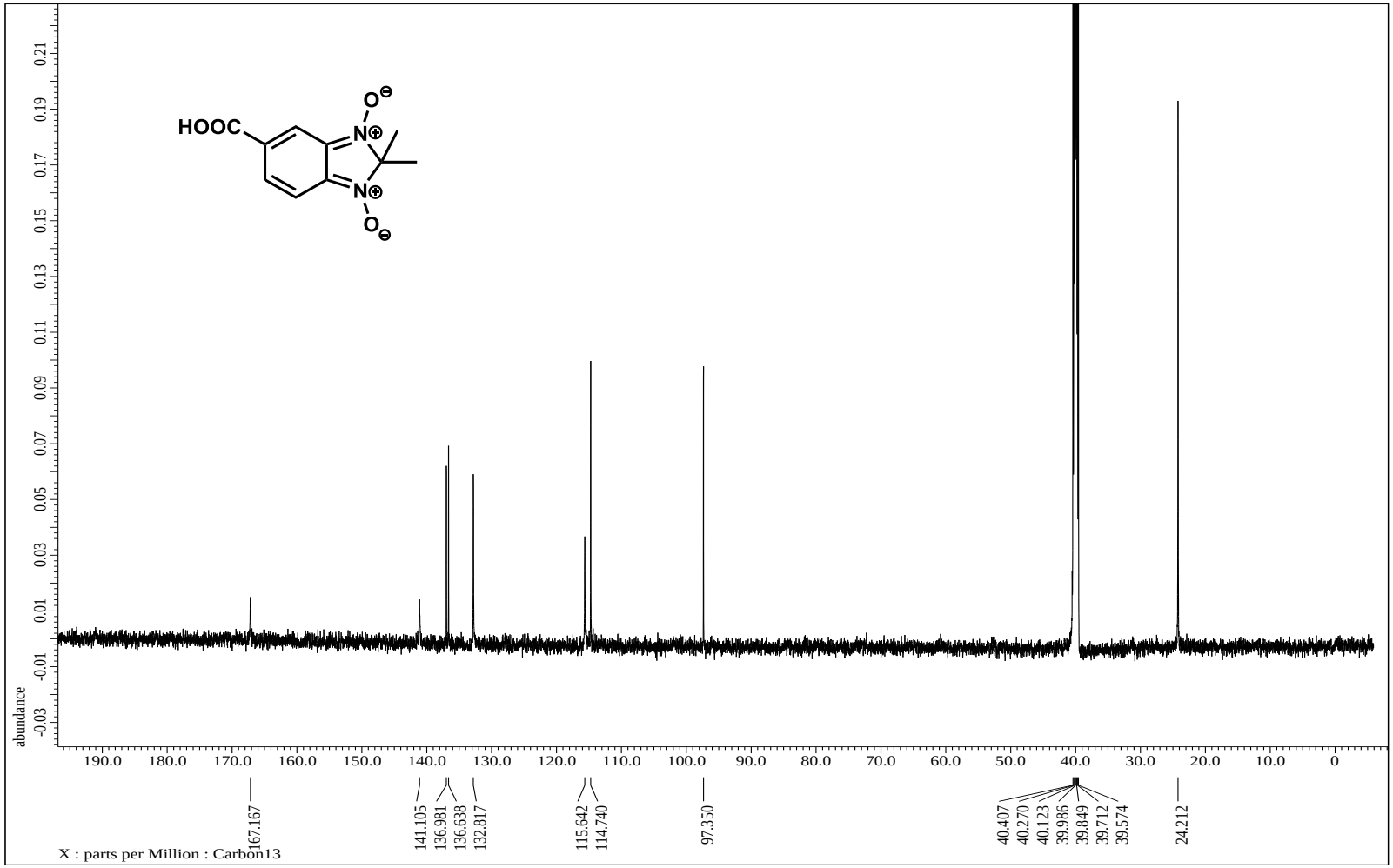

Figure 2.23. ^{13}C NMR (101 MHz, DMSO-d_6) of 2,2-dimethyl-*2H*-benzimidazol-1,3-dioxide-5-carboxylic acid (sepin1.2)

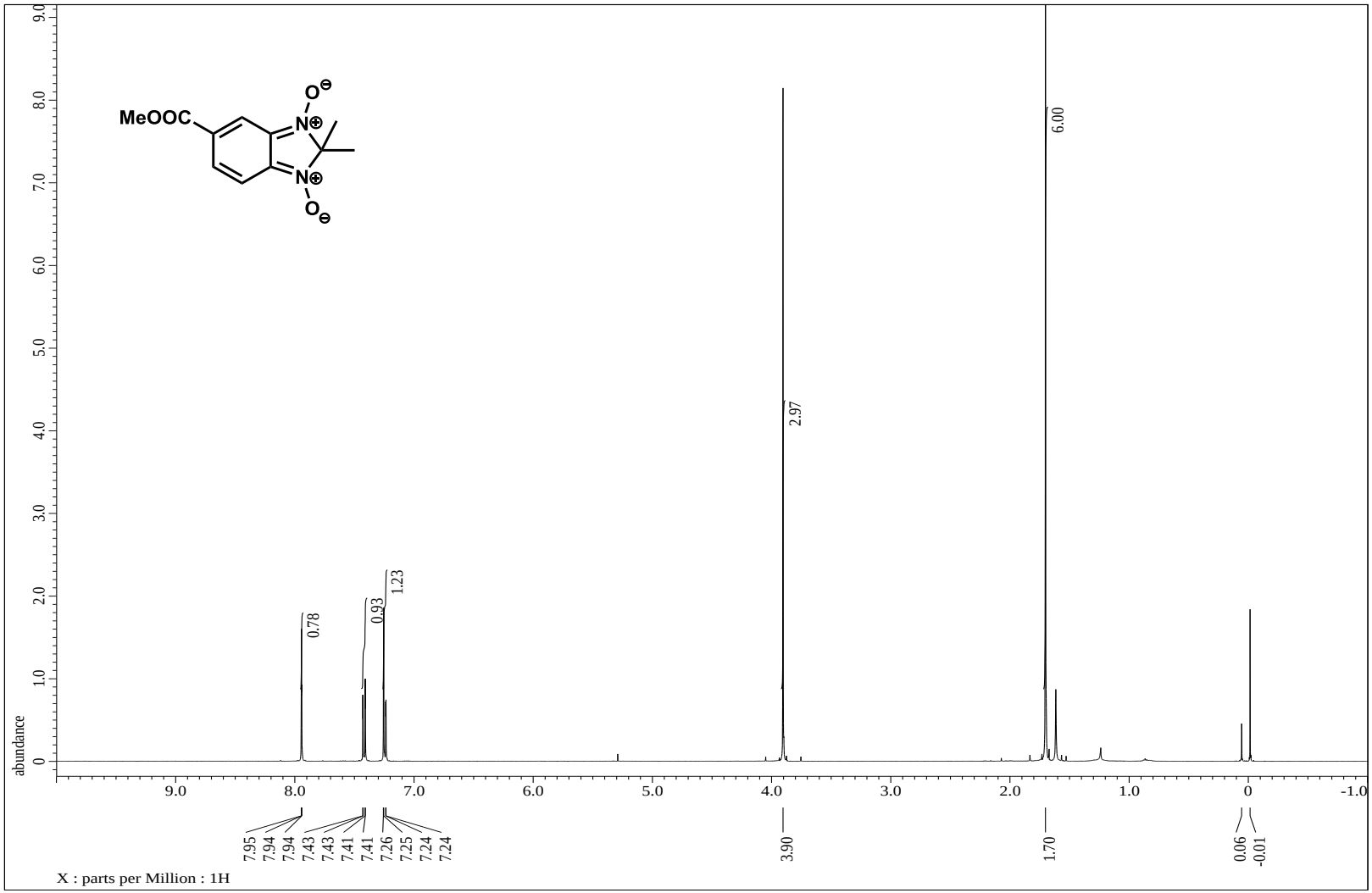

Figure 2.24. ^{1}H NMR (500 MHz, $CDCl_3$) of Methyl 2,2-dimethyl-*2H*-benzimidazol-1,3-dioxide-5-carboxylate (sepin1.3)

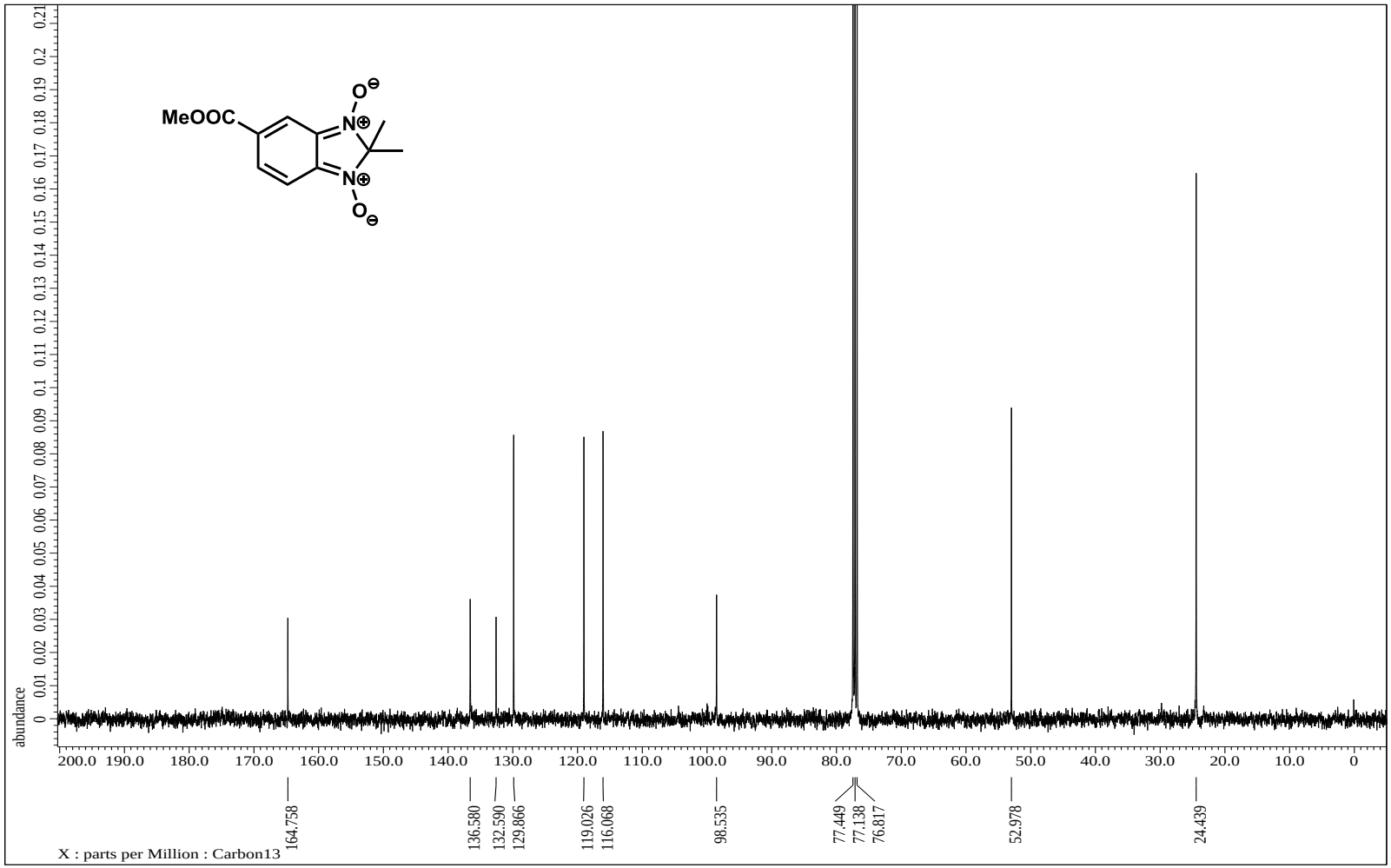

Figure 2.25. ^{13}C NMR (126 MHz, $CDCl_3$) of Methyl 2,2-dimethyl-*2H*-benzimidazol-1,3-dioxide-5-carboxylate (sepin1.3)

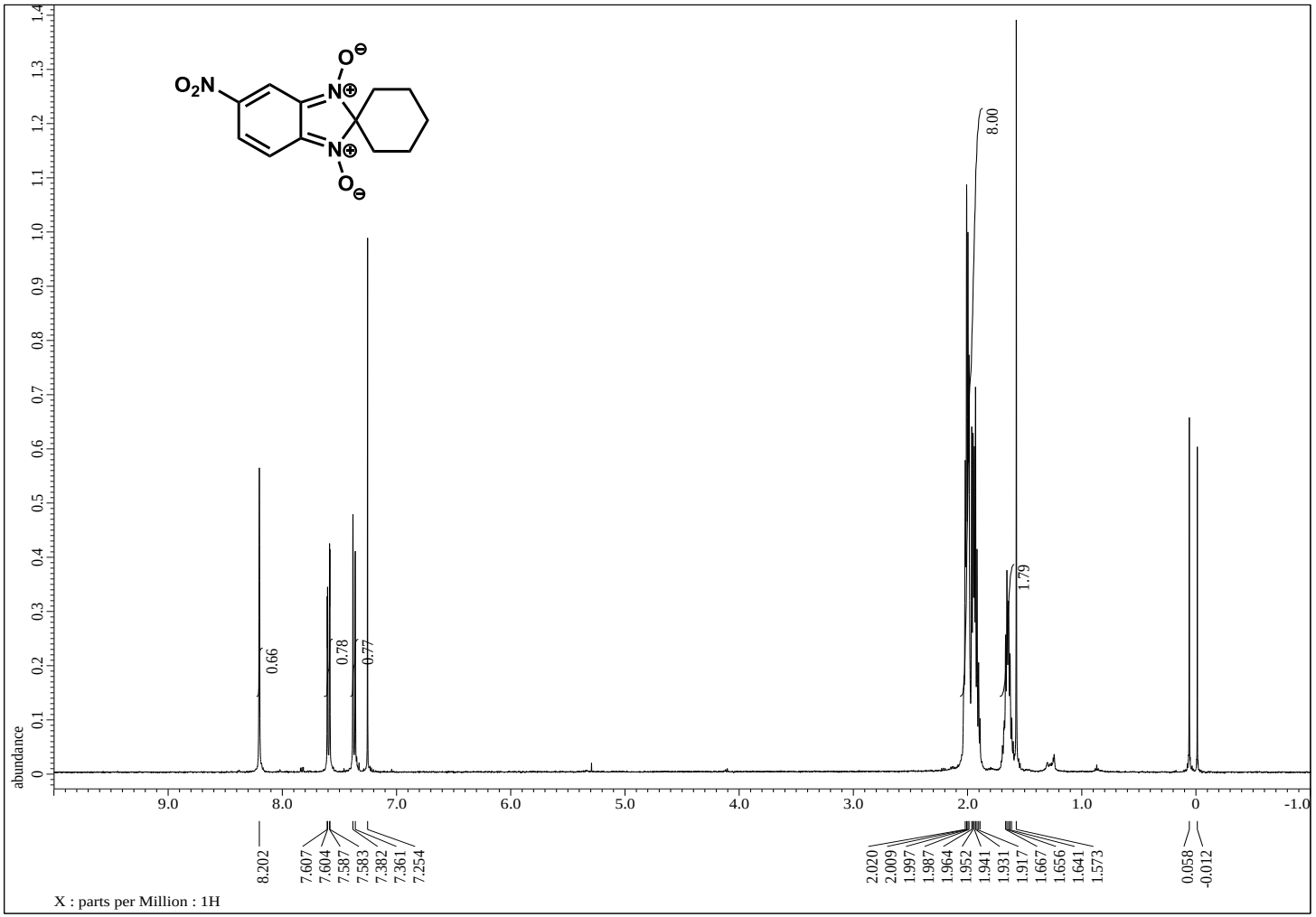

Figure 2.26. ^{1}H NMR (500 MHz, $CDCl_3$) of 5-nitro-2-spirocyclohexane-*2H*-benzimidazol-1,3-dioxide (sepin1.16)

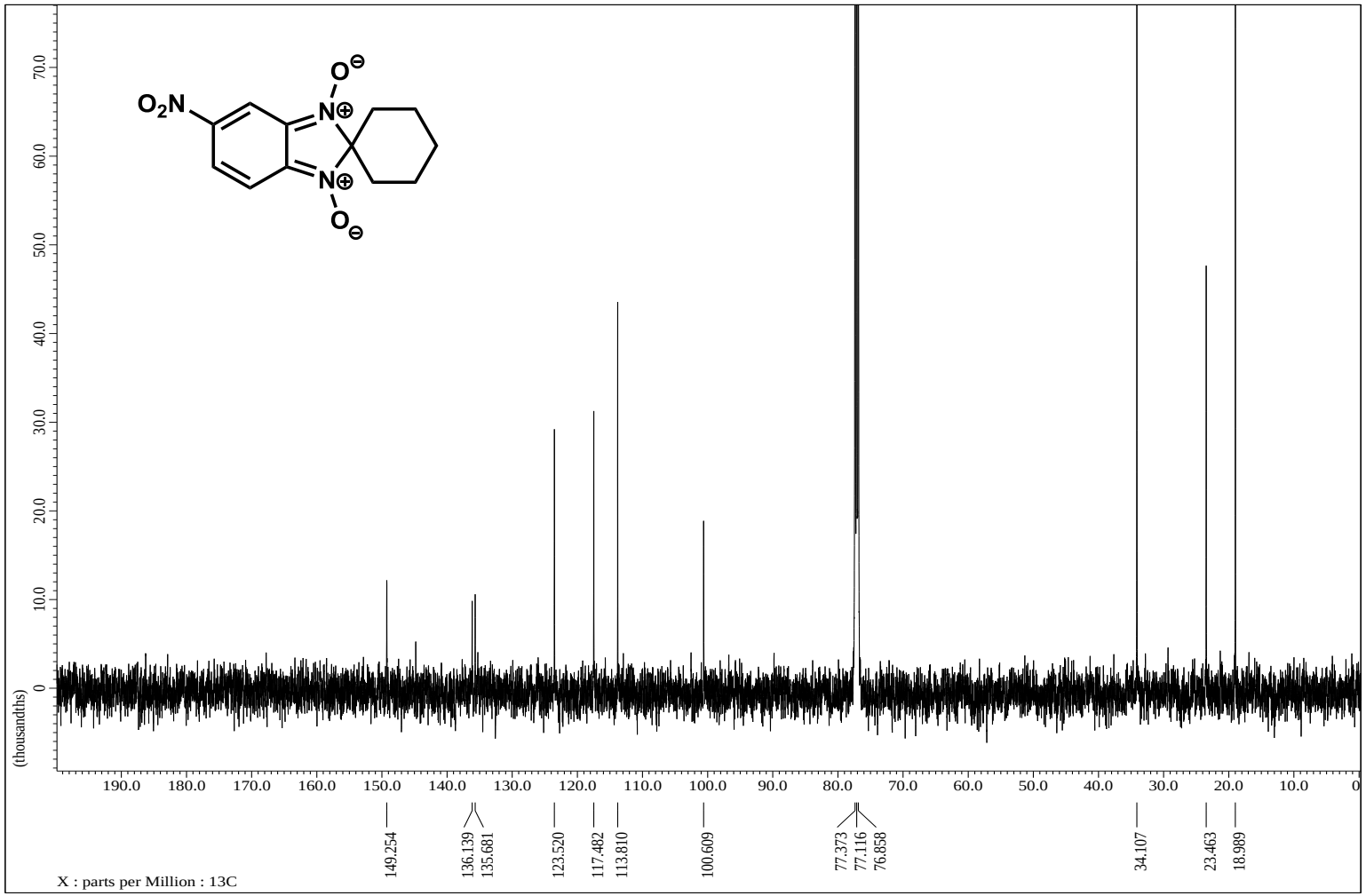

Figure 2.27. ^{13}C NMR (101 MHz, $CDCl_3$) of 5-nitro-2-spirocyclohexane-*2H*-benzimidazol-1,3-dioxide (sepin1.16)

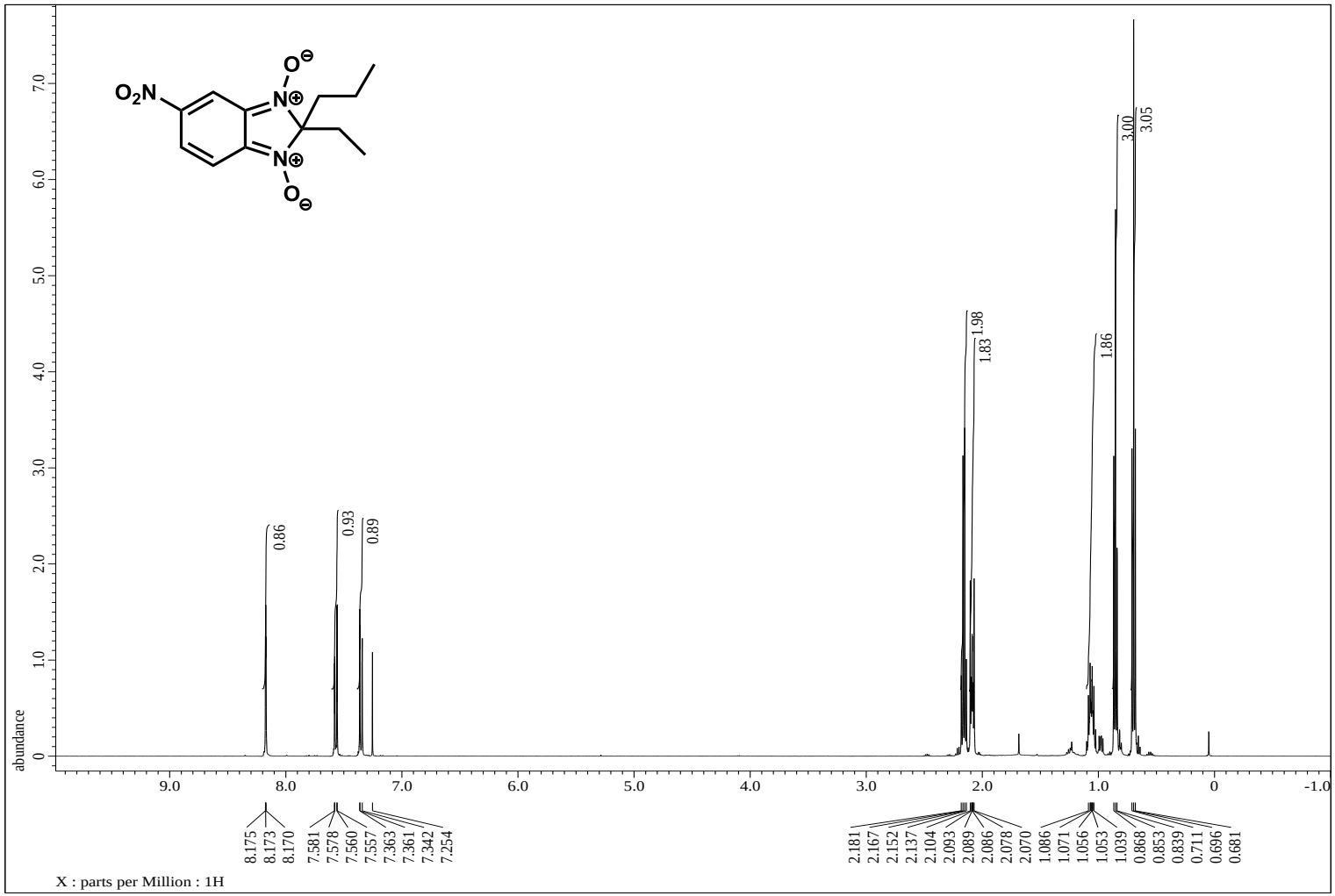

Figure 2.28. ^{1}H NMR (500 MHz, $CDCl_3$) of 2-ethyl-5-nitro-2-propyl-*2H*-benzimidazol-1,3-dioxide (sepin1.12)

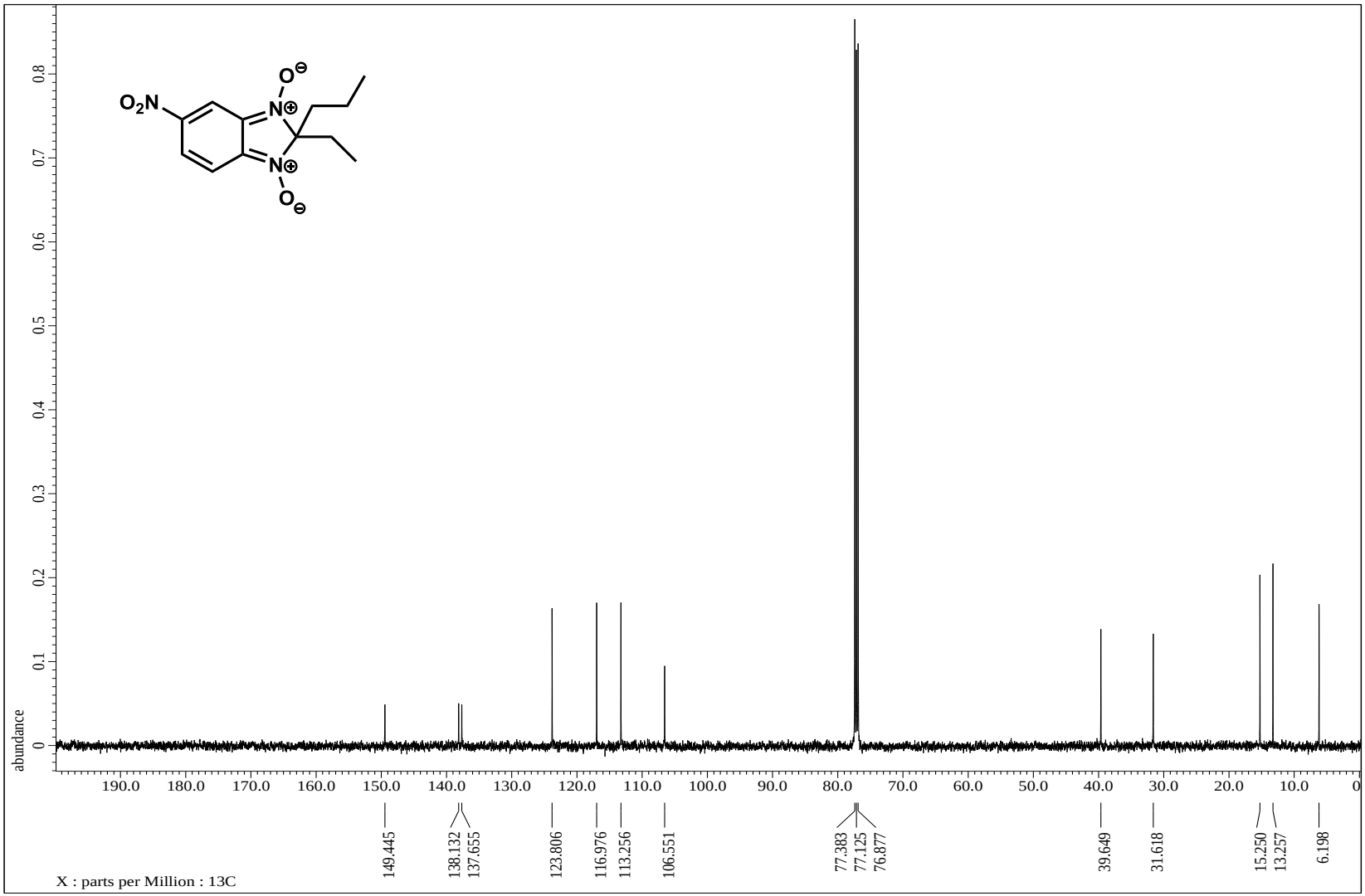

Figure 2.29. ^{13}C NMR (126 MHz, $CDCl_3$) of 2-ethyl-5-nitro-2-propyl-*2H*-benzimidazol-1,3-dioxide (sepin1.12)

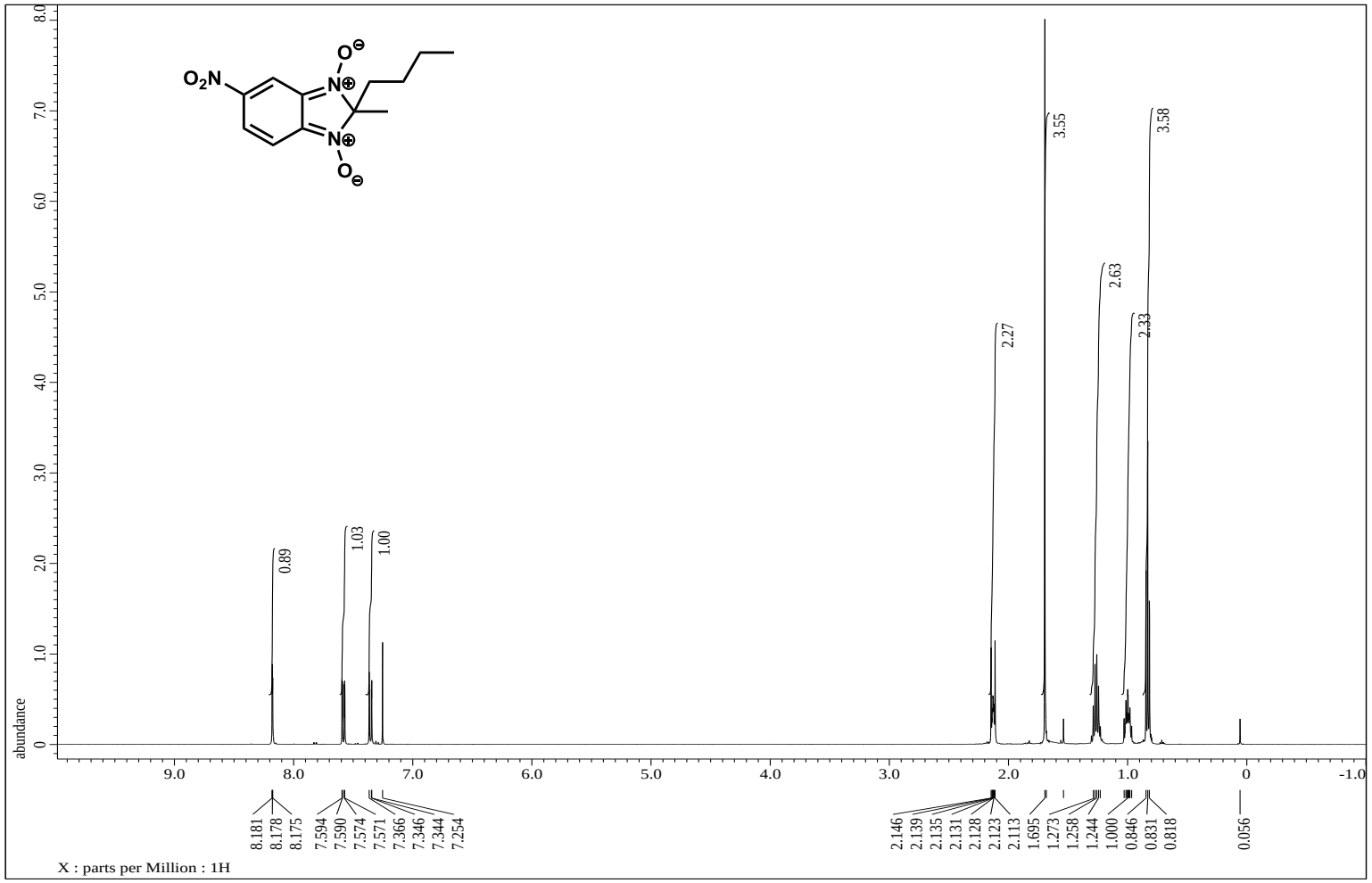

Figure 2.30. ^{1}H NMR (500 MHz, $CDCl_3$) of 2-butyl-2-methyl-5-nitro-*2H*-benzimidazol-1,3-dioxide (sepin1.13)

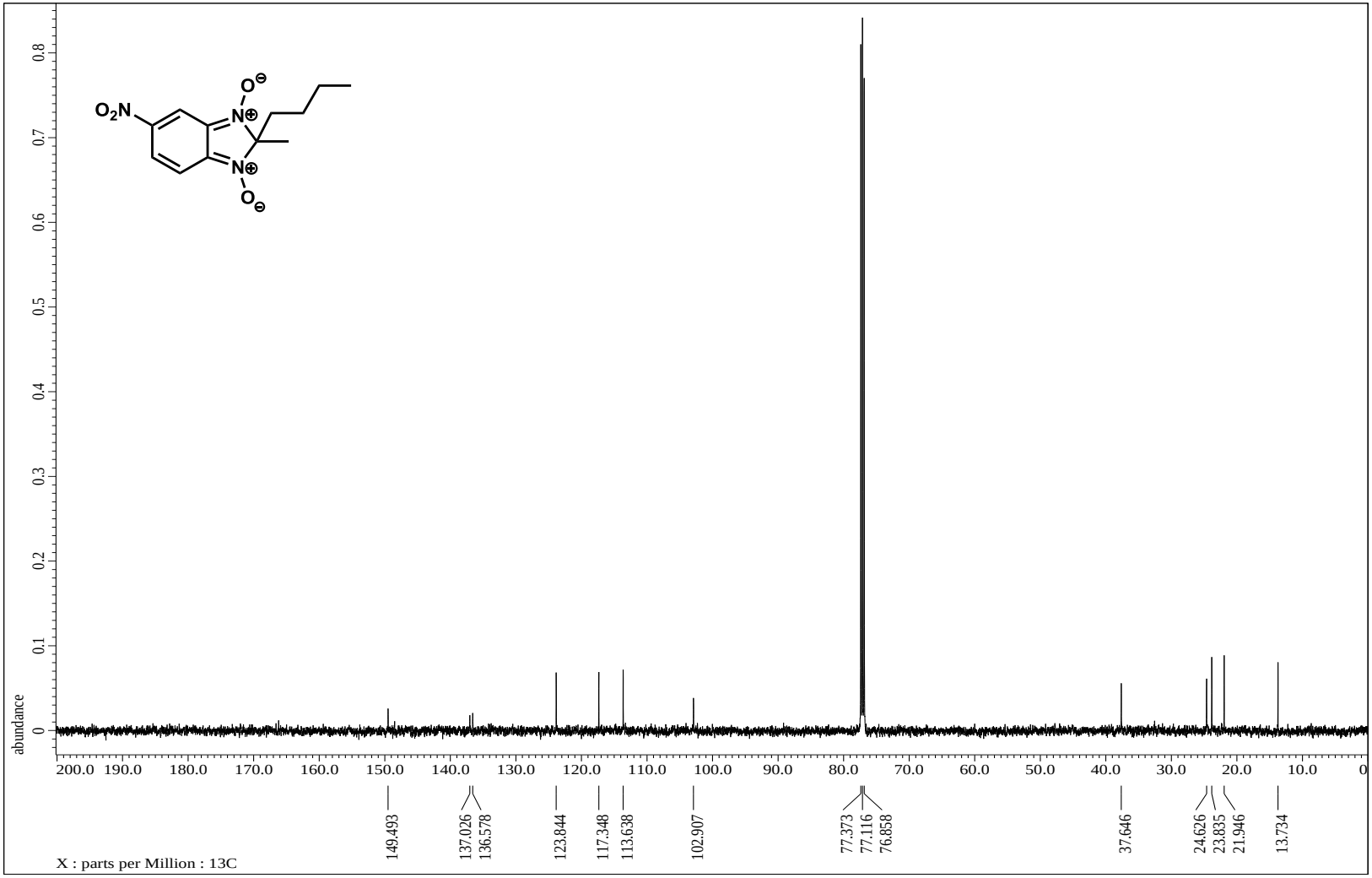

Figure 2.31. ^{13}C NMR (126 MHz, $CDCl_3$) of 2-butyl-2-methyl-5-nitro-*2H*-benzimidazol-1,3-dioxide (sepin1.13)

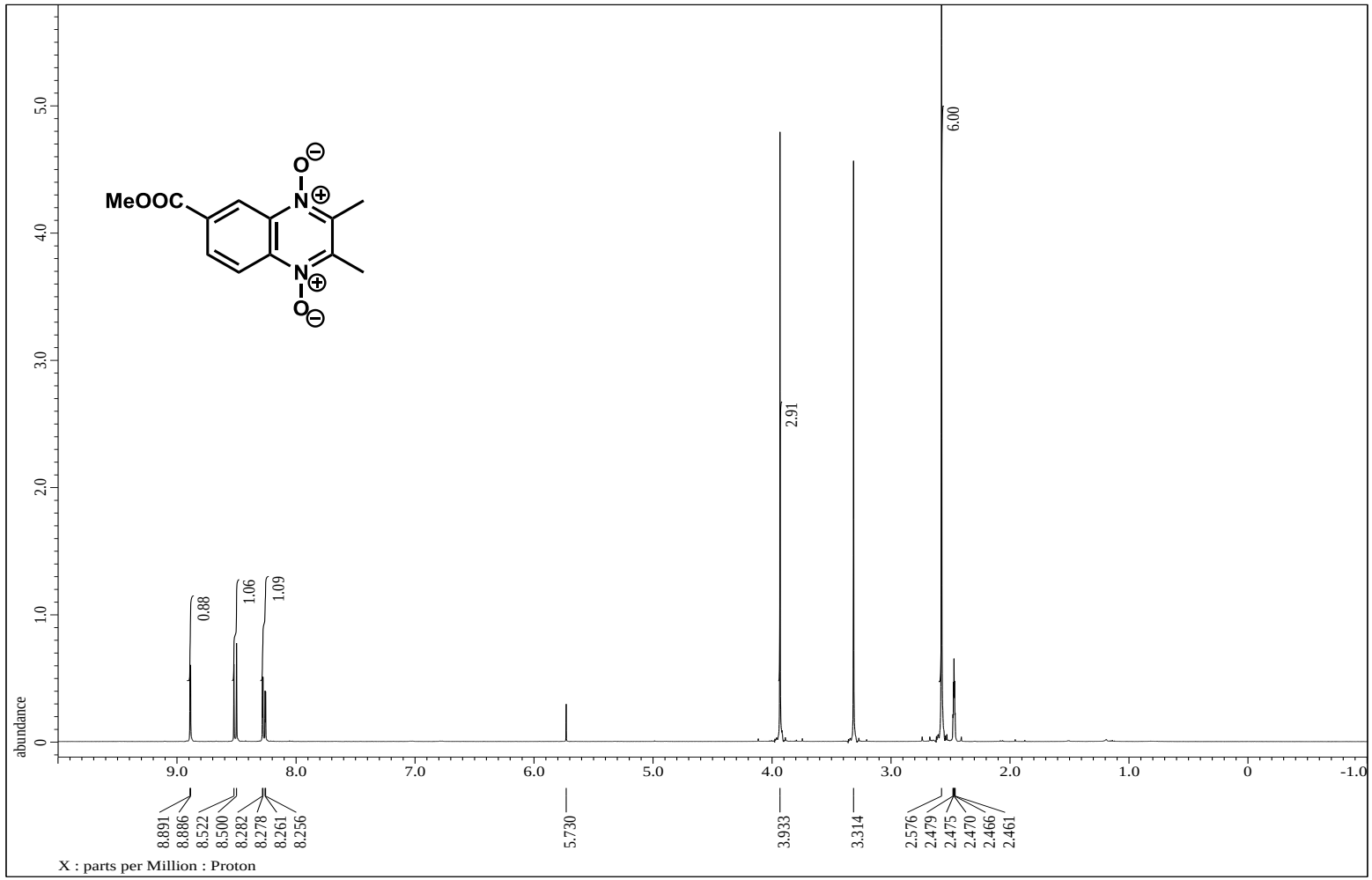

Figure 2.32. ^{1}H NMR (400 MHz, DMSO-d_6) of 2,3-dimethyl-6-(methoxycarbonyl)quinoxaline-1,4-dioxide (sepin1.22)

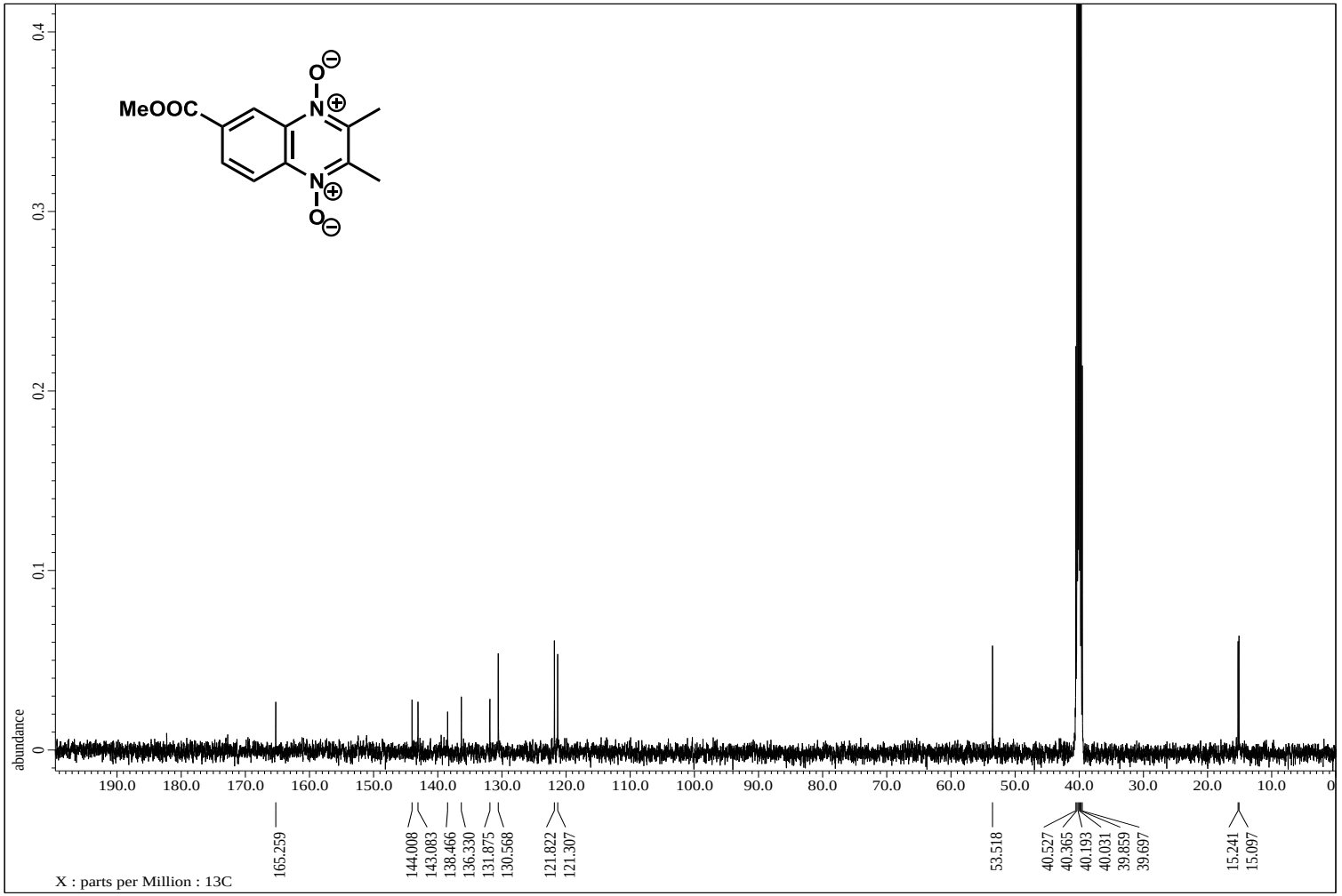

Figure 2.33. ^{13}C NMR (101 MHz, DMSO-d_6) of 2,3-dimethyl-6-(methoxycarbonyl)quinoxaline-1,4-dioxide (sepin1.22)

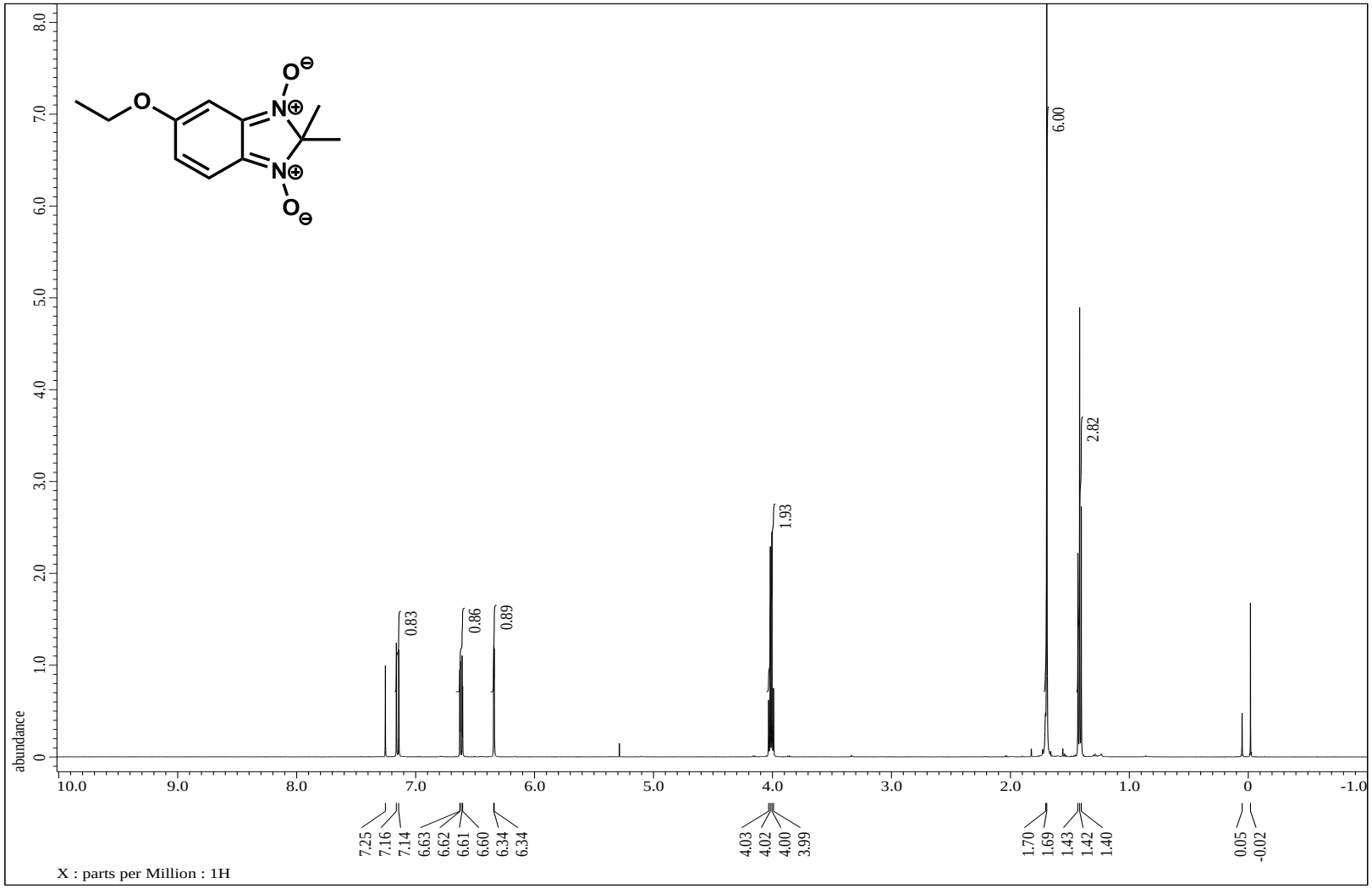

Figure 2.34. ^{1}H NMR (400 MHz, $CDCl_3$) of 5-ethoxy-2,2-dimethyl-*2H*-benzimidazol-1,3-dioxide (sepin1.4)

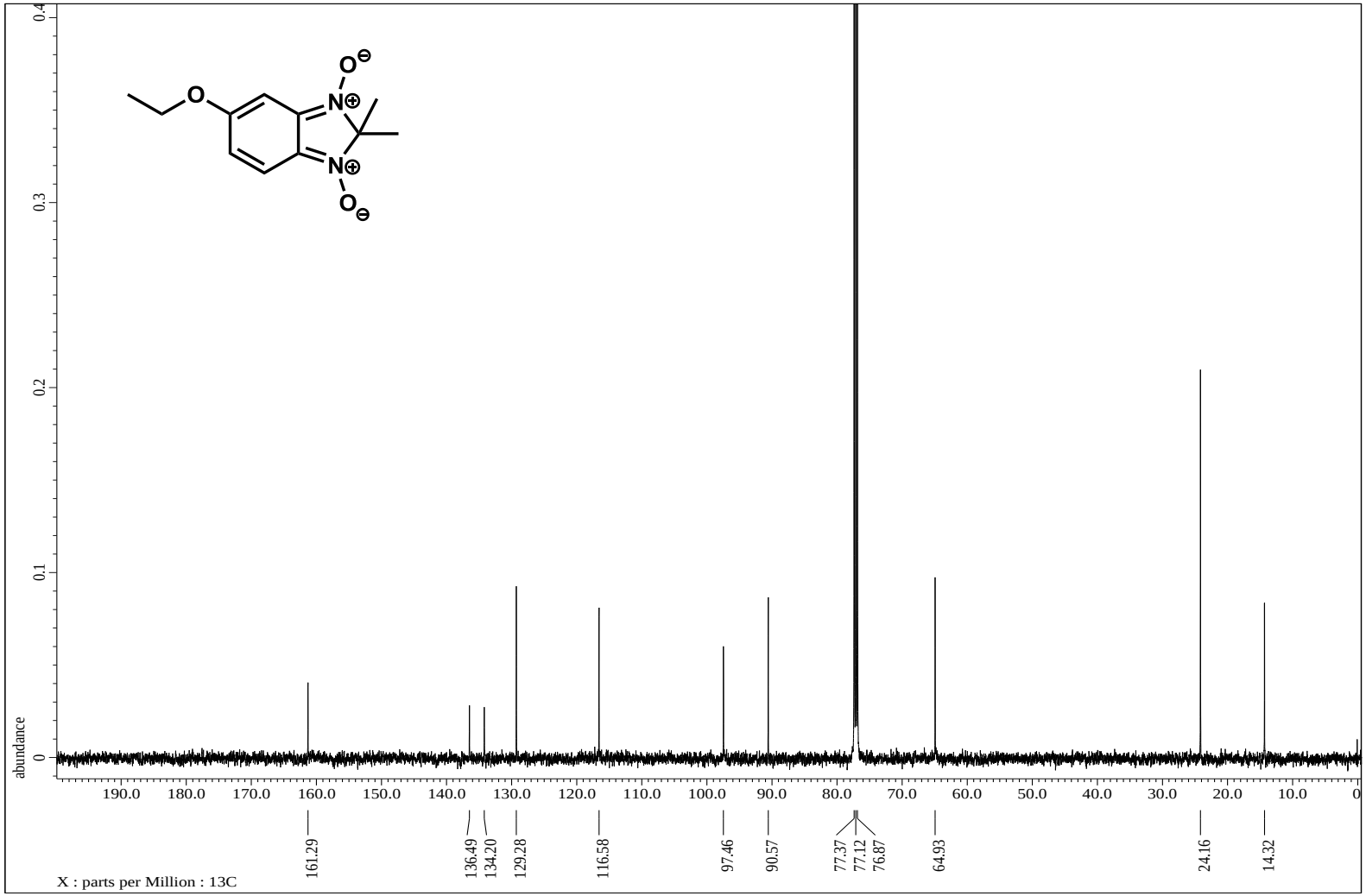

Figure 2.35. ^{13}C NMR (101 MHz, $CDCl_3$) of 5-ethoxy-2,2-dimethyl-*2H*-benzimidazol-1,3-dioxide (sepin1.4)

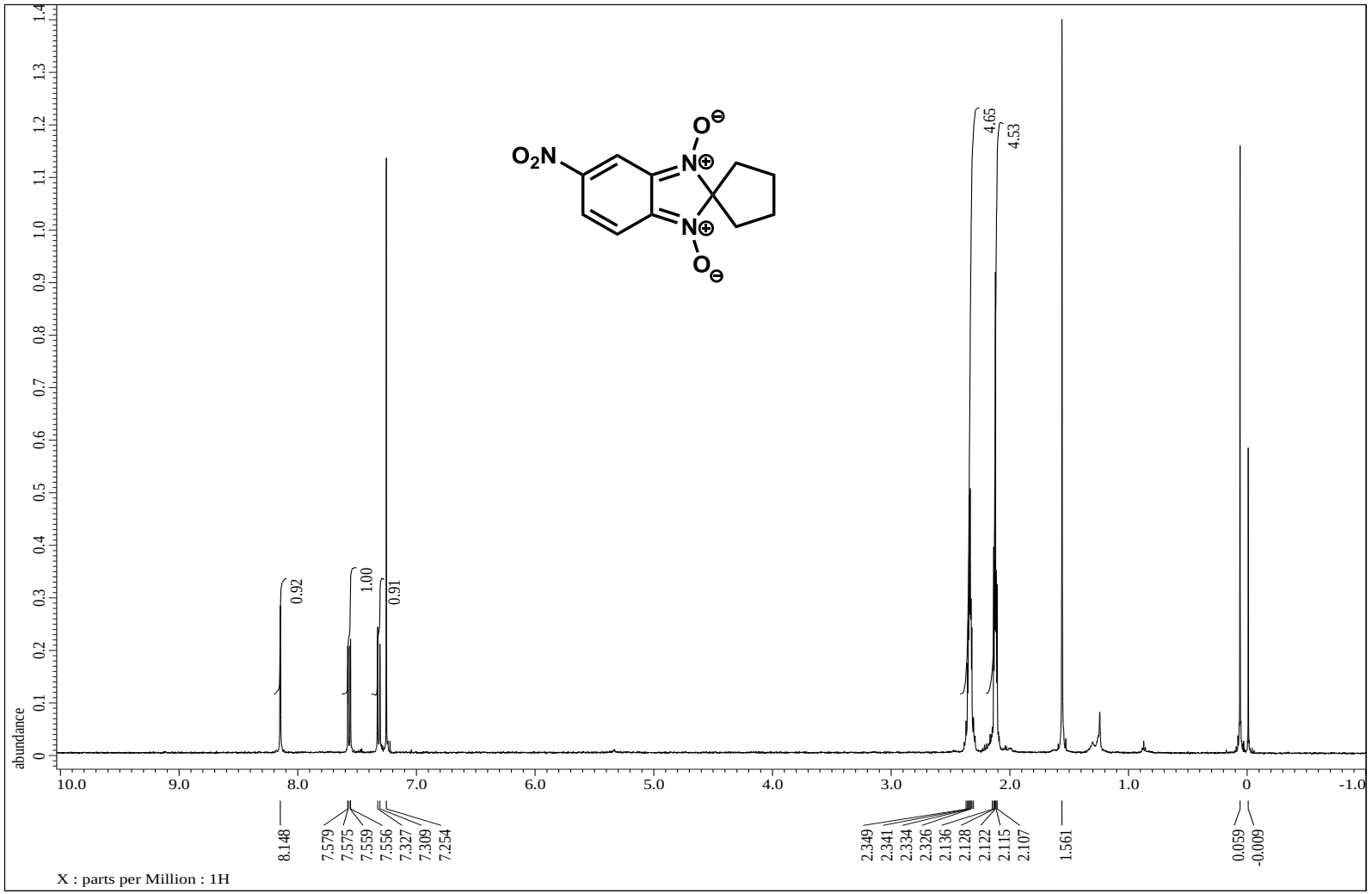

Figure 2.36. ^{1}H NMR (500 MHz, $CDCl_3$) of 5-nitro-2-spirocyclopentane-*2H*-benzimidazol-1,3-dioxide (sepin1.15)

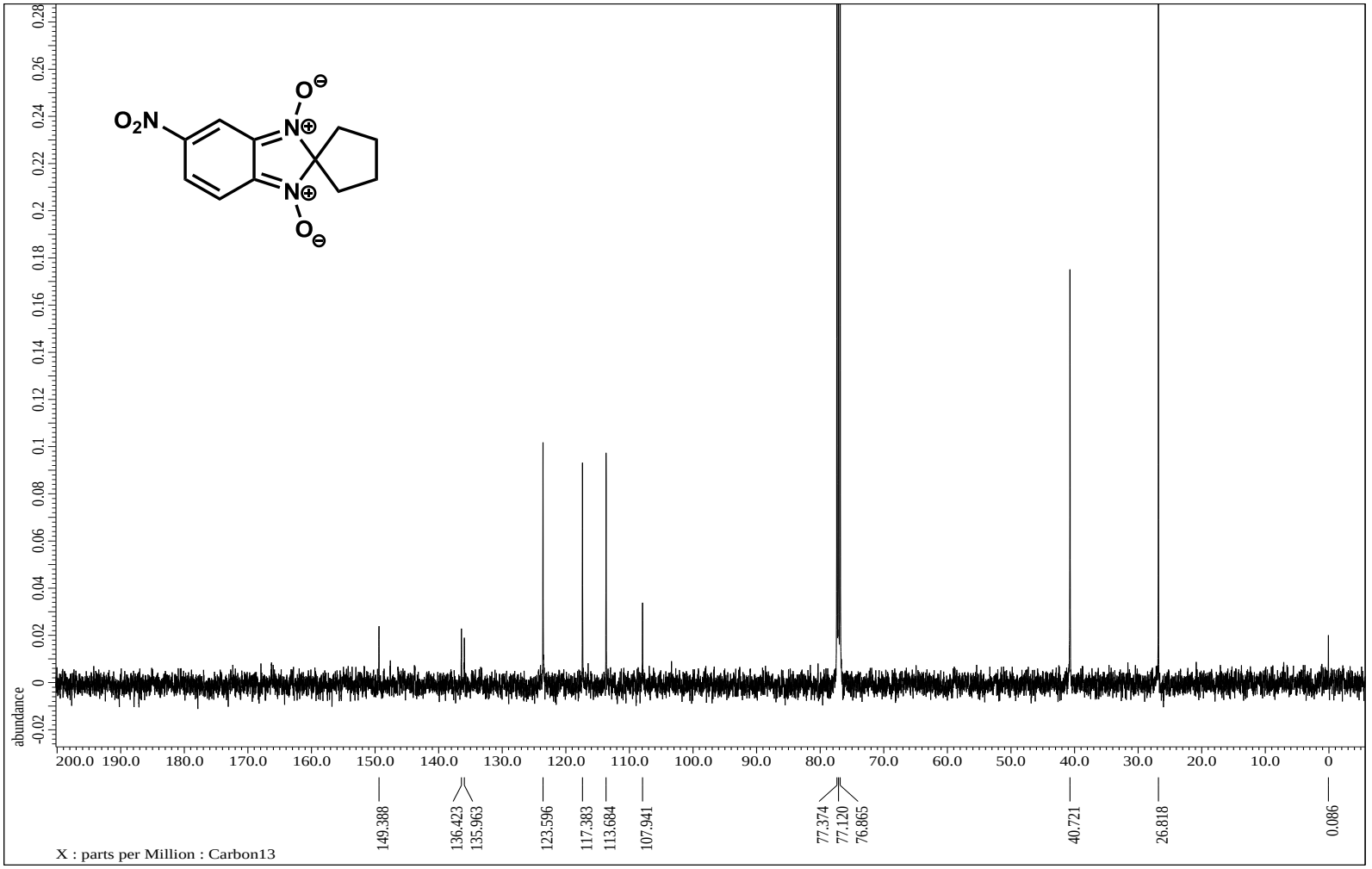

Figure 2.37. ^{13}C NMR (126 MHz, $CDCl_3$) of 5-nitro-2-spirocyclopentane-*2H*-benzimidazol-1,3-dioxide (sepin1.15)

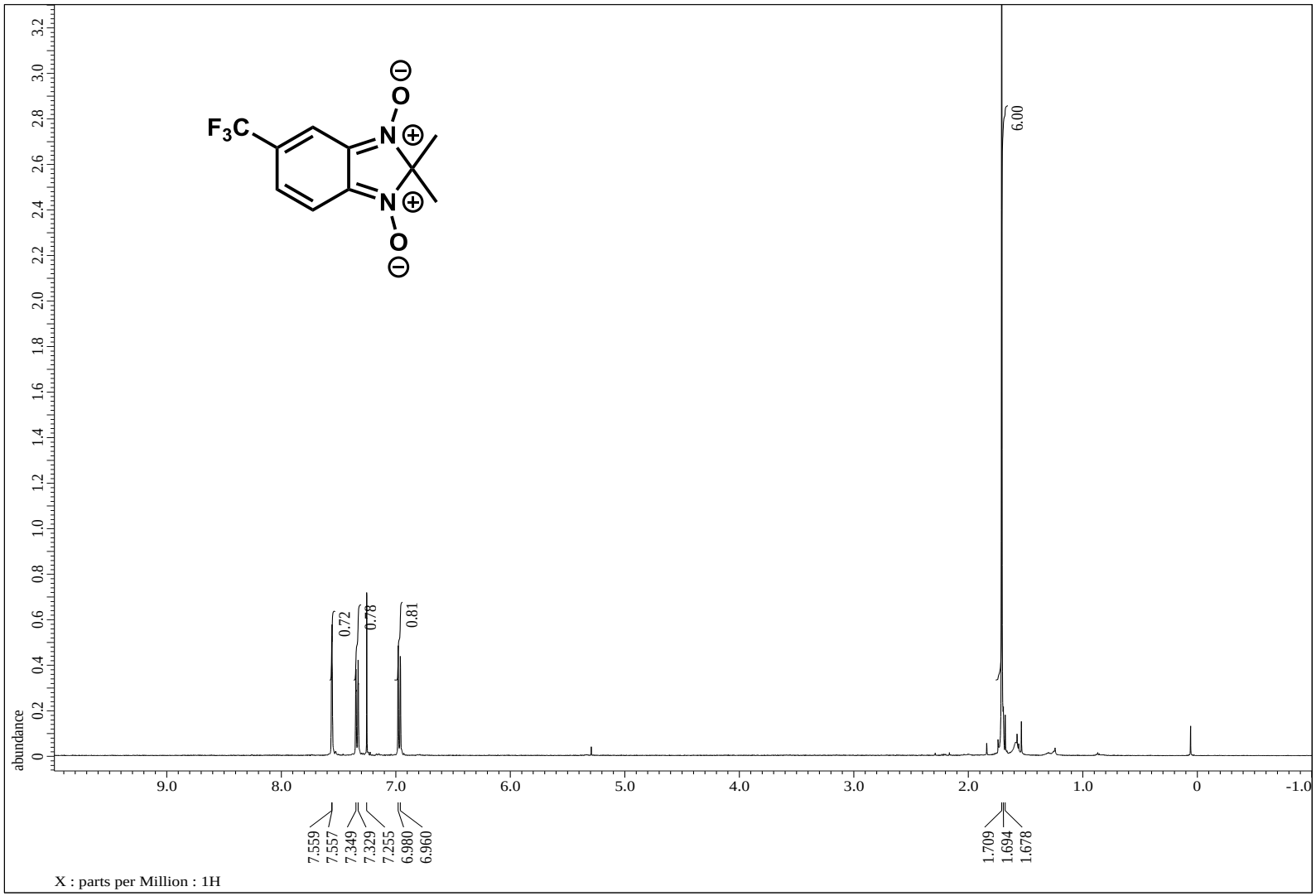

Figure 2.38. ^{1}H NMR (400 MHz, $CDCl_3$) of 2,2-dimethyl-5-(trifluoromethyl)-*2H*-benzimidazol-1,3-dioxide (sepin1.5)

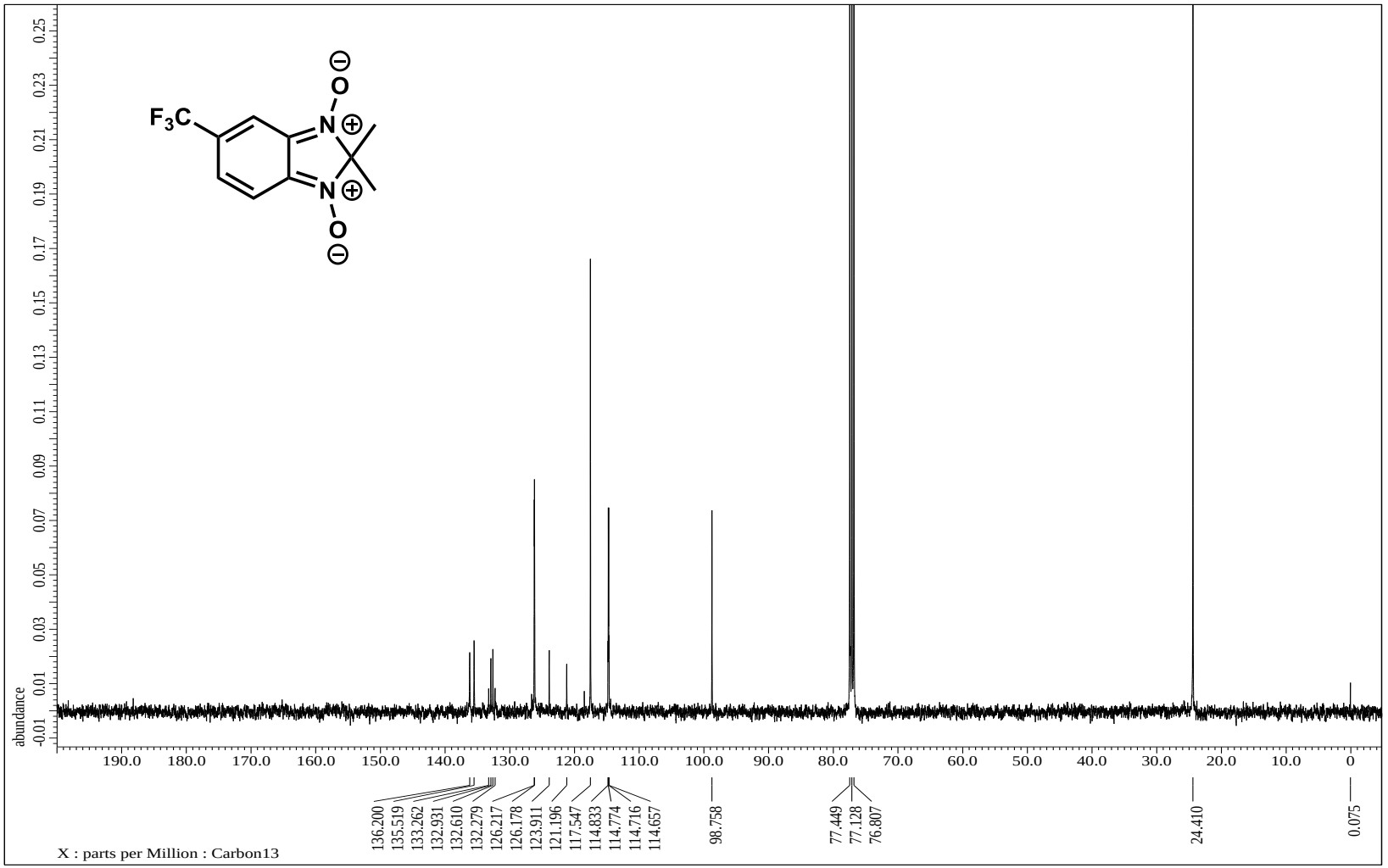

Figure 2.39. ^{13}C NMR (101 MHz, $CDCl_3$) of 2,2-dimethyl-5-(trifluoromethyl)-*2H*-benzimidazol-1,3-dioxide (sepin1.5)

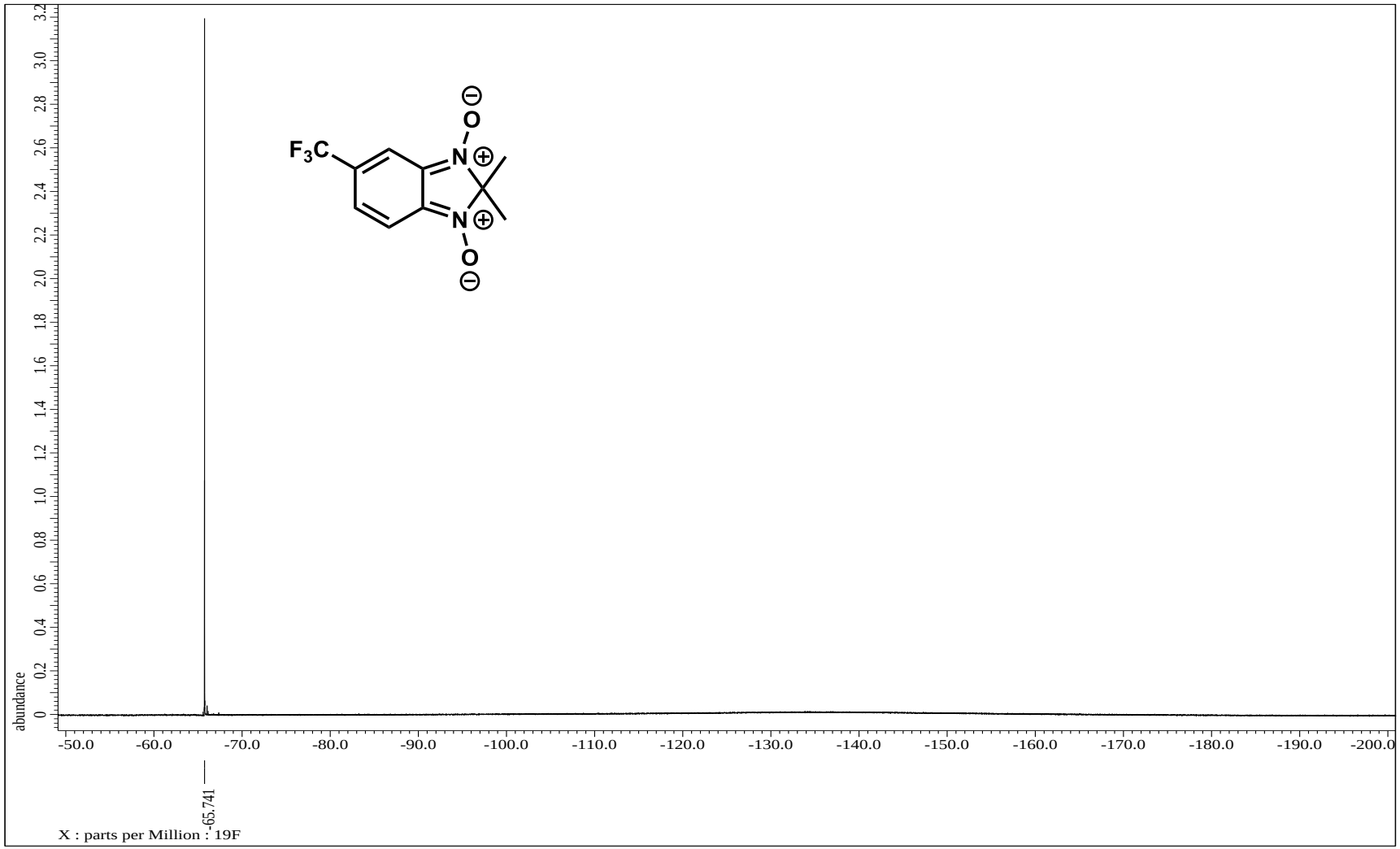

Figure 2.40. ^{19}F NMR (471 MHz, $CDCl_3$) of 2,2-dimethyl-5-(trifluoromethyl)-*2H*-benzimidazol-1,3-dioxide (sepin1.5)

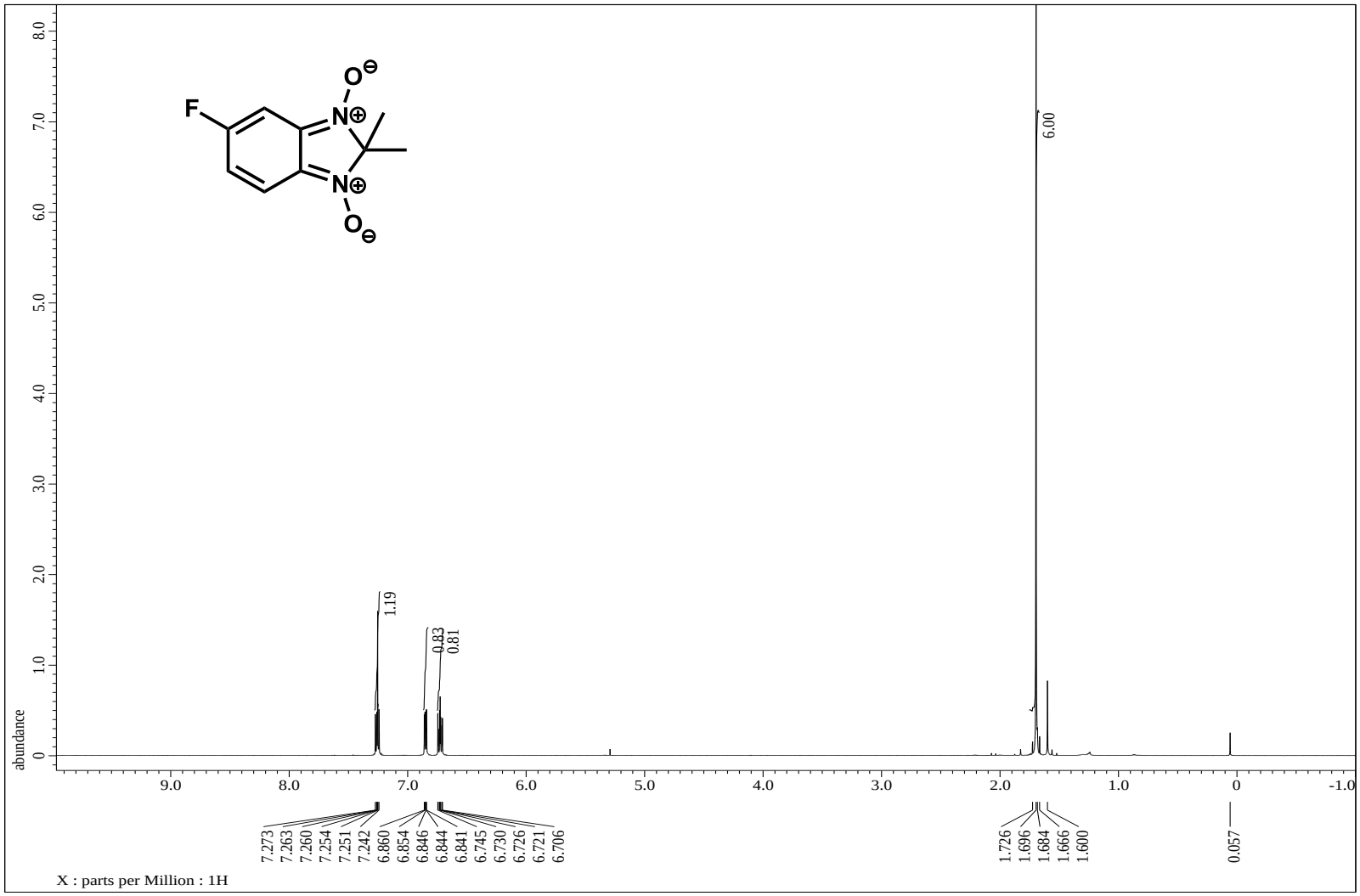

Figure 2.41. ^{1}H NMR (500 MHz, $CDCl_3$) of 5-fluoro-2,2-dimethyl-*2H*-benzimidazol-1,3-dioxide (sepin1.7)

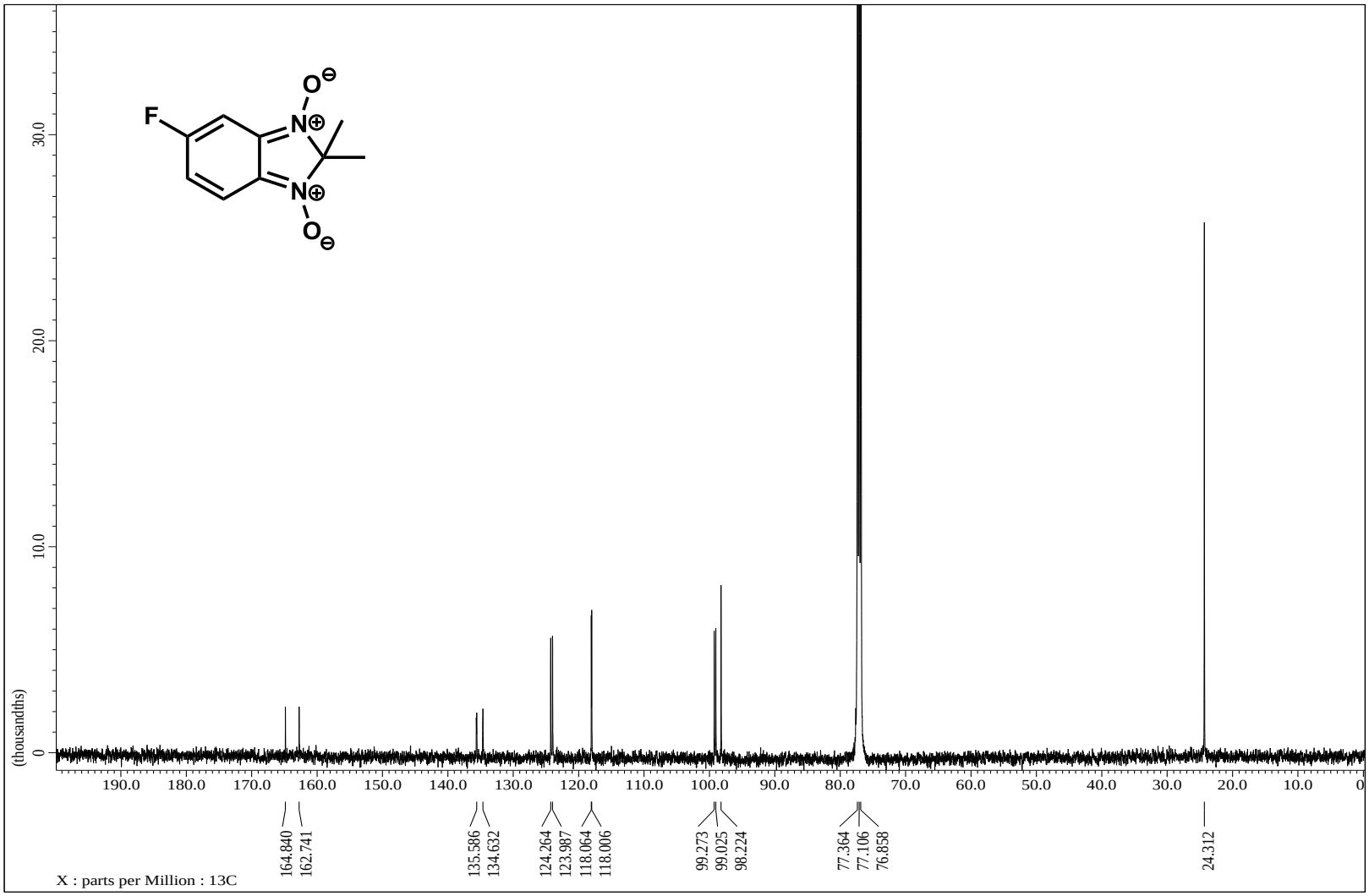

Figure 2.42. ^{13}C NMR (126 MHz, $CDCl_3$) of 5-fluoro-2,2-dimethyl-*2H*-benzimidazol-1,3-dioxide (sepin1.7)

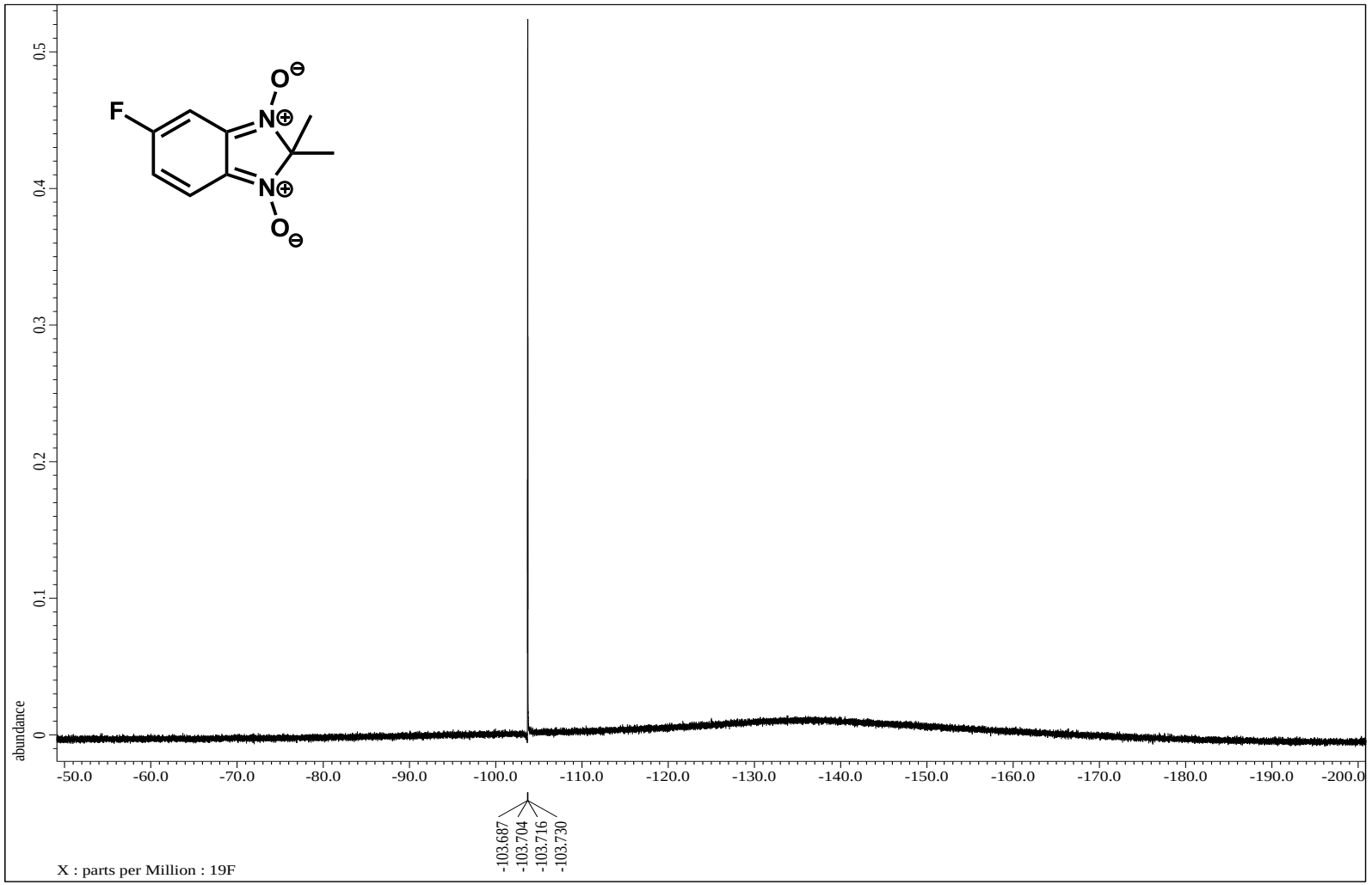

Figure 2.43. ^{19}F NMR (471 MHz, $CDCl_3$) of 5-fluoro-2,2-dimethyl-*2H*-benzimidazol-1,3-dioxide (sepin1.7)

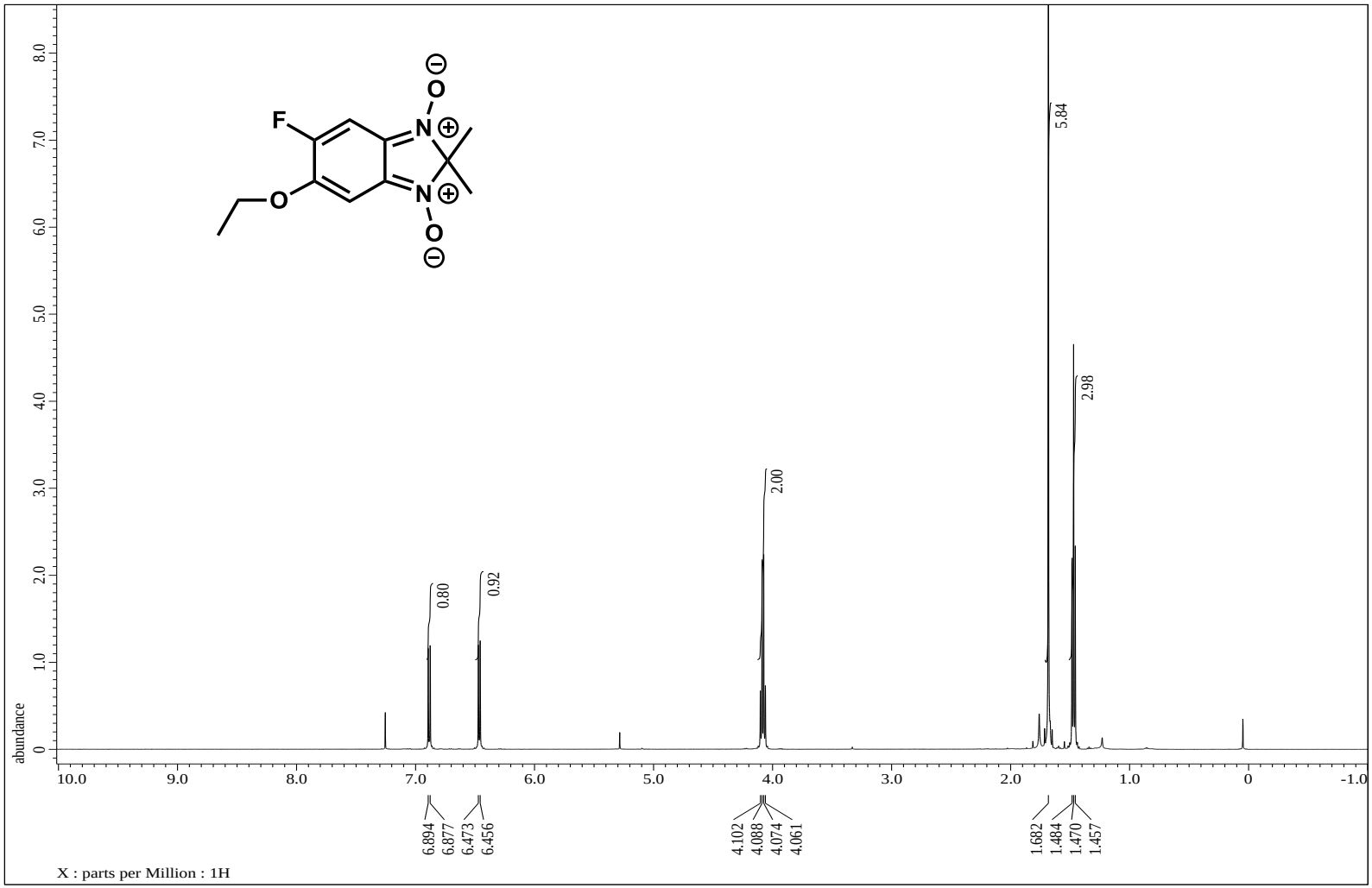

Figure 2.44. ^{1}H NMR (500 MHz, $CDCl_3$) of 5-fluoro-6-ethoxy-2,2-dimethyl-*2H*-benzimidazol-1,3-dioxide (sepin1.17)

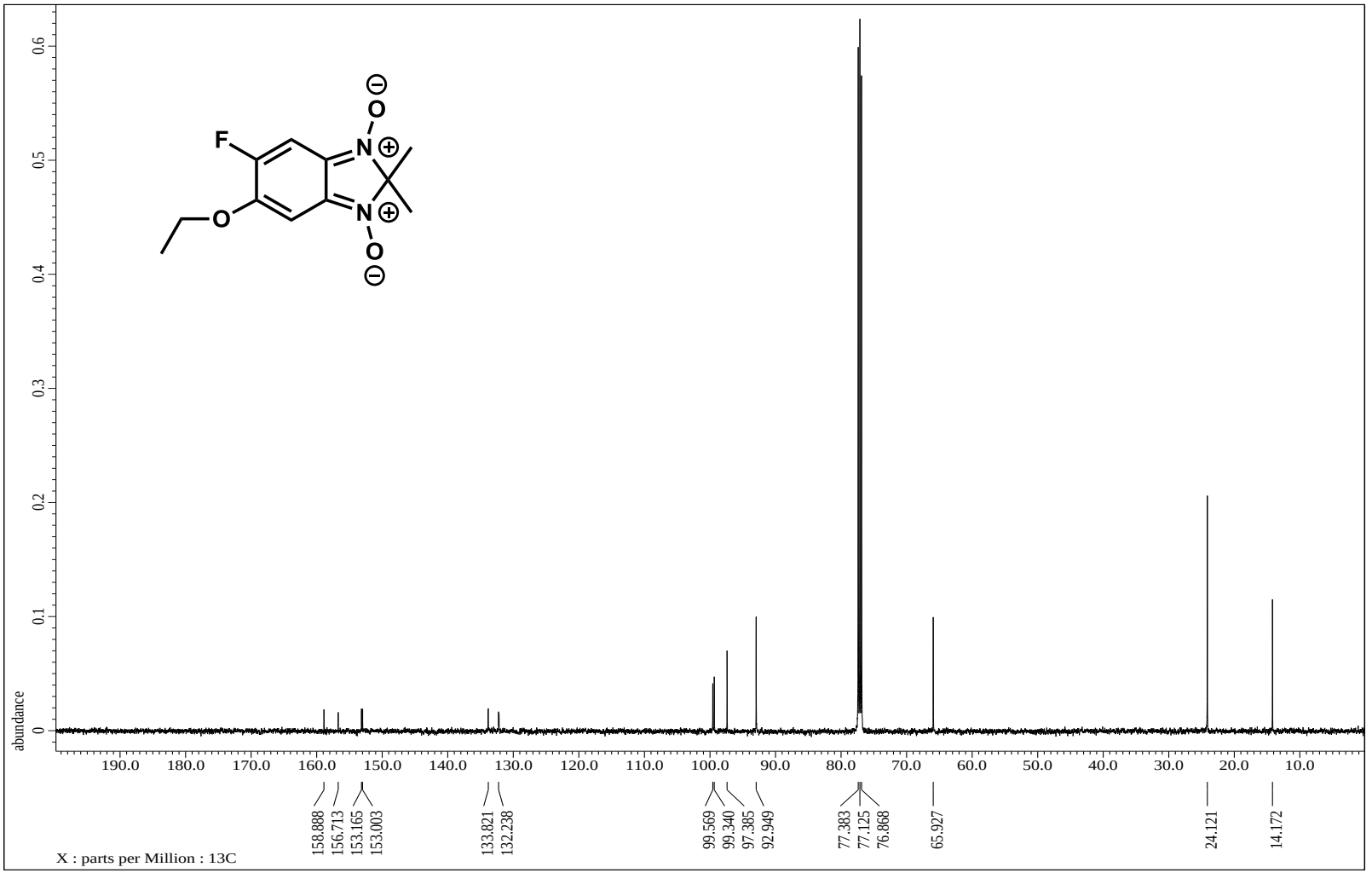

Figure 2.45. ^{13}C NMR (126 MHz, $CDCl_3$) of 5-fluoro-6-ethoxy-2,2-dimethyl-*2H*-benzimidazol-1,3-dioxide (sepin1.17)

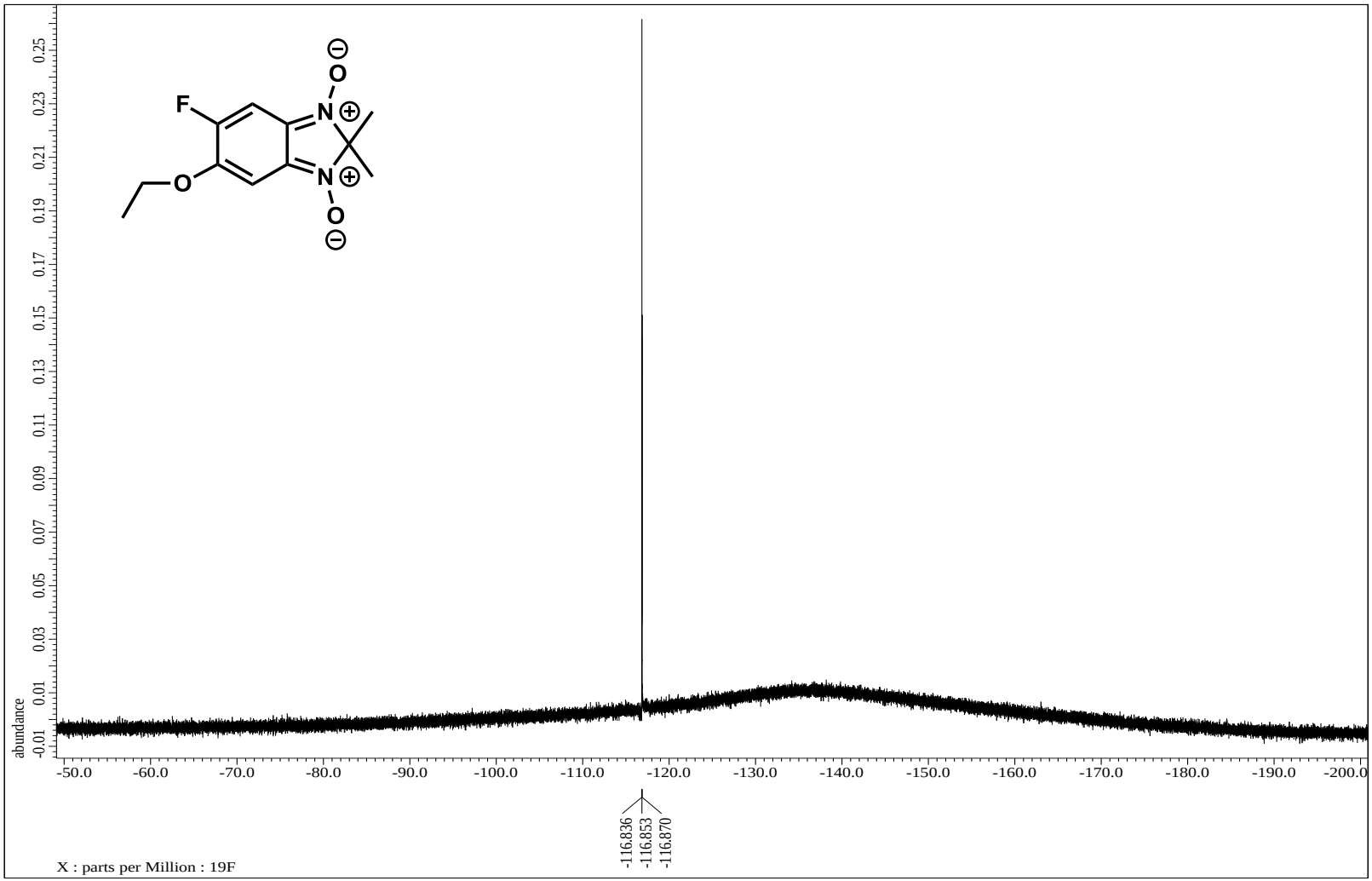

Figure 2.46. ^{19}F NMR (471 MHz, $CDCl_3$) of 5-fluoro-6-ethoxy-2,2-dimethyl-*2H*-benzimidazol-1,3-dioxide (sepin1.17)

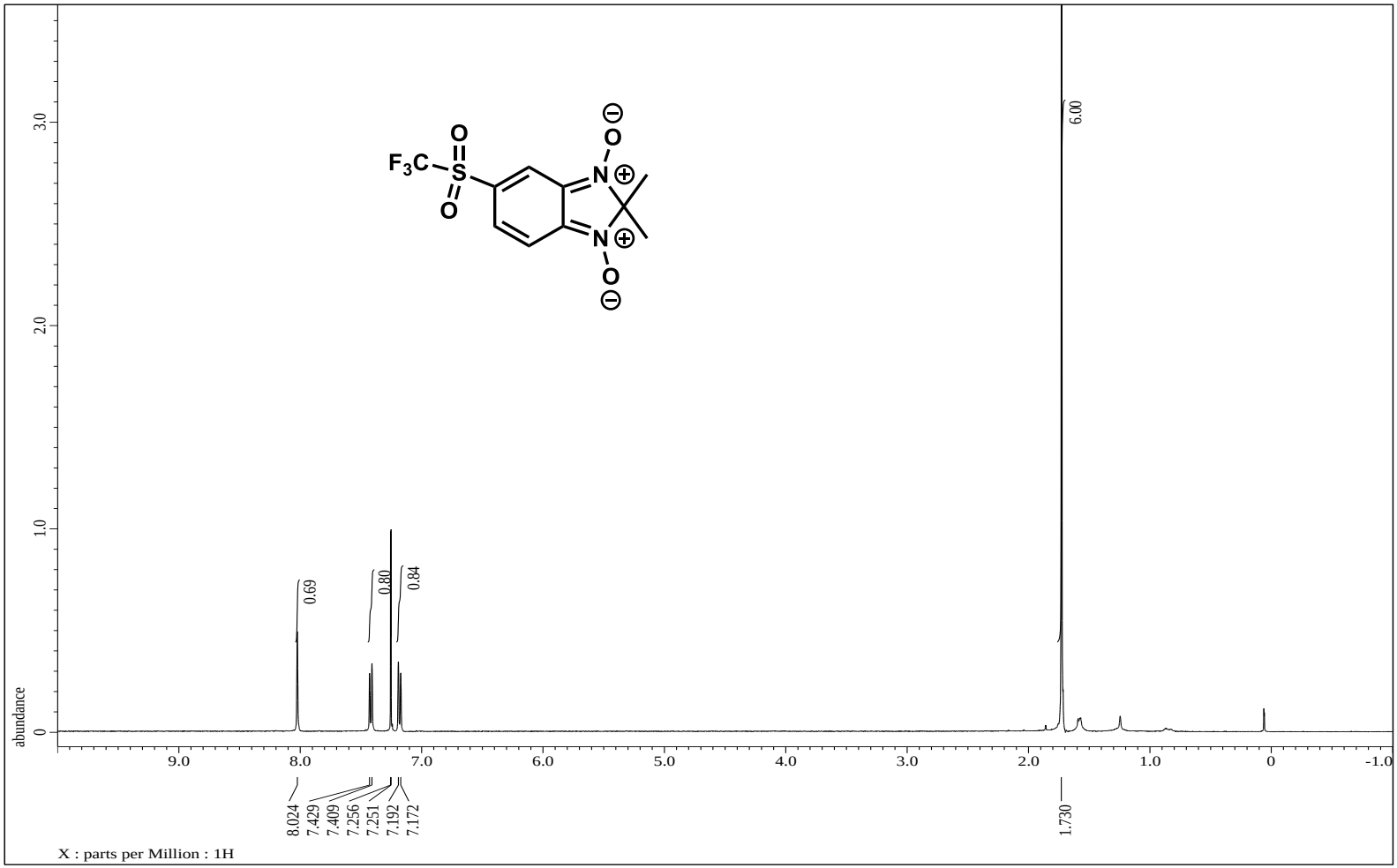

Figure 2.47. ^{1}H NMR (500 MHz, $CDCl_3$) of 2,2-dimethyl-5-(trifluoromethylsulfonyl)-*2H*-benzimidazol-1,3-dioxide (sepin1.6)

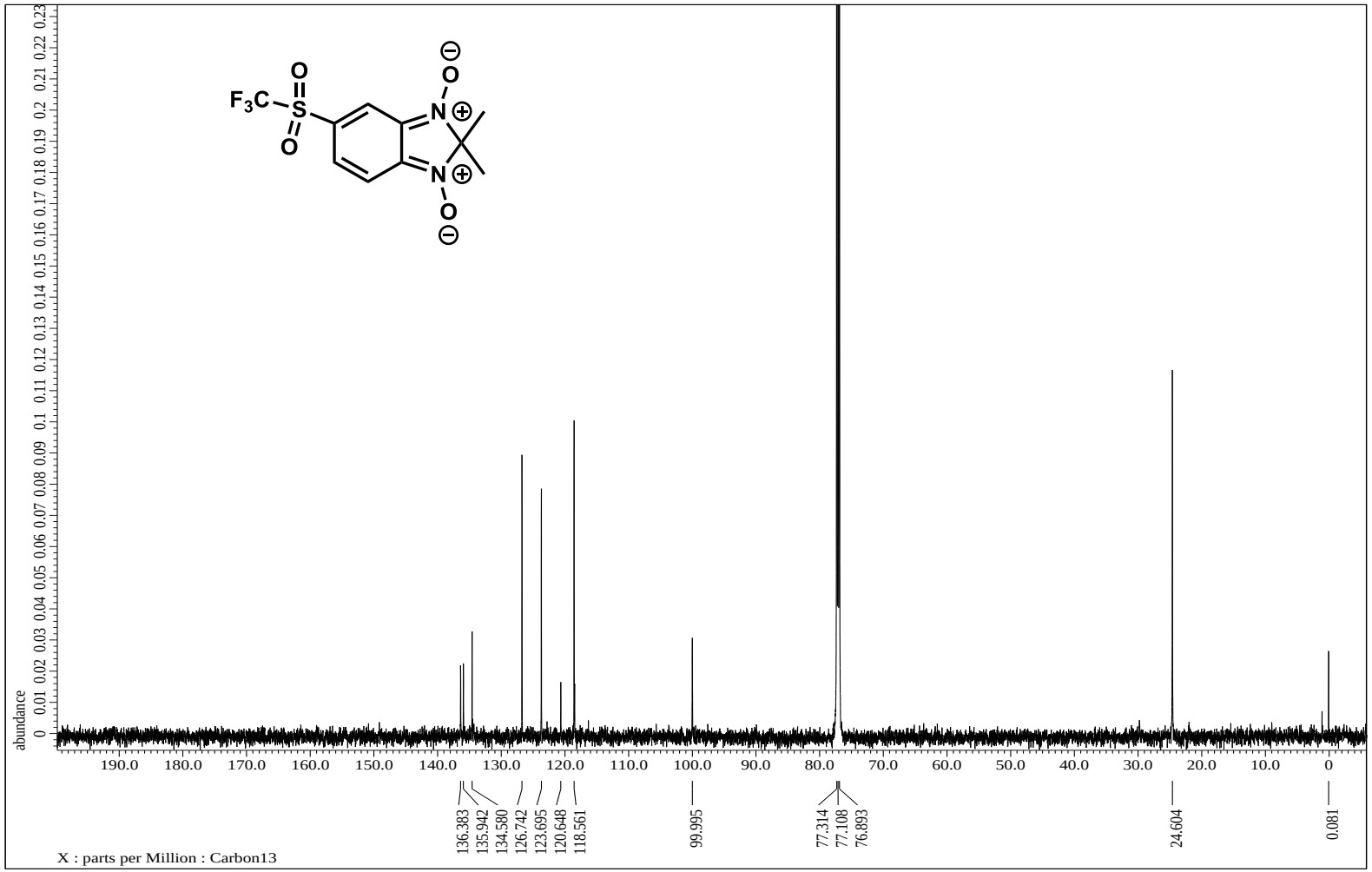

Figure 2.48. ^{13}C NMR (126 MHz, $CDCl_3$) of 2,2-dimethyl-5-(trifluoromethylsulfonyl)-*2H*-benzimidazol-1,3-dioxide (sepin1.6)

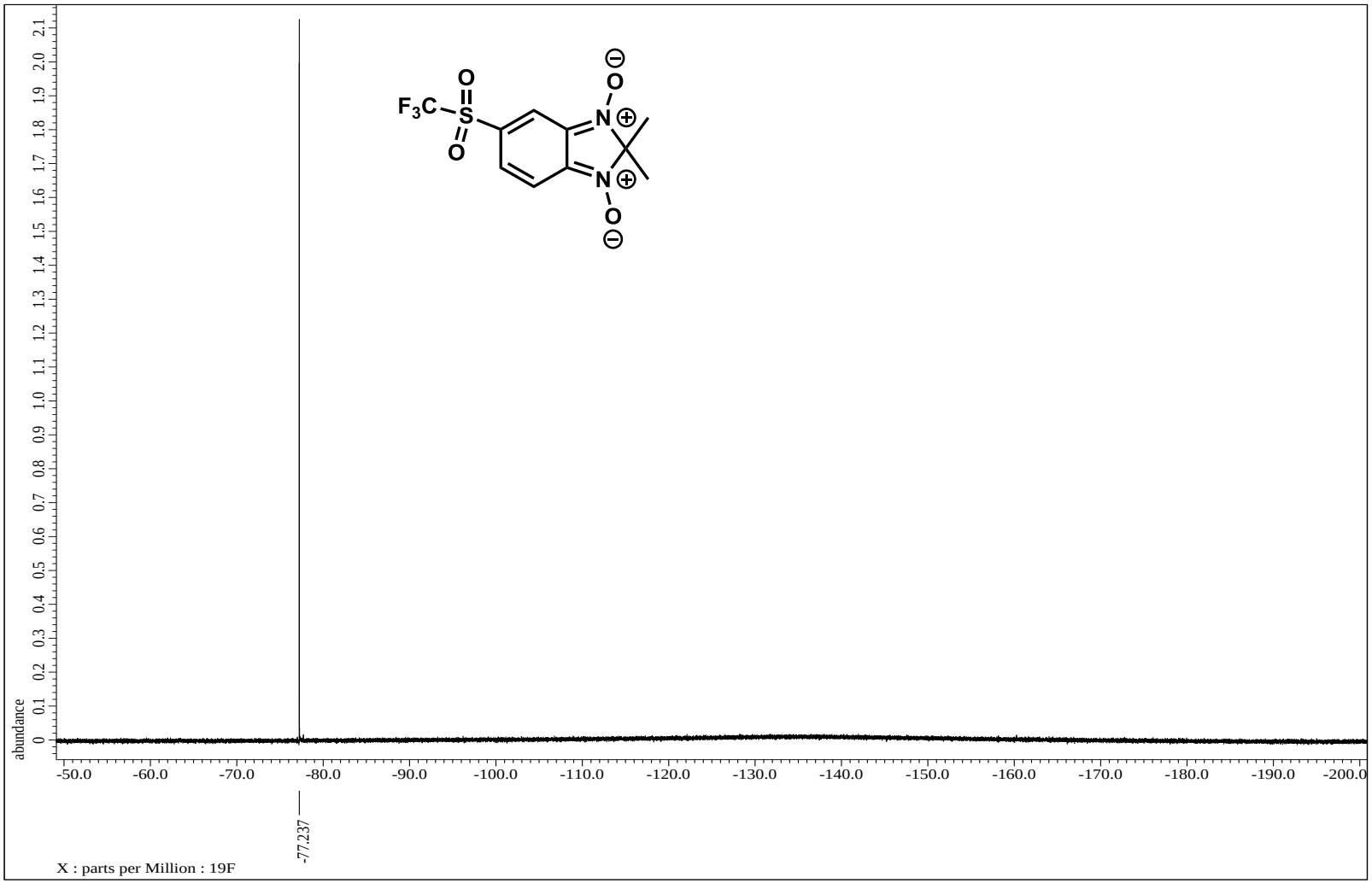

Figure 2.49. ^{19}F NMR (471 MHz, $CDCl_3$) of 2,2-dimethyl-5-(trifluoromethylsulfonyl)-*2H*-benzimidazol-1,3-dioxide (sepin1.6)

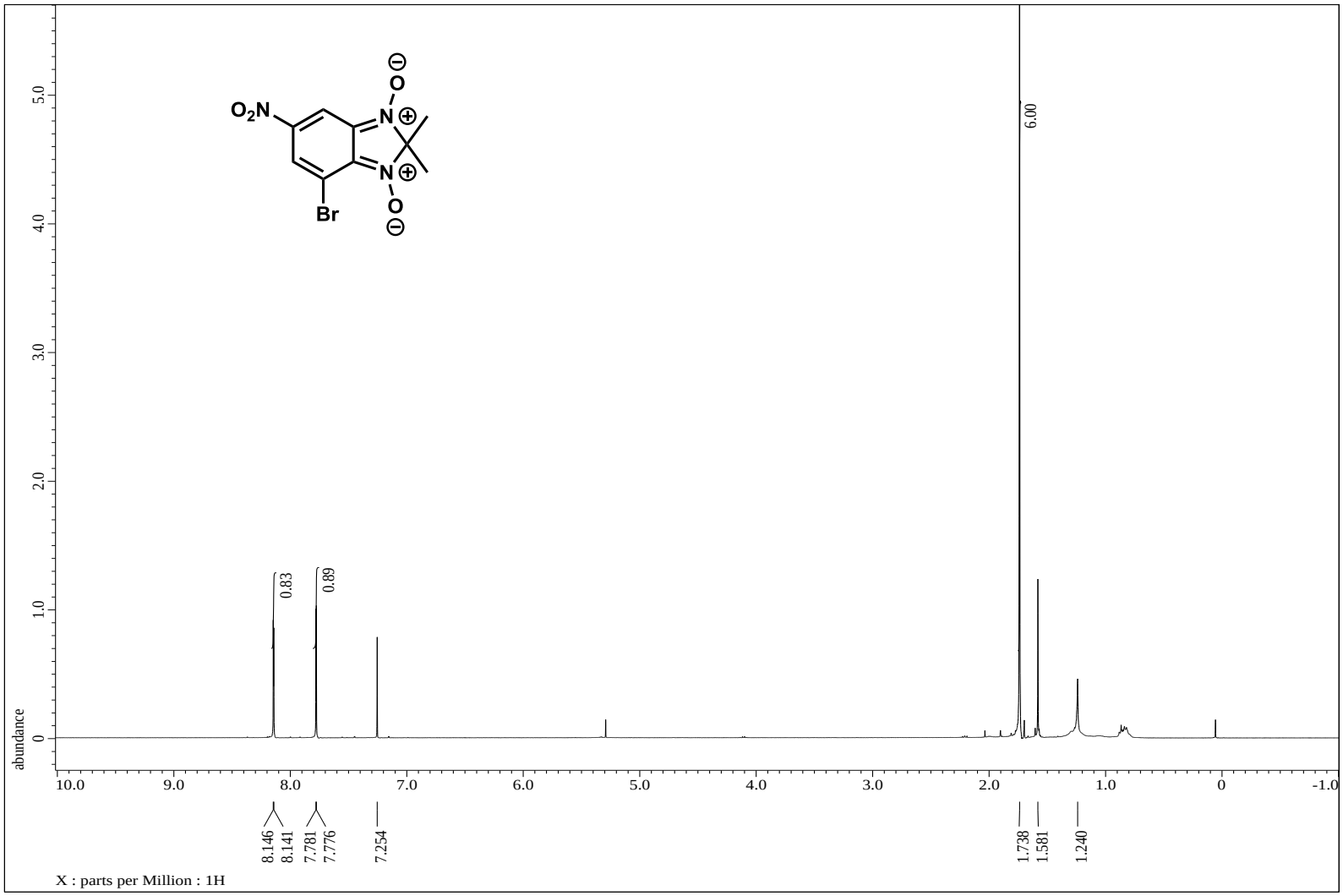

Figure 2.50. ^{1}H NMR (400 MHz, $CDCl_3$) of 4-bromo-2,2-dimethyl-6-nitro-*2H*-benzimidazol-1,3-dioxide (sepin1.18)

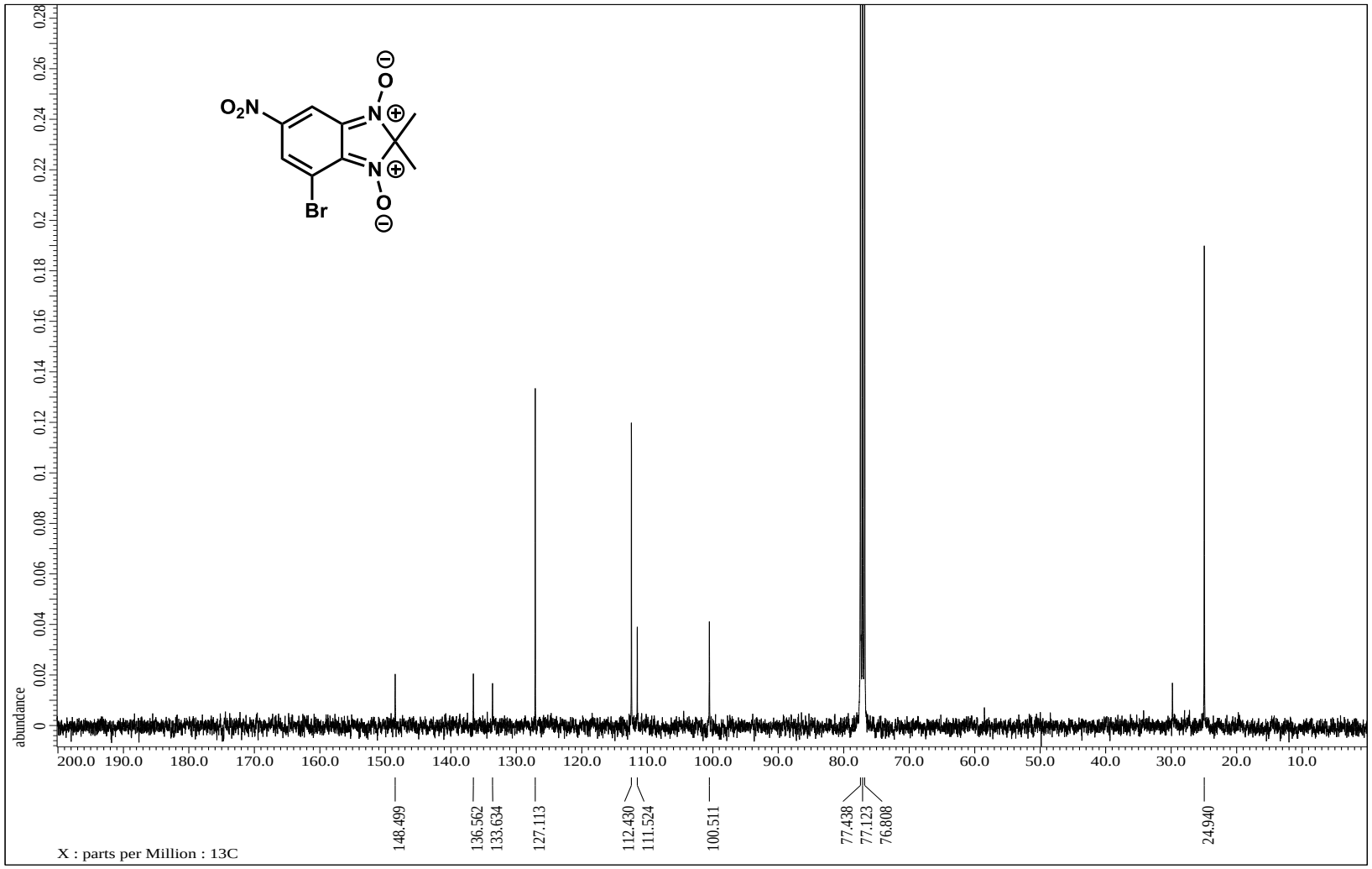

Figure 2.51. ^{13}C NMR (101 MHz, $CDCl_3$) of 4-bromo-2,2-dimethyl-6-nitro-*2H*-benzimidazol-1,3-dioxide (sepin1.18)

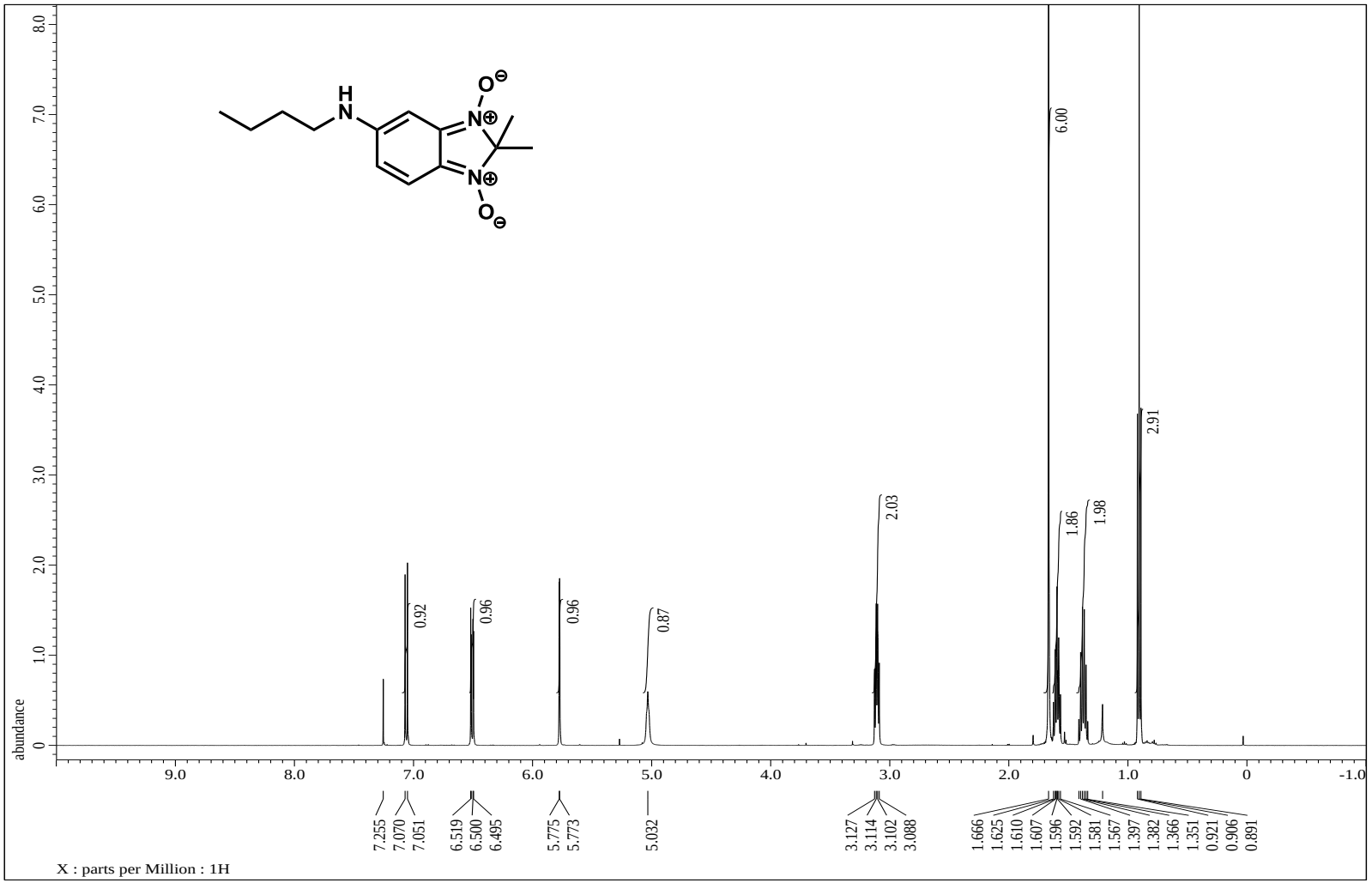

Figure 2.52. ^{1}H NMR (500 MHz, $CDCl_3$) of 5-(butylamino)-2,2-dimethyl-*2H*-benzimidazol-1,3-dioxide (sepin1.8)

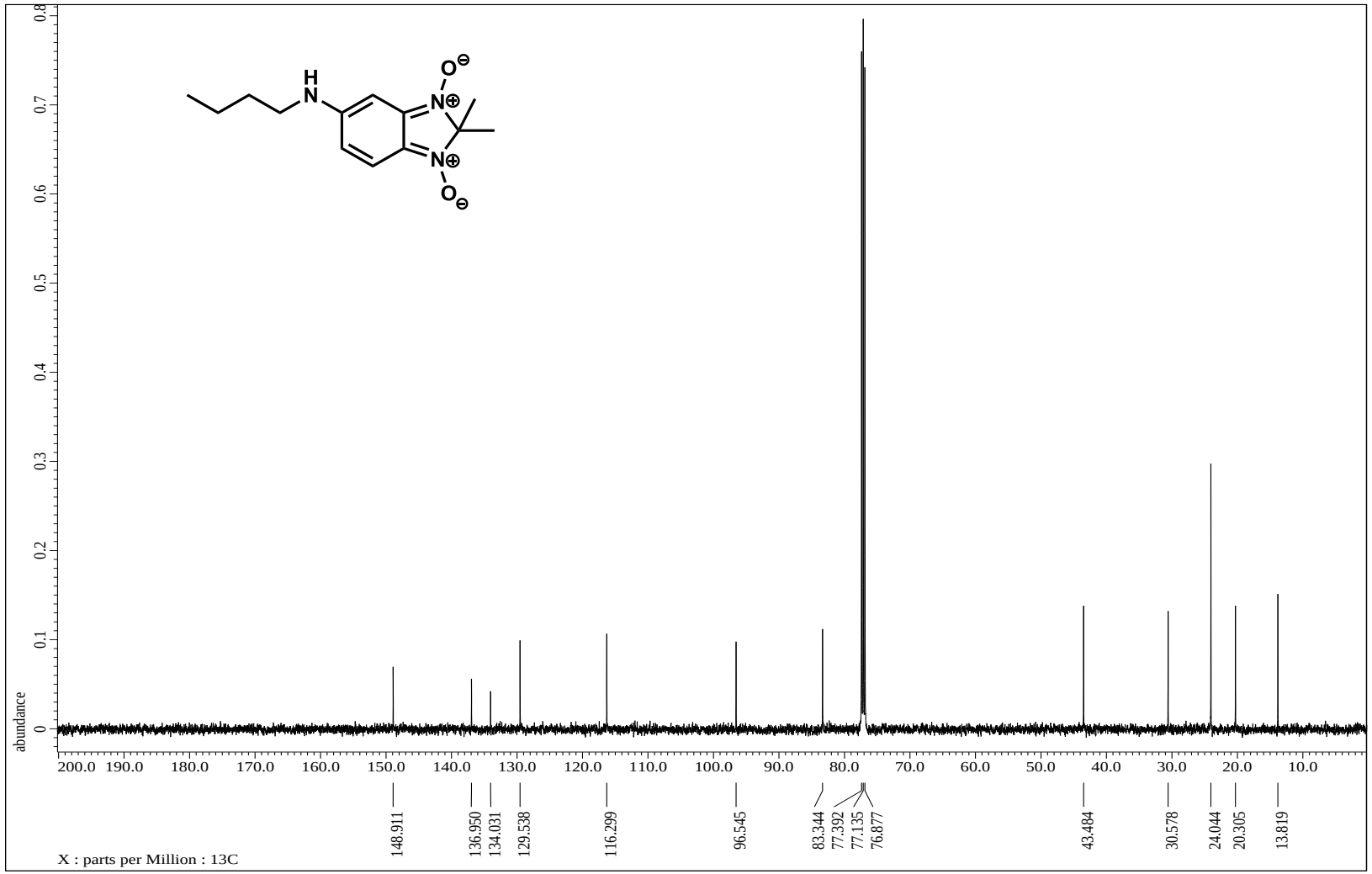

Figure 2.53. ^{13}C NMR (126 MHz, $CDCl_3$) of 5-(butylamino)-2,2-dimethyl-*2H*-benzimidazol-1,3-dioxide (sepin1.8)

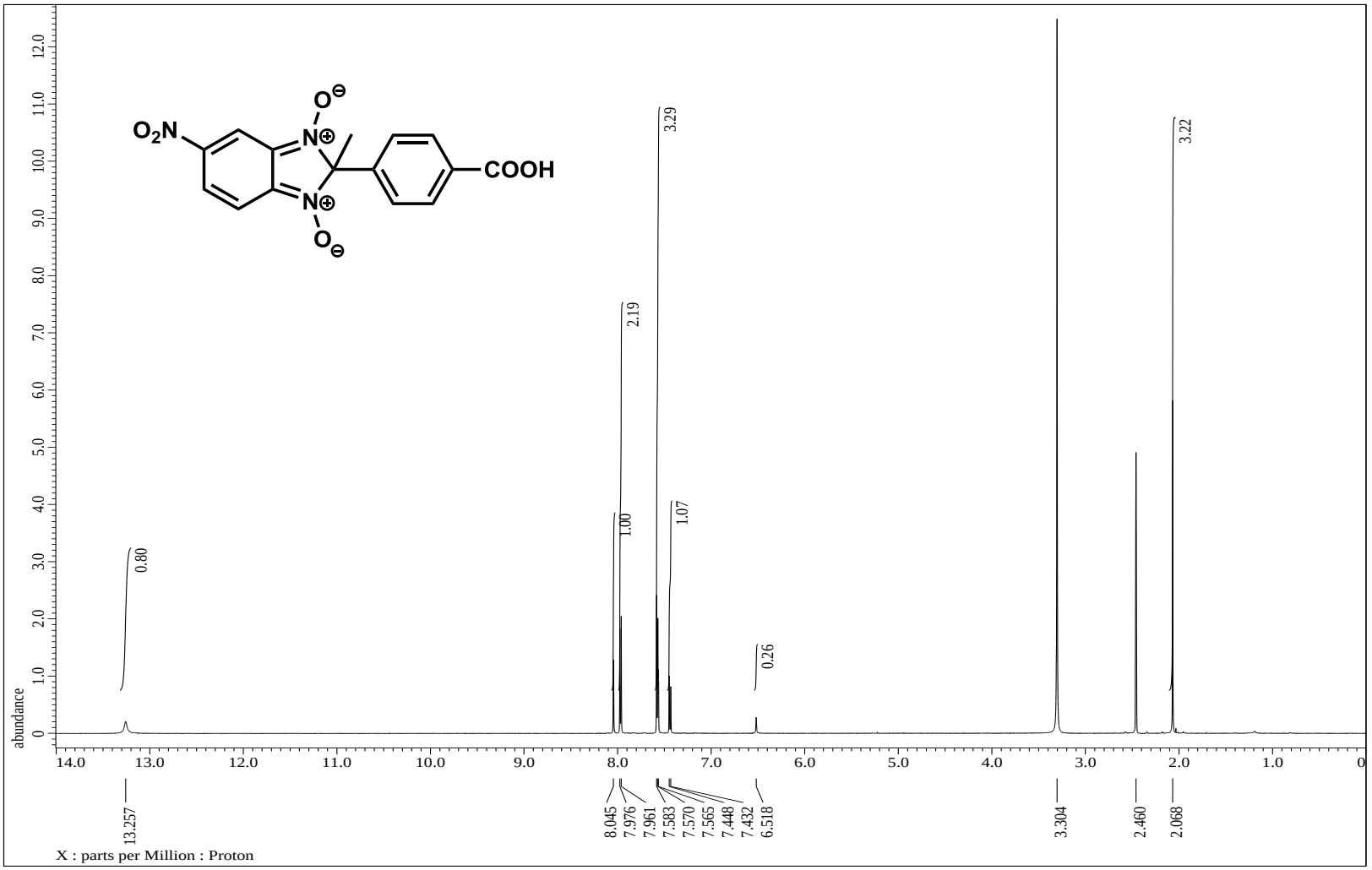

Figure 2.54. ^{1}H NMR (600 MHz, DMSO-d_6) of 2-(4-carboxyphenyl)-2-methyl-5-nitro-*2H*-benzimidazol-1,3-dioxide (sepin1.14)

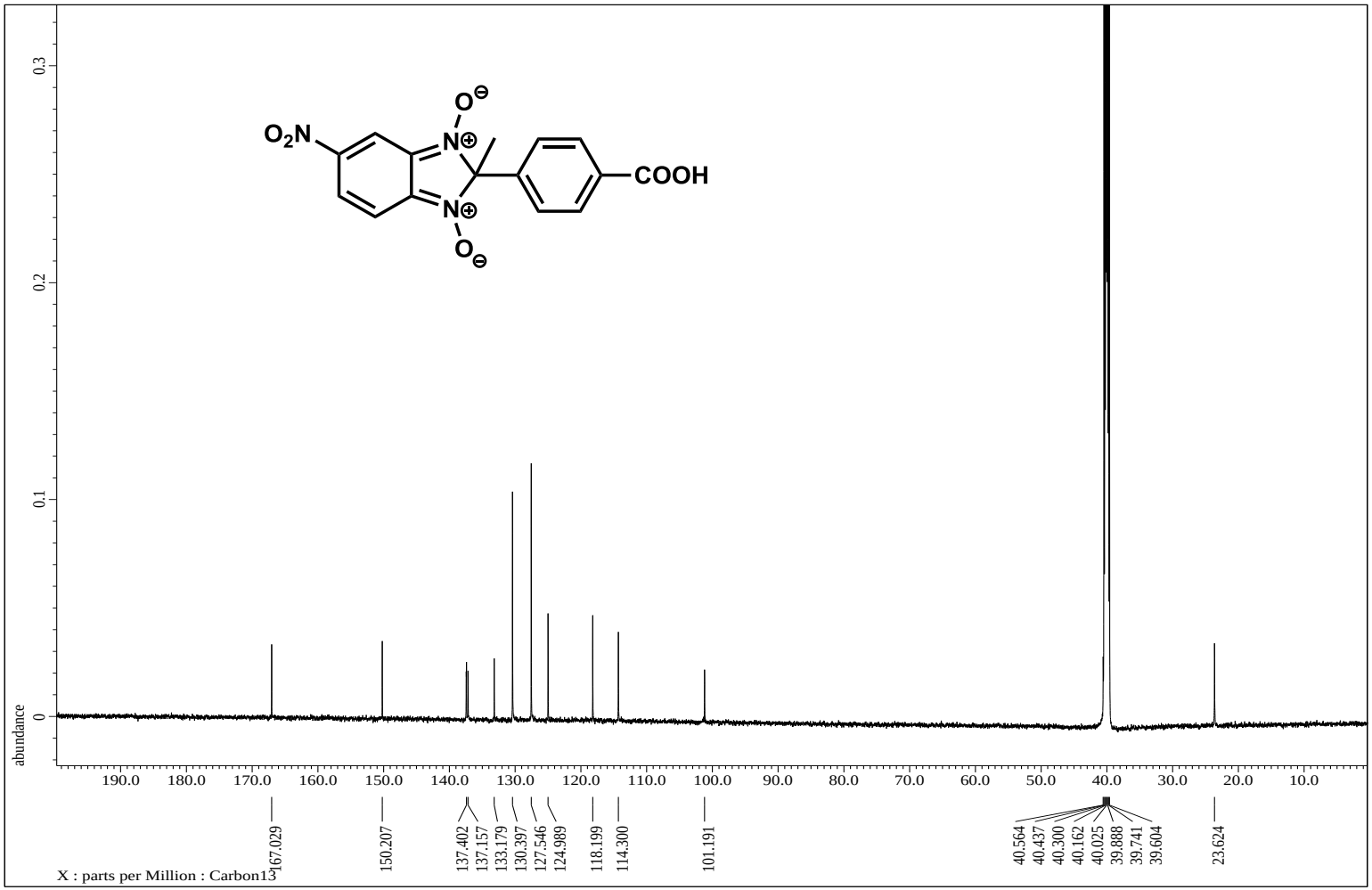

Figure 2.55. ^{13}C NMR (151 MHz, DMSO-d_6) of 2-(4-carboxyphenyl)-2-methyl-5-nitro-*2H*-benzimidazol-1,3-dioxide (sepin1.14)

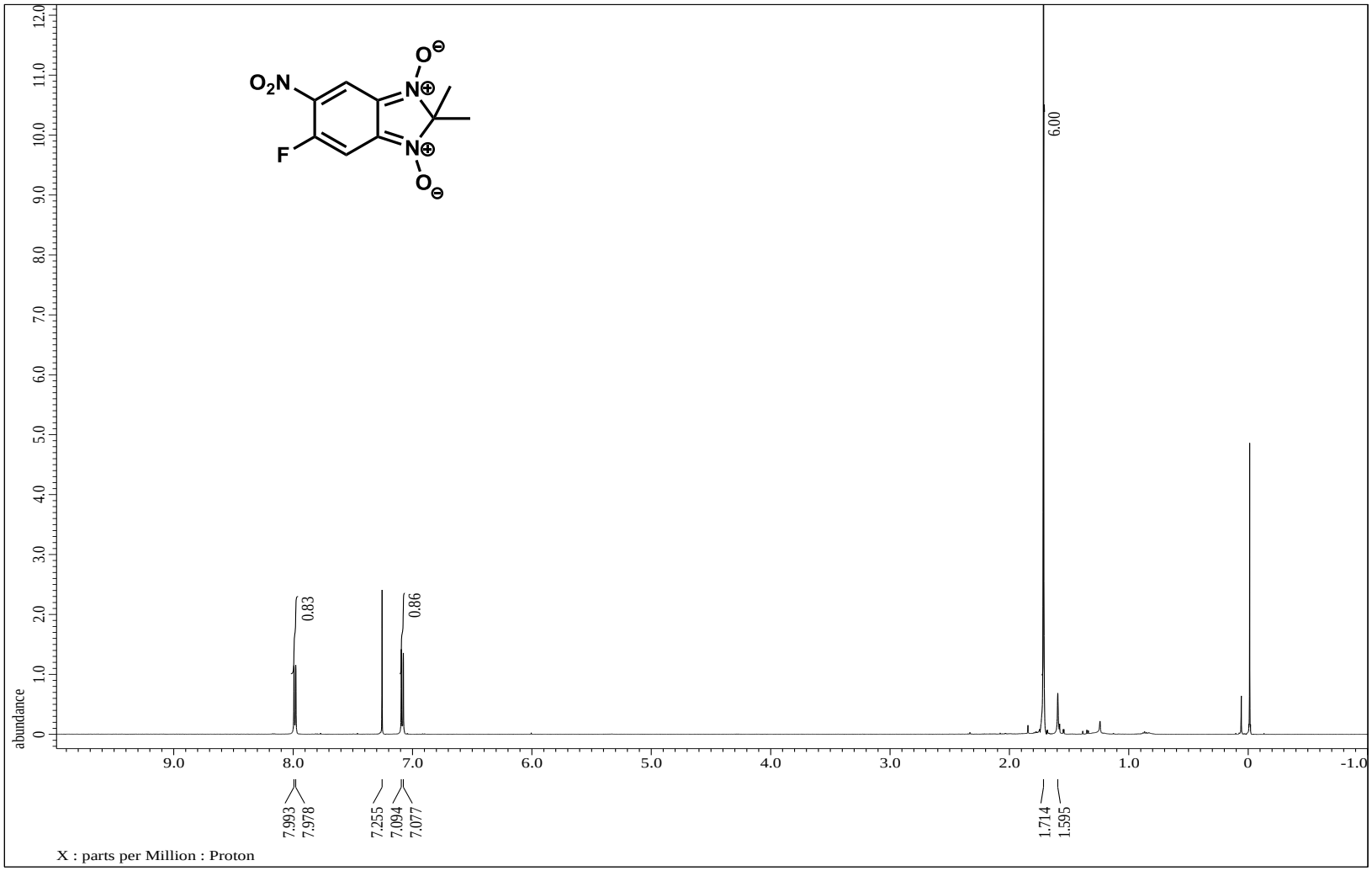

Figure 2.56. ^{1}H NMR (500 MHz, $CDCl_3$) of 6-fluoro-2,2-dimethyl-5-nitro-*2H*-benzimidazol-1,3-dioxide (sepin1.19)

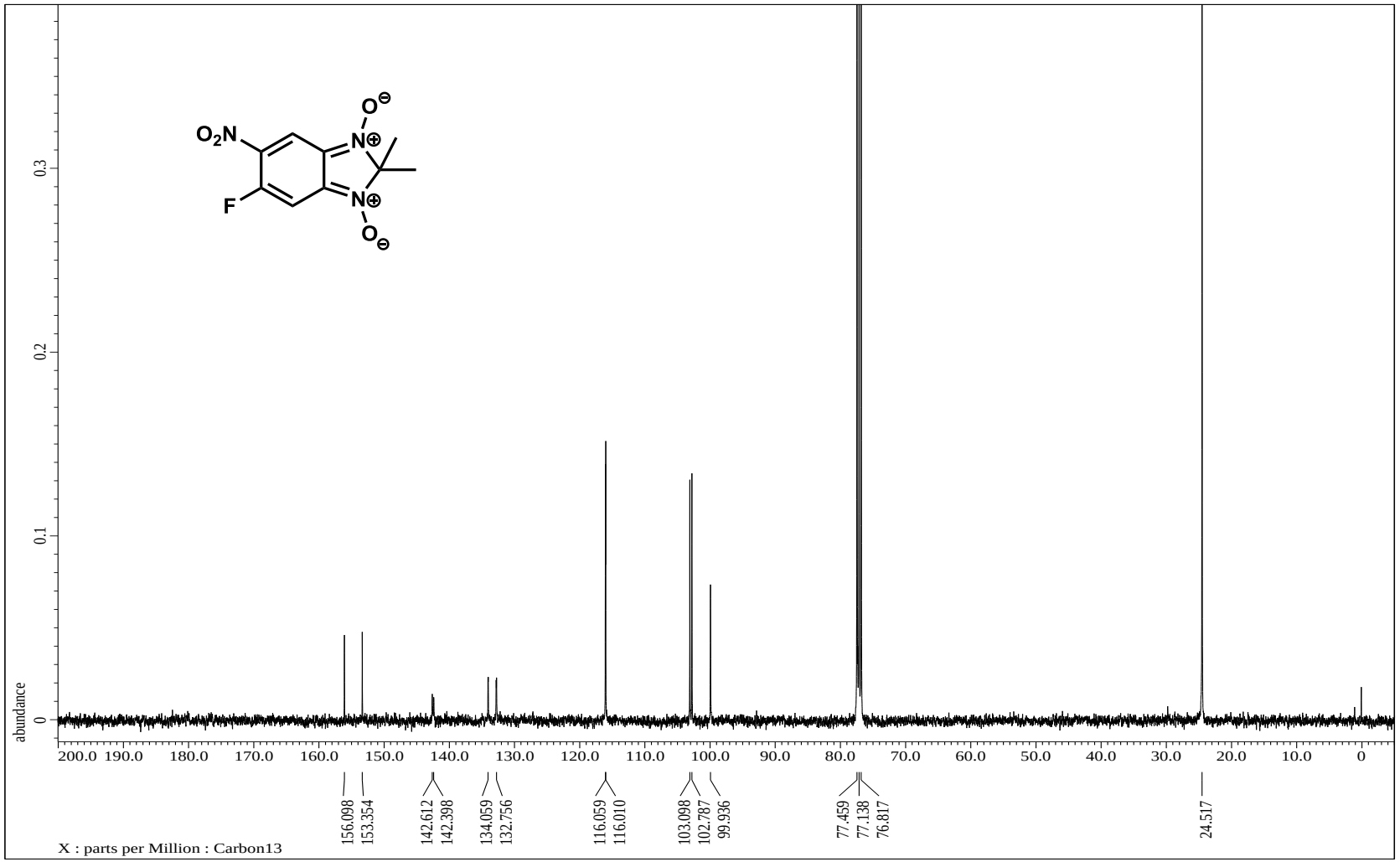

Figure 2.57. ^{13}C NMR (126 MHz, $CDCl_3$) of 6-fluoro-2,2-dimethyl-5-nitro-*2H*-benzimidazol-1,3-dioxide (sepin1.19)

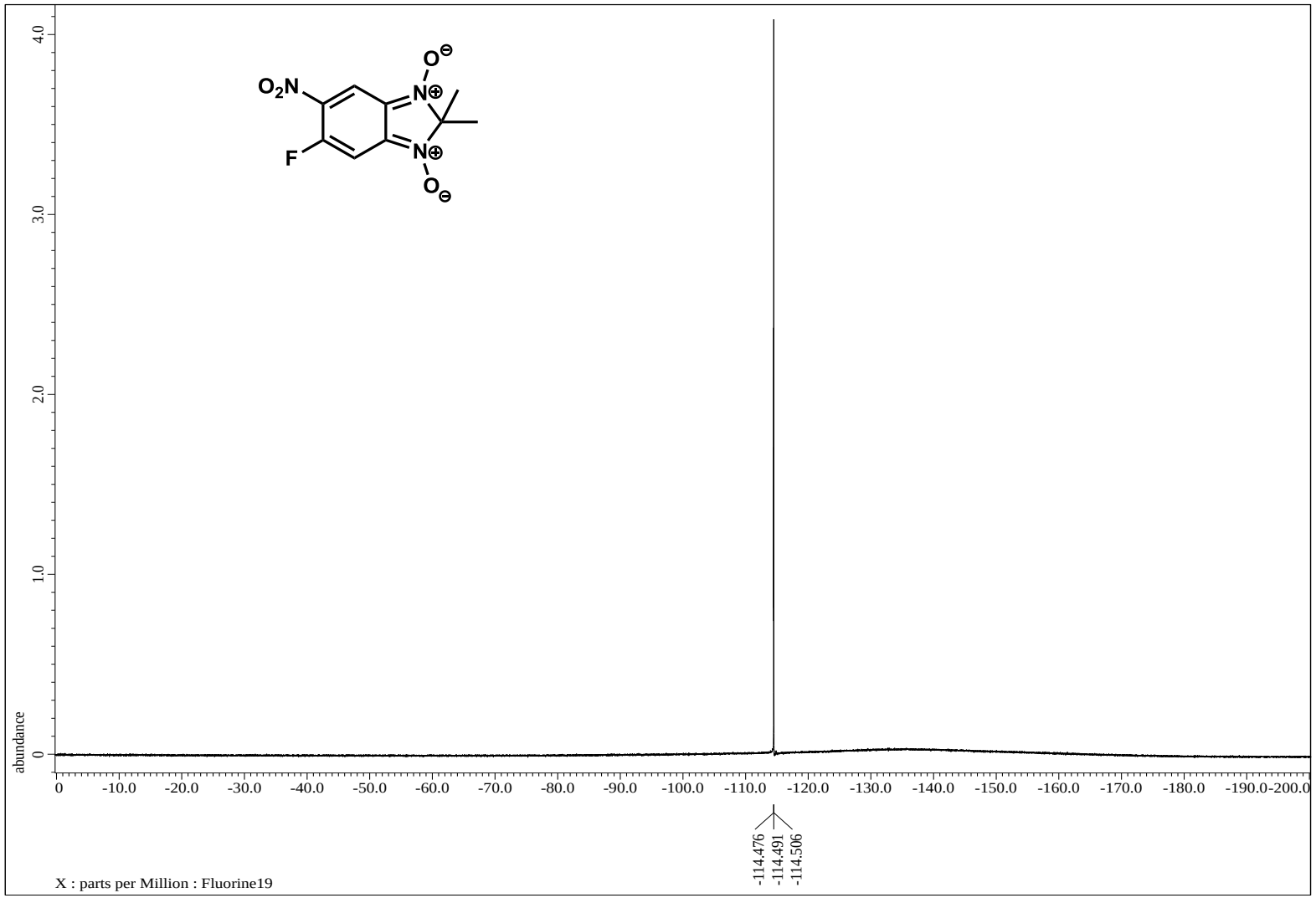

Figure 2.58. ^{19}F NMR (471 MHz, $CDCl_3$) of 6-fluoro-2,2-dimethyl-5-nitro-*2H*-benzimidazol-1,3-dioxide (sepin1.19)

O2N
N
N
.Et2O
abundance
0.76
0.83
0.85
0.59
6.00
0.86
X : parts per Million : 1H
8.227
8.225
7.757
7.753
7.731
7.728
7.420
7.395
7.251
3.494
3.477
3.460
3.442
1.629
1.587
1.570
1.546
1.529
1.216
1.199
1.181
0.057
-0.014

O2N
N
N
.Et2O
abundance
0
0.1
0.2
0.3
0.4
0.5
0.6
0.7
0.8
0.9
200.0
190.0
180.0
170.0
160.0
150.0
140.0
130.0
120.0
110.0
100.0
90.0
80.0
70.0
60.0
50.0
40.0
30.0
20.0
10.0
158.501
157.766
152.770
127.990
127.904
124.262
108.625
77.438
77.123
76.799
65.968
30.508
21.374
15.377
X : parts per Million : 13C

Chapter 3: General Conclusion and Future Directions

3.1. General Conclusion

We have successfully synthesized the natural product dysiherbaine and a library of small molecule inhibitors of saparase enzyme. These projects represents progress in developing new drugs for neural disorders and breast cancer. Dysiherbaine has shown high affinity and selectivity for kainate receptors, making it a unique ligand to explore the complexity of these receptors in central nervous system. Understanding the structure and the function of these receptors is critically important for developing potential therapies for neurological diseases. Our synthetic route to dysiherbaine allows the diversification of functional groups at biologically active centers at a late stage of the total synthesis. This approach therefore will maximize the number of possibly more pharmalogical active analogs which can be used for further investigation the roles of kainate receptors.

In addition to dysiherbaine, a library of small molecule inhibitors of saparase enzyme was also successfully synthesized by systematically modifying the structure of the lead compound obtained from a high throughput screening. Separase enzyme was found overexpressed and mislocalized in more than 60 % of breast cancer and 50 % of triple-negative breast cancer. The inhibition of this receptor can provide a new therapeutic strategy for targeting hard-to-treat breast cancer cells. We have conducted the SAR study on separase inhibitor analogs and the important sites for inhibitory activity in the lead molecule was identified. This information will efficiently guide further modifications in searching of stronger inhibitors and ultimately developing a new drug for breast cancer treatment.

3.2. FUTURE DIRECTIONS FOR DYSIHERBAINE

3.2.1. Modification at C8-C9

A small change in the structure of dysiherbaine by modifying the functionalities at C8-C9 can profoundly impact its pharmacological properties.[1] The preparation of new analogs with different functional groups at these positions will provide valuable molecules to investigate the roles of kainate receptors as well as develop potent antagonists which may have neuroprotective properties. Although our proposed key intermediate **1.1** was not achieved due to the unselective hydrogenation, an alternative intermediate **1.24** and its derivatives could be used to diversify the functional moieties at C8-C9 centers. The installation of amino acid side chain will be sequentially performed to access to dysiherbaine's analogs.

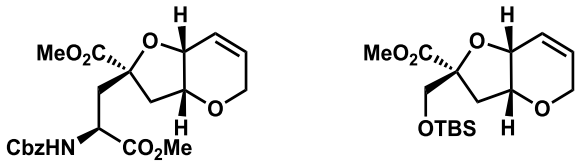

1.1 1.24

Figure 3.1. Structure of key intermediate **1.1** and early intermediate **1.24**

Woodward-Prevost reaction on intermediate **1.24** followed by dehalogenation can be used to access to monohydroxyl analog at C9 **3.4** (Scheme 3.1). Previous study has shown that this analog exhibits strong binding affinity for kainate subunit receptors GluK1 and GluK2.[2] Our synthetic route will efficiently access to this analog.

Scheme 3.1. Monohydroxyl analog at C9

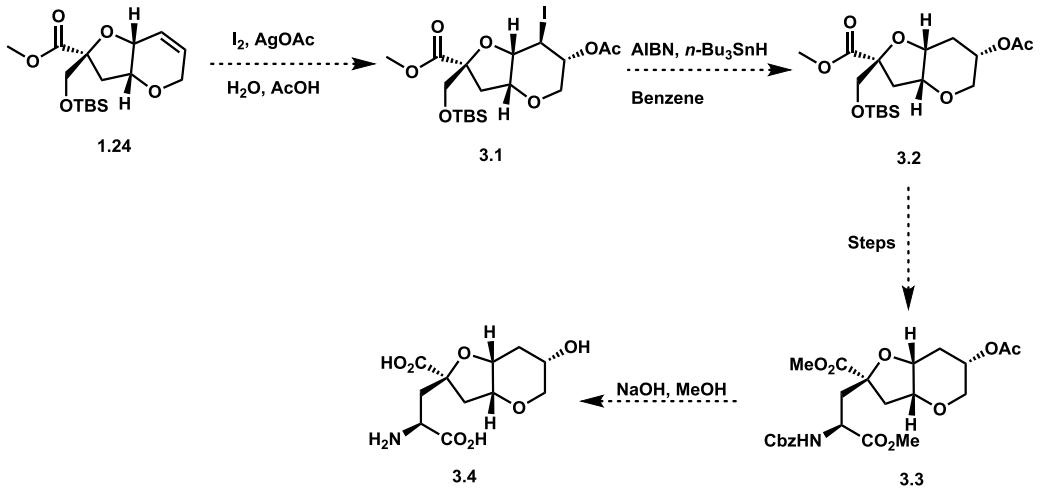

The amine analogs at C9 position, which was shown to play more important role in the binding affinity of dysiherbaine than C8,[1] will be unique and valuable to study kainate receptors. Our proposed synthetic route to these analogs starts with monoacetate derivative **3.2**. Hydrolysis of compound **3.2** followed by the installation of amino acid side chain will give intermediate **3.6** which can be oxidized to generate ketone **3.7**. The reductive amination of **3.7** with various amines will be performed to generate different amine analogs of dysiherbaine (Scheme 3.2).

Scheme 3.2. Monoamino analogs at C9

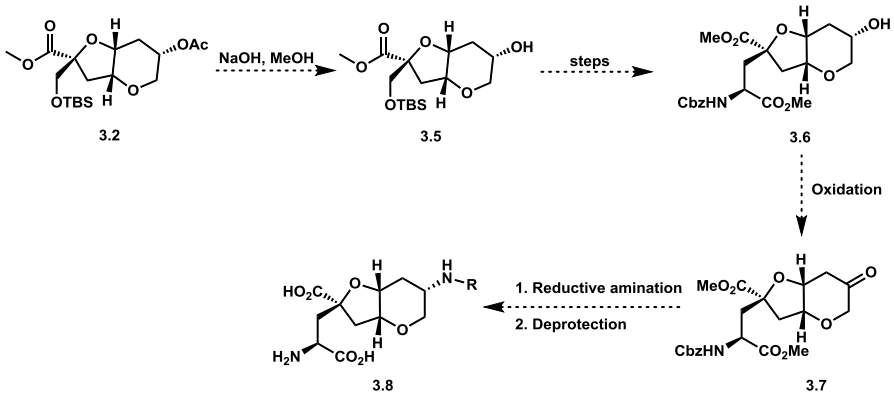

The modification of functional groups at C9 can also be achieved by using azidoalcohol **1.45**. The amino acid side chain will be attached in advance to optimize the efficiency of the synthetic route. Well-established Click chemistry and amide bond formation will be used to prepare the analogs due to the high yield and generality of these reactions. Treatment of a generated common intermediate **3.9** with alkyne under Click reaction condition will yield the triazo analog **3.11** (Scheme 3.3). In another pathway, reduction of **3.9** by Pd/C will provide a primary amine analog **3.12**. Treatment of amine **3.12** with acetyl chloride will give amide analog **3.13** (Scheme 3.3).

Scheme 3.3. Modification at C9 by Click chemistry and amide bond formation

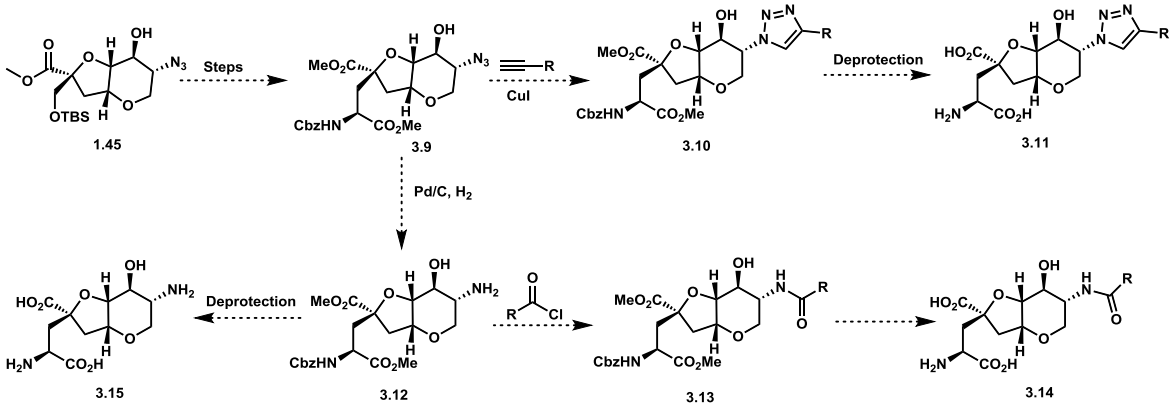

Scheme 3.4. Synthetic approach to MSVIII-19

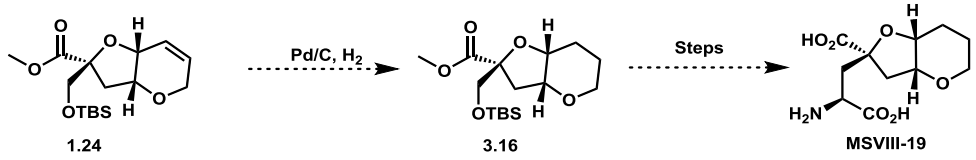

Additionally, MSVIII-19 analog can be achieved in a few steps from intermediate **1.24**. Hydrogenation of C8-C9 double bond in **1.24** followed by the attachment of amino acid side chain will effectively provide the desired analog (Scheme 3.4). This analog was

found to be a selective GluK1 partial agonist, although it induced full domain closure in the ligand binding core of this kainate receptor subtype.[3]

3.2.2. C2 and C4 epimers

Previous studies showed that C4 epimer of neodysiherbaine has a distinct pharmacological profile for the GluK1 subunit receptor,[1] suggesting that the C4 epimer of dysiherbaine could possess novel pharmacological properties toward kainate receptors. This analog can be easily synthesized from the C4 epimer of intermediate **1.24** (**1.24'**). The alkylation at C4 provided a mixture of diastereomers that are easily separated by column chromatography. The synthetic pathway for **1.24** can be carried on for **1.24'**, providing C4 epimer analog of dysiherbaine (Scheme 3.5).

Scheme 3.5. Synthetic approach to C4-epimer DH and C2, C4-epimer DH

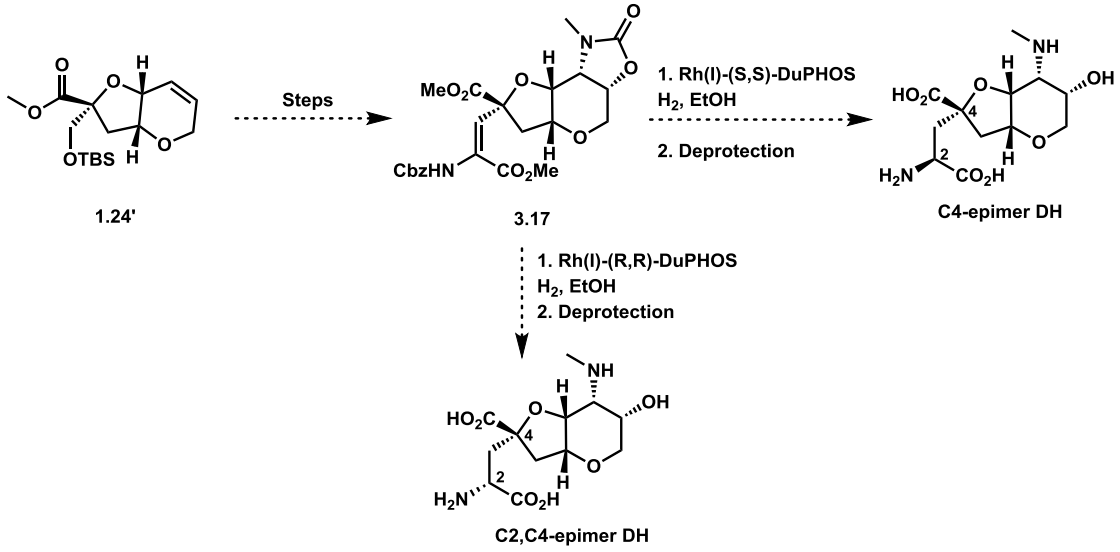

In addition to C4 epimer analog, the use of the other enantiomer of catalyst Rh(I)-(*R*,*R*)-DuPhos in asymmetric hydrogenation will potentially provide the C2,C4-epimer

analog of DH (Scheme 3.5). We believe this novel analog will be useful in the study of kainate receptor.

Scheme 3.6. Synthetic approach to C4-epimer and C2, C4-epimer analogs of MSVIII-19

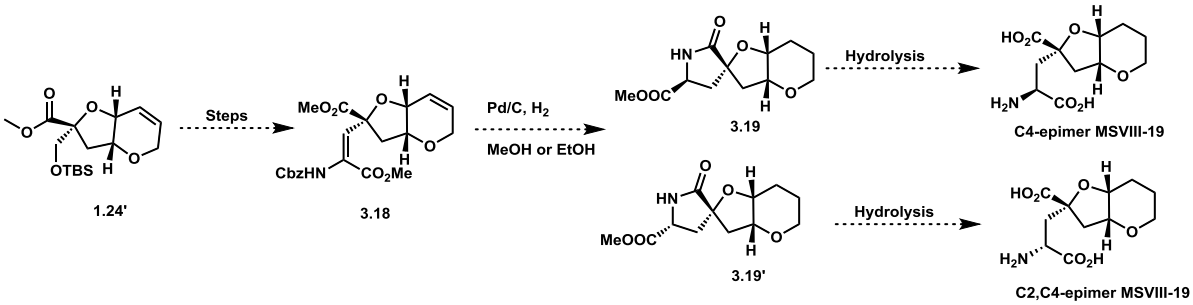

Intermediate **1.24'** can also be used to synthesize C4- and C2, C4-epimer analogs of MSVIII-19. Based on our preliminary results, the attachment of amino acid side chain to **1.24'** will generate a desired diene substrate **3.18** which could be reduced by Pd/C under H_2 atmosphere to concurrently access to both new analogs.

3.3. Future Directions for Separase Inhibitors

3.3.1 A general synthetic route to modify dimethyl position

In order to develop more potent inhibitors for separase enzyme, further modification of the lead compound is necessary. We have extensively modified the $-NO_2$ group at C5 position on the lead molecule and it appears to be essential for the activity. The diversification of the dimethyl group at C2 position on the other hand is limited due to the harsh conditions when using sulfuric acid as reaction solvent (Scheme 3.7). An alternative synthetic route to install different functional groups into C2 position will be

helpful in the search for more active inhibitors. We propose two synthetic approaches that can be used more generally to modify this position.

Scheme 3.7. The original synthetic route to modify C2 position

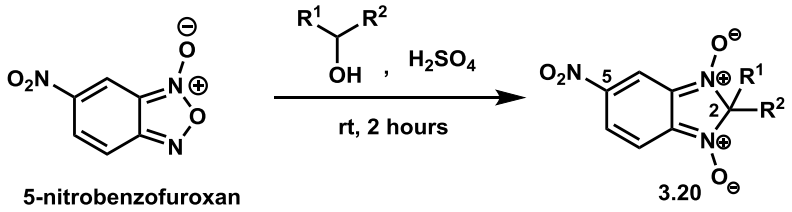

Scheme 3.8. Synthetic approach to modify at C2 position by using dioxime

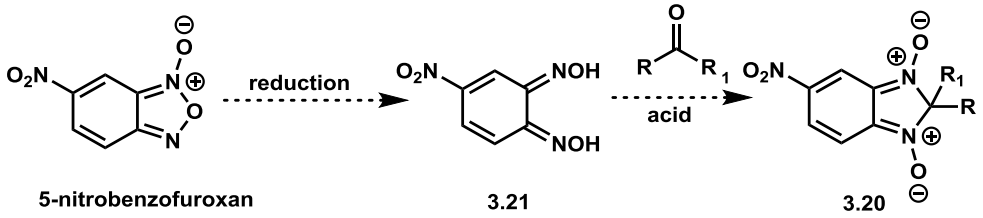

In the first approach, our strategy is using the condensation of *o*-benzoqinone dioxime **3.21** with various ketones under acidic conditions for the modification (Scheme 3.8).[4,5] The dioxime **3.21** could be synthesized from the reduction of benzofuroxan, a precursor in the original synthetic route (Scheme 3.7).[6,7] This chemistry has been successfully conducted when there is no substituent on the six-member ring. The existence of the $–NO_2$ group in the system may make the chemistry more challenging, especially for the formation of dioxime **3.21**.

In the second approach, the modification at C2 center can be achieved by the condensation of diamine **3.22** with different ketones, followed by the oxidation of a benzimidazoline **3.23** (Scheme 3.9). We have successfully synthesized **3.23** while

correcting the structure of the lead compound (chapter 2). The screening of an appropriate oxidant for the second step is necessary to achieve the desired product.

Scheme 3.9. Synthetic approach to modify at C2 position by using oxidation of benzimidazoline

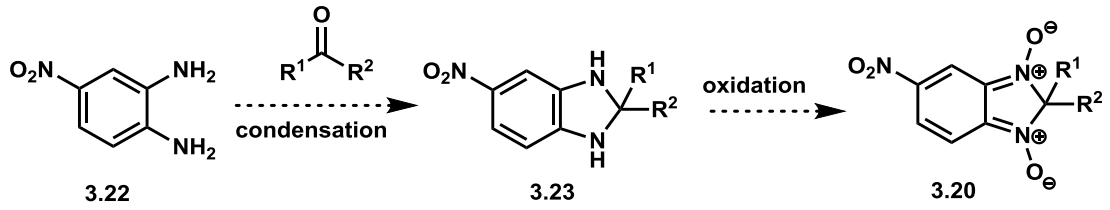

3.3.2 Photoaffinity labeling study

Photoaffinity labeling (PAL) is a valuable technique for studying the interaction of the inhibitors with their targeting enzymes, providing insight into the active site of the enzymes as well as assisting in designing more active inhibitors.[8] In order to conduct PAL studies, the preparation of photoaffinity probes is necessary. We have successfully synthesized sepin1.14, which has a –COOH group on the *para* position of a phenyl group attached to C2 position. Its inhibitory activity toward separase is comparable to the lead compound with an IC_{50} of 16.86 μM. Further modification on the carboxylic acid group of this compound will promisingly provide a probe for PAL studies.

A photoaffinity probe is typically composed of three main components, a ligand with good binding affinity, a photoreactive group which can form a covalent bond with receptor enzymes when irradiated, and an affinity tag such as biotin for purification or a fluorescence tag for detection. Based on this principle design, we propose the structure and a synthetic route to prepare a photoaffinity probe for separase enzyme by using sepin1.14 (Figure 3.2 and Scheme 3.10, respectively). Diaziridine will be chosen as a

photoreactive group due to its relative stability as well as its short lifetime upon irradiation which prevents side reactions with other biological systems.[9] The amide bond will be used to attach the inhibitor (sepin1.14) to a photoreactive group and an affinity tag component (**3.25**).

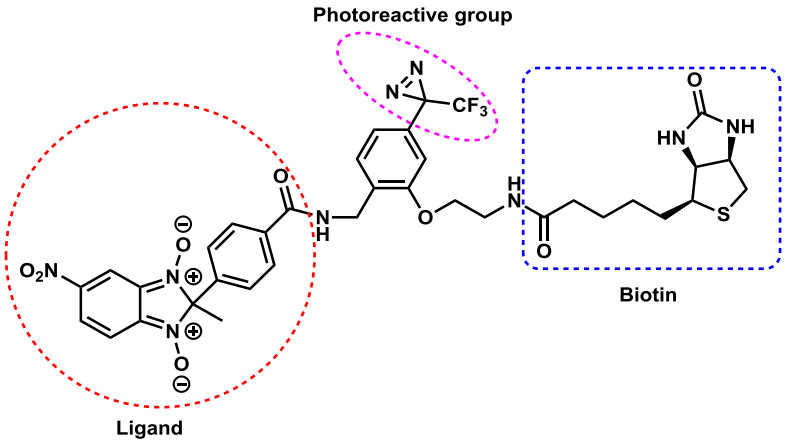

Figure 3.2. Proposed structure of photoaffinity labeling probe for separase enzyme

Scheme 3.10. Synthetic approach to photoaffinity probe for separase enzyme

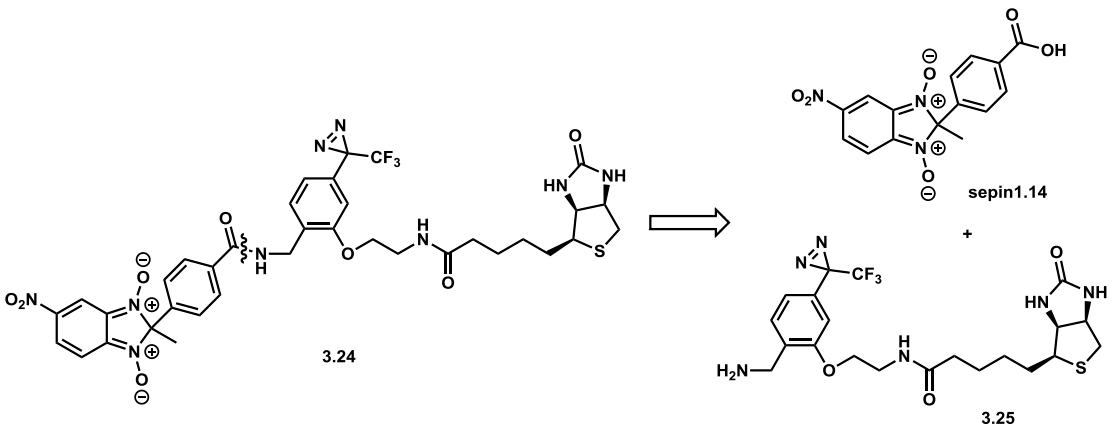

Scheme 3.11. Synthetic approach to a photoreactive group and an affinity tag component

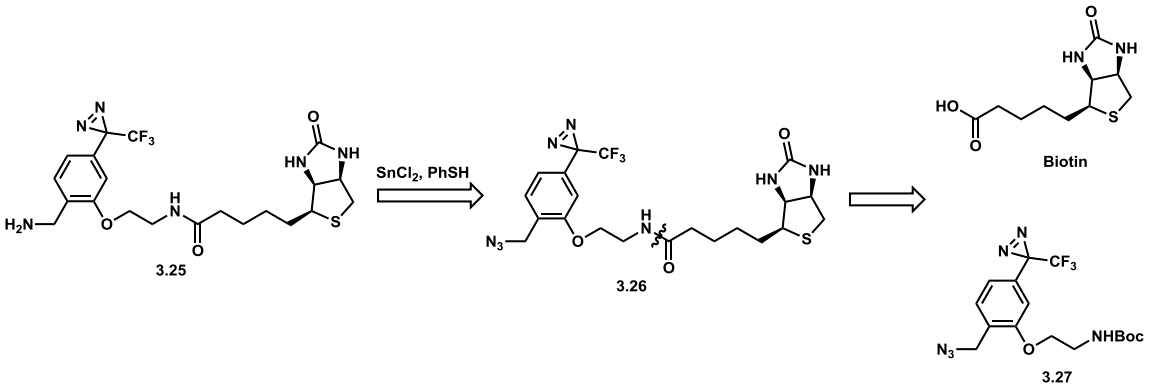

Compound **3.25** can be synthesized by the reduction of its corresponding azide adduct **3.26** using $SnCl_2$ and benzenethiol.[10] An amide bond will be used to construct **3.26** from biotin and photoreactive component **3.27** (Scheme 3.11).

Scheme 3.12. Synthetic approach to a photoreactive component

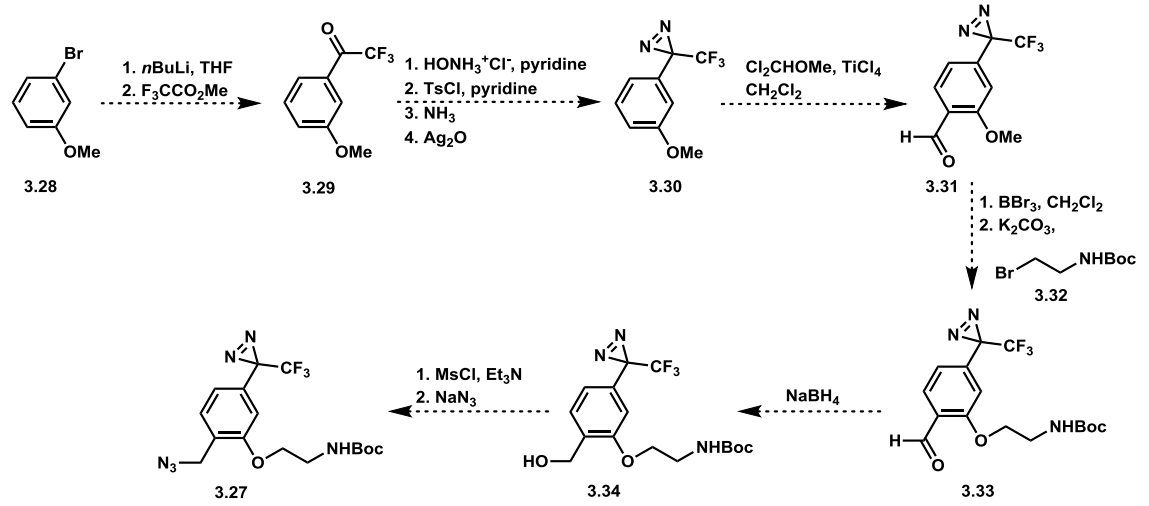

The synthetic route to **3.27** was proposed in Scheme 3.12, starting with 1-bromo-3-methoxybenzene **3.28** which is readily available. Firstly, trifluoroacetyl group will be installed and consequently transferred to diaziridine **3.30** in four steps.[11] An aldehyde moiety will be introduced for further transformation of the azide group. The

demethylation will then be performed by using BBr_3, followed by O-alkylation with **3.32** to provide a linker where biotin will be attached. Reduction of aldehyde with $NaBH_4$ will generate alcohol **3.34** which will be transferred to azide using MsCl and NaN_3, providing **3.27**.. Photoreactive component **3.27** will be ready for the attachment of biotin and sepin1.14, generating a photoaffinity tool to probe the active site of separase enzyme.

In summary, possible chemistries for both dysiherbaine and separase inhibitors were proposed. The generation of dysiherbaine's analogs will provide valuable molecules for further studying the roles of kainate receptors while the synthesis of photoaffinity probe will give insights into the active site of separase enzyme. These studies will substantially assist the progress in drug development for neural disorders and breast cancer.

REFERENCES

(1) Lash, L. L.; Sanders, J. M.; Akiyama, N.; Shoji, M.; Postila, P.; Pentikäinen, O. T.; Sasaki, M.; Sakai, R.; Swanson, G. T. *Journal of Pharmacology and Experimental Therapeutics* **2008**, *324*, 484.

(2) Shoji, M.; Akiyama, N.; Tsubone, K.; Lash, L. L.; Sanders, J. M.; Swanson, G. T.; Sakai, R.; Shimamoto, K.; Oikawa, M.; Sasaki, M. *The Journal of Organic Chemistry* **2006**, *71*, 5208.

(3) Frydenvang, K.; Lash, L. L.; Naur, P.; Postila, P. A.; Pickering, D. S.; Smith, C. M.; Gajhede, M.; Sasaki, M.; Sakai, R.; Pentikaïnen, O. T.; Swanson, G. T.; Kastrup, J. S. *The Journal of Biological Chemistry* **2009**, *284*, 14219.

(4) Samsonov, V. A.; Volodarskii, L. B. *Chem Heterocycle Compound* **1980**, *16*, 628.

(5) Pätzold, F.; Niclas, H. J.; Gründemann, E. *Journal für Praktische Chemie* **1990**, *332*, 345.

(6) Alexanian, V.; Haddadin, M.; Issidorides, C.; Nazer, M. *Heterocycles* **1981**, *16*, 391.

(7) Samsonov, V. A.; Volodarskii, L. B.; Shamirzaeva, V. *Chem Heterocycle Compound* **1994**, *30*, 460.

(8) Robinette, D.; Neamati, N.; Tomer, K. B.; Borchers, C. H. *Expert Review of Proteomics* **2006**, *3*, 399.

(9) Dubinsky, L.; Krom, B. P.; Meijler, M. M. *Bioorganic & Medicinal Chemistry* **2012**, *20*, 554.

(10) Kan, T.; Kita, Y.; Morohashi, Y.; Tominari, Y.; Hosoda, S.; Tomita, T.; Natsugari, H.; Iwatsubo, T.; Fukuyama, T. *Organic Letters* **2007**, *9*, 2055.

(11) Mayer, T.; Maier, M. E. *European Journal of Organic Chemistry* **2007**, *28*, 4711.